DIN: 68SD4266
3 JUNE 1968

PLANETARY VEHICLE THERMAL INSULATION SYSTEMS

FINAL REPORT

PREPARED FOR

JET PROPULSION LABORATORY

PASADENA, CALIFORNIA

UNDER JPL CONTRACT NO. 951537

GENERAL ELECTRIC

MISSILE AND SPACE DIVISION
Valley Forge Space Technology Center
P. O. Box 8555 • Philadelphia, Penna. 19101

DIN: 68SD4266
3 JUNE 1968

PLANETARY VEHICLE THERMAL INSULATION SYSTEMS

FINAL REPORT

BY

S.J. BABJAK
R.W. CARR
A.D. COHEN
C.S. LANKTON
R. LUDWIG
S. RUBENSTEIN
A. TWEEDIE

PREPARED FOR

JET PROPULSION LABORATORY
PASADENA, CALIFORNIA
UNDER JPL CONTRACT NO. 951537

THIS WORK WAS PERFORMED FOR THE JET PROPULSION LABORATORY, CALIFORNIA INSTITUTE OF TECHNOLOGY, AS SPONSORED BY THE NATIONAL AERONAUTICS AND SPACE ADMINISTRATION UNDER CONTRACT NAS 7-100.

GENERAL ELECTRIC
MISSILE AND SPACE DIVISION
Valley Forge Space Technology Center
P.O. Box 8555 • Philadelphia, Penna. 19101

PRECEDING PAGE BLANK NOT FILMED.

TABLE OF CONTENTS

TABLE OF CONTENTS (Cont)

LIST OF ILLUSTRATIONS

LIST OF ILLUSTRATIONS (Cont'd)

LIST OF ILLUSTRATIONS (Cont'd)

ABSTRACT

This report summarizes the results of the works performed on the subject contract. It contains the thermal analyses performed, results of the material evaluation tests, test fixture and blanket design details, and environmental test results. In addition a description of the thermal vacuum test is given, and results of the thermal vacuum tests are included. These tests indicated that excellent thermal performance was achieved with an insulation system that is relatively simple to fabricate and install.

SECTION 1.0

INTRODUCTION

PROGRAM OBJECTIVES AND SCOPE

The objective of the Planetary Vehicle Thermal Insulation program was to conduct a research and development program that would provide an efficient thermal insulation system for large interplanetary vehicles. Specifically, super insultation materials were to be selected and proven,an insulation system designed and fabricated, and a full-scale qualification test of the system was to be performed. The entire program was sponsored by the Jet Propulsion Laboratory of the California Institute of Technology.

The development of a super insulation system for large interplanetary vehicles must consider certain requirements which are unique in terms of size, thermal control constraints and the mission environments. Such an insulation system must be compatible with ethylene oxide (ETO) and heat sterilization, without significant degradation, in order to satisfy national planetary quarantine goals. The system must be capable of withstanding the physical loadings imposed by the vehicle operation and the environmental conditions presented by interplanetary travel. Furthermore, the insulation system should be designed to minimize installation and removal time and effort, as well as to be light in weight. Finally, and most important, the thermal insulation system developed should provide thermal protection for all mission phases with a minimum insulation system weight. Planetary missions to Mars were given exclusive attention in the course of this program, although the program results are, in many ways, applicable to a broad range of potential space explorations.

The thermal insulation development program, structured to investigate and reflect the aforementioned requirements, was initiated in October of 1966. The program was divided into the following four phases:

Phase I

During Phase I, the thermal insulation system requirements were defined and studied. Detailed thermal analyses were performed to assess potential insulation system capabilities. Extensive experimental activities were conducted to select insulation materials compatible with ethylene oxide decontamination and dry heat sterilization. Potentially suitable materials were subjected to simulated interplanetary irradiations and to rapid depressurization as associated with boost flight. Phase I was completed in February 1967 and was reported in Reference 1.

Phase II

Based on the analytical and experimental investigations of Phase I, the detailed design of the thermal insulation system was performed during Phase II. Additional material evaluation tests were performed and a small-scale model of the thermal insulation system was subjected to a long term thermal vacuum environment. The insulation system was subjected to simulated launch loads of vibration, shock, and acoustic, and a second series of rapid depressurization tests was run. A detailed thermal analysis was conducted to establish a priori insulation performance parameters. Phase II was completed in July 1967 and is reported in Reference 6.

Phase III

This phase consisted of the procurement, fabrication and assembly of the insulation system and the full-scale test fixtures.

Phase IV

The full-scale thermal vacuum tests were conducted in Phase IV. The test program was completed in January 1968.

This current report covers the entire thermal insulation research and development program. The aim of the report is to include, under one cover, a complete description of the program and a meaningful presentation of the experimental results and design conclusions developed. References to past reports are minimal, but are utilized where they add to the value of the text.

Although the development and test program was performed in sequential phases, this final report has not been so organized. Section 2.0 presents the technical discussion, relevant to the program, in a manner which is additive rather than chronological; i.e., the material selection, thermal blanket design, fabrication and test are presented as orderly reporting stepping stones toward the ultimate goal.

Section 1.0 Introduction

PROGRAM SUMMARY

The thermal insulation program has produced several significant and definitive results and conclusions which are briefly summarized below.

Results

a. A thermal insulation system has been developed for use on large interplanetary vehicles.
b. Outstanding thermal performance was achieved with multilayer gold-on-Mylar and Kapton film insulation blankets.
c. Effective and efficient insulation fabrication, installation and removal techniques and hardware were developed and demonstrated.
d. The gold-on-plastic film insulation was shown to be compatible with the decontamination and sterilization environments and capable of withstanding interplanetary irradiation.
e. The selected insulation system design was light in weight and capable of withstanding anticipated flight loads.

Conclusions

a. Large insulation blankets, up to at least 4 feet by 10 feet, are feasible, but require venting.
b. Deeply crinkled gold coated insulations have excellent thermal performance.
c. Aluminum-coated plastic film insulations are not reliably compatible with moist ethylene oxide environments.
d. Heat sterilization has no measurable affect on metallized plastic film insulations.
e. Kapton insulation is suitable for the high temperature radiation from an ablative rocket motor nozzle. Additional investigation is required to select insulation for a radiation cooled nozzle.

SECTION 2.0

TECHNICAL DISCUSSION

2.1 CANDIDATE INSULATION - MATERIAL EVALUATION

Section 2.1 Candidate Insulation-Material Evaluation

TEST OBJECTIVES

The design and selection of materials for the thermal insulation system of planetary vehicles must consider the constraints imposed by the NASA Planetary Quarantine Plan.[1] In order to avoid contamination of the planets by earth organisms, landing capsules will be heat sterilized prior to launch. Prior to heat sterilization, the capsule will be exposed to ethylene oxide decontaminants. The planetary spacecraft, or portions of the spacecraft, may also receive ethylene oxide (ETO) decontamination treatments to reduce the planetary contamination potential of these orbiting vehicles. Thermal insulation blankets, made of metallized plastic films, depend on the optical properties of the metal to reflect the incident heat flux and thereby develop a high value of thermal resistance. An oxide layer on the metal would reduce reflectance by increasing emittance of the surface. Therefore, the optical property effects of oxygen in the sterilization environment must be controlled. Furthermore, insulation materials employed on planetary missions will be exposed to the rigors of the space environment. Consequently, thermal insulation materials must be capable of withstanding the decontamination, sterilization and space environments without significant degradation, either physically or in their thermal insulating characteristics.

The material compatibility evaluation program for candidate thermal insulation materials consisted of a determination of the effects of exposures to decontamination, sterilization and space environments. Insulation samples and pressure-sensitive insulation tapes were studied in the following tests:

a. Tests were conducted to determine the effects of the ETO environment on the physical properties of candidate insulation materials. The tests evaluated the compatibility of both single sheet and small blanket samples of insulation material with the ETO decontamination environment. The effects of variations of the decontamination environment, including relative humidity, atmosphere and moisture injection techniques, were investigated.
b. Candidate insulation materials were subjected to the dry heat sterilization cycles prescribed in JPL Spec. Vol-50503-ETS. The effects of the presence of oxygen in the sterilization environment were studied.
c. Insulation samples were exposed to simulated space environmental factors including proton and ultraviolet radiation and high vacuum.
d. Pressure-sensitive insulation tapes were exposed to the ETO and sterilization environments.

All environmental exposures were followed by visual observations and physical property measurements.

[1] Planetary Quarantine Plan-Voyager Project; 15 March 1966, 3rd Revision dated 1 June 1967, NASA-OSSA, Voyager Project Office, Document #818-11-PQ001.

Section 2.1 Candidate Insulation-Material Evaluation

SCOPE

A comprehensive experimental evaluation program was conducted to select thermal insulation blanket materials that are compatible with dry heat sterilization, ethylene oxide (ETO) decontamination and the combined space environment. The material evaluation program consisted of exposures of several candidate insulation materials to ETO, dry heat and simulated space environments. The basic classes of insulation materials tested were:

a. Aluminized Mylar[2] (NRC-2[1])
b. Aluminized Kapton[2]
c. Dimpled Aluminized Mylar (Dimplar[3])
d. Aluminized Teflon[2]
e. Goldized Mylar
f. Goldized Kapton
g. Dacron[2] Mesh (a possible spacer material for insulation blankets)

In addition to the basic blanket materials, several insulation tapes, required for blanket assembly and installation on the planetary vehicle, were tested. The tapes tested were primarily of the pressure-sensitive adhesive variety although a hook and pile received considerable attention. The classes of tapes tested consisted of:

a. Aluminized Mylar with adhesive[4]
b. Kapton with adhesive[5]
c. Hook and pile[6]

The material evaluation consisted of the determination of the effects of the sterilization, decontamination and space environments on the physical properties of the insulation samples. The physical properties evaluated were:

a. Solar absorptance (α_S)
b. Normal emittance (ϵ_N)
c. Weight change (in air)
d. Outgassing (weight loss in vacuum and product analysis)
e. Adhesion
f. Dimensional Stability

In addition to the physical property measurements, visual observation of material degradation proved to be a significant source of information.

---

[1]Trademark of the National Research Corporation
[2]Trademark of the E. I. DuPont Company
[3]Trademark of the HITCO
[4]Manufactured by Permacel and 3M
[5]Technical Fluorocarbon, Inc.
[6]Velcro Industries, Ltd.

Section 2.1 Candidate Insulation-Material Evaluation

SUMMARY OF RESULTS

Table 2-1 summarizes the results of the material evaluation.

Ethylene Oxide Decontamination Effects

a. Aluminized coatings on plastic film are susceptible to degradation in humid environments.
b. Interior blanket layers are more severely damaged by humidity.
c. Blanket perforations reduce degradation.
d. No significant degradation is caused by dry ETO.
e. Goldized Mylar insulation was not affected by humid ETO environments.
f. Insulation experiences a weight gain due to decontamination (addition of moisture).
g. Adhesive properties of the pressure-sensitive tapes tested are not affected by ETO decontamination.

Dry Heat Sterilization Effects

a. No significant change in the emittance of aluminized or goldized films was produced by the range of oxygen-contaminated sterilization environments investigated.
b. Dry heat sterilization causes a small percentage dimensional shrinkage.
c. Most pressure sensitive tapes tested are significantly degraded by dry heat sterilization.
d. Technical Fluorocarbons Inc. clear Kapton and Velcro hook and pile tapes were most satisfactory.

Combined Space Environmental Effects

a. The combined exposure to ultraviolet and proton irradiation, in high vacuum, produced no significant change in the optical properties of the thermal insulation tested.
b. Aluminized Teflon insulation buckled after exposure to ultraviolet and proton radiation.

Table 2-1. Materials Evaluation - Overall Summary of Results

Materials	ETO Decontamination	Heat Sterilization	Combined Space Environment
NRC-2 (Alum. Mylar)	U	S	--
Aluminized Kapton (1/2 mil)	U	S	--
Aluminized Kapton (2 mil)	--	--	S
Gold on Kapton (3 mil)	--	--	S
Gold on Mylar (1/4 mil)	S	S	--
Dble. Sided Alum. Mylar (1/4 mil)	U	S	S
Aluminized Teflon (1 mil)	--	M	--
Aluminized Teflon (5 mil)	U	--	S
Dimpled Alum. Mylar (Dimplar)	M	M*	--
3M-850 Tape	S	U	--
Permacel-EE6600 Tape	S	U	--
Tech Floro (603-1) Tape	--	S	--
Velcro Hook and Pile	S	S	--

S - Satisfactory
M - Marginal
U - Unsatisfactory

*Large dimensional change

Section 2.1 Candidate Insulation-Material Evaluation

Subsection 2.1.1 Ethylene Oxide Decontamination Effects

A. ETO Effects on Single-Sheet Physical Properties

TEST PROCEDURES

The evaluation of the physical property effects of ETO decontamination environments was primarily concerned with single-sheet samples of candidate insulation materials. The samples were exposed to a series of ETO environments with differing moisture contents. Four different environments were investigated, namely:

a. ETO saturated (100 percent RH) with water
b. ETO in a dry (0 percent RH) atmosphere
c. ETO with a 45 percent RH atmosphere
d. Water vapor only

The exposures, with the exception of d., were performed in cycles, with each cycle requiring about 30 hours[1]. In all cases, the ETO mixture consisted of 12 percent ethylene oxide and 88 percent Freon 12. Figure 2-1 depicts the test program.

The basic test procedure for the combined ETO/moisture exposures for single sheets was as follows:

a. Insulation samples were placed in the preheated ($135^{\circ}F \pm 5^{\circ}F$) chamber.
b. The chamber was evacuated to 25 inches of mercury.
c. Approximately 50 ml of water was injected[2] (calibrated by the chamber manufacturer to provide 40 to 60 percent RH in an empty chamber) and allowed to equilibrate for 1 hour.
d. The ETO mixture was admitted to the chamber, raising the pressure to 6 ± 1 psig, providing a concentration of approximately 700 mg per liter of ethylene oxide.
e. Exposure time was 30 hours per cycle.
f. At the end of each cycle, the chamber was evacuated to 25 inches of mercury and then brought back to atmospheric pressure by admitting filtered air.
g. Some samples were withdrawn for physical property measurements.
h. After short hold times, the next cycle was initiated. The procedure was repeated until the required number of cycles had been completed. A copy of one of the recording charts is shown in Figure 2-2.

---

[1] A conservative approximation of the requirements of JPL Spec. VOL-50503-ETS, 12 January 1966

[2] This value was subsequently checked and found to produce a saturated environment.

Dry ETO exposures were conducted to determine whether the ETO mixture or water was the cause of degradation. These tests consisted of placing insulation samples in a large laboratory bottle and evacuating the air. The bottle was then pressurized with dry ETO to a pressure of 6 $\pm$ 1 psig and placed in an oven for each of six 30-hour cycles.

Aluminized and goldized plastic samples were subjected to exposures of water vapor only, at 122°F. The samples were placed over a beaker containing water and were visually observed after a period of approximately 15 hours. Subsequently, infrared transmission and emission spectrography techniques were employed to detect the presence of any visually transparent films.

The physical property measurements consisted of absorptivity, emissivity, weight change, dimensional change and outgassing. The outgassing tests were performed under vacuum for a period of approximately 20 hours at 200°F. A number of samples were elevated to 300°F. Mass spectrometer analysis was performed to establish the major outgassing products and vacuum weight loss was measured. Weight and dimensional measurements were made on the samples in air both before and after test exposures.

A complete set of control samples were prepared and measured for physical properties.

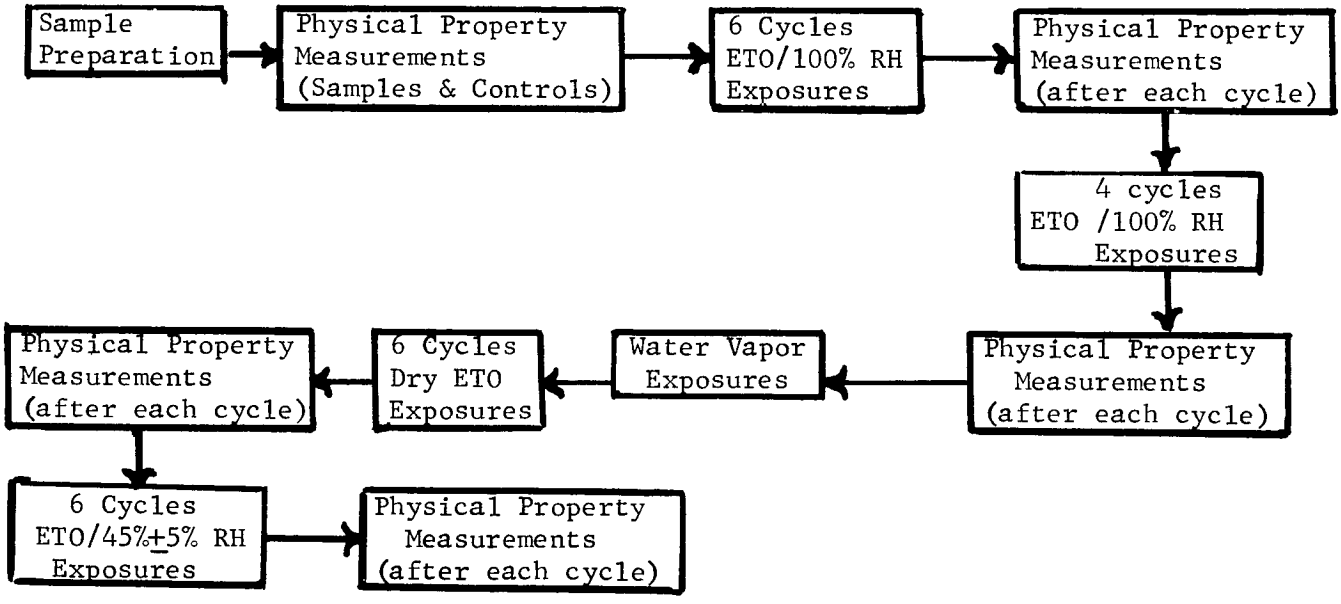

Figure 2-1. Evaluation of ETO Effects

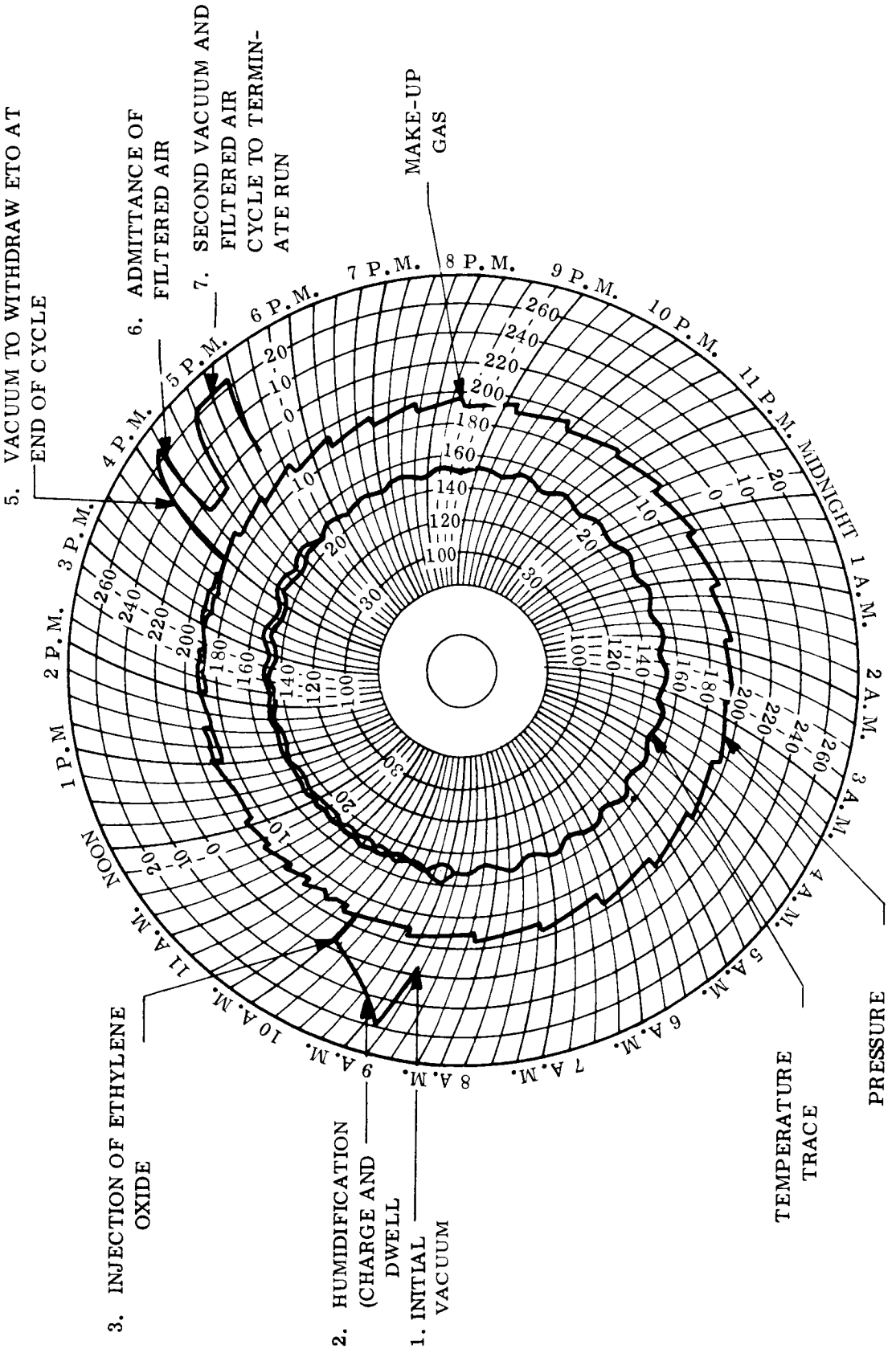

Figure 2-2. Typical ETO Exposure Cycle

Section 2.1 Candidate Insulation-Material Evaluation

Subsection 2.1.1 Ethylene Oxide Decontamination Effects

A. ETO Effects on Single-Sheet Physical Properties

TEST SAMPLES

A wide variety of metallized plastic film insulation materials were prepared for the evaluation of the deleterious effects of ETO decontamination. Table 2-2 lists the insulation materials investigated during the study. The table also indicates that not all of the materials were subjected to all of the test conditions; a weeding out process was employed to minimize the number of required tests. Some materials were eliminated early due to physical weakness or the impracticality of their use for a full scale insulation system. Other materials were added as test results indicated the need for a broader sample range.

Samples of the candidate materials were fabricated in the General Electric - MSD Materials Laboratory. All samples were handled with white gloves, cut with scissors and stored in polyethylene bags. It was found that the use of white Nylon gloves, even when used fresh each time, resulted in fingerprints that showed up in degraded spots after ETO exposure. Polyethelene or polyvinyl chloride gloves were found to be satisfactory.

Samples were prepared in different sizes dependent upon the specific tests for which they were to be used. Outgassing samples were 12 inches by 3 inches; dimensional and weight change samples were 5 inches by 5 inches; and the optical properties samples were 2 inch squares.

Table 2-2. Test Samples

Sample of Material	TYPE OF EXPOSURE				
	ETO +100% RH (6 cycles)	ETO +100% RH (4 cycles)	ETO +45% RH (6 cycles)	DRY ETO (6 cycles)	WATER VAPOR (15hr)
Alum. Mylar (NRC-2)*	X	X	X	X	X
Alum. Kapton (1/2 mil)	X	X	X	X	X
Gold on Kapton (1/2 & 1 mil)	X	X	X	X	
Gold on Mylar (1/4 & 1 mil)	X	X	X	X	X
Dimpled Alum Mylar (Dimplar)	X	X	X	X	X
Alum. Teflon (1 mil)	X	X	X	X	
SiO_2 on Alum. on Kapton	X	X		X	
Al_2O_3 on Alum. on Mylar	X	X		X	
Alum. backed w/Fiberglass	X		X	X	
Hanovia Gold on Kapton	X		X		
Alum. Mylar on Dimplar	X	X	X	X	
Kapton on Dimplar	X	X		X	
Double Sided Alum. Mylar*			X		X
Dacron Mesh	X	X	X	X	
Vanadium on Kapton	X	X	X	X	
Electrodeposited Nickel on Kapton			X	X	

*Folded samples of these materials were included as well as the sample sheets

Section 2.1 Candidate Insulation-Material Evaluation

Subsection 2.1.1 Ethylene Oxide Decontamination Effects

A. ETO Effects on Single-Sheet Physical Properties

TEST APPARATUS

ETO Exposures

The ETO decontamination chamber, used for these tests, was a 20-by-20 by 36 inch cryotherm sterilizer manufactured by the American Sterilizer Company. The test samples were protected from direct impingement of humidification water and ETO by plastic cover sheets. The test setup included six thermocouples in the chamber to measure temperature distribution, manual water injection via a circulator, a humidity indicator and heaters at the front and rear chamber doors to reduce temperature differentials. Gas chromatography was employed to accurately determine the amount of water in the chamber. The details of the development of this equipment are presented in Reference 1.

Dry ETO Exposures

The dry ETO exposures utilized a large laboratory bottle within an oven. Six sets of insulation samples were placed in the bottle. The bottle was fitted with vent and evacuation valving and a pressure gage.

Physical Property Measurements

Outgassing - A block diagram of the outgassing test facility is shown in Figure 2-3. The samples were placed within the black box heater, as shown in Figure 2-4, thereby maintaining temperature uniformity without the need for thermocouples on the samples. Figure 2-5 is a photograph of a portion of this facility. A Cahn RG Electrobalance was used to continuously measure vacuum weight loss and a GE Monopole Mass Spectrometer, viewing through an aperture in the black box, was employed for product analysis.

Optical Properties - A Beckman DK-2 Spectrophotometer equipped with a magnesium oxide coated integrating sphere was used for the measurement of the spectral reflectance of the metallized films in the wavelength region from 0.3 to 2.6 microns. Applying Kirchoff's law, the spectral absorptance of the opaque material is determined from:

$$\alpha_{s} = 1 - \rho_{s_{\lambda}}$$

where $\rho_{s\lambda}$ is the measured spectral reflectance. The total solar absorptance (α_s) is then determined by numerically integrating the expression:

$$\alpha_{s} = \frac{\int_{0}^{\infty} \alpha_{s_{\lambda}} \, s_{\lambda} \, d\lambda}{\int_{0}^{\infty} s_{\lambda} \, d\lambda}$$

where S_λ is the monochromatic solar irradiance at wavelength λ.

The spectral reflectance of the metallized films in the wavelength region from 2 to 24 microns was obtained utilizing a Perkin-Elmer 205 Spectrophotometer in conjunction with a Leeds and Northrup Hohlraum heated cavity. The total normal emittance (ϵ_n) is determined from infrared spectral reflectance measurements by numerically integrating the following definition:

$$\epsilon_n = \int_0^\infty (1 - \rho_\lambda) \frac{I_{b_\lambda}}{\sigma T^4} \, d\lambda$$

where ρ_λ is the absolute spectral reflectance
Ib_λ is the monochromatic "blackbody" intensity at wavelength λ
T is the absolute temperature of the sample
σ is the Stefan-Boltzmann constant

Mechanical Tests - Dimensional change measurements were made using a steel ruler; the accuracy approximated $\pm$ 1/16 of an inch due to the irregularities of crinkled and dimpled material. Weight measurements in air were made on a Mettlar Microanalytical Balance.

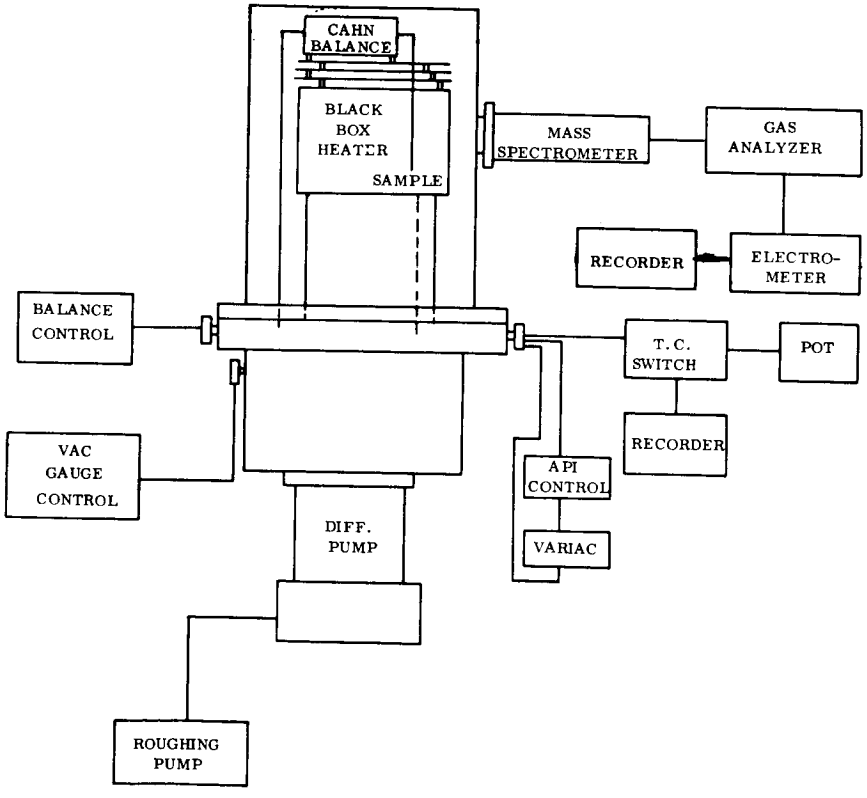

Figure 2-3. Outgassing Test Facility Schematic

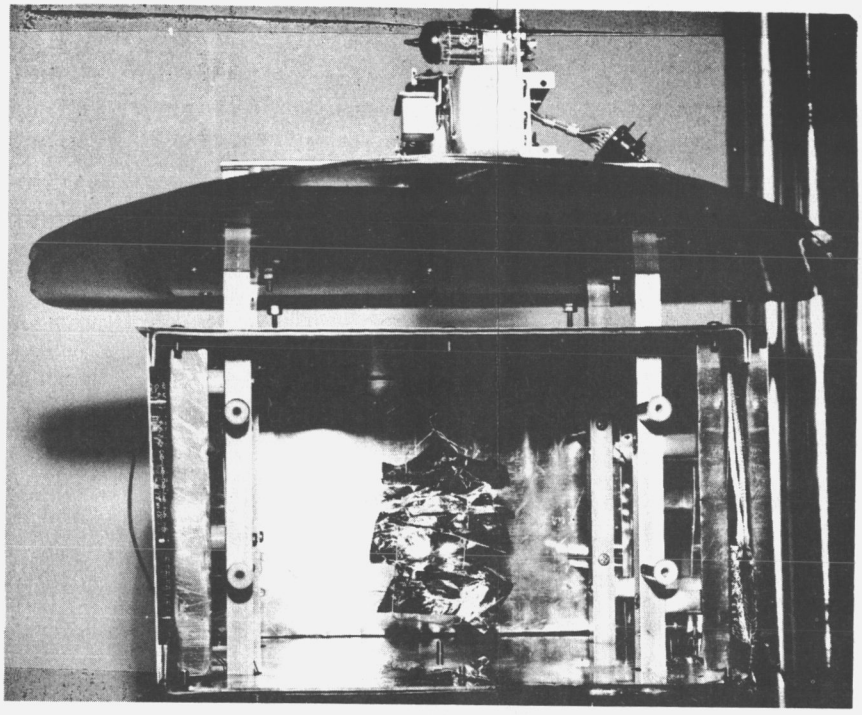

Figure 2-4. Sample Position in Black Box

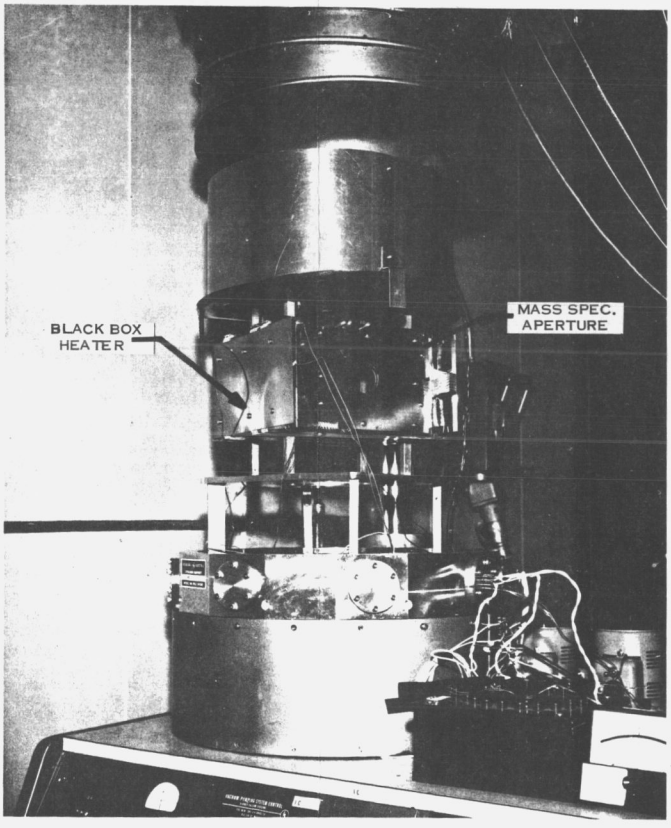

Figure 2-5. Outgassing Test Apparatus

Section 2.1 Candidate Insulation-Material Evaluation

Subsection 2.1.1 Ethylene Oxide Decontamination Effects

A. ETO Effects on Single-Sheet Physical Properties

TEST RESULTS - VISUAL OBSERVATIONS

ETO Plus 100 Percent Relative Humidity

Two series of ETO exposures were conducted in the presence of a water-saturated atmosphere. Post-test visual observations revealed that:

a. Aluminized Kapton had much of the aluminum removed.

b. NRC-2 (aluminized Mylar) was also almost devoid of aluminum. Figure 2-6 shows the extent of this damage.

c. Double-sided aluminized Mylar, dimpled aluminized Mylar and aluminized Teflon all displayed similar degradation.

d. All the aluminum was removed from the folded samples of aluminized Mylar as shown in Figure 2-7.

e. Gold on both Mylar and Kapton did not exhibit any degradation.

f. SiO_2 on aluminized Kapton and Al_2O_3 on aluminized Mylar did not degrade until the second cycle of exposure, but by the fourth cycle severe discoloration and aluminum removal were evident.

Dry ETO Exposures

No visible degradation of any of the samples occurred with exposure to dry ETO.

ETO Plus 45 Percent Relative Humidity

Exposures to ETO in the presence of a 45 percent relative humidity atmosphere produced no visibly detectable effects to the insulation sheet samples. However, extensive aluminum damage was noted to have occurred in the interior of the folded samples.

Water Vapor Exposures

Figure 2-8 depicts the extensive removal of aluminum from the plastic films when exposed to a water vapor atmosphere. The figure shows circular areas devoid of aluminum representing the shape of the test beaker rim. The presence of a visually transparent Al_2O_3 film could not be detected. Gold on Mylar exhibited no adverse effects to the same exposure.

FOLDOUT FRAME 1

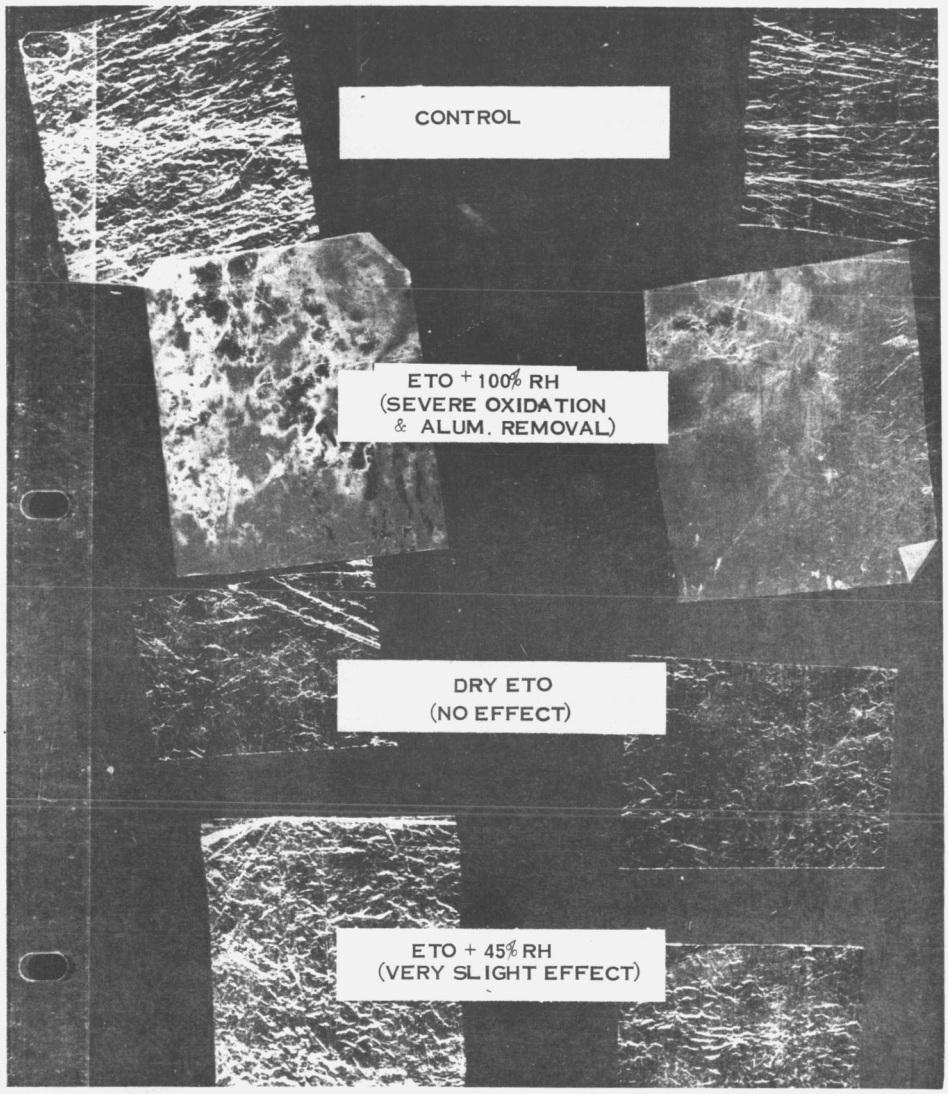

Figure 2-6. NRC-2 - ETO Results

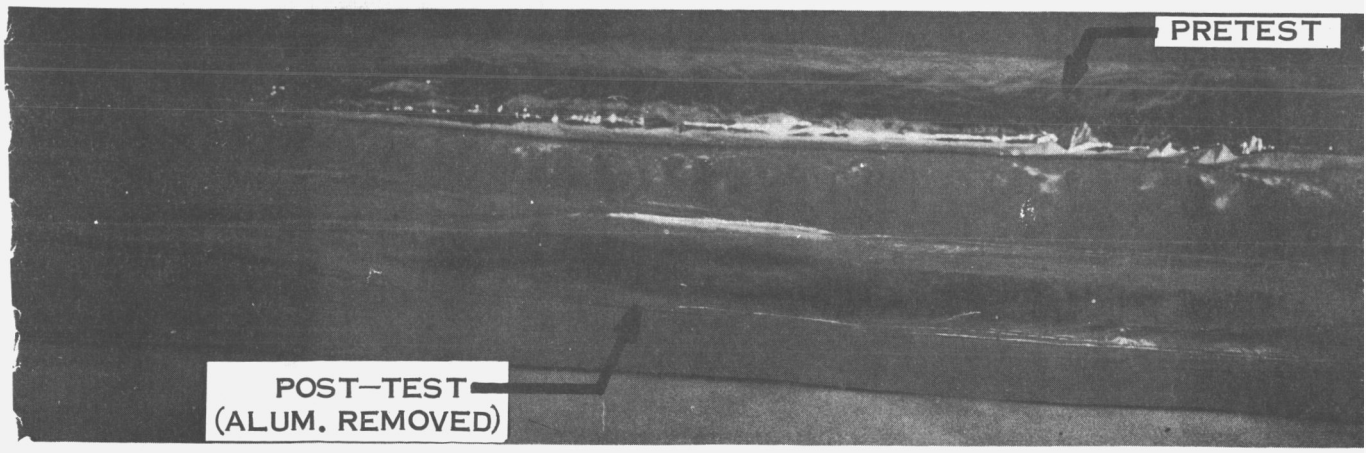

Figure 2-7. Folded Sample, Double-Sided Aluminized Mylar Before and After ETO Exposure

FOLDOUT FRAME 2

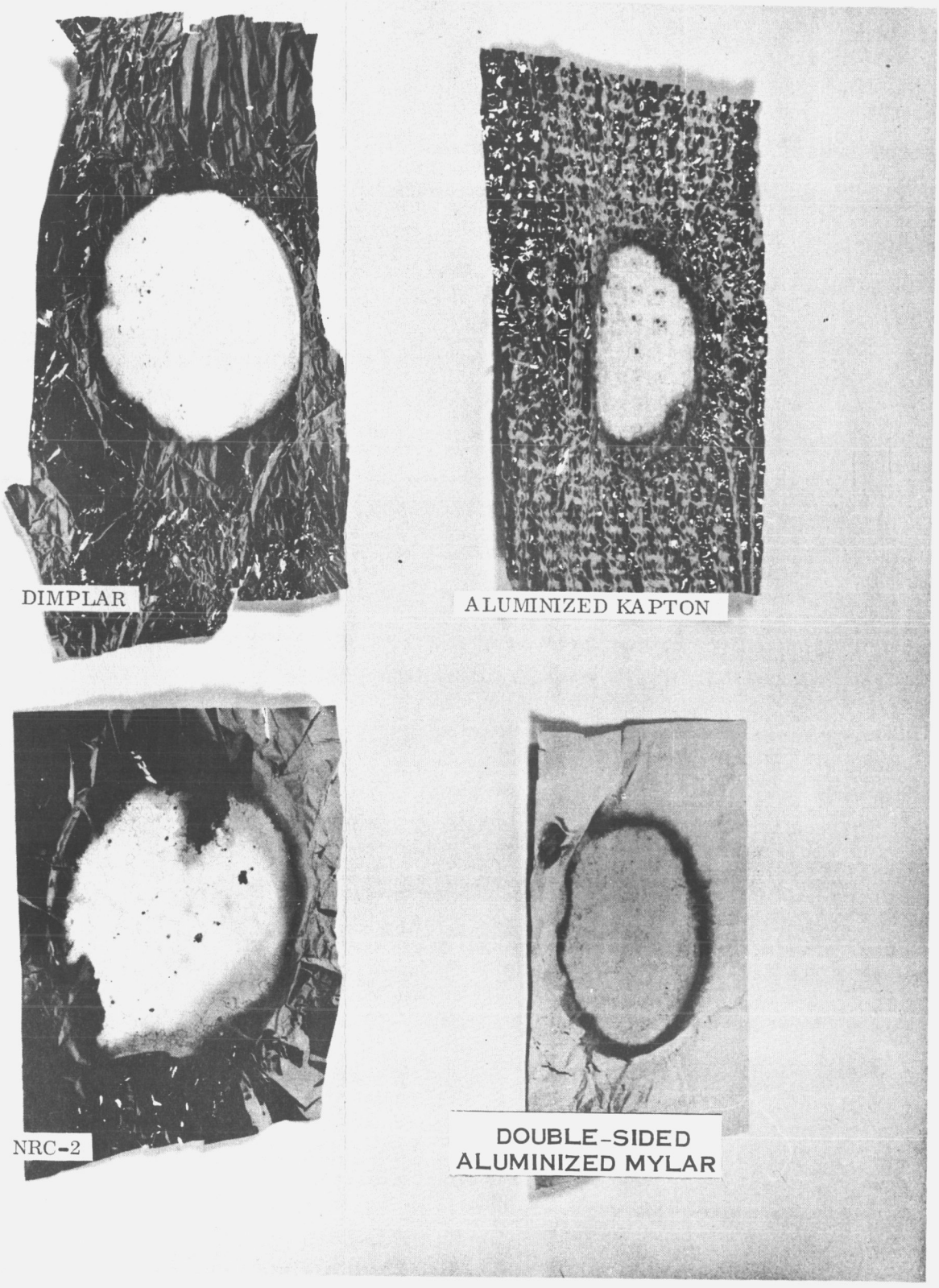

+ 100% RH

Figure 2-8. Water Vapor Exposure Results

Section 2.1 Candidate Insulation-Material Evaluation

Subsection 2.1.1 Ethylene Oxide Decontamination Effects

A. ETO Effects on Single-Sheet Physical Properties

TEST RESULTS - PHYSICAL PROPERTY MEASUREMENTS

Table 2-3 summarizes the results of the weight and dimensional change investigations. Reference 1 presents the test data in detail. Dimensionally, aluminized Mylar was the most stable, and Dimplar showed the greatest change due to expansion.

Weight measurement in air, after exposure to humid ETO environments, indicated a consistent increase in weight. As shown in Table 2-3, this increase in weight is manifested by an increase in weight loss in vacuum. Mass spectrometer analysis of the vacuum outgassing products indicates the major product to be water; thereby both the increased weight in air after the exposure to humid ETO and the resultant vacuum weight loss. Figure 2-9 depicts the vacuum weight loss analysis for NRC-2 samples (control and after ETO exposure). Elevating the temperature, to 300°F, further increases the weight loss in vacuum.

Table 2-4 presents the data from optical property measurements both before (control) and after ETO exposures. Measurements were not performed where the aluminum was removed. The table shows that the ETO exposures produce only slight changes to the insulation material optical properties.

Table 2-3. ETO Effects on Weight and Dimensions

Material	Wt Chge in Air (After ETO) (%)	Weight Chge in Vacuum				Dimensions* (After ETO) (inches)
		Control		ETO		
		Time (hr)	200°F %Loss	Time (hr)	200°F %Loss	
Alum. Kapton (½ mil)	+1.30	21	0.47	43	1.00	5 X 5
NRC-2 (Preshrunk)	+0.55	25	0.57	22	0.88	4 15/16X4 15/16
Dimplar	+0.62	19	0.31			5 ½ X 5 1/16
Dble Sided Alum Mylar	+0.46	18	0.81	22	0.99	4 7/8 X 5
Alum Teflon (1 mil)	+0.20	19	0.21	19	0.17	4 7/8 X 5
Dacron Mesh	+0.26	79	0.21	43	0.57	4 7/8 X 4 3/4

* Dimension prior to ETO exposures = 5 X 5 inches
Accuracy = ± 1/16 inch

FOLDOUT FRAME 1

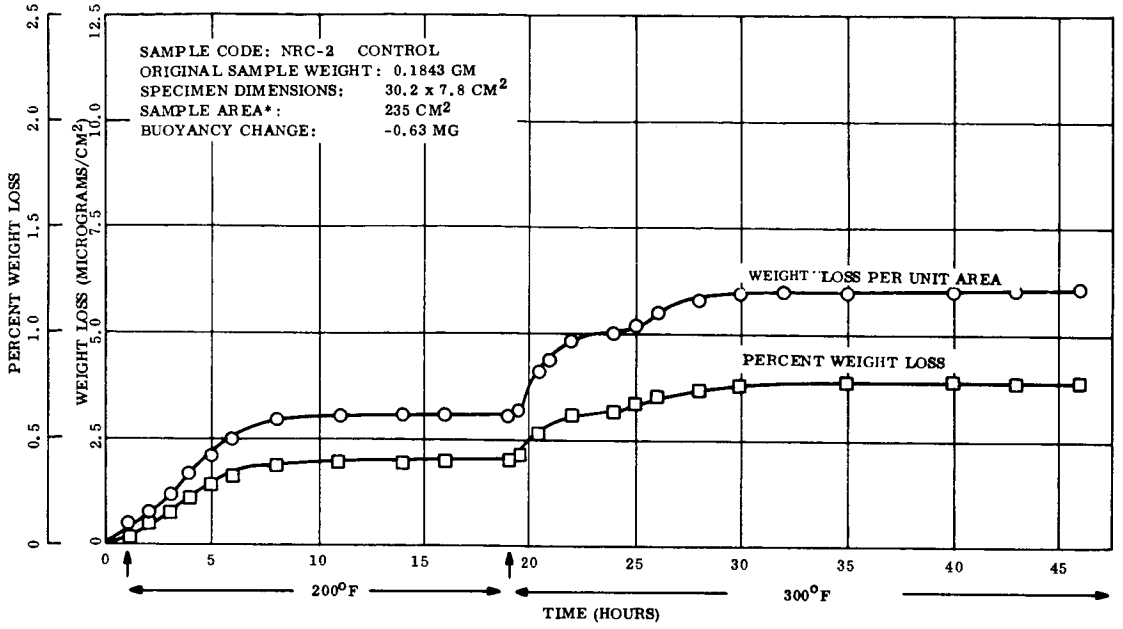

Control Sample

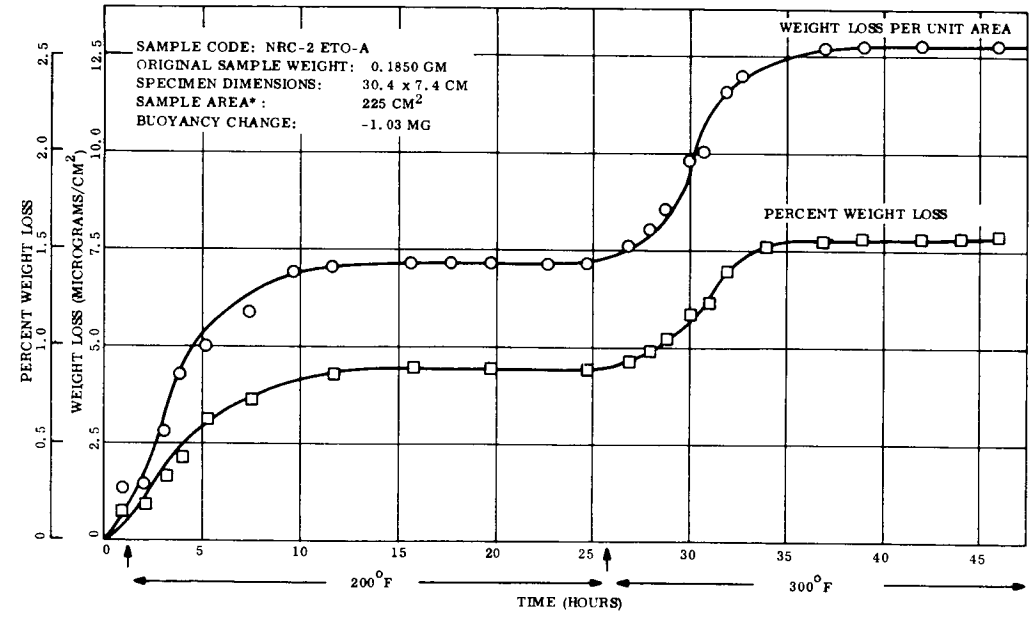

After ETO Exposure

* AREAS USED FOR COMPUTATION ARE FOR ONE SIDE ONLY ON FILM AND MESH SPECIMENS.

Figure 2-9. NRC-2 Vacuum Weight Loss Analysis

FOLDOUT FRAME 2

Table 2-4. Effect of ETO on Optical Properties

Material	Control		Wet ETO 4 Cycles		Wet ETO 6 Cycles		Dry ETO 6 Cycles		ETO 45% RH 6 Cycles	
	(α_S)	(ϵ_N)	(α_S)	(ϵ_N)	(α_S)	(ϵ_N)	(α_S)	(ϵ_N)	(α_S)	(ϵ_N)
Gold on Mylar (1 mil)		0.040				0.061				
Mylar on gold (1 mil)		0.610				0.606				
Gold on Mylar (1/4 mil)		0.051		0.049	0.256	ok*		0.045		0.042
Mylar on gold (1/4 mil)	0.361	0.446	0.381	0.472	0.276	ok		ok		ok
Gold on Kapton (1 mil)		0.041		0.047		ok		0.032		ok
Kapton on gold (1 mil)	0.275	0.645	0.344	0.644		ok		ok		ok
Gold on Kapton (1/2 mil)		0.030		0.030		ok		ok		ok
Kapton on gold (1/2 mil)		0.655		0.656		ok		ok		ok
Aluminum disc		0.037				0.068		ok		ok
Embossed Aluminum Mylar - Aluminum up		0.054				0.229		0.049		
Aluminum on TFE (1 mil)		0.045	Aluminum Removed		Aluminum Removed			0.058		0.062
TFE on Aluminum (1 mil)	0.153	0.594	Aluminum Removed		Aluminum Removed		0.194	0.624	0.194	0.624
Dimplar Aluminum		0.160	Aluminum Removed		Aluminum Removed			0.144		0.276
NRC-2 (preshrunk) Aluminum up		0.040	Aluminum Removed		Aluminum Removed			0.037		0.048
NRC-2 - Aluminum up		0.39	Aluminum Removed		0.685	0.204		0.045		
NRC-2 - Aluminum down	0.194	0.339	Aluminum Removed					ok		ok
Aluminum on Kapton (1/2 mil)		0.049	Aluminum Removed		0.314	0.150		0.073		0.051
Kapton on Aluminum (1/2 mil)	0.328	0.478	Aluminum Removed		Aluminum Removed			ok	0.353	0.550
SiO_2 on Aluminum on Kapton			Aluminum Removed		Aluminum Removed			ok		
Al_2O_3, on Aluminum on Mylar			Aluminum Removed		Aluminum Removed			ok		
Aluminum backed with Fiberglass		0.030				0.030		ok		ok
Hanovia Gold on Kapton (JPL)		0.106				0.080		ok		ok
Vanadium on Kapton			Metal removed			0.098		ok		ok
Hanovia gold on Kapton (AGC)								ok		ok
Narnco electrodeposited nickel on Kapton		0.121						ok		ok
Lash Electrodeposited nickel on Kapton		0.035						ok		ok
Aluminum on Mylar on aluminized Dimplar		0.038	Aluminum Removed		Aluminum Removed			0.037		ok
Kapton on aluminum embossed	0.345	0.054	Aluminum Removed		Aluminum Removed					
Aluminum Mylar double side		0.040								0.054

* OK = SATISFACTORY VISUAL INSPECTION

Section 2.1 Candidate Insulation-Material Evaluation

Subsection 2.1.1 Ethylene Oxide Decontamination Effects

B. ETO Effects on Thermal Insulation Blankets

TEST PROCEDURES

Several candidate thermal insulation materials were fabricated into multilayer blankets and subjected to ETO/moisture environments to determine the visually observable effects of such exposures. Thermal insulation blankets were exposed to three different environments.

Blanket Test No. 1

The first series of tests consisted of 6 cycles of sample exposure to ETO in a humid environment. Figure 2-10 depicts the test procedure. The relative humidity in the test chamber was varied for each of the six cycles, ranging from 35 to 73% RH. Both horizontal and vertical blanket samples were employed in these tests. Each of the samples were removed and partially disassembled after each cycle.

Blanket Test No. 2

In order to isolate the effects of the ETO/Freon mixture from those associated with the presence of moisture, the ETO mixture was replaced with nitrogen for this second series of blanket tests. The test procedure was similar to that described for Blanket Test No. 1. At approximately halfway through the third cycle, the relative humidity was increased from 50 to 76 percent (average attained level was 60 percent). This was done to determine if the higher humidity would accelerate the degradation of the aluminized materials. These tests included perforated NRC-2 blankets to determine if the vent holes would reduce degradation.

Blanket Test No. 3

One explanation for the degradation of aluminized film during ETO decontamination may be the condensation of relatively stagnant water vapor in the blankets. This could occur when the ETO/Freon mixture is injected (see Figure 2-10) after vacuum and water vapor equilibration (about one hour). In an effort to minimize this occurrence, the ETO/Freon mixture in Blanket Test No. 3 was injected and allowed to equilibrate; then water vapor (in the form of steam) was injected. This is the inverse water injection procedure from that generally employed.

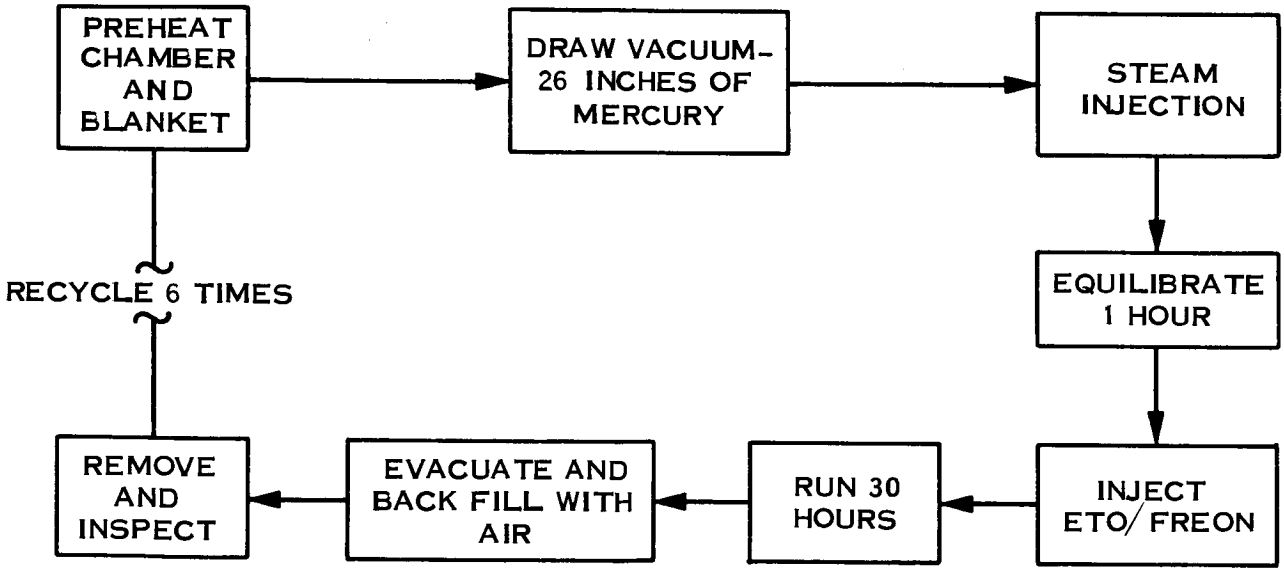

Figure 2-10. Typical ETO Exposure Cycle

Section 2.1 Candidate Insulation-Material Evaluation

Subsection 2.1.1 Ethylene Oxide Decontamination Effects

B. ETO Effect on Thermal Insulation Blankets

TEST SAMPLES

The thermal insulation blanket samples utilized in the evaluation of ETO effects are described in Tables 2-5 and 2-6.

Table 2-5. Test Samples for Blanket Tests Nos. 1 and 2

BLANKET MATERIAL	CONSTRUCTION
NRC-2 Aluminized Mylar (¼ mil) (Horizontal)	35 layers, 18 x 30 inches, TC* on 17th layer
NRC-2 Aluminized Mylar (¼ mil) (Vertical)	35 layers, 18 x 30 inches, TC on 17th layer
Aluminized Kapton (½ mil) and NRC-2	15 layers Kapton/20 layers NRC-2, 18 x 30 inches, TC on 17th layer
Dimpled Alum. Mylar, Aluminized on both sides (Dimplar)	8 pair layers, 18 x 30 inches, TC on 4th layer
Gold on Mylar (¼ mil)	35 layers, 15 x30 inches, TC on 17th layer
Embossed Alum. Mylar (½ mil)	35 layers, 18 x 30 inches, TC on 17th layer

*Thermocouples placed in the center of blanket.

During Blanket Test No. 2 the following nonblanket (sheet) samples were also evaluated:

a. Kapton
b. NRC-2
c. Gold on Mylar
d. Double Sided Aluminized Mylar
e. Mylar

Insulation blanket samples used in Blanket Test No. 1 and 2 were assembled by stitching through the layers. Some of the blankets exposed in the third test series were assembled with Nylon retainer posts.

Table 2-6. Test Samples for Blanket Test No. 3

BLANKET MATERIAL	CONFIGURATION *
Gold on Mylar ** (¼ mil)	34 layers, 18 inch diameter, blanket held at edge by four Nylon posts and pinched in center with a Nylon post and washer.
Aluminized Kapton (½ mil)	34 layers, 18 x 30 inches
Dimpled Aluminized Mylar (Dimplar) (Double Sided)	8 pair layers, 18 x 30 inches
Double Sided Aluminized Mylar (¼ mil)	34 layers, 18 x 30 inches
NRC-2 (perforated)	34 layers, 18 x 30 inches held together by 4 Nylon posts. (Perforations were ¼ inch diameter holes on 2 inch centers.)
NRC-2	34 layers, 18 x 30 inches, held together by 4 Nylon posts.
NRC-2	34 layers, 18 x 30 inches, held together by 4 Nylon posts on the corners and pinched together at the center with two Nylon posts and washers.

* All samples, with the exception of aluminized Kapton, were mounted vertically.
** The gold on Mylar blanket had undergone six previous ETO decontamination cycles.

Section 2.1 Candidate Insulation-Material Evaluation

Subsection 2.1.1 Ethylene Oxide Decontamination Effects

B. ETO Effects on Thermal Insulation Blankets

TEST APPARATUS

The ETO decontamination chamber, employed for all three blanket tests, was a 20 x 20 x 36 inch cryotherm sterilizer manufactured by the American Sterilizer Company. The unit was modified to provide automatic humidity control; the control being calibrated via gas chromatography. A baffle and fan were installed to provide uniform temperature distribution and circulation of the decontamination gases. Figure 2-11 is a schematic of the modified test equipment.

Steam, for humidity control, was taken from an autoclave using distilled water, since the plant steam contains a "depositing amine" lubricant (octadecylamine). This could perturbate the optical properties of the test materials. The steam was supplied to the chamber through a heated 3/8 inch OD copper tubing line fitted with a return line and trap. This arrangement minimized the amount of condensation injected into the chamber. Figure 2-12 is a photograph of the chamber and autoclave.

Heat was supplied to the chamber via a steam-heat jacket. Heating ribbons were attached to both doors (front and back) to provide a uniform temperature distribution. The temperature was monitored by eight copper-constantan thermocouples spaced around the chamber. Additional thermocouples were placed in the center of the sample blankets.

The chamber ETO concentration was indirectly controlled via the chamber pressure. The chamber pressure was controlled by a regulator set at 6 $\pm$ 1 psig. At low pressure, a solenoid on the ETO/Freon 12 storage bottle line opened. The gas passed through a heat exchanger and into the chamber until the chamber pressure reached 7 psig.

A metal shelf was hung 2 inches below the chamber top. Steel clips were attached to the shelf for holding the vertical blankets; the blankets being folded approximately 3 inches from one 30 inch edge, and the clips being attached to the outside of this fold. The horizontal blankets were placed on the shelf.

During Blanket Test No. 3, the steam heating of the chamber was replaced by a water reservoir temperature bath and pump. This produced better temperature control and distribution.

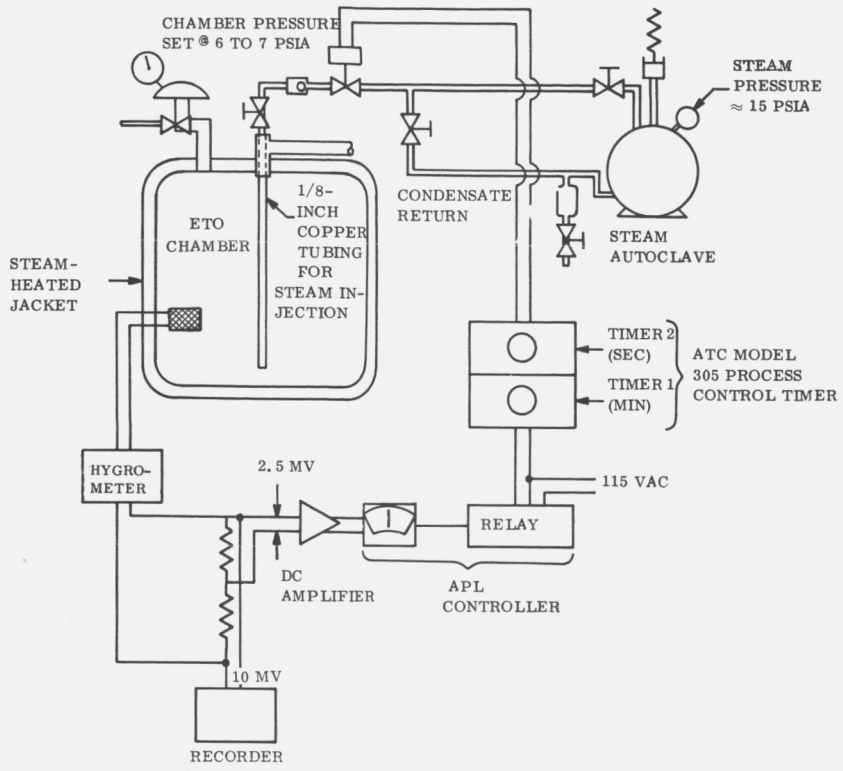

Figure 2-11. ETO Exposure Apparatus

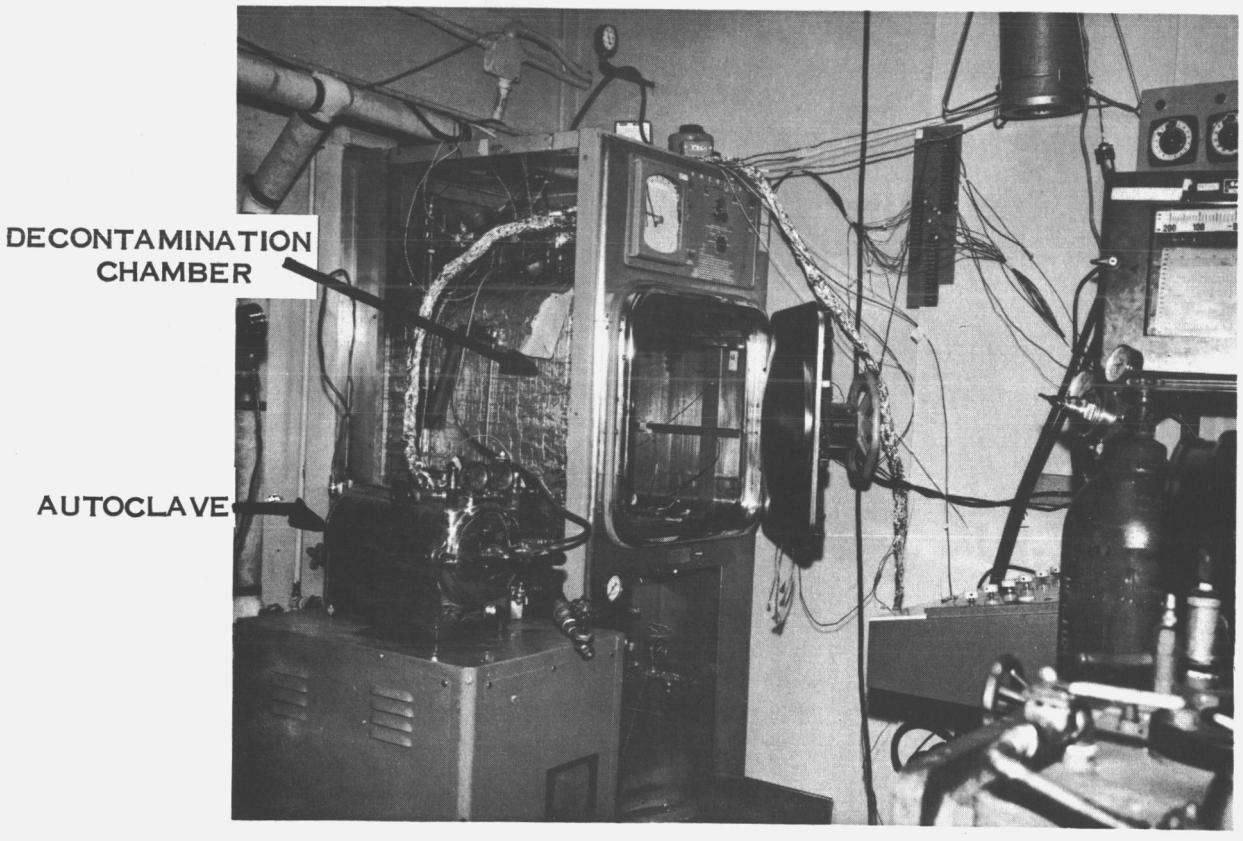

Figure 2-12. ETO Facility

Section 2.1 Candidate Insulation-Material Evaluation

Subsection 2.1.1 Ethylene Oxide Decontamination Effects

B. ETO Effects on Thermal Insulation Blankets

TEST RESULTS

Blanket Test No. 1

Table 2-7 summarizes the results of the first series of ETO exposures. After two cycles of ETO exposure, the blankets were removed from the chamber. The 35 layers of NRC-2 (horizontal) appeared in good condition on the surface and edges. However, after removing the stitches and folding back the first layer, an adhesion was noted between the first and second layers. The adhesion was so severe that it tore the NRC-2 in spots. This same adhesion was noted for the remaining layers. After the third layer, slight haziness and discoloration of the aluminum was noted. This discoloration became progressively worse towards the center of the blanket. The vertical NRC-2 blanket exhibited the same adhesion and discoloration between layers.

The eight layer pairs of Dimplar, vertically mounted, showed no degradation. No degradation occurred on the gold-on-Mylar blanket. The composite sample did not show any signs of degradation or stickness for the 15 layers of aluminized Kapton. When the NRC-2 layers were reached, discoloration and adhesion were present. NRC-2 blankets were not exposed during the third cycle.

The samples were removed again after the third cycle. Dimplar, aluminized Kapton, and gold on 1/4 mil Mylar did not show any signs of degradation. A new NRC-2 blanket and a 35 layer embossed aluminized unstitched Mylar blanket were placed in the chamber for the fourth cycle. After the fourth cycle, the blankets were again inspected. The Dimplar, aluminized Kapton, gold on 1/4 mil Mylar and embossed aluminized Mylar blankets did not exhibit any degradation. The NRC-2, however, was discolored and hazy in the region where it was supported in the chamber. It should be noted that the samples in the chamber were less compact than in the earlier cycles because of the removal of the stitches for inspection. Adhesion of the layers of aluminized material was a recurring factor in the presence of water vapors. The samples were inspected after the fifth and sixth cycles with the same general results.

Blanket Test No. 2

In this series of exposures, the ETO atmosphere was replaced by a nitrogen atmosphere. The relative humidity was 50 percent for the first two cycles and was increased to 76 percent halfway through the third cycle. Table 2-8 presents the test observations.

No material degradation was observed after the first two cycles at 50 percent RH. However, after the third cycle, the NRC-2 blankets showed discoloration and aluminum removal. The NRC-2 blanket with perforations showed only slight discoloration. On successive cycles the NRC-2 blankets continued to degrade.

Gold-on-Mylar, aluminized Kapton and the embossed aluminized Mylar showed no signs of degradation. Figure 2-13 compares perforated and unperforated NRC-2 blankets after six cycles. Note the large darkened area in the unperforated blanket. No degradation was evident on the perforated blanket.

As indicated in Table 2-8, the sheet samples, including NRC-2, did not degrade. This is significant in that the degradation in multilayer blankets is more prevalent than in single sheets

Blanket Test No. 3

The third series of exposures, including the use of retainer posts for blanket assembly and inverse water injection procedures, further demonstrated that aluminum is a marginal material in a humid ETO environment. Most degradation occurred in the areas of handling, at posts and near folds, indicating the effects of moisture from fingerprints. The blanket observations are summarized in Table 2-9.

Table 2-7. Blanket Test No. 1 Summary

Blanket	Cycle 1	Cycle 2	Cycle 3	Cycle 4	Cycle 5	Cycle 6
NRC-2 horizontal	No inspection	Degraded and removed				
NRC-2 vertical	No inspection	Degraded and removed				
Kapton/ NRC-2 (composite)	No inspection	Kapton OK/ NRC-2 degraded	Kapton OK/ NRC-2 more degraded	Kapton OK/ NRC-2 degraded	Kapton OK/ NRC-2 same	Kapton - degradation on layer adjacent to NRC-2 NRC-2 - same
DIMPLAR	No inspection	OK	OK	OK	OK	OK
Gold on Mylar	No inspection	OK	OK	OK	OK	OK
Replacement NRC-2					Degradation in fold	Further degradation in fold
Emb. Alum. Mylar (Unstitched)				OK	OK	OK
Cycle remarks	T = 118°F P = 60 psi RH - 73% Condensed water in chamber	T = 118°F for 12.5 hr, T = 140 for 17.5 hr P = 60 psi RH = 73% for 12.5 hr = 40% for 17.5 hr	T = 116 to 120°F P = 6.0 psi RH = 71%	T = 130 to 140°F P = 610 psi RH = 62%	T = 140 to 147 P = 6.0 psi RH = 35%	T = 130 to 140 P = 6.0 psi RH = 46%

*Blank space indicates no sample present in chamber.

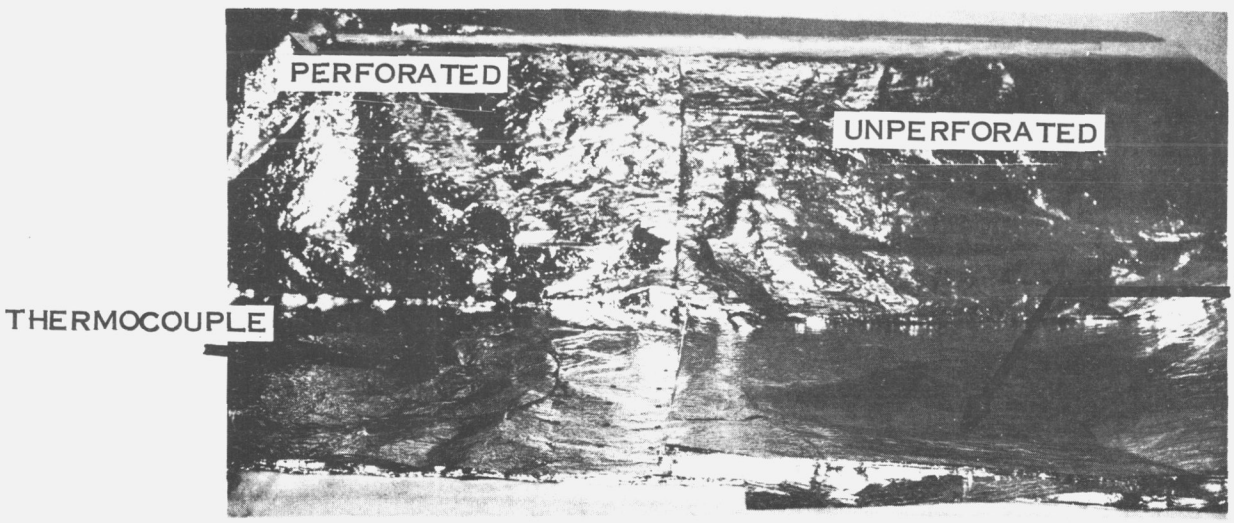

Figure 2-13. NRC-2 Perforated and Unperforated Blanket After Blanket Test No. 2

FOLDOUT FRAME 2

Table 2-8. Blanket Test No. 2 Summary (Simulated Decontamination with Nz/Moisture)

Material	Cycle 1	Cycle 2	Cycle 3	Cycle 4	Cycle 5	Cycle 6
NRC-2 (Horizontal)	G	G	discoloration	discoloration	discoloration	discoloration
NRC-2 (Vertical)	G	G	G	P	P	P
NRC-2 (vertical perforated)	G	G	G	G	G	G
Dimplar	G	G	G	G	G	G
Hastings	G	G	-	G	G	G
Non-blanket material	G	G	G	G	G	G
Kapton	G	G	G	G	G	G
NRC-2	G	G	G	G	G	G
Gold on Mylar	G	G	G	G	G	G
Mylar	G	G	G	G	G	G
Temp. °F	143	140	144	135	143	125
Pressure (Psig)	7±1	7±1	7±1	7±1	7±1	7±1
% RH	50	50	* 50 for 18 hours 60 for 18 hours	>75.5	>75	>75

* The relative humidity was increased to duplicate the moisture content of Blanket Test No. 1; 60% is average value for Cycle 3.

G = No degradation (or very slight)
P = Degradation

Table 2-9. Blanket Test No. 3 Summary

Blanket Material	Cycles						Remarks
	1	2	3	4	5	6	
Gold-on-1/4-mil Mylar	G	G	G	G	G	G	
1/2-mil aluminized Kapton	G	G	G	G	G	G	A few fingerprints
Dimplar	G	G	G	G	G	G	A few fingerprints on outer sheets around post
1/4-mil DS aluminized Mylar	G	G	F	F	F	F	Discoloration
NRC-2 perforated	G	G	F	F	F	F	Discoloration around fold and post
NRC-2	G	G	G	F	F	F	Discoloration
NRC-2 tightly packed	G	G	G	F	F	F	Discoloration around posts, fingerprints, and a few transparent spots

G - No degradation
F - Small degradation

Section 2.1 Candidate Insulation-Material Evaluation

Subsection 2.1.2 Heat Sterilization Effects

A. Effects of Sterilization Atmosphere Oxygen Concentration

TEST PROCEDURES AND APPARATUS

Aluminized Mylar and gold-on-Mylar insulation samples were exposed to nitrogen atmospheres with varying oxygen concentrations. The evaluation of the effects of oxidation consisted of environmental exposures and optical and electrical resistance measurements. The oxidation test apparatus is shown in Figure 2-14. Each of the three test bottles was operated to provide a different concentration of oxygen in the nitrogen atmosphere. Three concentrations were evaluated; specifically 0.31, 0.66, and 2.69 percent oxygen by volume. The bottles, containing the insulation samples, were placed into a Trent oven and six sterilization cycles[1] (at $135^{\circ}C \pm 2^{\circ}C$ for 96 hours per cycle) were run. Following the test, the samples were removed for investigation.

The nitrogen gas supply was obtained from standard, 200 cu. ft, 2000 psig bottles. The nitrogen gas oxygen concentration was analyzed in triplicate: by the vendor, by GE in the as received state, and as effluent from the oxidation test bottles. Table 2-10 shows the results of these analyses. As is most apparent in the low concentration specimens, small leaks in the gas flow stream allowed additional oxygen to enter the gas. Consequently, the effluent oxygen percentages were assumed to be most valid.

In reference to Figure 2-14, the lines upstream of the test bottles were leak tight and under 2 psig pressure at the regulator. The nitrogen gas inlet was at the base of the bottles and the entering gas was evenly dispersed by fritted glass. The system was purged with test gas for 30 minutes prior to heatup and for at least 20 minutes during temperature buildup, thereby accomplishing approximately eight complete test bottle volume changes.

The normal emittance (ϵ_N) of the test samples was determined via spectral reflectance measurements, with a Perkin-Elmer 205 Spectrophotometer, as previously described in Subsection 2.1.1. The ϵ_N accuracy is $\pm$ 0.02.

The test setup for measuring electrical resistance is shown schematically in Figure 2-15. The fixture was constructed of a fiber base with brass rods used as connectors. With the sample clamped firmly at the ends, the voltage of the source was adjusted to provide the test current, the voltage probe was placed gently on the sample and measurements taken. The measure of electrical resistance determines the relative thickness of the aluminum coating from:

$$R = \rho \frac{\ell}{A} = \rho \frac{\ell}{wt}$$

Where: R = resistance
ℓ = length of sample
w = width of sample
A = cross-sectional area
ρ = resistivity coefficient dependent upon material and temperature

[1] JPL Spec. VOL-50503-ETS, 12 January 1966.

Table 2-10. Nitrogen Gas/Oxygen Concentration Analysis

Gas Bottle	Vendor Certified Analysis	General Electric Analyses (As Received)	General Electric Analysis (Effluent)
1	0.0275	0.046 0.061	0.31
2	0.26	0.268	0.66
3	2.44	2.51	2.68

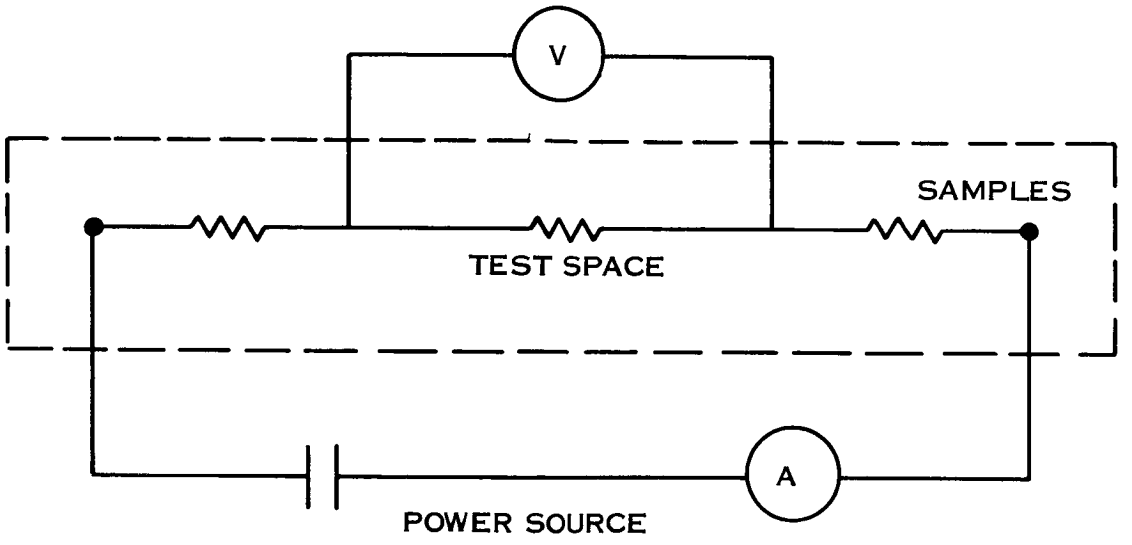

Figure 2-15. Electrical Resistance Apparatus Schematic

$$\text{or } t = \frac{\rho}{R \text{ per square}}$$

In using this method for determining relative thickness, it was assumed that the temperature and purity of aluminum are constant. Calculations indicated that temperature rise from current in the 100 microampere to 1 milliampere range will be from 0 to 1.5°F, which, using the temperature coefficient of pure aluminum, would cause a maximum error of 0.33 percent. Furthermore, this voltammeter method circumvents any error introduced from the test fixture electrically mating with the aluminum, since a differential voltmeter (which will draw zero current from the test setup) is used within a series circuit. By using low currents, the error due to temperature rise is minimized to the point that it is insignificant.

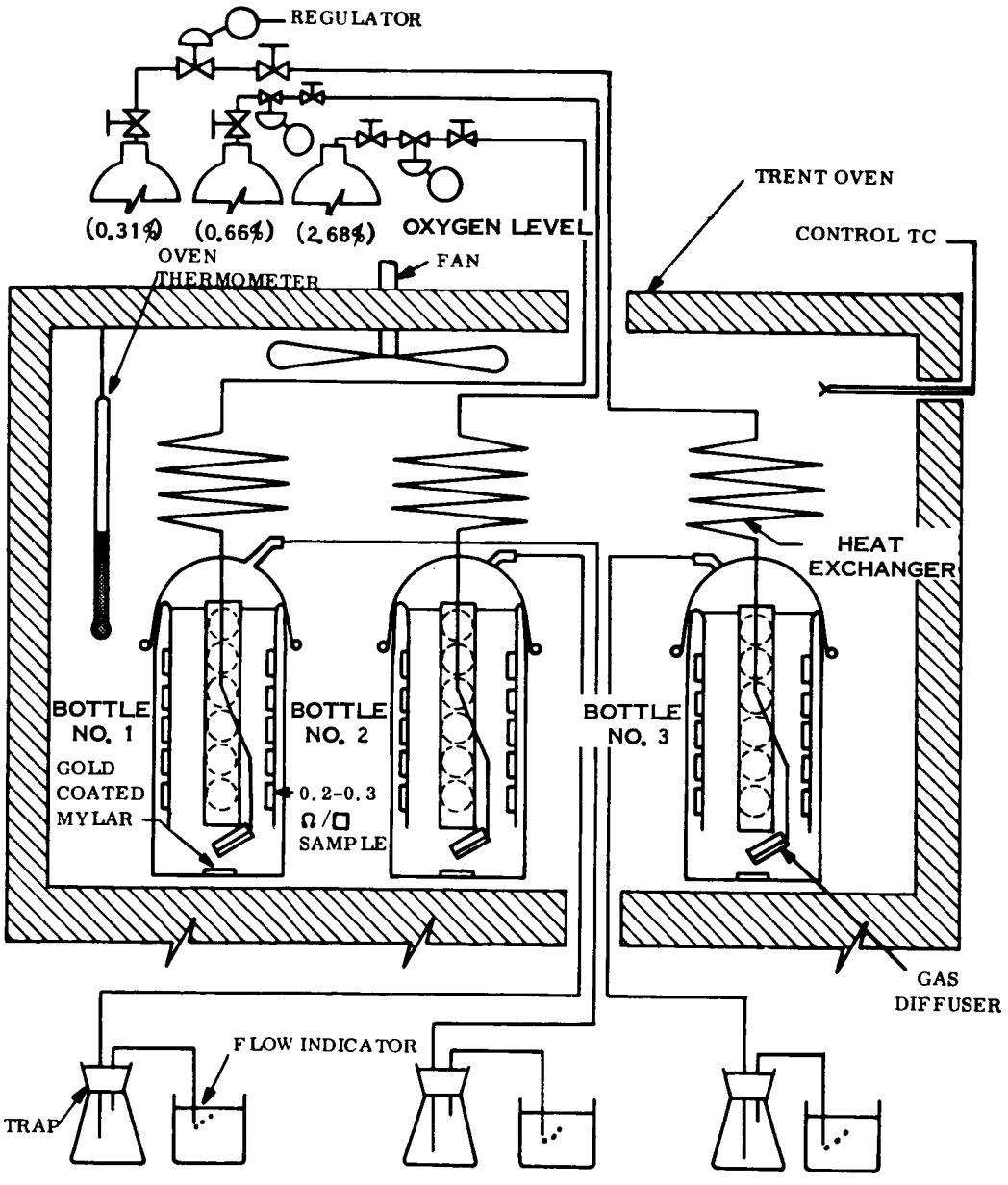

Figure 2-14. Oxidation Test Apparatus

Section 2.1 Candidate Insulation-Material Evaluation

Subsection 2.1.2 Heat Sterilization Effects

A. Effects of Sterilization Atmosphere Oxygen Concentration

TEST SAMPLES

The test samples, for the oxidation effects investigation, consisted of aluminized Mylar, Hanovia gold and gold on Mylar. Three batches of aluminized Mylar (NRC-2) were obtained, each batch having a different film resistance indicative of the thickness of the aluminum coating. The resistance ranges for each batch were:

Batch 1 - 0.2 to 0.3 ohms per sq dimension (Ω/sq.); thickness = 0.0042 mil

Batch 2 - 0.7 to 0.9 Ω/sq ; thickness = 0.0013 mil

Batch 3 - 2.5 to 3.0 Ω/sq ; thickness = 0.00042 mil

Samples from each batch were placed in each of the oxidation test bottles.

Three sheets, approximately 1 inch wide by 9 inches long, were cut from each film. It was found that an electrical measurement of film resistance was necessary to establish the aluminized side of the film. Six aluminum disks, 1 inch in diameter by 20 mils thick, were bonded to the Mylar side of the film using SR 585 (General Electric silicone-based pressure sensitive) adhesive. The 0.2 to 0.3 Ω/sq film was then trimmed around the aluminum disk. These disks were bonded to aluminum foil by using SR 585 on the side opposite the film. The purpose of this step was to provide a support for the disks in the test chamber in such a manner as to require a minimum of sample manipulation during the removal operation. For the 0.7 to 0.9 and 2.5 to 3.0 Ω/sq films, this method was replaced by the simpler procedure of supporting the samples by the uncut test film where enough sample material was available.

Strips 1 inch wide by 5 inches long by gauge thickness were cut from each film for electrical resistance measurements. A sample of dimpled aluminized Mylar (Dimplar) was also evaluated for electrical resistance effects. Disk samples of Hanovia gold and gold on Mylar were also exposed to the oxidation test environments.

Section 2.1 Candidate Insulation-Material Evaluation

Subsection 2.1.2 Heat Sterilization Effects

A. Effects of Sterilization Atmosphere Oxygen Concentration

TEST RESULTS

Optical Properties

Table 2-11 summarizes the results of variable oxygen-concentration exposures on the aluminiz Mylar optical properties. The table presents averaged emissivity measurements from all of the six cycles: detailed data is presented in Reference 1. No significant change occurred in the normal emittance of aluminized Mylar when exposed to nitrogen with an oxygen contaminati of up to 2.68 percent by volume. A typical plot of the variation of the normal emittance during the six cycles of 2.68 percent oxygen exposure is shown in Figure 2-16. Very little variation, within the accuracy of the emittance measurements, is noted.

Table 2-12 summarizes the normal emittance variations of gold on Mylar in an oxidation atmosphere. Again, only slight effects are indicated.

Electrical Resistance

Table 2-13 presents the electrical resistance data, indicating resistance measurements with both high (1 milliampere) and low (100 microampere) applied currents. The data indicates good correlation between results for the different current levels prior to oxidation exposure. Similarly, repeatable results were obtained during re-tests of the same sample. However, the data from the exposed test samples exhibits less repeatability. Due to the nature of the electrical tests, the condition of the samples probably had more influence on the results than the exposures to oxygen. The test depended on an even flow of current through a square area of sample, but the heat and handling caused a good deal of crinkling and bending of the samples. Therefore, evaluation of subtle changes in the resistance data should be regarded as inconclusive.

Table 2-11. Averaged Normal Emittance (ϵ_N) of Aluminized Mylar after Oxidation Test

Film Resistance ($\Omega/\square$)	Oxygen Concentration (percent volume) 0.31	0.66	2.68	Control (No Exposure)
0.2 to 0.3	0.0394	0.0391	0.0391	0.030
0.7 to 0.9	0.0355	0.0346	0.0350	0.042
2.5 to 3.0	0.0536	0.0469	0.0450	0.060

Note: Values are an average of six tests
Accuracy = $\epsilon_N = \pm 0.02$

FOLDOUT FRAME 2

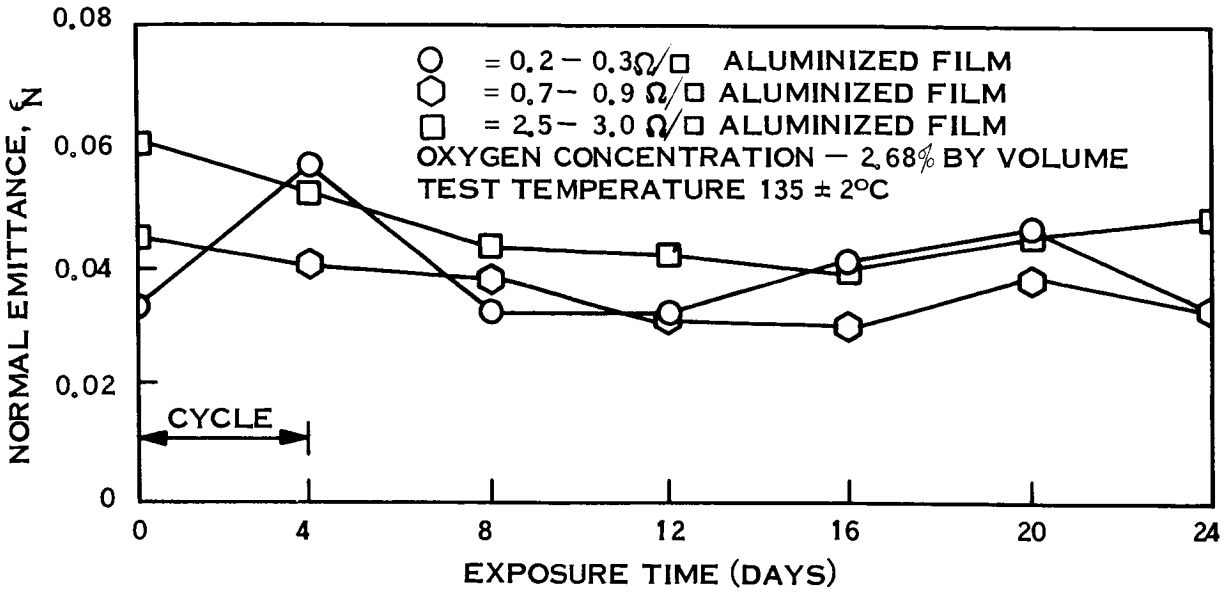

Figure 2-16. Effect of 2.68 Percent of Oxygen on Aluminized Mylar

Table 2-12. Normal Emittance of Gold Coated Mylar After Oxidation Tests

Oxygen Concentration (percent by volume)	Hanovia Gold	Vacuum-Deposited Gold
Control[1]	0.129	0.027
0.31	---	0.039
0.66	---	0.047
2.55	0.092	0.033
Control[2]	0.144	0.027

1 - Pre-test
2 - Post-test

Table 2-13. Electrical Resistance Data

Material Designations	Before Exposure (ohms/square)	After Exposure to Oxygen Concentration at 135°C 0.31% (ohms/square)	0.66% (ohms/square)	2.68% (ohms/square)
NRC (2.5-3.0)	←	not measureable		→
NRC (0.2-0.3)	0.21/0.21*	0.44/0.29	0.42/0.29	0.50/0.35
NRC (0.7-0.9)	1.05/1.05	6.7/7.1	1.25/1.2	1.27/1.2
Dimplar	--	4.4/4.7	4.4/4.75	4.7/5.25

*Resistance at 1 millampere/100 microampere current.

Section 2.1 Candidate Insulation-Material Evaluation

Subsection 2.1.2 Heat Sterilization Effects

B. Effects of Dry Heat Sterilization

TEST PROCEDURES AND APPARATUS

A wide range of candidate thermal insulation materials were subjected to dry heat sterilization per JPL Spec. VOL-50503-ETS, and were subsequently measured for physical property changes and visually observed.

The dry heat sterilization facility is schematically presented in Figure 2-17. Based on the oxidation effect test results, the facility was designed for the use of a nitrogen atmosphere containing 2.5 percent (by volume) of oxygen. Test sample material was arranged on a special fixture within the retort and thermocouples inserted within the material folds. Six sterilization cycles were conducted at 135°C, for 96 hours per cycle. The following procedure was employed for each of the cycles:

a. The retort was evacuated to approximately 20 mm of mercury pressure and backfilled twice with dry nitrogen. Nitrogen was then allowed to purge the retort at 2 cu ft/min.
b. After the second backfill, the air line needle valve was opened to allow the oxygen content of the gas to increase. The concentration was controlled by balancing the retort pressure against the air stream pressure (constant head of 10 inches of mercury) at 2.5 psi.
c. The retort was purged until the moisture content of the effluent gas was less than 15 ppm.
d. When the oxygen concentration and moisture content of the gas was acceptable, the oven heater and fan were turned on. The temperature of the oven and reference thermocouple was recorded with a potentiometer during the heatup and cool-down cycle. The 92 hour dwell was begun when all thermocouples read between 133 and 137°C. After 92 hours, the oven heat was turned off, and the oven door opened. The temperature of the reference and oven thermocouples were recorded during the cooldown.
e. When the retort thermocouples read below 40°C, the oven fan and gas purge were turned off, and the retort door opened. Material samples were removed, and the next cycle initiated.

After the completion of six sterilization cycles, the samples were removed and submitted for material tests. Figure 2-18 is a flow diagram of a single sterilization cycle.

Optical and physical property measurements of solar absorptance, normal emittance, weight change (in air), outgassing and dimensional stability were performed using the techniques and apparatus described for the evaluation of ETO effects, Subsection 2.1.1.

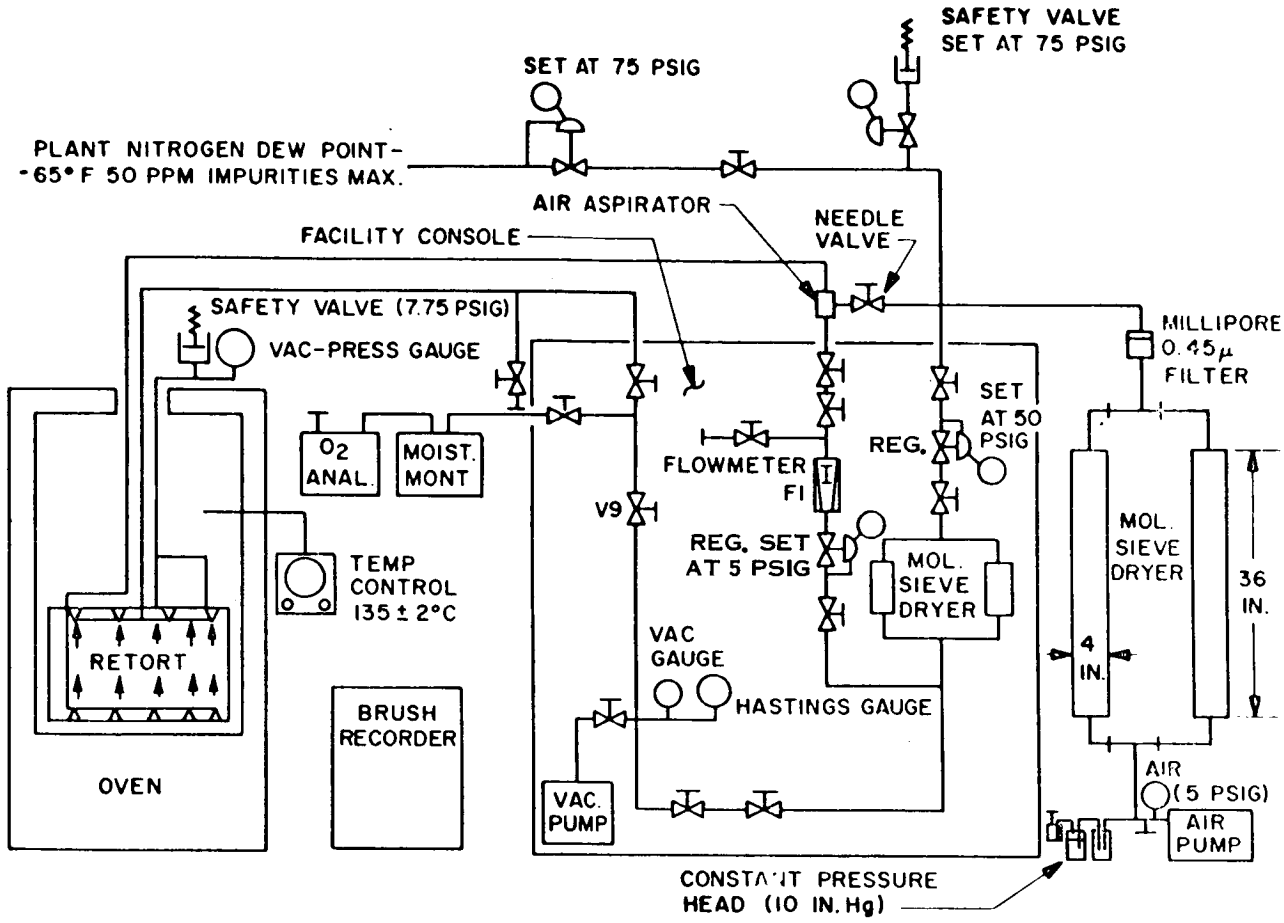

Figure 2-17. Thermal Sterilization Facility

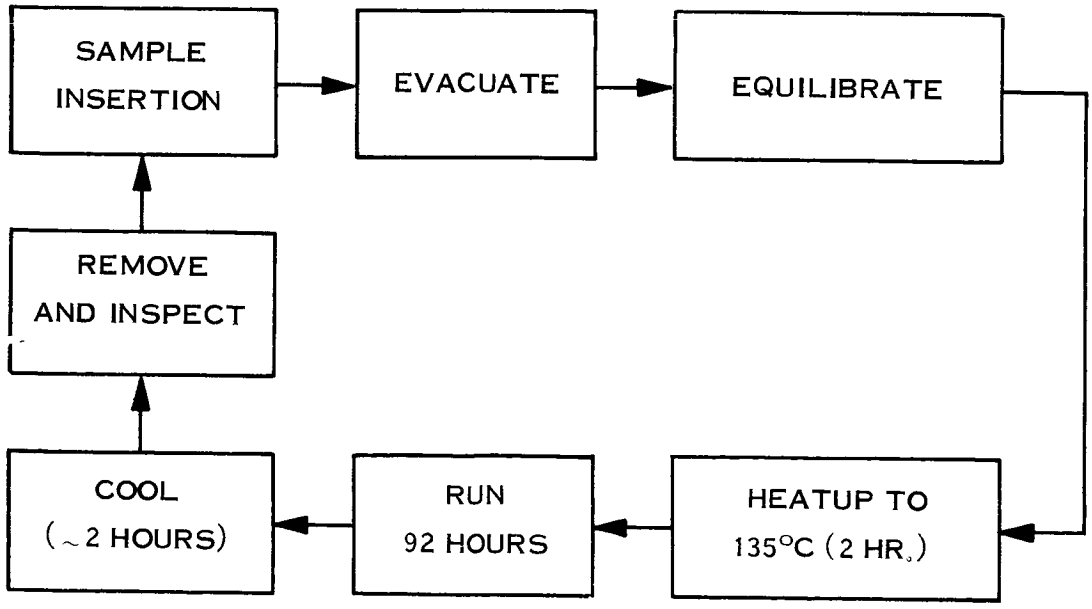

Figure 2-18. Heat Sterilization Cycle-Test Procedure

Section 2.1 Candidate Insulation-Material Evaluation

Subsection 2.1.2 Heat Sterilization Effects

B. Effects of Dry Heat Sterilization

TEST SAMPLES

Flat sheet and rolled samples of candidate thermal insulation materials were prepared for exposure to the dry heat sterilization environment, with the size of the samples varying with the intended post-test measurements to be accomplished. The insulation material test samples were prepared in two complete sets: one set having undergone prior exposure to the ETO decontamination cycle. The sample sizes for each of the post-sterilization test were as follows:

optical property tests - 2 x 3 inches

dimensional change measurements - 5 x 5 inches

outgassing (weight loss and product analysis) - 12 x 3 inches

Table 2-14 lists the specific materials evaluated. In addition to the tabulation, rolled samples of NRC-2, doublesided aluminized Mylar and Dacron mesh (spacer material) were also subjected to the sterilization cycles and visually observed post-test.

Table 2-14. Dry Heat Sterilization Test Samples

Material	Optical Prop. Samples	Dimen. Chge. Samples	Outgassing Samples
Aluminized Kapton (1/2 mil)	X	X	X
Aluminized Teflon (1 mil)	X	X	X
Alum. Mylar (doublesided)	X	X	X
Dimplar		X	X
NRC-2 (preshrunk)	X		
Gold on Mylar (1/4 mil)	X	X	X
Dacron Mesh			

FOLDOUT FRAME 1

Section 2.1 Candidate Insulation-Material Evaluation

Subsection 2.1.2 Heat Sterilization Effects

B. Effects of Dry Heat Sterilization

TEST RESULTS

Table 2-15 summarizes the results of the post-sterilization weight change analysis, both in air and in a vacuum environment. The table compares the results of weight change measurements after ETO, dry heat and cumulative ETO and dry heat exposures. In air, in contrast to ETO exposure results, the samples lose weight as a result of heat sterilization. Presumably, the dry sterilization atmosphere dehydrates the sample materials whereas the moist ETO environment adds water. Table 2-15 further shows that weight loss in vacuum, after heat sterilization, is decreased as compared to the unexposed control samples and those exposed to ETO environments, which further supports the dehydration analysis.

Table 2-16 depicts the results of dimensional measurements after decontamination and sterilization treatments. Aluminized Kapton was the most stable under both conditions, and none of the samples exhibited dimensional changes in excess of 10 percent.

Optical measurement data is presented in Table 2-17. As with the ETO-exposed optical samples, there does not seem to be any significant optical degradation attributable to heat sterilization.

Table 2-15. Post-Sterilization Weight Change Analysis

Material	Weight Change in Air (%)			Weight Change in Vacuum							
	ETO	Heat	ETO & Heat	Control Time (hr)	Control 200°F %Loss	ETO Time (hr)	ETO 200°F %Loss	Heat Time (hr)	Heat 200°F %Loss	ETO & Heat Time (hr)	ETO & Heat 200°F %Loss
Alum. Kapton (1/2 mil)	+1.30	-0.57	-0.16	21	0.47	43	1.0	26	0.31	25	0.12
NRC-2 (preshrunk)	+0.55	-0.54	-0.65	25	0.57	22	0.88	20	0.45	19	0.22
Dimplar	+0.62	-0.40	-0.30	19	0.31						
Dble. Sided Alum. Mylar	+0.46	-0.34	-0.34	18	0.81	22	0.99	25	0.25	21	0.33
Alum. Teflon (1 mil)	+0.20	-0.13	-0.04	19	0.21	19	0.17	25	0.11	25	0.18
Dacron Mesh	+0.26	-0.69	-0.15	79	0.21	43	0.57	25	0.30	25	0.10

Table 2-16. Post Sterilization Dimensional Change Analysis

MATERIAL	DIMENSIONS (INCHES)*			
	PRE-TEST	AFTER ETO	AFTER HEAT	AFTER ETO + HEAT
Alum. Kapton (½ mil)	5 x 5	5 x 5	4 15/16 x 5	5 x 5
NRC-2 (preshrunk)	5 x 5	4 15/16 x 4 15/16	4 15/16 x 4 7/8	4 13/16 x 5 1/16
Dimplar	5 x 5	5 1/2 x 5 1/16	4 7/8 x 5 1/2	4 7/8 x 5 1/2
Dble. Sided Alum.Mylar	5 x 5	4 7/8 x 5	4 7/8 x 5 1/16	4 13/16 x 5
Alum. Teflon (1 mil)	5 x 5	4 7/8 x 5	4 13/16 x 5	4 13/16 x 5
Dacron Mesh	5 x 5	4 7/8 x 4 3/4	4 3/4 x 4 13/16	4 13/16 x 4 7/8

*Accuracy = ± 1/16 inch or 1 percent

Table 2-17. Post-Sterilization Optical Property Measurements

	CONTROL		ETO		HEAT		ETO + HEAT	
	α_S	ϵ_N	α_S	ϵ_N	α_S	ϵ_N	α_S	ϵ_N
Alum. Teflon (1 mil)		0.045		0.062		0.063		0.066
Alum. Teflon (film up)	0.153	0.594	0.194	0.624	0.186	0.548	0.165	0.577
NRC-2 (preshrunk)		0.040		0.048		0.038		0.053
Alum. Mylar (Dble. Sided)		0.040		0.049		0.070		0.077
Alum. Kapton (½ mil)		0.049		0.051		0.039		0.052
Alum. Kapton (film up)	0.328	0.478	0.353	0.550	0.346	0.523	0.347	0.528
Gold on Mylar (¼ mil)		0.051		0.042		0.033		0.051

Accuracy: $\epsilon_N = \pm 0.02$

Section 2.1 Candidate Insulation-Material Evaluation

Subsection 2.1.3 Combined Space Environmental Effects

TEST PROCEDURES

Candidate insulation cover materials were subjected to combined ultraviolet and photon irradiation under high vacuum to ascertain the effects of these space environmental factors on the materials. Pre-and post-test optical property measurements were performed. Fourteen samples of candidate cover materials were irradiated to simulate the anticipated exposures during interplanetary travel. The basic test procedure was as follows:

a. Solar absorptivity (α_S) and normal emittance (ϵ_N) measurements were performed on all samples. The samples were then placed on a turntable in the Combined Effects Chamber.

b. Solar absorptivity measurements were taken on the samples in place in the chamber at ambient pressure.

c. The test chamber was evacuated to 10^{-7} torr and α_S measurements again taken.

d. Mercury-Xenon (H_gX_e) lamps were turned on and the samples subjected to 116 ultraviolet equivalent sun hours (UVESH). Exposure required 58 hours, followed by α_S measurements (in situ).

e. A proton dose of 10^{15} protons per square centimeter was then delivered to the samples; followed by α_S (in situ) measurements.

f. The H_gX_e lamps were turned on again to complete the 1000 UVESH exposure. Ultraviolet exposure was equivalent to 25 percent of the dosage that would be received by a spacecraft intransit from Earth to Mars. Experience has shown that 1000 hours of ultraviolet exposure will normally show up any degradation.

g. The H_gX_e lamp housing was removed for visual observations of the samples.

h. Photon irradiation was resumed. Most of the samples completed a total dosage of 10^{16} protons per sq. cm. However, due to sample buckling, some of the samples had lesser total exposures, as discussed under Test Results. The proton total exposure (10^{16}) was based on the expected dose equivalent to solar wind effects during a Mars mission.

i. The chamber was vented to atmosphere and a complete set of optical measurements was performed on the samples.

Figure 2-19 outlines the test procedure.

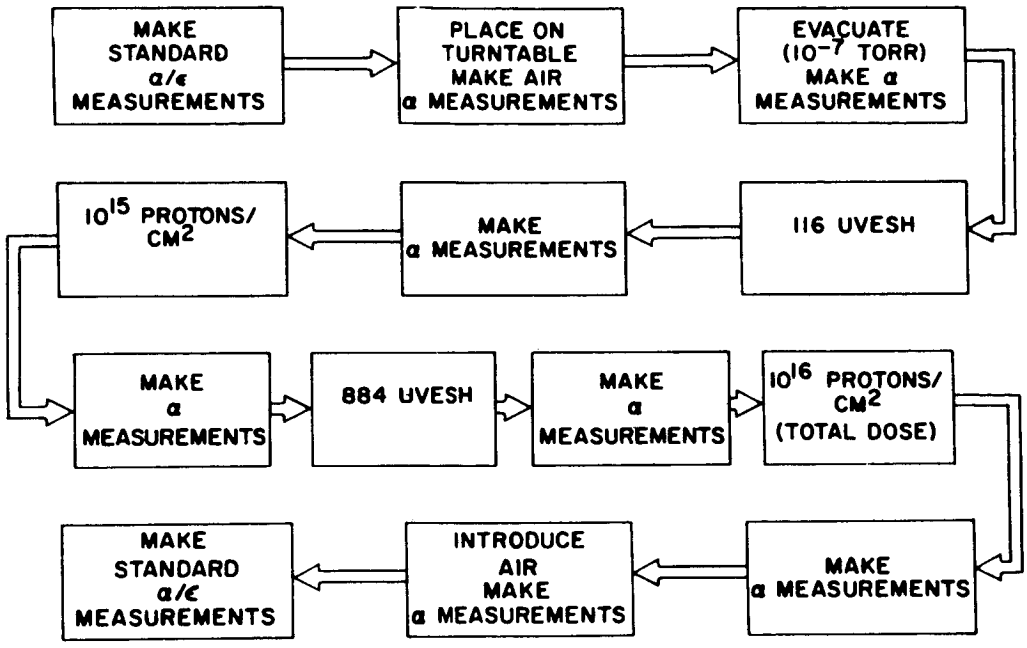

Figure 2-19. Combined Effects Test Procedure

TEST SAMPLES/TEST APPARATUS

Fourteen samples of candidate insulation cover materials were subjected to simulated interplanetary environmental exposures in a Combined Effects Chamber. Both disc and sheet samples were employed. Disc samples were 0.93 inches in diameter, and the sheets were 2 x 3 inches. Table 2-18 describes the samples tested.

The Combined Effects Chamber is shown schematically in Figure 2-20. The chamber can readily maintain a vacuum of 10^{-7} torr. Ultraviolet radiation is applied via mercury xenon lamps; their output being equivalent to two ultraviolet suns (2 UVES). Proton irradiation is provided by a 2 KEV hydrogen-ionization proton gun. The chamber has the capability for in situ optical measurements.

The test samples are mounted in the chamber on a turntable, as shown in Figure 2-21; sample numbering corresponds to that of Table 2-18. The 2 x 3 inch sheet samples are held on one end with clips and, on the other end, with a central 8 inch copper disc. The disc samples fit into holes provided in the turntable. During the tests, the turntable was maintained at 25°C and the test chamber shroud (see Figure 2-20) was cooled with liquid nitrogen.

Optical measurements were performed using the Beckman DK-2 spectrophotometer and Perkin Elmer Reflectometer as described in Subsection 2.1.1.

Table 2-18. Test Samples - Combined Effects Tests

Sample No.	Sample Material	Sample Configuration
1	Alum. Kapton (2 mils)	Sheet, Film Side Up
2	Alum. Kapton (2 mils)	Sheet, Film Side Up
3	Alum. Kapton (2 mils)	Disc, Film Side Up
4	Alum. Kapton (2 mils)	Sheet, Film Side up
5	Alum. Kapton (2 mils)	Sheet, Film Side Up
6	NRC-2	Disc, Alum. Side Up
7	Gold on Kapton (3 mils)	Disc, Gold Side Up
8	Gold on Kapton (3mils)	Sheet, Gold Side Up
9	Alum. Teflon (5 mils)	Sheet, Film Side Up
10	Dble. Sided Alum. Mylar	Disc
11	Alum. Teflon (5 mils)	Sheet, Film Side Up
12	Alum. Teflon (5 mils)	Sheet, Film Side Up
13	Alum. Teflon (5 mils)	Sheet, Film Side Up
14	Alum. Teflon (5 mils)	Disc, Film Side Up

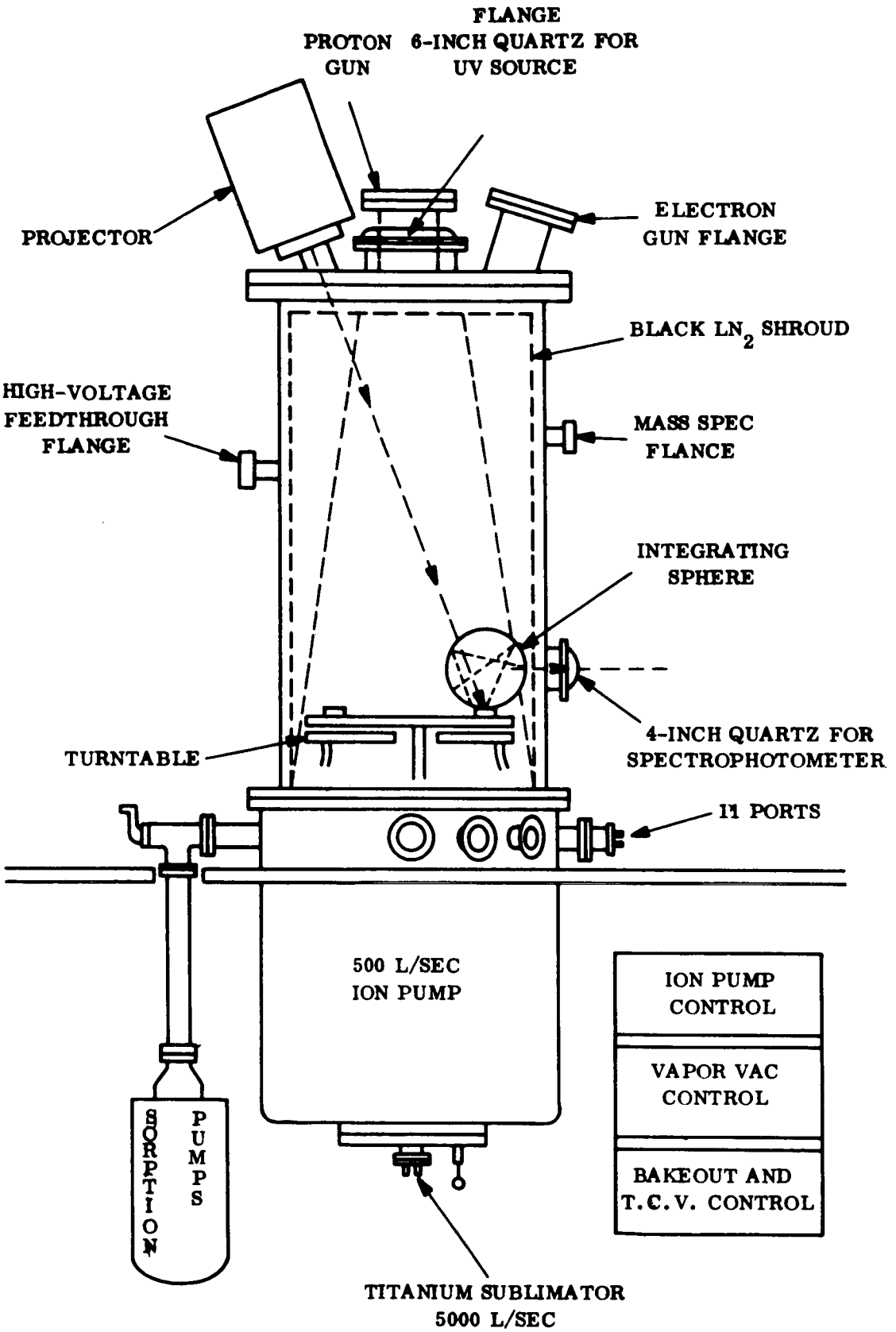

Figure 2-20. Combined Effects Facility Schematic

FOLDOUT FRAME 2

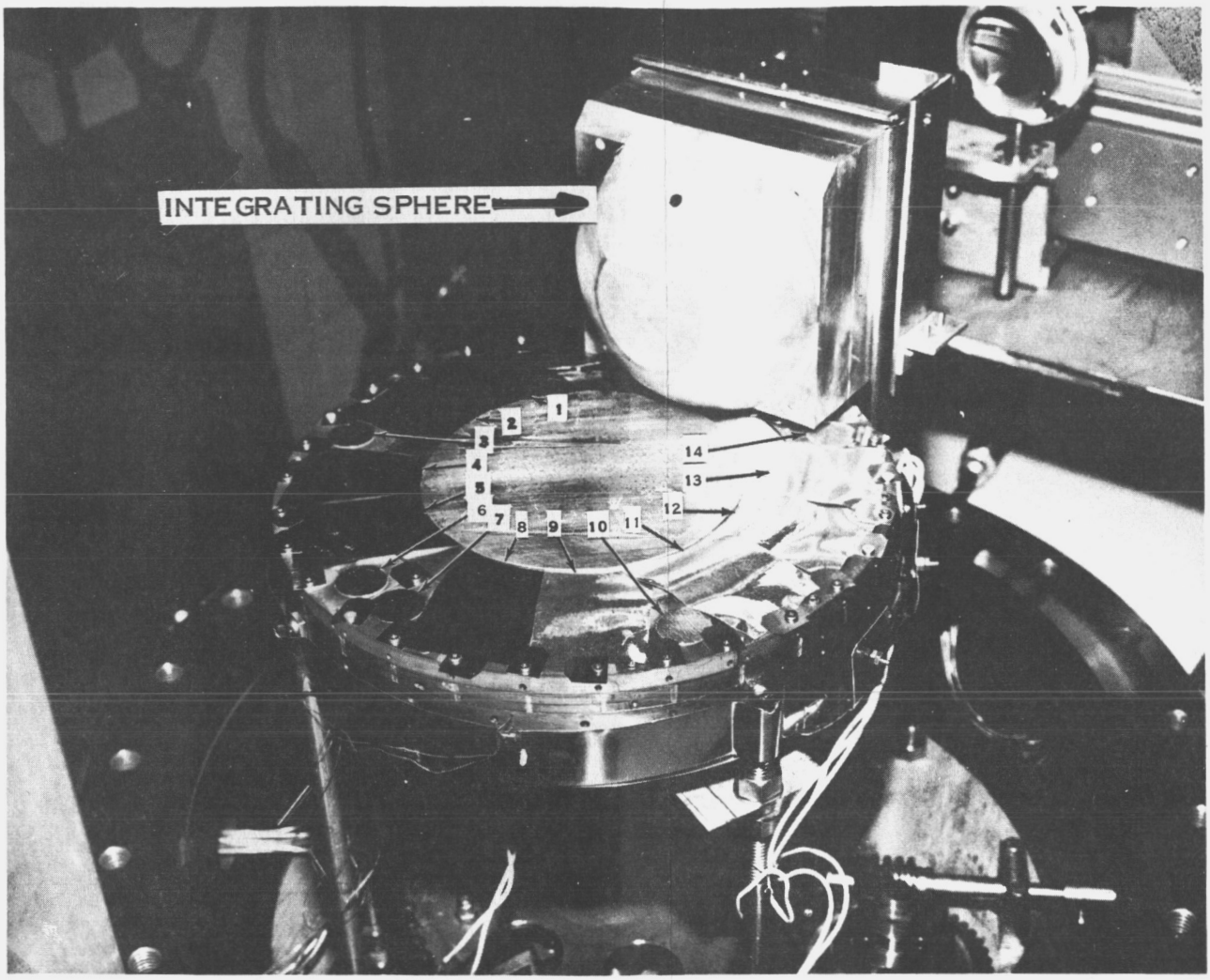

Figure 2-21. Combined Effects Sample Location

Section 2.1 Candidate Insulation-Material Evaluation

Subsection 2.1.3 Combined Space Environmental Effects

TEST RESULTS

Table 2-19 summarizes the optical property measurements of the test samples before, during and subsequent to irradiation. The sample numbers correspond to the descriptions given in Table 2-18.

After the total 1000 UVESH exposure, the lamp housing was removed for visual observations of the samples. The aluminized Teflon sheet samples had buckled. It is suspected that buckling occurred during either the 116UVESH or the 884UVESH exposures since these are the only portions of the test that can produce sufficient energy to cause a bulk effect. Proton energy is limited to surface reactions.

The buckling of the aluminized Teflon inhibited the movement of the turntable. Consequently, some of the samples could not be positioned for the final proton irradiation. Table 2-20 shows the doses actually received. Only three aluminized Teflon samples received α_s measurements after 1000 UVESH exposures, due to the buckling.

Figure 2-22 shows the effects of irradiation on reflectance of goldized Kapton and aluminized Kapton. Figure 2-22 (a) represents the pre-radiation measurements for vapor deposited gold on Kapton and Figure 2-22 (b) presents measurements after proton and UV exposure. Comparing Figure 2-22 (a) and Figure 2-22 (b) very little change due to irradiation is noted. The figure also depicts the good correlation between in situ and spectrophotometer measurements.

Table 2-19. Combined Space Environments Effects on Cover Materials

Sample Material	Air Convection Before Irradiation			In Situ					Air Convection After Irradiation		
				Air Vac	116 UVESH	116 UVESH 10^{15}p/cm^2	1000 UVESH 10^{15}p/cm^2	1000 UVESH 10^{16}p/cm^2			
	α_s	ϵ_N	α_s/ϵ_N	α_s	α_s	α_s	α_s	α_s	α_s	ϵ_N	α_s/ϵ_N
2-mil aluminized Kapton (2 in. x 3 in.)				0.460	0.472	0.447	0.477	0.507 (Vac) 0.447 (Air)			
2-mil aluminized Kapton (2 in. x 3 in.)				0.443	0.449	0.425	0.460	0.491 (Vac) 0.449 (Air)			
2-mil aluminized Kapton (Disc)	0.391	0.674	0.58	0.472	0.444	0.510	0.489	0.457 (Air) 0.450 (Vac)	0.415	0.751	0.56
2-mil aluminized Kapton (2 in. x 3 in.)				0.480		0.450	0.413	0.429 (Vac) 0.438 (Air)			
2-mil aluminized Kapton (2 in. x 3 in.)				0.488	0.441	0.463	0.429	0.433			
NRC-2 (Disc)	0.150	0.030	5.0	0.209	0.237	0.221	0.198		0.134	0.024	5.6
3-mil Gold Kapton (Disc)	0.412	0.811	0.52	0.450	0.447		0.419	0.410	0.414	0.795	0.52
3-mil Gold Kapton (2 in. x 3 in.)				0.430	0.426	0.396	0.415	0.409			
3-mil Al Teflon (2 in. x 3 in.)				0.240	0.264	0.258	0.293	0.315			
D.S. aluminized Mylar (Disc)	0.220	0.04	5.0	0.216	0.230	0.175	0.220		0.218	0.036	6.1
5-mil aluminized Teflon (2 in. x 3 in.)				0.251	0.234	0.266	0.297	0.251			
5-mil aluminized Teflon (2 in. x 3 in.)				0.225	0.292	0.244	0.312	0.260 (Air)			
5-mil aluminized Teflon (2 in. x 3 in.)				0.241	0.247	0.243	Sample out of position				
5-mil aluminized Teflon (Disc)	0.195	0.822	0.24	0.256	0.292	0.225	0.321 0.369		0.189	0.809	0.23
$\alpha_s \pm .02$ Beckman $\alpha_s = \pm .06$ in-situ $\epsilon_N \pm .02$											

From Table 2-19, it may be observed that there was no variation in α_s greater than 0.06 for aluminized Kapton, goldized Kapton and NRC-2. The measurements of α_S/ϵ_N before and after combined effects testing do not show a significant change for aluminized Teflon, goldized Kapton, aluminized Kapton, NRC-2, and double-sided aluminized Mylar.

Visual observations of the aluminized Kapton and gold on Kapton revealed a slight darkening of the irradiated portions of the Kapton as compared to the shielded portions. This effect was not observed on the aluminized Telfon samples.

Table 2-20. Actual Proton Dosage

Sample No.	Sample Material	Dosage (Protons/cm^2) 10^{16}	5×10^{15}	10^{15}
1	Alum. Kapton	X		
2	Alum. Kapton	X		
3	Alum. Kapton	X		
4	Alum. Kapton	X		
5	Alum. Kapton	X		
6	NRC-2	X		
7	Gold on Kapton	X		
8	Gold on Kapton	X		
9	Alum. Teflon	X		
10	Dble. Sided Alum. Mylar		X	
11	Alum. Teflon		X	
12	Alum. Teflon			X
13	Alum. Teflon			X
14	Alum. Teflon			X

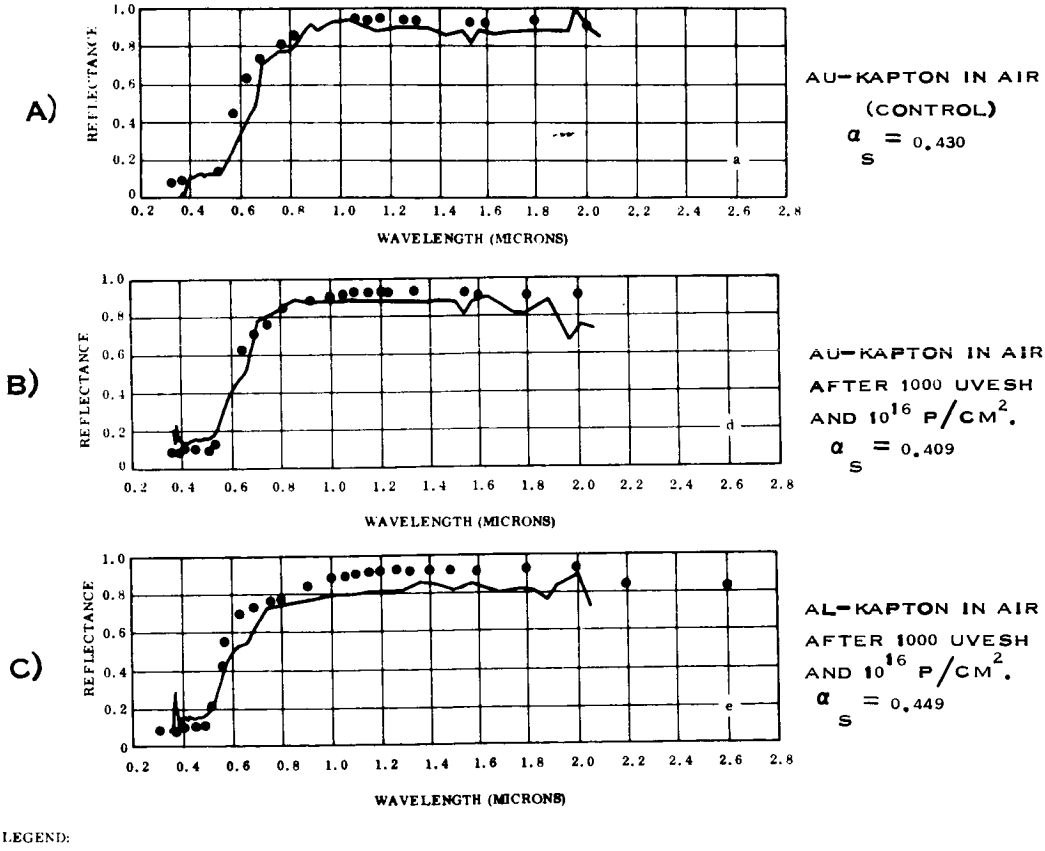

Figure 2-22. Effects of Proton and Ultraviolet Exposures

Section 2.1 Candidate Insulation-Material Evaluation

Subsection 2.1.4 Decontamination and Sterilization Effects on Pressure-Sensitive Tapes

TEST PROCEDURES/SAMPLES/APPARATUS

During the course of the ETO exposures of candidate insulation materials (Subsection 2.1.1) several samples of pressure-sensitive tapes were subjected to the ETO cycle. The tapes were primarily metallized film with a silicone adhesive on the film side. A pressure-sensitive hook and pile (Velcro) tape was also exposed. With the exception of the Velcro, the tapes were subjected to ETO while bonded to the metallized side of several candidate insulation materials. Velcro was bonded to itself, e.g., hook to pile. Table 2-21 presents the sample descriptions.

A set of pressure-sensitive tapes was also subjected to dry heat sterilization while bonded to insulation materials. Table 2-21 is indicative of the samples exposed during the heat sterilization of candidate materials, described in Subsection 2.1.2. In addition, clear (non-metallized) Kapton tapes and hook and pile tapes were subjected to dry heat sterilization[1], while hung in a small oven. Table 2-22 lists these additional tapes.

After both decontamination and sterilization, mechanical tests were performed on the adhesion properties of the pressure-sensitive tapes. The test performed was the "T-Peel" for adhesives, as described in ASTM-D1876. The tests consisted of taking the T-shaped samples, as shown in Figure 2-23, and pulling the tape and metallized film apart at the rate of 12 inches per minute on a tensile test machine. The load was measured in pounds per inch for continuously peeling the sample apart.

The tapes in Table 2-22 were subjected to "lap-shear" tests after sterilization. These tests, conducted on a tensile tester, evaluate the shear strength of the adhesive by measuring the force required to pull apart overlapped tape at 0.2 inches per minute. Lap-shear tests were also performed on tapes at -200°F.

[1] In accordance with JPL Spec. VOL-50503-ETS.

Table 2-21. ETO and Sterilization Exposure Test Samples

BONDED TO:	TAPE		
	E E6600(1)	3M 850(2)	Velcro
Alum. Teflon	X	X	
NRC-2	X	X	
Dimplar	X	X	
Dble. Sided Al. Mylar	X	X	
Alum. Kapton	X	X	
Tin on Mylar	X	X	
Gold on Mylar	X	X	
Velcro			X

(1) Manufactured by Permacel (2) Manufactured by 3M Company

Table 2-22. Additional Tape Candidates

VENDOR	TYPE	FILM	ADHESIVE	MANUFACTURER'S SPECIFIED OPERATING RANGE
Tech Floro	603-1	1 mil Kapton	Silicone PS*	-450°F to 750°F
3M	Y91845	1 mil Kapton	Silicone PS*	-200°F to 550°F
Permacel	EE6379	1 mil Kapton	Silicone PS*	to 400°F
Velcro	SA0142		Solvent Activated	to 325°F
Velcro	PS0100		PS	to 325°F
Velcro	SA0140		Pliobond	to 325°F
Velcro	SA0140		Resiweld	to 325°F

*PS = Pressure sensitive

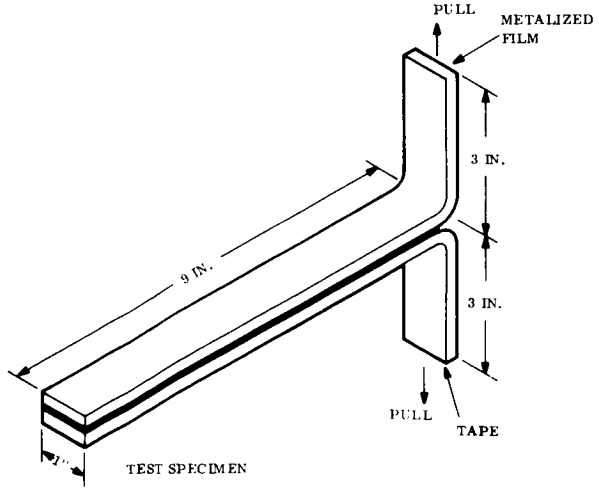

Figure 2-23. T-Peel Test Specimen

RESULTS

Table 2-23 depicts the T-peel test results after exposure to decontamination, sterilization and the combined effects of the two treatments. As compared to the control samples, ETO exposures produced no significant degradation of adhesive properties.

T-peel measurements taken after sterilization produced the most dramatic effects. Heat exposure greatly reduced the adhesive properties of the pressure-sensitive tapes. In many cases, the aluminum was removed from the plastic film of the insulation material. Figure 2-24 shows the removal of aluminum from aluminized Teflon. The dry heat exposures caused the adhesives to run, ultimately resulting in discoloration and drying. Figure 2-25 shows this condition for Permacel EE6600 tape on aluminized Teflon. The adhesive can be seen to have run to the back (metallized side) of the tape. Figure 2-26 shows the T-peel curves for each of the exposures. The control and ETO curves are relatively smooth as compared to those for sterilization.

Velcro hook and pile tapes, particularly the pressure-sensitive adhesive, as compared to the solvent-activated adhesive, performed well throughout the program. Lap-shear tests indicated that the hook and pile slips before the adhesive peels.

Lap shear tests on Kapton film tapes indicate an increase in shear strength after sterilization, which is probably due to the adhesive setting. At - 200^{o}F, lap-shear strength was seen to decrease by approximately 15 percent.

On the basis of these tests, Tech Floro Kapton film tape (Type 603-1) was selected for future use at the joints between insulation blankets. Velcro hook and pile was selected for blanket assembly to the vehicle.

FOLDOUT FRAME 1

Table 2-23. T-Peel Results

Candidate Materials	T-Peel Measurements							
	Control		ETO		Heat		ETO + Heat	
	EE 6600 lb/in.	3M 850 lb/in.	EE 6600 lb/in.	3M 850 lb/in.	EE 6600 lb/in.	3M 850 lb/in.	EE 6600 lb/in.	3M 850 lb/in.
1 mil aluminized Telfon	2.25	1.24	1.65	1.40	0.42	0.46	0.40	0.59
1 mil aluminized Teflon	2.07	1.19	0.81	1.39	0.62	0.30	0.40	0.73
1 mil aluminized Teflon (film up)								
NRC-2 preshrunk	1.50	0.750	1.60	1.68	Film broke when		0.5	Film
NRC-2 preshrunk	2.00	0.858	1.40	1.60	sample was being		Film	broke
NRC-2 preshrunk (film up)					placed in machine.		broke	
Dimplar	0.38	0.64	1.10	0.91	0.6	Film	0.4	Film
Dimplar	0.62	0.69	0.85	0.94	0.55	broke	0.4	broke
1/4 mil D.S. aluminized Mylar	1.46	1.61	1.74	1.60	Film broke at		Film	Film
1/4 mil D.S. aluminized Mylar	1.50	1.63	1.49	1.55	start of test		broke	broke
1/2 mil aluminized Kapton	1.20	1.49	1.72	1.60	0.54	1.5	0.7	0.7
1/2 mil aluminized Kapton	1.38	1.01	1.85	1.55	0.8	1.2	0.9	0.6
1/2 mil aluminized Kapton								
1/2 mil Sn on Mylar	1.8	1.7	1.5	1.56	0.8	1.39	Film	Film
1/2 mil Sn on Mylar			1.7	1.70	0.9	1.63	broke	broke
1/4 mil gold on Mylar	0.04	0.04	0.04	0.038	0.8	Film	Film	0.07
1/4 mil gold on Mylar					0.6	broke	broke	
Velcro/Velcro	0.508		0.54		0.50		0.50	
Velcro/Velcro	0.510		0.64		0.52		0.55	

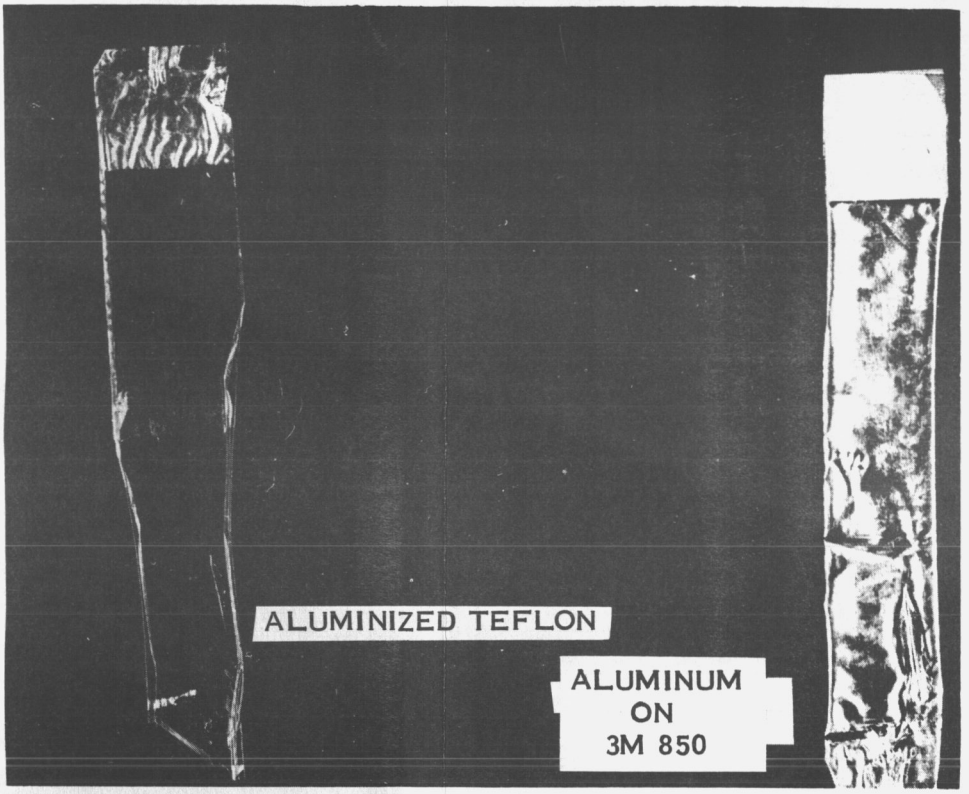

Figure 2-24. Aluminum Removal from Teflon After ETO and Heat Exposures

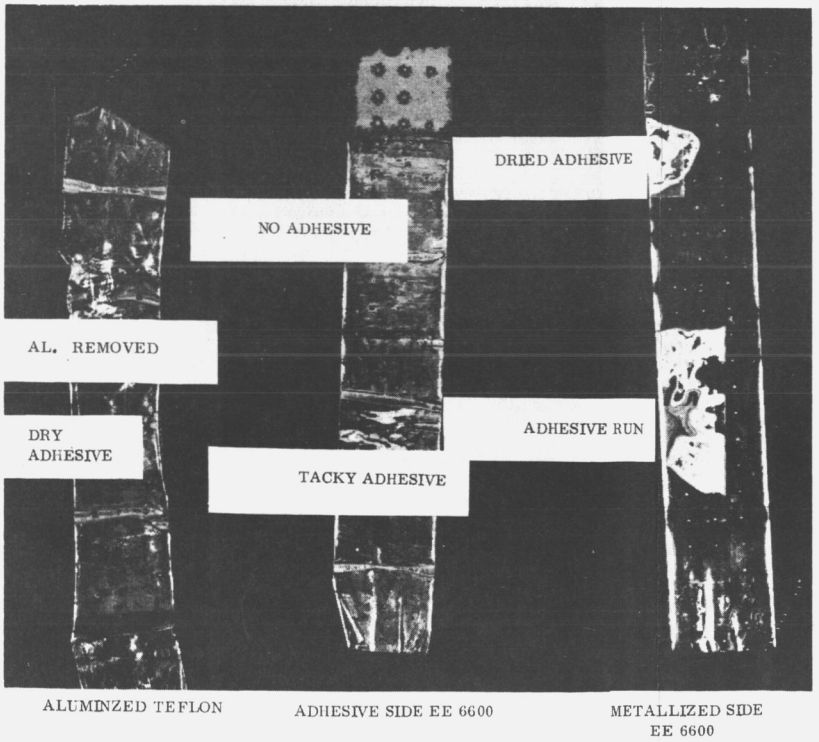

Figure 2-25. Aluminized Teflon After Heat Sterilization

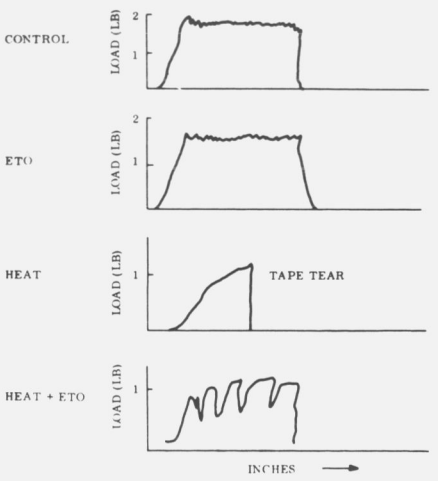

Figure 2-26. T-Peel Test Comparison

SECTION 2

TECHNICAL DISCUSSION

2.2 CANDIDATE INSULATION—THERMAL PROPERTIES EVALUATION

Section 2.2 Candidate Insulation-Thermal Properties Evaluation

SCOPE/OBJECTIVES

A test program was conducted to determine the thermal conductivity of various insulation configurations. The principal test objective was to define the heat leak that would exist with the various blanket configurations and to, thereby, identify those materials and/or configurations most desirable from a thermal standpoint.

Specifically the test objectives were as follows:

a. Evaluate the thermal effects of Dacron net spacers in insulation blankets.
b. Compare the thermal conductivity of various metallized film insulations.
c. Assess the effects of blanket density (layers per inch) on thermal conductivity for the several candidate insulation materials.
d. Evaluate the heat flow effects of joints and insulation support posts.
e. Assess the heat flow effects of different insulation materials with similar joints and supports.
f. Evaluate the effects of a change in warm-side insulation temperature for different materials.
g. Provide conductance data applicable to a controlled heat leak at the sun-facing end of a planetary vehicle.
h. Determine the thermal effects of vent holes in the insulation blankets.

Section 2.2 Candidate Insulation-Thermal Properties Evaluation

Subsection 2.2.1 Thermal Conductance Measurements

TEST APPARATUS

The thermal conductance of candidate insulation configurations was determined in a guarded hot plate apparatus. The guarded hot plate apparatus is the basic type employed at the General Electric Spacecraft System's Thermal Laboratory for measuring the apparent thermal conductivity of evacuated multilayer insulations. The apparatus used was a second generation improvement of that described in Reference 2. The construction of this apparatus generally follows that outlined in ASTM Standard C-177. Figure 2-27 shows the test apparatus. Two identical test samples are used, one on either side of the hot plate, thereby providing a mean value of insulation sample characteristics. The hot plate contains electrical resistance elements sandwiched between two aluminum plates. The hot plate is in two separate sections: a main heater and a guard heater, with the main heater supported by the guard heater. Each cold plate is made of copper, to which is soldered a copper tube. Liquid nitrogen flows through this tube by gravity from a reservoir at the top of the apparatus to cool the copper plate. The test sample thickness is controlled by hot plate to cold plate spacing. The entire hot plate apparatus is operated in a vacuum environment of about 10^{-5} torr.

The temperatures of the guard heater and main heater are matched by feeding the output of a deviation thermopile between the main and guard heaters to a deviation amplifier. The amplifier output is the input to a controller which governs a magnetic amplifier that powers the guard heater. The main heater power is set manually, with the control system used to match the guard heater temperature to that of the main heater. The heat transferred through the test samples is obtained by measuring the applied voltage and current to the main heater. The current is measured by the potential drop across a calibrated resistance in series with the main heater.

Accuracy of Apparatus

There are several sources of error inherent with testing low-conductance multilayer insulation in a guarded hot plate apparatus: (1) inadequate radial guarding of the insulation being tested, (2) heat losses (or additions) caused by radial conductance between the guard and main heater plates, and (3) heater plate heat capacity. Items 2 and 3 are essentially eliminated by pretest heat flow measurements and the application of appropriate correction factors. With few exceptions, the corrections for either of these items amount to less than 5 percent of the insulation sample heat flow.

Radial guarding of the insulation is more of a problem. The thousand-times higher conductance in the lateral direction, as compared to the transverse, makes the results very sensitive to the insulation perimeter guarding. If the perimeter guard has the same temperature profile as the insulation in the thickness direction and either direct or reflected radiation from other temperature regions is prevented, then radial transfer would be eliminated. Lacking means to specifically accomplish that, a method was adopted wherein a peripheral temperature was

imposed below that of the insulation at a given axial position, as illustrated by Figure 2-28. Th peripheral guard ring was made of adhesive aluminized Mylar tape with the aluminum coating o the face opposite the adhesive. The tape was folded lengthwise so that only enough adhesive wa left exposed to attach to the cold plate, resulting in a low-emittance surface facing the insulatio and the exterior, as well.

It is believed that the peripheral guard tape results in a higher heat flow from the heater plate than would be the case for an adiabatic boundary. For an insulation thickness of 0.85 inch, a thermocouple placed in the tape near the heater plate edge read -80°F when the heater plate was at 75°F and the cold plate edge at -310°F. Thus some heat must flow by radiation and by conductive contact from the insulation to the tape. Heat flow in this direction will increase the required heater power as compared with the ideal case of transverse transfer only, resulting in higher calculated conductivity. Tests by the National Bureau of Standards, NRC data (Reference 3) and work of other investigators, including Reference 4, substantiate the assumption that the present data is conservative; i.e., measured conductivity is high. However, data in Reference 5 agrees with the present results. Data agreement between different test methods will improve for insulation samples of higher conductivity as the preciseness of peripheral guarding becomes less sensitive.

FOLDOUT FRAME 2

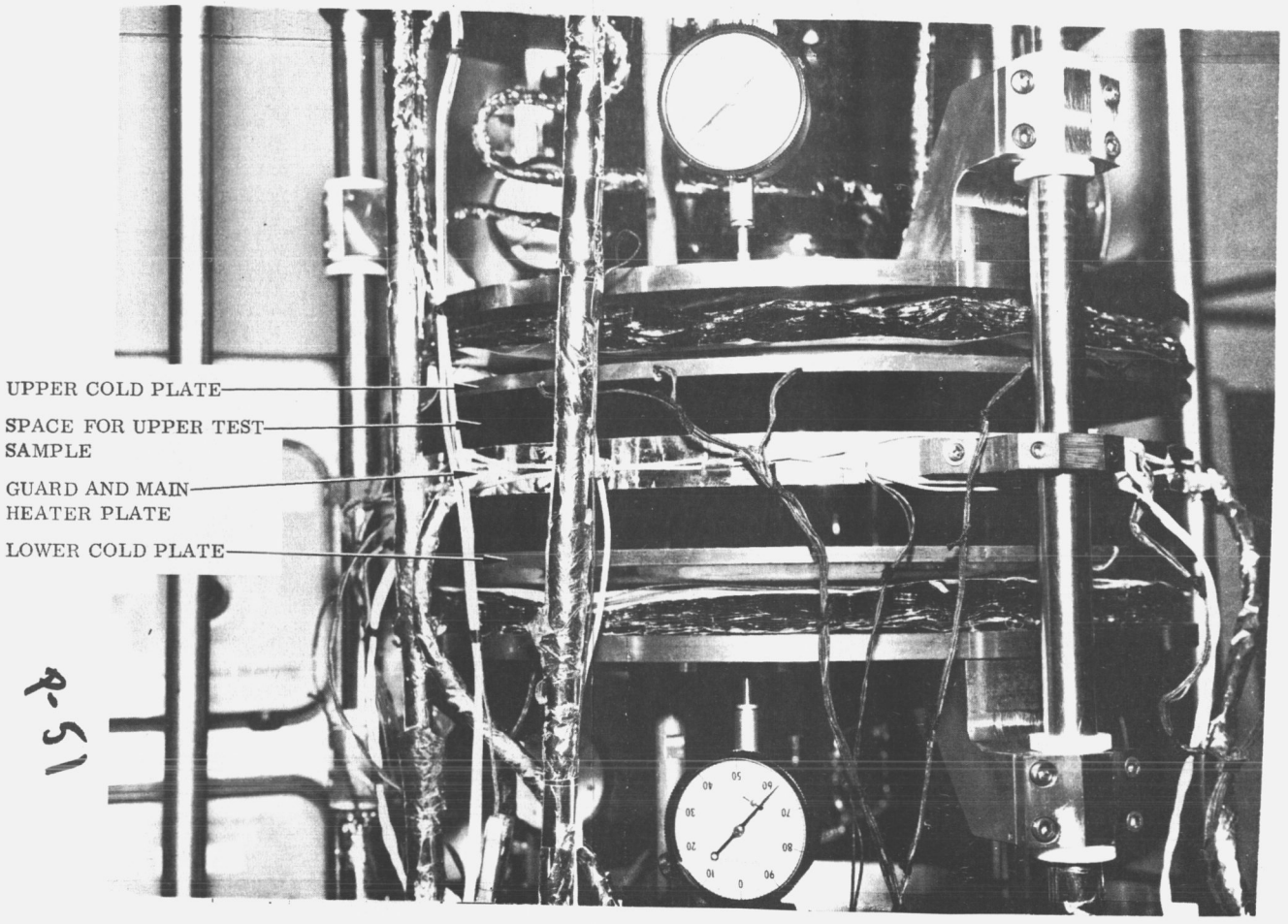

Figure 2-27. Thermal Conductivity Rig

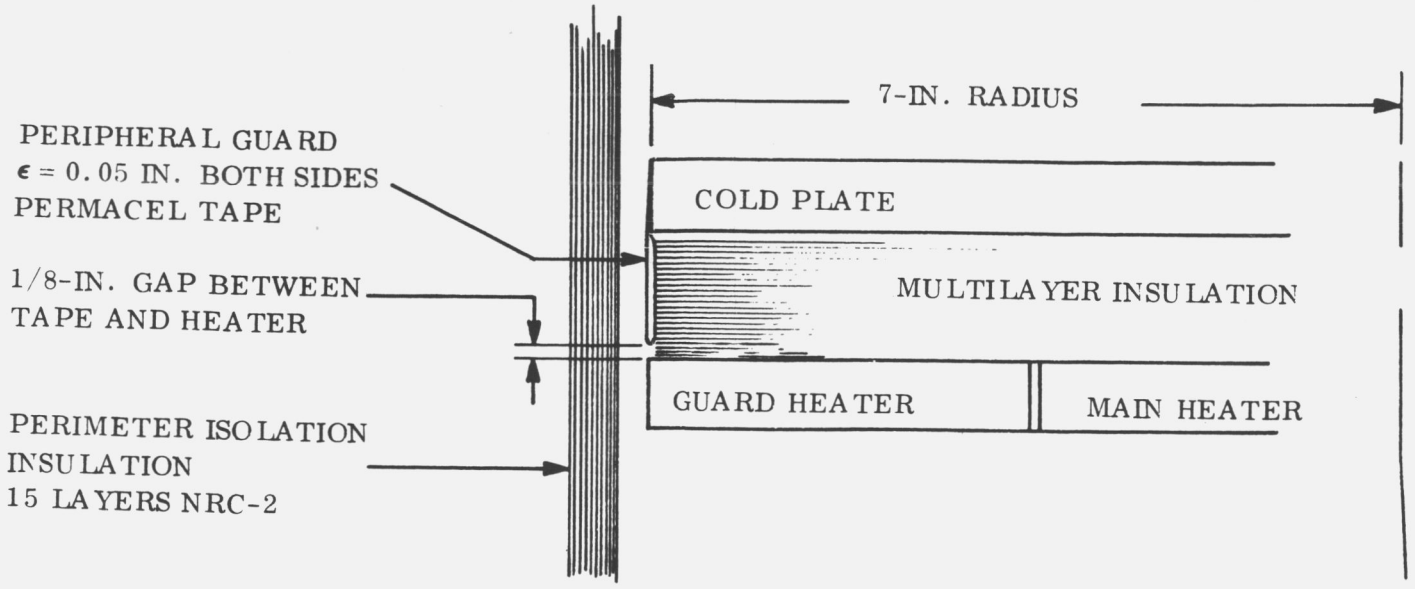

Figure 2-28. Method of Peripheral Guarding

Section 2.2 Candidate Insulation-Thermal Properties Evaluation

Subsection 2.2.1 Thermal Conductance Measurements

TEST PROCEDURES/ TEST SAMPLES

The thermal conductivity of a comprehensive range of insulation materials and configurations was determined under simulated space thermal environments. Table 2-24 delineates the thermal insulation configurations which were evaluated. The samples were all tested on the guarded hot plate apparatus. For most of the tests, the hot plate was held at about 70°F, simulating average spacecraft temperature, and the cold plates at -320°F, simulating an insulation face radiating into space.

Based on NRC data (Reference 3), 70 layers of insulation per inch was considered desirable. A flat blanket, built from "as-manufactured" 1/4-mil crinkled aluminized Mylar, stacks up to a greater layer density than 70 per inch. Consequently, the material was subjected to additional hand wrinkling to make the specimen less dense. Tests No. 1, 1A, 2, 3 and 6 were conducted to evaluate the effects of such crinkling.

Tests No. 7 and 9 were conducted to determine the advantages or disadvantages of using Dacron or Nylon spacers between the insulation layers.

One-quarter-mil, double-sided, embossed, aluminized Mylar was evaluated in Test No. 5 to determine the value of this significantly more dense (128 layers/inch) blanket. Test No. 12 determined the conductivity of uncoated Mylar.

The type of multilayer insulation trademarked "Dimplar" was evaluated. This material is composed of alternate layers of deeply corrugated aluminized Mylar film separators between smooth reflector sheets of the same material. One corrugated and one flat layer are referred to as a layer pair. Because of the deeply corrugated separators, a fewer number of layers of Dimplar is required than for other insulations tested, but at least 1/2 mil-thick film is necessary for the dimpled layers. Normally the same thickness material is used in both layers of a pair, but it is possible to use thinner sheets for the reflectors to reduce weight. The Dimplar samples in Tests No. 10, 11, 17, 18, 18A, 19, and 20 all were of 1/2-mil separators and reflectors designated by Dimplar number T-7342.

Test No. 23 through 27 investigated gold-coated film insulations, both Mylar and Kapton, while No. 25 through 27 evaluated the heat loss due to blanket vent holes. Samples 24 through 27 were made of die crinkled material.

A controlled heat leak at the sun-facing end of the vehicle was simulated in Test No. 21 and 22. The cold side was maintained at spacecraft temperature (about 70°F), and the warm side was operated at typical temperatures (150 and 250°F) for sunheated surfaces.

Several tests (No. 8, 14, 19 and 20) were conducted to show the effect of reduced warm-side (spacecraft) temperature, as might occur at the capsule heat shield insulation if insufficient

electrical power is available to maintain normal temperatures. For these tests, the "hot plate" (simulating the capsule) was operated at temperatures ranging from -3 to -43°F.

Lastly, tests were conducted to investigate the thermal penalty of the rabbeted joint and support post shown in Figure 2-29. Test No. 13, 13A, 15, 16 and 16A evaluated this configuration for NRC-2 material; Test No. 17, 18, and 18A did so for Dimplar.

Table 2-24. Thermal Conductance Test Samples

Sample/Test No.	Sample Configuration*	No. of Layers	Thickness (inches)	Density (lb/ft^3)
1	¼ mil Alum. Mylar-crinkled (NRC-2)	35	0.50	1.52
1A	Same as No. 1	35	0.50	1.45
2	¼ mil Alum. Mylar (preshrunk)-double crinkled	35	0.50	1.46
3	Same as No. 2	35	0.85	0.86
4	½ mil Mylar-One side tin coated	35	0.50	3.22
5	¼ mil Mylar-Aluminized 2 sides, embossed	51	0.40	2.79
6	¼ mil Alum. Mylar (33 layers), crinkled + ½ mil Alum. Kapton (2 layers), crinkled. Kapton on cold plate side.	35	0.50	1.54
7	¼ mil Mylar-Alum. 2 sides (23 layers) + Dacron net spacers (24 layers)	23	0.50	5.52
8	Retest of No. 7			
9	¼ mil Mylar-Alum. 2 sides (23 layers) + Nylon tulle spacers (24 layers) + 1 mil Alum. Kapton on cold plate side.	24	0.50	2.44
10	½ mil Alum. Mylar (Dimplar)	8 layer pairs	0.75	1.03
11	Same as No. 10	8 layer pairs	0.85	0.91
12	¼ mil Mylar-uncoated	35	0.50	1.50
13	Same as No. 1 with rabbeted joint and support post per Figure 2-29.	35	0.50	
13A	Same as No. 13	35	0.50	
14	Retest of No. 13			
15	Same as No. 1 with center support	35	0.50	
16	Same as No. 1 with rabbeted joint	35	0.50	
16A	Retest of No. 16	35	0.50	
17	Same as No. 10 with center support	8 layer pairs	0.85	
18	Same as No. 10 with joint, post and stitching as in Figure 2-29.	8 layer pairs	0.85	
18A	Same as No. 18	8 layer pairs	0.85	
19	Retest of No. 18			
20	Retest of No. 18			
21	Two layers 1 mil Alum. Kapton Dimplar between 3 layers ½ mil crinkled Alum. Kapton.	5	0.312	1.16
22	Retest of No. 21			
23	¼ mil gold-coated Mylar (crinkled)	34	0.50	1.84
24	¼ mil gold-coated Mylar-crinkled	24	0.625	0.98
25	Same as No. 24 with nine-1/8 inch dia. holes per sq. foot.	24	0.625	0.97
26	½ mil gold-coated Kapton-crinkled, with nine-1/8 inch dia. holes/sq.ft.	24	0.625	1.61
27	½ mil gold-coated Kapton-crinkled, with four-1/8 in. dia. holes/sq.ft.	19	0.3125	3.11

*All metallized film samples are so metallized on one side only except as noted.

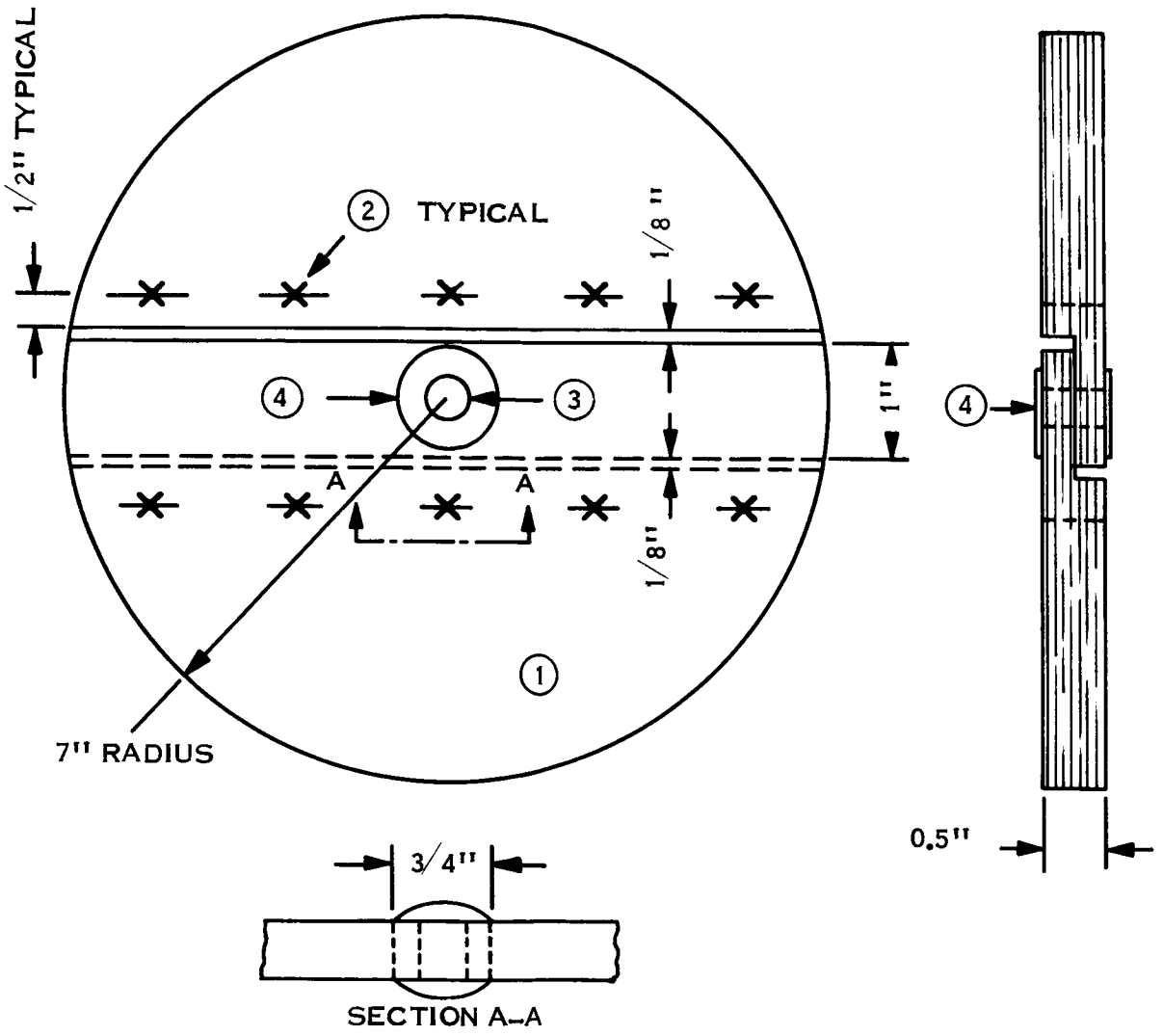

1. Insulation Blanket.
2. Single fiberglass thread stitch, stitch begins 1/2 inch from periphery, evenly spaced.
3. 1/4 inch dia. Nylon (Nylatch) post, cut 0.485±0.005 inch long (for NRC-2) (0.225 inch dia. post, 0.30 inch dia hole, cut 0.835 inch long (for Dimplar).
4. 1/2 inch dia. aluminized Mylar tape (Permacel) to retain post in sample blanket.

Figure 2-29. Rabbeted Joint and Support Post Configuration

Section 2.2 Candidate Insulation-Thermal Properties Evaluation

Subsection 2.2.1 Thermal Conductance Measurements

TEST RESULTS - BLANKET MATERIALS

Table 2-25 presents the test results for the blanket material evaluation.

Insulation Blanket Materials (Test No. 1 thru 6, 10, 11, 12, 23 and 24)

Aluminized Mylar (NRC-2) - Sample No. 1, 1A, 2, and 6 consisted of 35 NRC-2 layers at a one-half inch thickness. Sample No. 6 was deviated by the use of 2 layers of aluminized Kapton on the cold side. The average NRC-2 conductivity was 4.0×10^{-5} Btu/hr-ft-^{o}F, with the deviation being approximately $\pm$ 25%. The deviation is possible due to the hand wrinkling that was added to the production crinkling normally applied to NRC-2. Sample 3, with a greater depth of wrinkling, had a low heat flow value but resulted in a higher heat cunductivity because of its greater thickness. It is not included in the average value for NRC-2 conductivity.

Tin-coated Mylar (Sample No. 4) - The heat flow rate through this material was nearly twice the average of the crinkled aluminum-coated specimens and, consequently, tin-coated material was rejected as a potential insulation candidate.

Embossed Aluminized Mylar - Sample No. 5, although providing a density of 128 layers per inch (2.79 lb/ft^3), yielded a low value of conductivity. If similar material with deeper embossing to give lower density would not have a degraded conductivity, such material could have been considered a likely candidate; however, General Electric experience with embossed material indicates the inconsistency with which sufficient depth is obtained.

Aluminized Mylar (Dimplar) - Test Nos. 10 and 11 showed that this material like other multilayer insulation is sensitive to compression. The measured conductivity times density ($k \times \rho$) value for eight layer pairs at 0.85 inch thickness was 9.5×10^{-5} Btu lb/hr-ft^4-^{o}F, in contrast to 5.9×10^{-5} Btu lb/hr-ft^4-^{o}F for NRC-2, using average values of k and ρ. If 1/4-mil reflectors are used and conductivity increases by 10 percent, as stated in Dimplar literature, the $k \times \rho$ product for Dimplar would reduce to 8.0×10^{-5} Btu lb/hr-ft^4-^{o}F, including the takeup effect of the dimpled separator.

Gold coated Mylar (Sample No. 23) - This sample showed that vapor deposited gold on 1/4 mil Mylar produced a thermal conductivity that was slightly lower than NRC-2 for similar layer densities. The $k\rho$ valve was higher, probably due to the high density of gold compared to aluminum. Sample No. 24 was die crinkled, as contrasted to the hand wrinkling for Sample 23, resulting in a less dense blanket with superior thermal performance. Sample 24 had the same heat flow as No. 23, despite 10 less layers. This reduced the $k\rho$ product to 4.42×10^{-5} from 6.77×10^{-5} Btu-lb/hr-ft^4-^{o}F.

Uncoated Mylar (Sample No. 12) - The thermal conductivity of the uncoated Mylar specimen was 20 times greater than that for the wrinkled aluminum multilayer material.

Spacers

Test No. 7 and 9 evaluated the desirability of Dacron and Nylon spacers, respectively. The Dacron-spaced aluminized Mylar resulted in the lowest conductivity of any specimen tested, but the weight of the spacers produces an extremely high density. The Nylon, although about half as dense, produced about a 60 percent increase in conductivity. Considering the relatively high ρk product, insulations containing Nylon or Dacron spacers were not considered further.

Effect of Warm Side Temperature

Test No. 8, 14, 19 and 20 were run to show the effect of a change in warm side temperature on different specimens. These tests showed that effective emittance is more constant with temperature for this predominantly radiative material than is effective conductivity. With the exception of Test No. 8, which is of questionable accuracy due to test anomalies, all of the tests show that the effective emittance increases somewhat as the warm side temperature is reduced. The reversal of this trend between Test No. 19 and 20 is believed within the noise of data accuracy.

Table 2-25. Test Result-Blanket Materials

Sample/ Test No.	Brief Description	Test Temp. (°F) T_H	Test Temp. (°F) T_c	Heat Flow (Btu/hr-ft^2)	k Conductivity (Btu/hr-ft-°F)	ρk ($\times 10^5$) Btu-lb/ hr-ft-°F	ϵ Emittance
1	35 layers-NRC-2	73	-322	0.304	3.2×10^{-5}	4.86	0.0022
1A	35 layers-NRC-2	71	-322	0.472	5.0×10^{-5}	7.25	0.0035
2	35 layers-NRC-2	71	-323	0.369	3.9×10^{-5}	5.69	0.0027
3	35 layers-NRC-2	72	-323	0.317	5.7×10^{-5}	4.89	0.0023
4	35 layers-Tin on Mylar	68	-322	0.686	7.3×10^{-5}	23.50	0.0052
5	51 layers-Emb. Alum.	68	-322	0.391	3.3×10^{-5}	9.21	0.0030
6	35 layers-NRC-2/ Alum. Kapton	72	-323	0.382	4.0×10^{-5}	6.16	0.0028
7	23 layers-NRC-2/ Dacron	73	-322	0.303	3.2×10^{-5}	17.70	0.0022
8	Retest of No. 7	-3	-322	0.128	1.7×10^{-5}	9.27	0.0017
9	24 layers-NRC-2/ Nylon/Al. Kapton	68	-323	0.476	5.1×10^{-5}	12.40	0.0036
10	8 layer pairs-Dimplar	70	-321	0.819	13.1×10^{-5}	13.50	0.0061
11	8 layer pairs-Dimplar	72	-323	0.586	10.5×10^{-5}	9.50	0.0043
12	35 layers-Mylar (uncoated)	72	-322	8.310	88.0×10^{-5}	132.40	0.0609
14	Retest of No. 13	-4	-322	0.216*			0.0042
19	Retest of No. 18	-24	-323	0.628*			0.0147
20	Retest of No. 18	-43	-323	0.513*			0.0144
23	34 layers-Gold on Mylar	71	-324	0.349	3.7×10^{-5}	6.77	0.0026
24	24 layers-Gold on Mylar	76	-323	0.345	4.5×10^{-5}	4.42	0.0025

* Heat flow per 0.695 sq. ft.

Section 2.2 Candidate Insulation-Thermal Properties Evaluation

Subsection 2.2.1 Thermal Conductance Measurements

TEST RESULTS - CONFIGURATIONS

Table 2-26 presents the test results for the evaluation of joints, supports and vent holes.

Insulation Joints and Supports

NRC-2 Blankets - Test No. 13, 13A, 15, 16 and 16A were performed to demonstrate the amount of heat flow perturbation to the basic NRC-2 material caused by a particular type joint and a specific type of insulation support. In order to extract the amount of thermal penalty caused by each type perturbation, the thermal performance for the joint and support post tests is presented in "as-measured" terms.

Test No. 16 and 16A gave an average heat flow of 0.342 Btu/hr. in the test apparatus for NRC-2 material incorporating only the joint shown on Figure 2-29. Using the average unperturbed NRC-2 conductivity of 4.0×10^{-5} Btu/hr-ft-^{o}F, from Aluminized Mylar (NRC-2), page 54, results in a calculated sample heat flow of 0.265 Btu/hr at average test conditions. The heat difference, 0.077 Btu/hr, is the joint thermal penalty. The test samples included 16 inches of joint length, and the joint penalty reduces to 0.058 Btu/hr-ft of joint at the tested temperature and thickness conditions. Test No. 15, including only a center post in the NRC-2 test samples, gave a heat flow of 0.308 Btu/hr in the apparatus at a warm side temperature of 69^{o}F. This heat flow corrects to 0.316 Btu/hr at 72^{o}F to make it comparable with the other data points. Subtracting 0.265 Btu/hr from 0.316 Btu/hr results in a 0.051 Btu/hr difference. Each of the two simultaneously tested samples contained a post, and the post penalty reduces to 0.026 Btu/hr-post. The test apparatus has a main heater area of 0.695 ft^2 so the unperturbed calculated average NRC-2 heat flow of 0.265 Btu/hr results in 0.381 Btu/hr-ft^2. Adding the heat flow penalties of 0.058 and 0.026 Btu/hr, respectively, for a foot of joint and a post results in a calculated overall loss of 0.47 Btu/hr-ft^2. This is for an insulation panel containing 35 layers of NRC-2 material in 1/2 inch thickness, including one support post and one foot of joint per square foot of surface area, when operated between the temperatures of 72 and -320^{o}F. The effective emittance for such a composite is 0.0034.

If the measured heat flow average of 0.342 Btu/hr, from Test No. 16 and 16A, is added to the penalty for posts*, a heat flow rate of 0.393 Btu/hr results. This compares favorably with the average rate of 0.396 Btu/hr from Test No. 13 and 13A. These latter tests were performed on samples that included both the joints and posts per Figure 2-29.

Dimplar Blankets - Test No. 17, 18, and 18A determined the heat flow penalty that the same type of support post and rabbeted joint would cause in Dimplar. Test No. 17, employing only the center post, yielded a heat flow through the apparatus of 0.520 Btu/hr for a specimen pair* that included a 0.30-inch diameter hole with a 0.835-inch-long, 0.225-inch diameter Nylon post. Compared

* Two samples are tested simultaneously in the apparatus.

to the unperturbed material, two posts added 0.125 Btu/hr after the heat flow of Test No. 17 had been corrected to the specimen temperature of 72°F for Test No. 11. This heat loss of 0.063 Btu/hr-post is three times the penalty measured with the NRC-2 due, in part, to the fact that the NRC-2 tests included a 0.25-inch hole for the post instead of the 0.30-inch hole in the Dimplar.

Test No. 18 gave an apparatus heat flow of 1.073 Btu/hr for the Dimplar perturbed by both the post and joint. Combining this value with Test No. 17, results in a calculated joint perturbation of 0.40 Btu/hr-foot of joint. For an insulation panel design of one post and 1 foot of joint per square foot area, this combination, with eight layer pairs of Dimplar, would yield a heat loss of 1.05 Btu/hr-ft^2. Thus, eight layer pairs of Dimplar in an attached panel should result in over twice the heat flow of an insulation panel of 35 layers of NRC-2.

Test No. 18A was performed to confirm the results of Test No. 18, with one difference. The hole for the attachment post was reduced to 0.25 inch in an endeavor to improve the performance of this configuration. The reduced hole size resulted in a 57 percent reduction in heat flow. Combining Test No. 18A with Test No. 17 data, gives a joint perturbation of only 0.059 Btu/hr-ft of joint and a composite heat flux of 0.71 Btu/hr-ft^2 for this configuration with one post and 1 foot of joint per square foot.

Blanket Vent Holes

Test No. 25, 26 and 27 utilized goldized Mylar and Kapton blankets to determine the effects of vent holes.

Comparing the results for Test No. 25 versus the unperforated goldized Mylar (Test No. 24) indicates no appreciable effect due to vent holes. Unfortunately, Test No. 26 and 27, employing goldized Kapton, are not very representative. Due to gold being partially removed from Sample No. 26 during crinkling, its thermal performance was poor. Furthermore, an effort to reduce the crinkling for Sample No. 27 produced a more dense stack-up, resulting in an unsatisfactory ρk factor.

Table 2-26. Test Results-Configurations

Sample Test No.	Brief Description	Test Temp. (^{o}F) T_H	Test Temp. (^{o}F) T_c	Heat Flow (Btu/hr-ft^2)	k Conductivity (Btu/hr-ft-^{o}F)	ρk ($\times 10^{-5}$)	ϵ Emittance
13	No. 1 with joint & post	73	-322	0.380*			0.0040
13A	No. 1 with joint & post	73	-321	0.412*			
15	No. 1 with center post	69	-322	0.308*			
16	No. 1 with joint only	70	-322	0.353*			
16A	Retest of No. 16	71	-318	0.330*			
17	No. 10 with center post	69	-323	0.520*			
18	No. 10 with joint & post	73	-323	1.073*			0.0112
18A	No. 10 with joint & post	72	-323	0.610*			
21	Dimplar/Alum. Kapton	150	73	1.70	57.4×10^{-5}	65.90	0.0170
22	Retest of No. 21	151	72	4.57	66.0×10^{-5}	76.80	0.0152
25	24 layers-Vented Gold Mylar	73	-323	0.344	4.5×10^{-5}	4.39	0.0025
26	24 layers-Vented Gold Kapton	72	-322	0.723	9.6×10^{-5}	15.40	0.0053
27	24 layers-Vented Gold Kapton	69	-321	0.850	5.7×10^{-5}	17.60	0.0064

*Heat flow per 0.695 sq ft

SECTION 2.0
TECHNICAL DISCUSSION

2.3 CANDIDATE INSULATION—STRUCTURAL PROPERTIES EVALUATION

Section 2.3 Candidate Insulation - Structural Properties Evaluation

TEST OBJECTIVES/SCOPE

Multilayer thermal insulation blankets for interplanetary vehicles are, by design, loosely packed and light weight with low conductive and radiative heat transfer characteristics. Launch and flight operations, for such vehicles, will expose the insulation blankets to a variety of structural and mechanical loadings. Effective thermal performance requires that the insulation system be capable of physically withstanding these loads without significant degradation. Consequently, a series of tests were conducted to evaluate the structural and mechanical capabilities of multilayer metallized film insulation blankets.

The structural properties evaluation consisted of simulated exposures to pertinent launch and flight mechanical loadings. The tests encompassed the following three major categories:

Rapid Depressurization

Air is trapped between layers of the insulation blanket during manufacture and installation. The rapid reduction of ambient pressure during early flight could potentially cause the entrapped air to balloon the blankets. Ballooning is undesirable because the membrane forces produced may tear the blanket at fasteners, block sensor fields of view, change antennae patterns or interfere with deployment of components. Hence, ballooning must be controlled. The purpose of the rapid depressurization tests was to determine the magnitude of the ballooning problem and to develop effective solutions, as necessary. The program was conducted in two parts: (a) an evaluation of the ballooning problem and (b) an assessment of the effectiveness of blanket perforations for venting. In conjunction with the rapid depressurization tests, various blanket installation and joining configurations were evaluated.

Shock, Acoustic and Vibration Loadings

Planetary vehicles experience intensive shock, acoustic and vibration environments during the launch mode and subsequent propulsion system operations, e.g. midcourse corrections and orbit insertion. Therefore, metallized film insulation blankets were subjected to two separate series of dynamic mechanical tests simulating flight environments. The test samples were subjected to ethylene oxide decontamination between the two test series to determine if the intervening treatment had any debilitating effects.

Long Term Vacuum Environment

The planetary vehicle thermal insulation material, when assembled into blankets, must be capable of surviving vibration, caused by firing an orbit insertion motor, after several months of exposure to space vacuum and temperature conditions. A test program was conducted during which insulation blankets were exposed to a simulated space vacuum ($\sim 10^{-8}$ Torr) and temperature ($\sim -280^{\circ}$F) for sixty days. At the conclusion of the exposure period, and while still under vacuum and low temperature conditions, the specimen was vibrated at levels approximating those produced by a liquid rocket engine.

Section 2.3 Candidate Insulation - Structural Properties Evaluation

SUMMARY OF RESULTS

Rapid Depressurization Tests

a. Ballooning is a function of blanket size: 2x6 foot blankets ballooned only slightly and showed only minimal damage due to ballooning while larger blankets were more excessively damaged.
b. Ballooning is reduced by removal of stitches.
c. Ballooning varies with the ratio of interlayer air volume to edge vent area (V/A).
d. Four 1/8-inch diameter vent holes per square foot of surface area, are sufficient to prevent ballooning damage of 4x10-foot blankets.
e. The step (rabbet) type insulation joint is satisfactory.
f. "Tinger" fasteners, employing a 1 3/8-inch diameter base Velcro hook and pile tape, satisfactorily supported the insulation.

Shock, Acoustic and Vibration Tests

a. Acoustic and vibration loadings did not cause any significant damage to the insulation blankets.
b. Shock loadings caused the blankets to tear at the support post holes. Subsequent enlargement of the holes, from 0.250 inches to 0.296 inches, eliminated this problem.
c. ETO decontamination had no effect on the ability of the insulation to withstand the environmental loads, nor did the testing effect the ability of the materials to withstand decontamination.
d. The integrity of the joints and post attachments was maintained in the presence of shock, acoustic, and vibration loads.

Long Term Vacuum Exposure

Sixty day exposure to space vacuum and temperature conditions, followed by vibration loadings of approximately 4.0G RMS, produced no apparent physical damage to the insulation and no measurable change in thermal performance.

Section 2.3 Candidate Insulation - Structural Properties Evaluation

Subsection 2.3.1 Rapid Depressurization Tests

TEST PROCEDURE

Two series of depressurization tests were conducted. The initial tests were designed to assess the magnitude of the problem of insulation ballooning during early flight, while the second series determined the value of perforating the insulation as a means for minimizing the effects of ballooning.

The procedures for both series of tests were similar. Insulation blankets were mounted vertically in the test chamber, and the chamber was purged with dried air to minimize condensation during subsequent depressurization. The desired depressurization profile was accomplished through manual control of air flow between the test chamber and an adjacent evacuated chamber (see TEST APPARATUS). The depressurization profile was equivalent to a typical Saturn V ascent trajectory: from 760 Torr to 50 Torr in about 90 seconds.

Blanket expansion during depressurization was recorded via motion picture camera. Two insulation blankets were tested simultaneously, since the camera could view only two blankets. After testing, blankets were inspected for fit, insulation tears, loose fasteners, permanent distortion and general soundness.

Prior to the second series of depressurization tests, static blanket load tests were conducted to determine the amount of deflection (expansion) to be expected for a given pressure difference. This indicated the pressure within the blanket during the depressurization test. The unloaded deflection of horizontally hung test blankets was measured. Then, weights of paper, in 1/2 lb increments, were evenly distributed over the upper insulation face until a total load of 3.0 lb was reached. Deflection of the blanket was measured after each 1/2 lb increment. Deflection measurements were also taken during load removal and subsequent to the second series of depressurization tests to ascertain the occurrence of permanent deformation. A one-half pound load on a 4x10 ft blanket results in a 0.0125 pound per square foot pressure.

Section 2.3 Candidate Insulation - Structural Properties Evaluation

Subsection 2.3.1 Rapid Depressurization Tests

TEST APPARATUS

The test chamber for the depressurization tests was the air lock of a 32x54 ft thermal vacuum chamber. Figure 2-30 depicts the test facility. The main vacuum (32x54 ft) chamber and its air lock (depressurization test chamber) are connected with a 6 inch pipe and bleeder valve. The desired depressurization chamber pressure was provided by manually opening the 6 inch line to permit air lock pressure to dump into the evacuated main chamber.

Two blanket frames are vertically suspended in the air lock. A 64 frame per second motion picture camera was focused on a scale and clock behind the specimens. The camera and blankets were carefully positioned to minimize parallax errors and a geometric correction factor was applied to the camera data to account for the remaining error.

An x-y plotter was used to record air lock pressure versus time with the desired pressure profile being preplotted on the x-y chart paper. Test chamber lights, clock, camera and x-y plotter were all connected to a single control switch, and their operations synchronized. Figure 2-31 shows portions of a test film: Part A shows no deflection at T=0, and Part B shows expansion about half-way through the depressurization period.

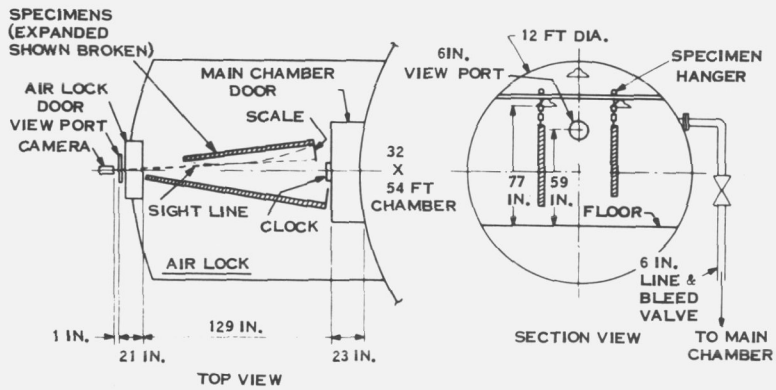

Figure 2-30. Depressurization Test Facility

A

T = 0 sec

B

T = 40 sec

Figure 2-31. Film Segment-Depressurization Test

Section 2.3 Candidate Insulation - Structural Properties Evaluation

Subsection 2.3.1 Rapid Depressurization Tests

TEST SAMPLES

Blanket Materials

The basic insulation material for the depressurization tests was aluminized Mylar (NRC-2). The NRC-2 was selected because it is representative of the candidate materials and no major effect of material on expansion was considered likely.

The thermal blankets evaluated in the initial depressurization tests consisted of 35 layers of NRC-2, with a surface layer of 1-mil Teflon (FEP), all loosely stitched together with fiberglass thread. Four insulation blankets were tested: 2x6 feet, 3x7 feet, 4x8 feet and 4x10 feet. The stitches were removed from the 4x8 foot blanket when it became evident that stitching increased the likelihood of tearing during depressurization.

The blankets for the second series of tests consisted of 23 layers of die-crinkled NRC-2 with a 2-mil Kapton cover sheet. These blankets were all 42-1/8 x 114-1/2 inches in size and were perforated. Each blanket incorporated a step joint. A venting analysis, described in Reference 6, predicted that satisfactory venting of 4 foot wide blankets could be accomplished within the range of 4, 9 or 16 holes (1/8 inch diameter) per square foot. The test blankets were perforated accordingly.

Table 2-27 describes the thermal blankets tested during both depressurization series.

Blanket Mountings

Figure 2-32 depicts the blanket support frame employed for the initial depressurization tests. The frame is capable of supporting any of the blanket sizes tested, although only one blanket per frame was tested at any one time. Nylon (Nylatch) fasteners were used to mount the blankets in the frame. The fasteners were spaced, at 6 inch intervals, around the blanket periphery; the 1/4 inch diameter fasteners reducing the edge vent area by about 4 percent. Flat frame panels were employed for simplicity, rather than curved panels which would more closely simulate vehicle surfaces. The stretching of layers due to expansion is nearly the same for flat and curved panels, i.e. the arc length of a layer that expanded 1/2 inch over an originally flat 10 foot span is 0.36 percent greater, in contrast to an expansion of 1/2 inch for a panel of 10 foot span originally curved to a six foot radius whose arc length becomes 0.44 percent greater. The frame "edge plate" (Figure 2-32) simulated edge vent area blockage due to butting blankets and structures.

The support frame for the second series of depressurization tests is shown in Figure 2-33. "Tinger" fasteners, developed during this program, were used to mount the blankets in the frame. The Tinger fastener, shown in Section YY of Figure 2-31, consists of an approximately 1/4 inch diameter Nylon mast, undercut at the top to accept a retainer washer. One inch diameter Velcro "hook" material is cemented to the mast base. A corresponding square patch

of Velcro "pile" is cemented to the frame. In essence, the Tinger holds the insulation between base and retainer washer, and the hook and pile holds the Tinger in place. The Tinger fasteners are employed around the blanket periphery and, for Blanket No. 7 only, along a center span as shown in Figure 2-33. A step joint was incorporated around the periphery of the blanket.

Table 2-27. Depressurization Test Specimens

Blanket No.	Material	Size (ft)	Stitching	Vents per ft^2	Fastener Support
1	NRC-2/Teflon	2x6	yes	none	peripheral
2	NRC-2/Teflon	3x7	yes	none	peripheral
3	NRC-2/Teflon	4x8	no	none	peripheral
4	NRC-2/Teflon	4x10	yes	none	peripheral
5	NRC-2/Kapton	4x10*	no	4	peripheral
6	NRC-2/Kapton	4x10*	no	9	peripheral
7	NRC-2/Kapton	4x10*	no	4	peripheral & center span
8	NRC-2/Kapton	4x10*	no	16	peripheral

* approximate; actual size: 42-1/8 x 114-1/2 inches.

FOLDOUT FRAME 2

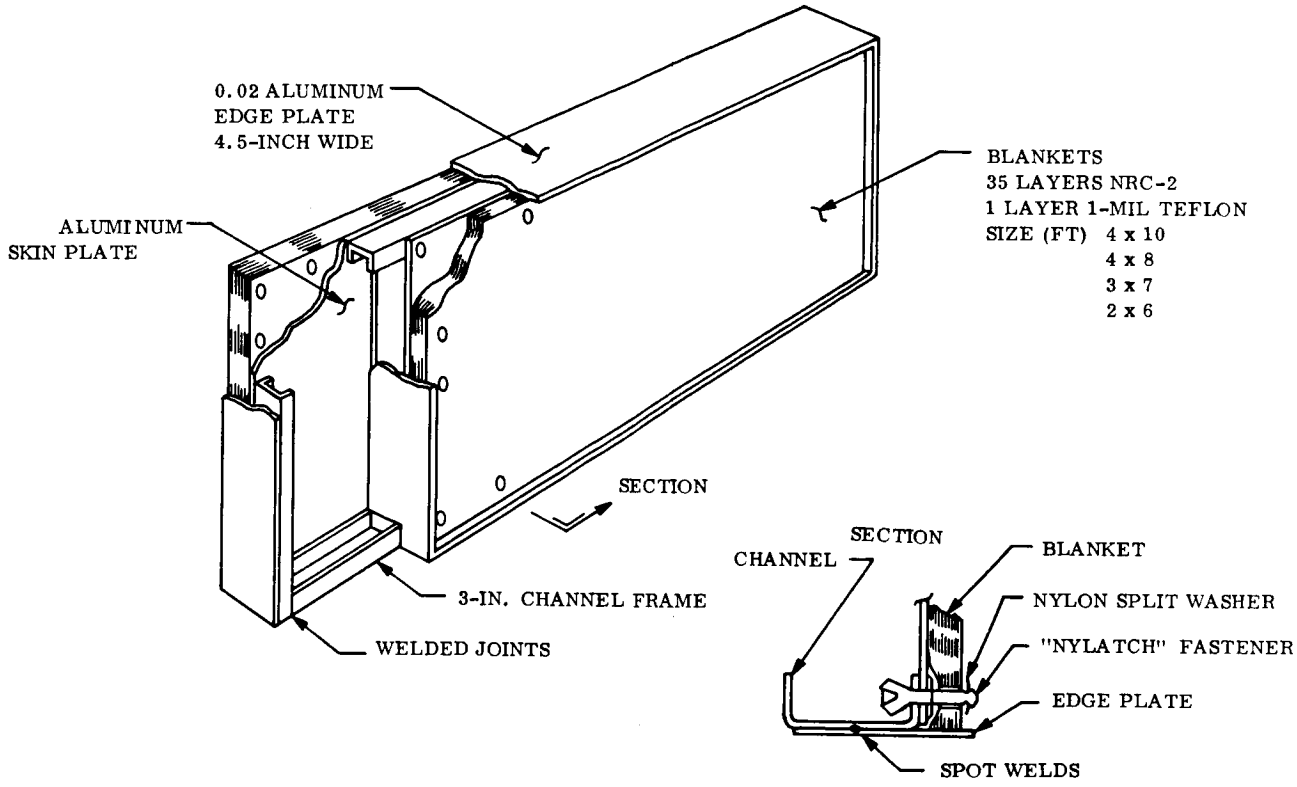

Figure 2-32. Blanket Support Frame - Initial Test

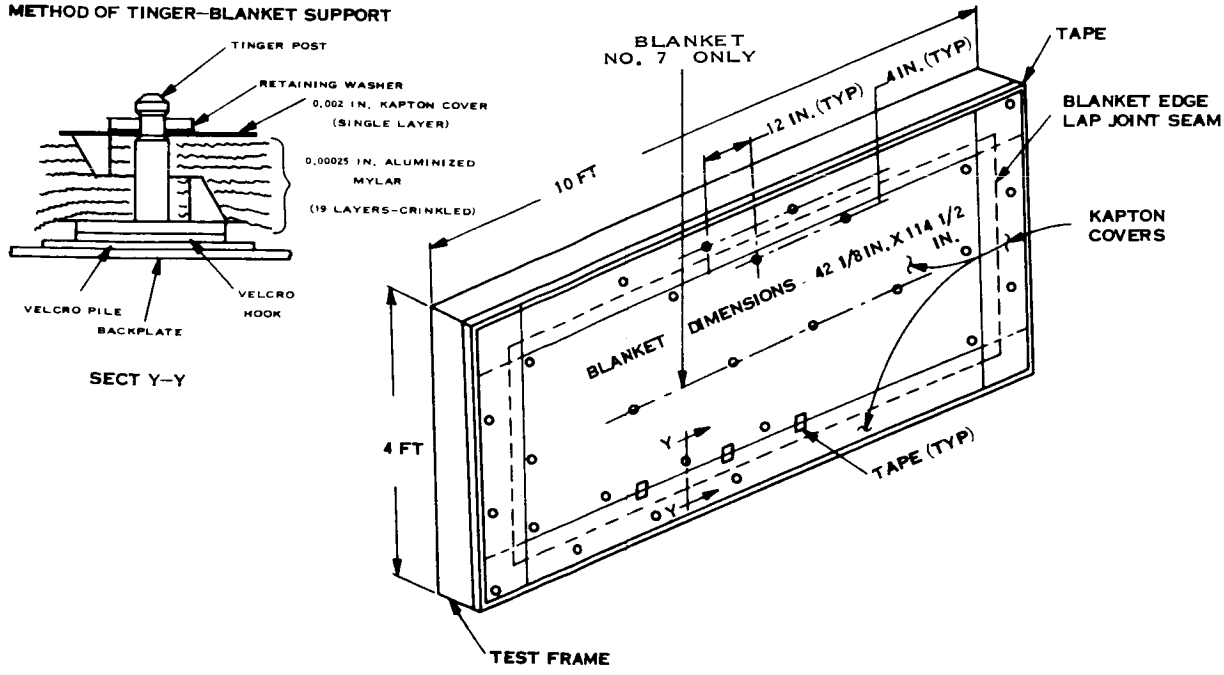

Figure 2-33. Blanket Support - Second Test

Section 2.3 Candidate Insulation - Structural Properties Evaluation

Subsection 2.3.1 Rapid Depressurization Tests

TEST RESULTS

Initial Test Series

By close examination of the motion pictures and the application of parallax correction factors, blanket expansion versus time data was obtained and is superimposed on the pressure-time profiles in Figures 2-34 and 2-35. The figures show close correlation between the desired and actual pressure profiles and illustrate that the greatest expansion rate corresponds (roughly) to the greatest depressurization rate, lagging by about 15 seconds. Figure 2-36, a plot of deflection versus pressure, clearly shows the effect of blanket size on expansion and that the absence of stitching increases vent area and, hence, reduces expansion (see Blanket No. 3). Figure 2-37 shows the interlayer volume-vent area ratio against the maximum deflection, for each blanket size.

Table 2-28 presents the test results, describing expansion data and the results of visual inspection. The 4x8 foot blanket, without stitching, had less extensive damage than either the 4x10 or 3x7 foot blankets. The smallest blanket (2x6 foot) was least damaged. In all cases, slight permanent deformation of the Teflon cover sheets was noted.

Second Test Series

The depressurization expansions for the perforated blankets in the second test series are plotted in Figures 2-38 and 2-39. The maximum expansion of each test blanket is shown in Figure 2-40.

Results of the static loading tests indicate that the minimum blanket loading, i.e. loading caused by its own weight when held horizontally, produced more deflection (between 1.0 and 3.0 inches) than was observed during depressurization with the blanket held vertically. Blanket weight results in a loading of about 0.05 pounds per sq. foot. Thus, actual venting pressure differential is less than 0.05 psf.

Visual post-test examination revealed no degradation of any of the blankets due to depressurization. No permanent stretching of the Kapton cover sheet occurred. The integrity of the step joint and Tinger fasteners was maintained throughout the test.

Table 2-28. Test Results

Blanket Size (ft)	Thickness at Stitches (inches)	Maximum Ballooning at Center (inches)	Final Condition of Blanket
4x10	1/4	6.3	Poor - extensive tears
4x8	No stitches 1/2 at posts	2.5	Fair - some tears
3x7	1/2	4.2	Poor - extensive tears
2x6	1/2	0.8	Good - tears on back stitches

FOLDOUT FRAME 1

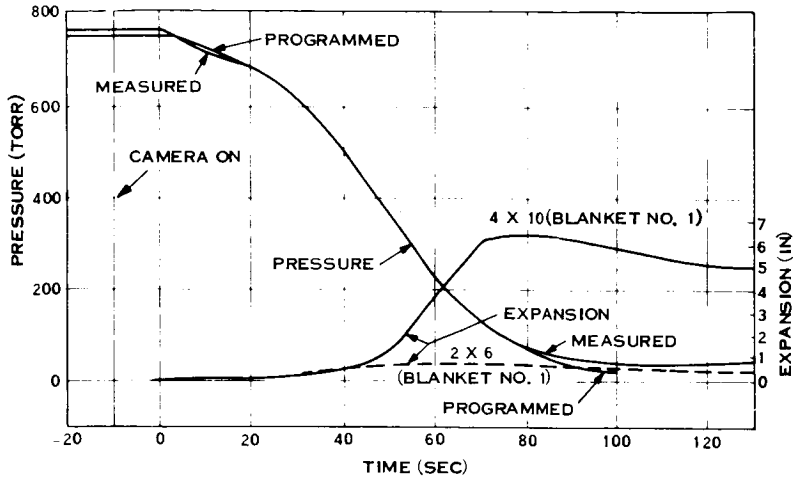

Figure 2-34. Depressurization Profile, First Series

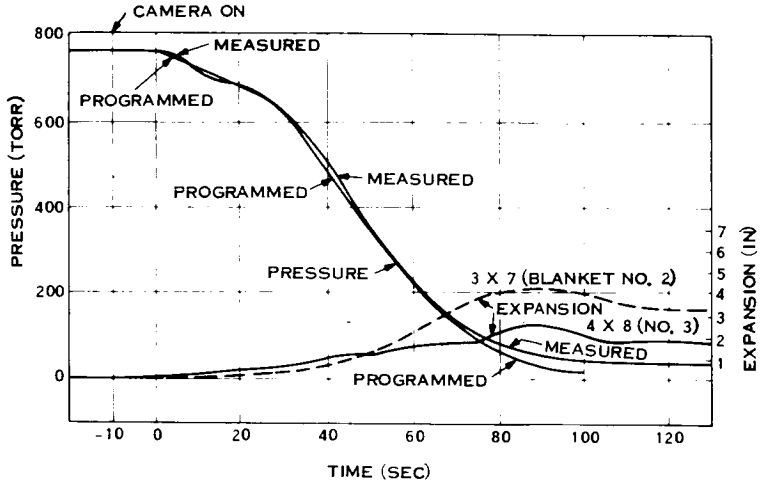

Figure 2-35. Depressurization Profile, First Series

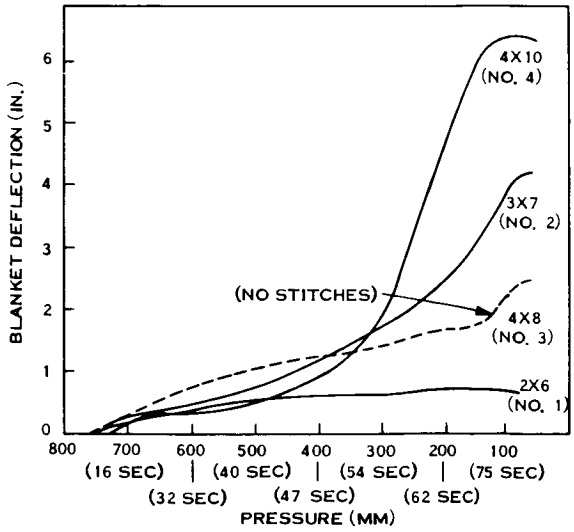

Figure 2-36. Blanket Deflection versus Pressure

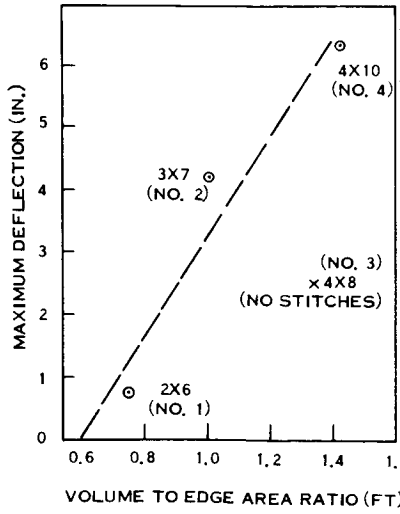

Figure 2-37. Maximum Deflection

FOLDOUT FRAME 2

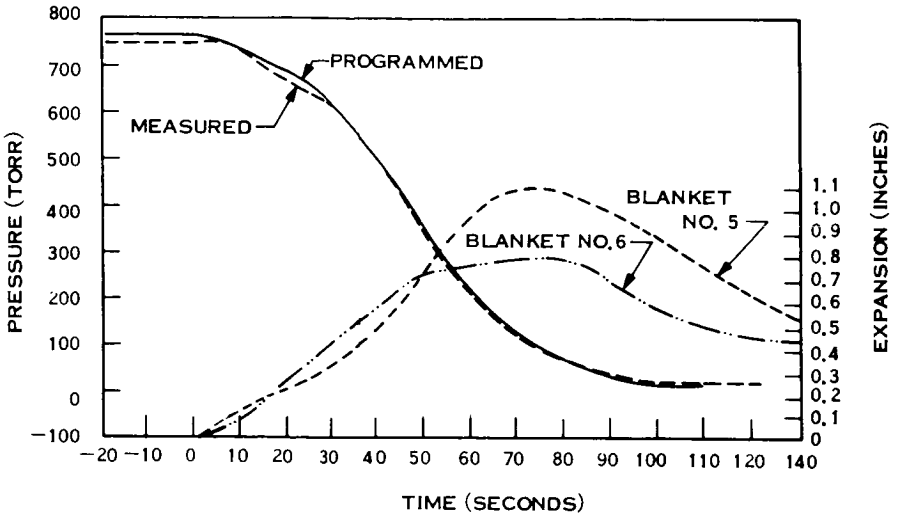

Figure 2-38. Depressurization Profile, Second Series

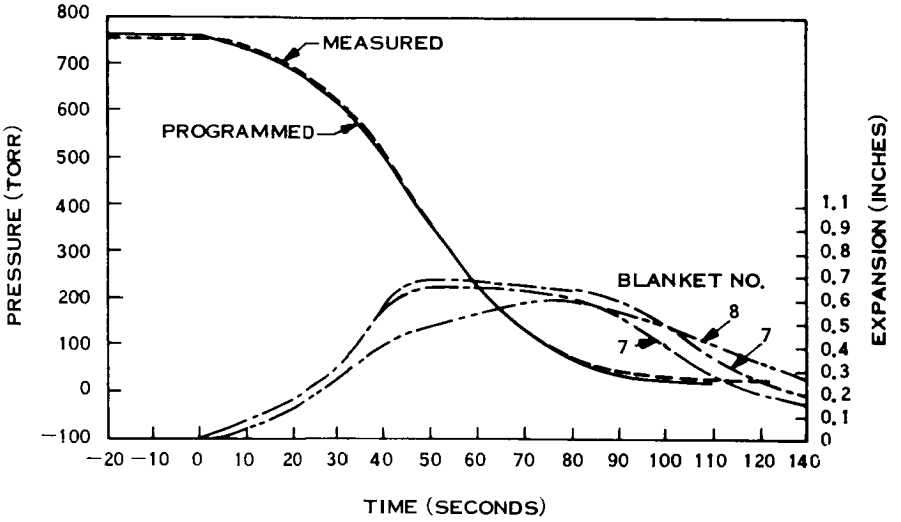

Figure 2-39. Depressurization Profile, Second Series

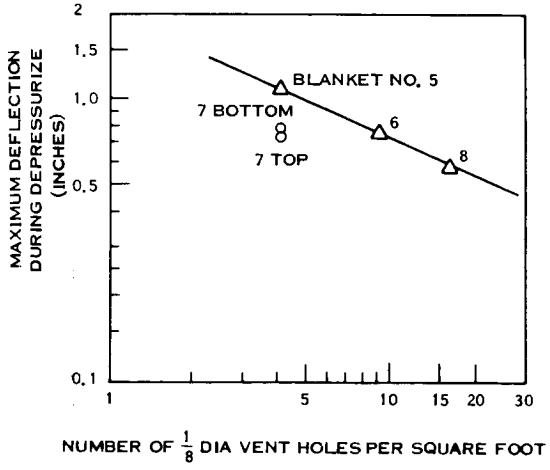

Figure 2-40. Maximum Deflection versus Number of Vent Holes per Square Foot

versus V/A

Section 2.3 Candidate Insulation - Structural Properties Evaluation

Subsection 2.3.2 Shock, Acoustic and Vibration Tests

TEST PROCEDURE/TEST FACILITIES

Tests were conducted to evaluate the capability of insulation blanket configurations to withstand the dynamic environments typically associated with the operation of space vehicles. The dynamic mechanical tests were conducted in two series, both consisting of shock, acoustic and vibration environments simulating flight conditions. The insulation specimens were exposed to six cycles of ethylene oxide decontamination between the two test series.

Shock Test

The insulation shock test was performed on an Avco model SM 220 shock machine at the Associated Testing Laboratories, Inc., Wayne, New Jersey, according to General Electric Test Procedure PVTIS 19. The insulation test fixture was mounted to the platform of the shock machine, and an accelerometer was mounted near the center of the base plate of the test fixture. The accelerometer was connected through a bandpass filter to a Memo Scope. The cutoff settings of the bandpass filter were 0.2 cps and 900 cps. The shock machine was then calibrated for the required shock pulse. The shock pulse approximated a one-half sine wave with a peak intensity of 200 g $\pm$ 10 percent and a time duration of 2 milliseconds $\pm$ 15 percent.

After calibration, the insulation blanket samples were mounted to the test fixture. The blanket samples were then subjected to one shock impact in a direction perpendicular to the test fixture base plate. The shock pulse recorded during the impact is shown in Figure 2-41. Post-test visual inspections were performed.

Acoustic Test

Following the shock test, the insulation blankets, mounted on the same test fixture, were exposed to acoustic excitation at Noise Unlimited, Inc., Somerville, New Jersey. Dummy blankets were installed on the test fixture and were exposed to approximately 30 minutes of high intensity noise for facility checkout. The test blankets were then installed. Figure 2-42 compares the excitation levels achieved versus the test objective. Although the test did not achieve the specified levels, particularly below 250 cycles per second, it is felt that the intent of the test was achieved. The average overall intensity was within 4 db of the desired 151.5 db level. This intensity was maintained for 7-1/4 minutes. Visual inspection was made after acoustic testing.

Vibration Test

After the acoustic exposure, the test fixture was installed in the General Electric Dynamic Simulation Laboratory at Valley Forge, Pa. on a MB Model C210 exciter. The insulation blankets were subjected to broad band random vibration in the vertical direction. A test level

of 15 g rms for a period of 120 seconds was maintained. Figure 2-43 shows the averaged response of six accelerometers. Dummy blankets were again employed for facility checkout and were exposed to 10 to 15 g rms for about 30 minutes.

Ethylene Oxide Decontamination Exposure

The insulation blankets were subjected to six 30 hour ethylene oxide cycles, per JPL Specification VOL-50503 ETS, following the first series of shock, acoustic, and vibration tests.

Second Series of Shock, Acoustic, and Vibration Tests

The same set of insulation blanket assemblies were subjected to a second series of mechanical excitation tests to determine if the intervening decontamination treatment had debilitating effects. These insulation assemblies, for the second series, included a number of tears at support post holes from prior testing and handling.

The second shock test was similar to the initial test. During the equipment checkout for the second test, a set of dummy blankets was installed and subjected to two shocks approximating 200 g each. The second acoustic and vibration tests exposures followed the same procedure as the initial series.

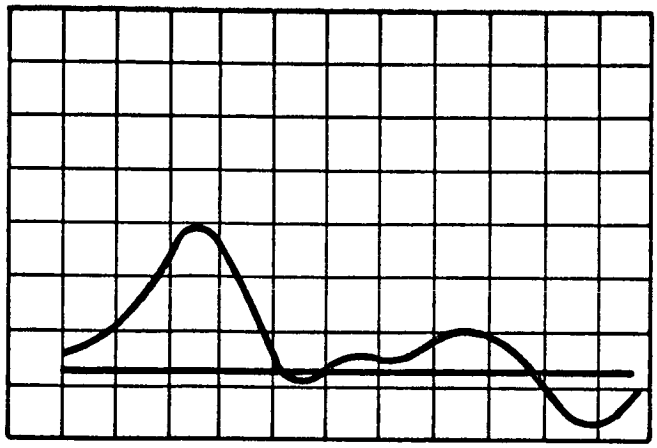

ACCELEROMETER SENSITIVITY:	0.735 PK MV/PK G
OSCILLOSCOPE VERTICAL SETTING:	50 MV/DIVISION (70G/DIVISION)
OSCILLOSCOPE HORIZONTAL SETTING:	0.5 MS/DIVISION
PEAK INTENSITY:	200G
TIME DURATION:	2 MS

Figure 2-41. Test Shock Pulse

FOLDOUT FRAME 2

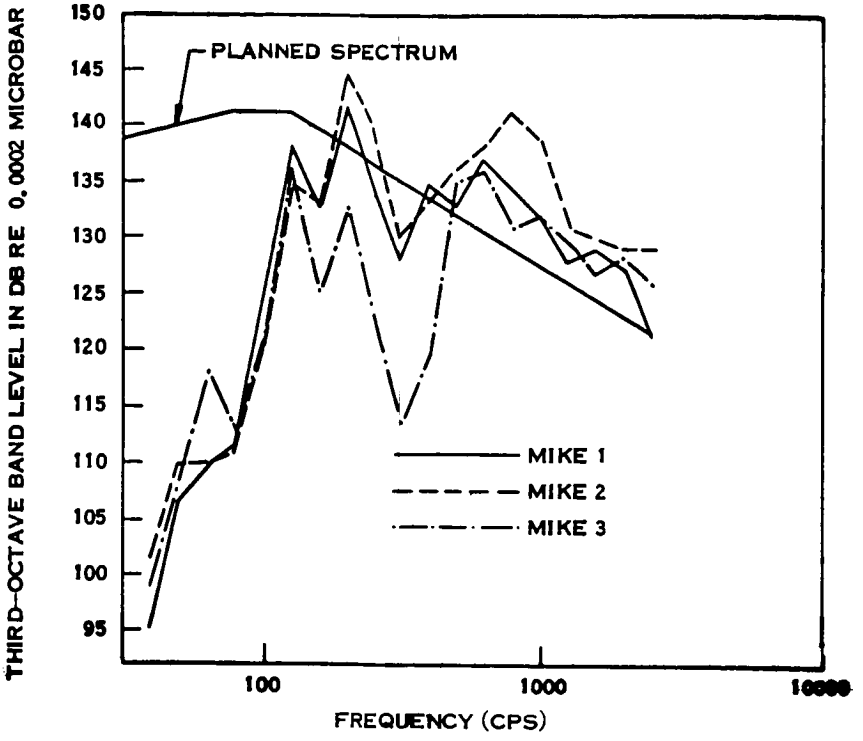

Figure 2-42. Acoustic Levels

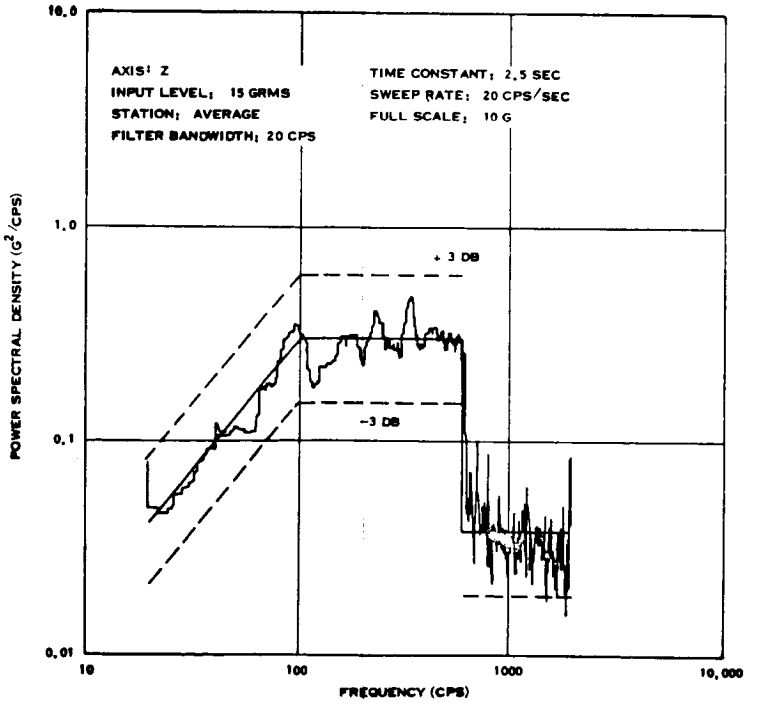

Figure 2-43. Vibration Levels

Section 2.3 Candidate Insulation - Structural Properties Evaluation

Subsection 2.3.2 Shock, Acoustic and Vibration Tests

TEST SAMPLES/APPARATUS

A 30 inch cubic test fixture was used for the shock, acoustic and vibration tests. The fixture, as depicted in Figure 2-44, was a cross-braced welded frame constructed of 4 inch square aluminum tubing and covered with aluminum skins. One face of the cube was attached to the test apparatus through a suitable adapter, leaving 5 faces for test specimens. No adapter was required for the acoustic tests. The insulation blanket specimens were attached to the frame with Tinger fasteners. The fastener holes in the insulation specimens were 0.250 inches in diameter. During the second shock test, the clear Mylar dummy blankets utilized 0.296 inch diameter fastener holes.

The insulation blanket specimens were as follows:

Side 1	Nineteen layers of 1/4 mil gold coated Mylar and one layer of 2 mil Kapton held with four fasteners.
Side 2	Same as Side 1 except 6 fasteners used.
Side 3 and 4	Two blankets, one of which covers 1-1/2 sides and the other 1/2 side. A step joint was used between the two. Both blankets used 19 layers of 1/4 mil gold coated Mylar with one layer of 2 mil Kapton. (Figure 2-45 shows sides 2 and 3 prior to test.)
Top	Ten layers of gold coated 1/2 mil Kapton and one layer of clear 2 mil Kapton with four fasteners.

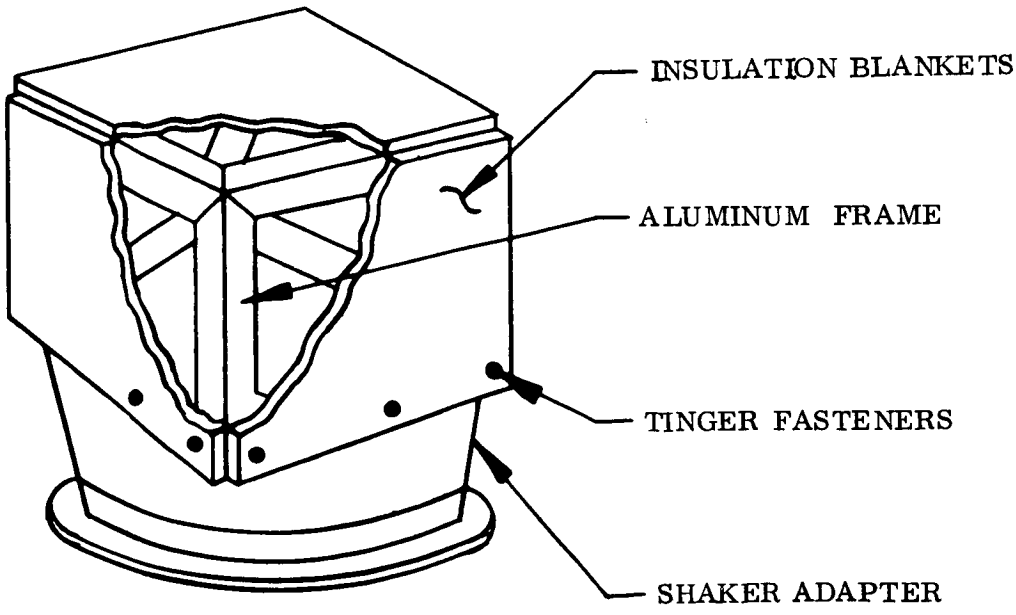

Figure 2-44. Dynamic Test Fixture

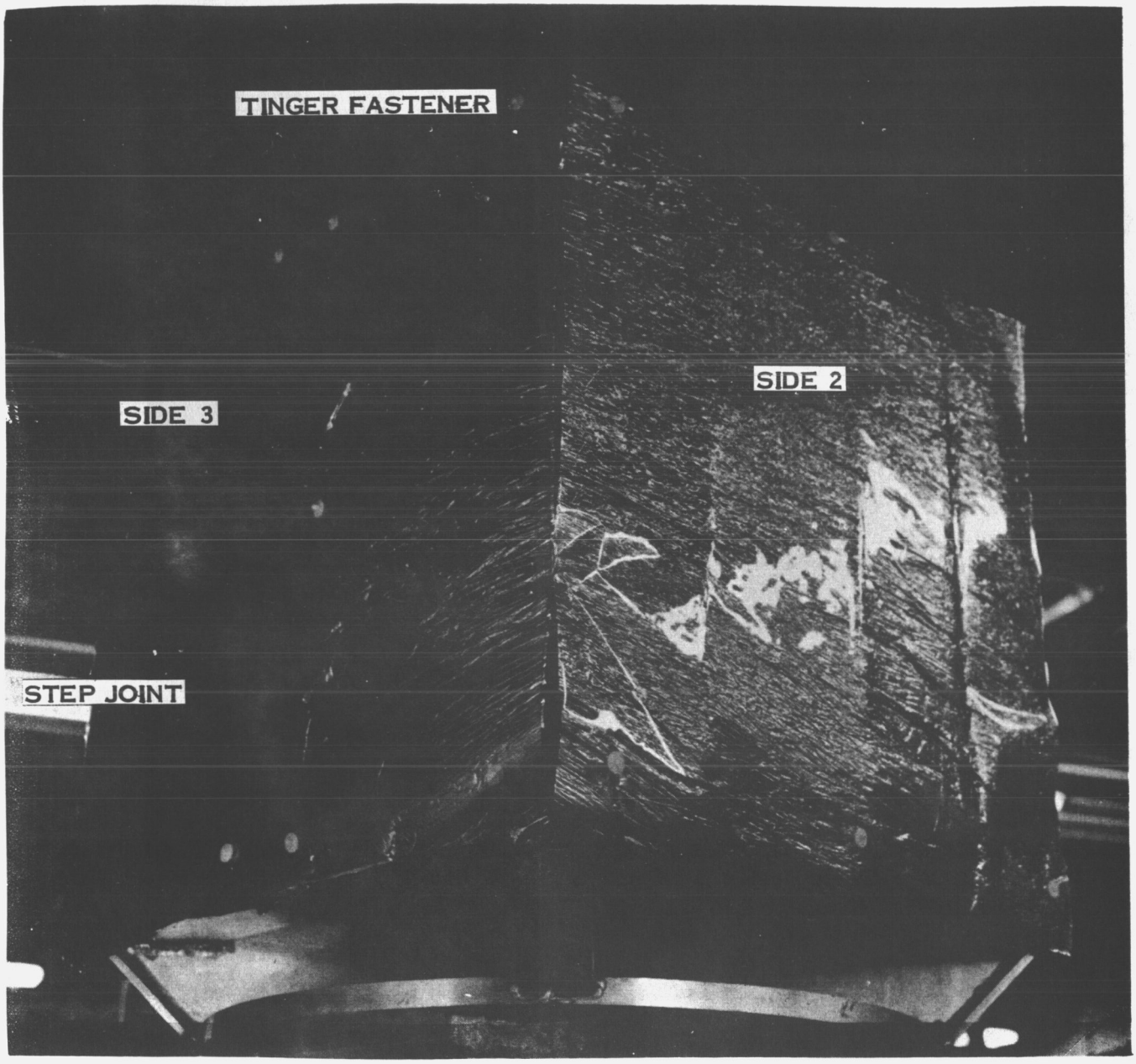

Figure 2-45. Insulated Dynamic Test Fixture

TEST RESULTS

Initial Series

Shock Test Results - The shock pulse to the insulation blanket samples was within the specified limits of 200 g ± 10 percent for 2 milliseconds ± 15 percent. Inspection after the shock test showed that some tears had developed at the support post holes in both the outer 2 mil Kapton cover sheet and in the 1/4 mil gold Mylar underlayers. Had these tears occurred on a flight vehicle, it is not likely that blanket performance would have been noticeably affected. However, the tears were sufficiently numerous to require remedial action to be taken. None of the attachment posts were dislodged.

Acoustic Test Results - Examination after the test did not reveal any additional damage to the insulation blankets beyond that sustained during the shock test. Also significant is the fact that dummy blankets, installed on the fixture for facility checkout, did not sustain any damage during approximately 30 minutes of high intensity noise.

Vibration Test Results - Inspection after test showed that insulation blanket damage had not increased beyond that noticed after the shock test. Neither were the dummy insulation blankets damaged during an approximate 30 minute exposure to 10 to 15 g rms during test facility checkout.

ETO Exposure

Examination of the gold coated Mylar and Kapton material after ETO decontamination did not reveal any signs of surface degradation. Restricted inspection between the multilayers, without removing the blanket fasteners, did not disclose any areas where materials were stuck together.

Second Series

Shock Test Results - The second shock test was similar to the initial test. During the equipment checkout for this second test, a set of dummy blankets made of clear Mylar was installed and subjected to two shocks approximating 200 g each. These dummy blankets had 0.296 inch diameter post holes instead of 0.25 inch holes in the gold coated blankets. Inspection of the dummy blankets after removal from the fixture did not reveal any tears in the Mylar. Thus enlargement of the post holes apparently eliminates the tearing problem.

After shock machine checkout to establish the desired pulse contour, the gold coated blankets were installed on the fixture and subjected to the 200 g shock. Examination after the second shock test did not indicate any noticeable enlargement of the previous tears. However, some post holes in one blanket had tears near the top that were not in evidence after the first test.

After the first test, the tears were primarily at post holes near the top of the fixture, tearing from the holes toward the adjacent edge. The tears at the new locations were also toward the adjacent edge. This leads to the conclusion that at the second installation, the blanket in question was inadvertently turned around so that untorn holes from the bottom were located at the top. During the second shock, these untorn holes then developed tears as the blanket material was restrained by the upper posts. No new tears appeared in the other blankets, nor did the tears that were there appear enlarged.

Acoustic and Vibration Test Results - The second acoustic test exposure followed the same procedure as the first, and no further damage to the insulation blankets was noted. Similarly, the second random vibration exposure did not produce any additional blanket damage or cause any of the fasteners to loosen.

Section 2.3 Candidate Insulation - Structural Properties Evaluation

Subsection 2.3.3 Long Term Vacuum Effects

TEST PROCEDURE

A test program was conducted during which multilayer thermal insulation blankets were exposed to a simulated space vacuum and temperature for 60 days.

Prior to starting the vacuum test, the vibration spectrum was run under ambient pressure and temperature conditions to check out operation of the vibration setup. The vibration levels simulated, as closely as possible, vibration levels measured in static tests of the LEMDE thrust chamber assembly. The total vibration time was 3-1/2 minutes. Visual inspection was performed prior to vacuum testing.

The vacuum level throughout the test was maintained between 1.6×10^{-7} and 2.5×10^{-8} torr. Test chamber shroud temperatures were below $-280^{\circ}F$ during the test. A reference internal temperature of the test model was held between $+36^{\circ}F$ and $+51^{\circ}F$. The total exposure to the test conditions was 1440 hours (60 days) before vibration excitation, plus four days for evaluation of thermal conductance change.

At the conclusion of the 60 day thermal vacuum exposure, and with vacuum and temperature conditions maintained, the model was again subjected to vibration. Figures 2-46 and 2-47 depict the power spectral density for the control accelerometer and accelerometer No. 2, respectively. Two accelerometers were used for redundancy purposes, in case of failure of one of the units. The frequency spectrums were essentially unchanged from the values recorded prior to the start of the vacuum exposure cycle. As may be seen from Figure 2-46, the overall vibration spectrum showed reasonable correlation with the specified levels. Several peaks at 160, 460, 550, 650, 730, and 840 cycles are considerably above the specification levels, and peaks at 900, 960, 1700, and 1800 cycles are below specification levels. These correspond to resonances in the test fixture, which were confirmed by a plot of acceleration/exciter voltage versus frequency.

Total vibration time for the vacuum vibration test was 5 minutes and 18 seconds, with 120 seconds at the specified test levels. Post-test, visual inspections were performed and the thermal conductance of the specimens was evaluated.

FOLDOUT FRAME 1

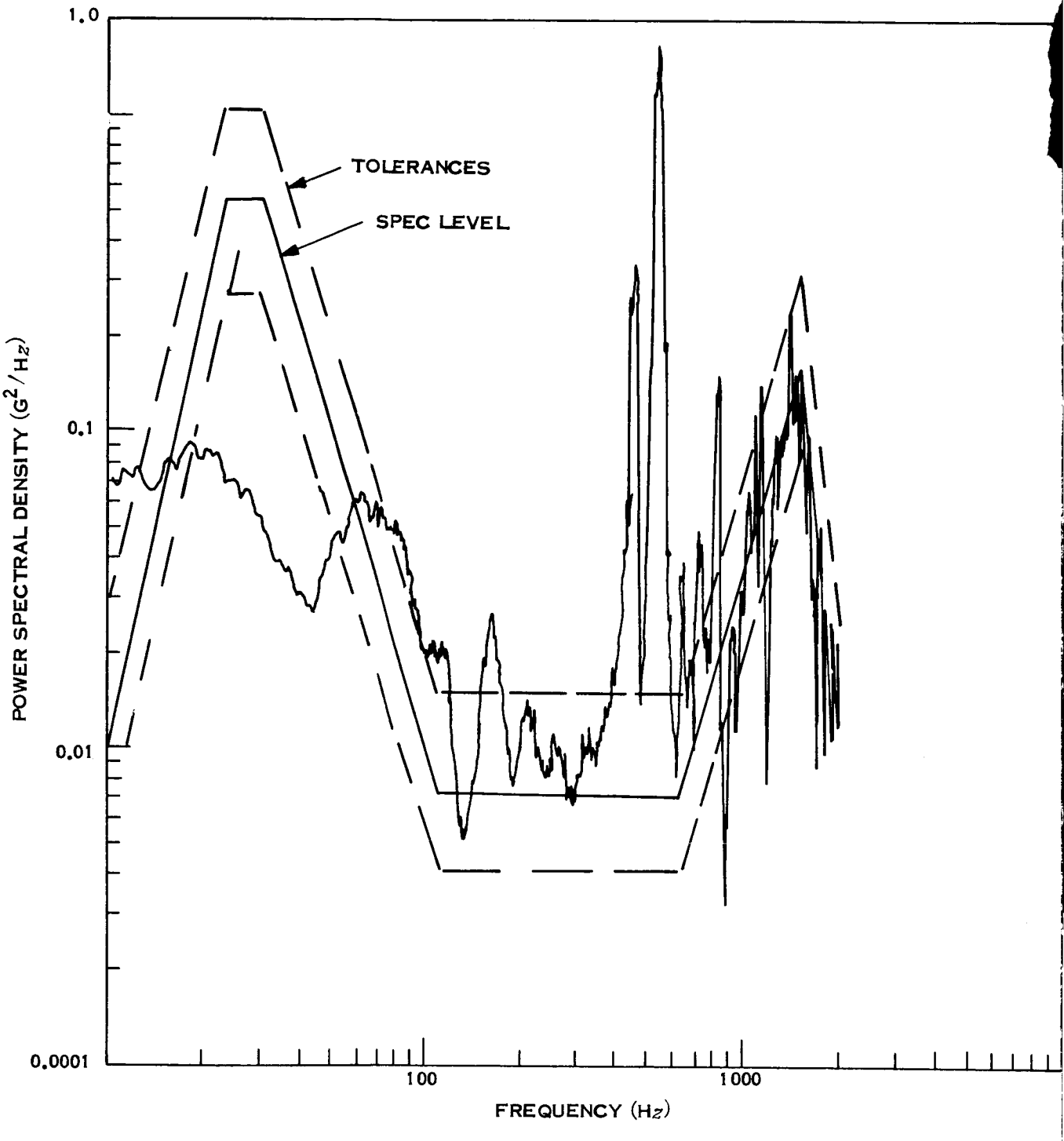

Figure 2-46. Power Spectral Density - Control Accelerometer

FOLDOUT FRAME 2

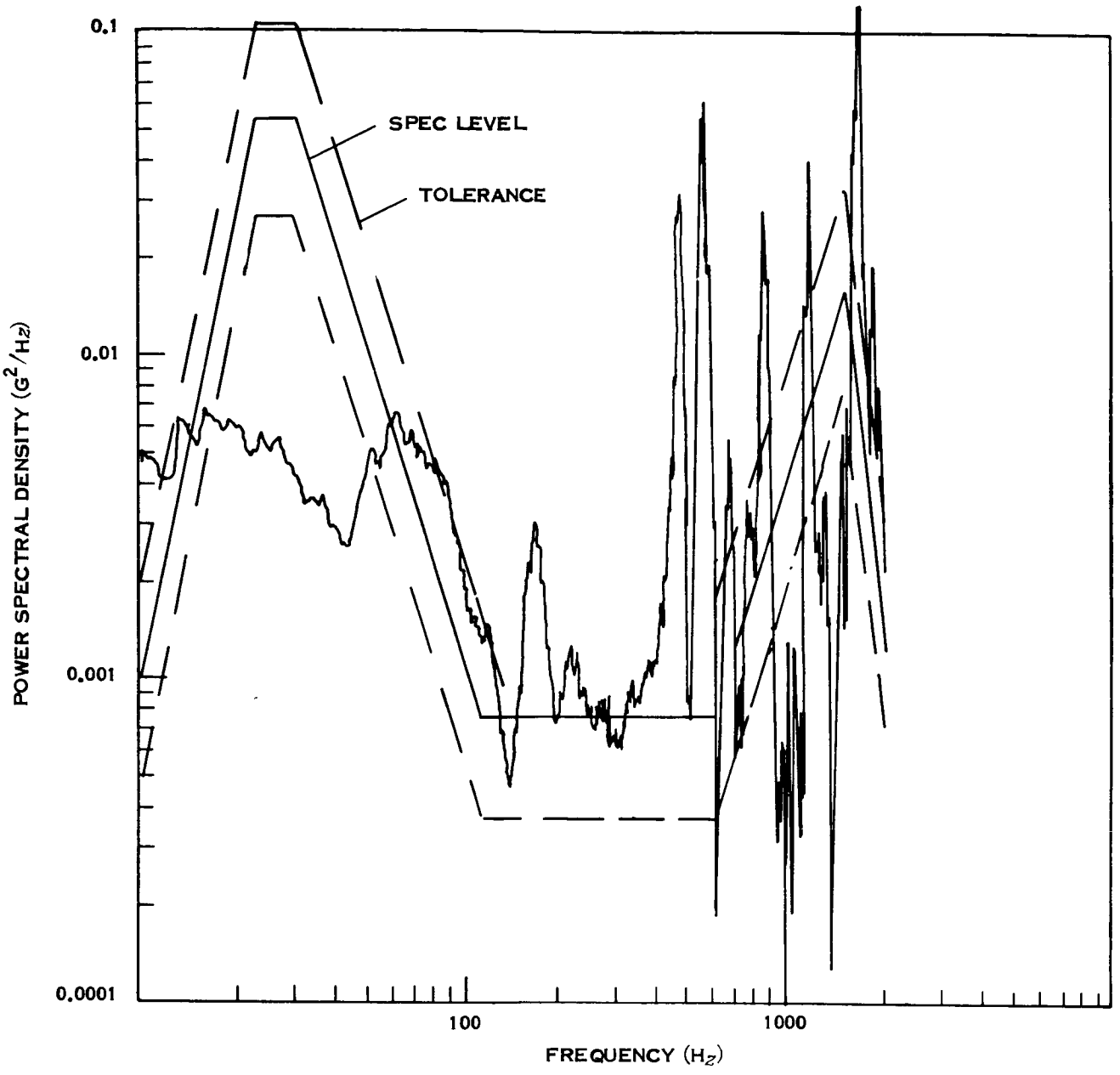

Figure 2-47. Power Spectral Density - Accelerometer No. 2

Section 2.3 Candidate Insulation - Structural Properties Evaluation

Subsection 2.3.3 Long Term Vacuum Effects

TEST APPARATUS

The long term vacuum exposure was performed in a 2 x 2 foot thermal vacuum chamber at the General Electric Valley Forge facility.

Figures 2-48 and 2-49 depict the test fixture. Basically, the fixture was a 14 inch diameter by 14 inch long right circular cylinder. As shown in the figures, the insulation test fixture and vibration exciter were supported from the chamber lid. The test fixture cylinder was made in two sections. A sheet metal cone was mounted inside the upper half and the armature of a vibration exciter was mounted to the small end of the cone, inside the lower half of the cylinder. The exciter body was supported by springs from the joint between the upper and lower halves of the cylinder. The entire external surface of the cylinder was insulated with the specimen blankets. The entire assembly was supported by springs in the cold walled vacuum chamber.

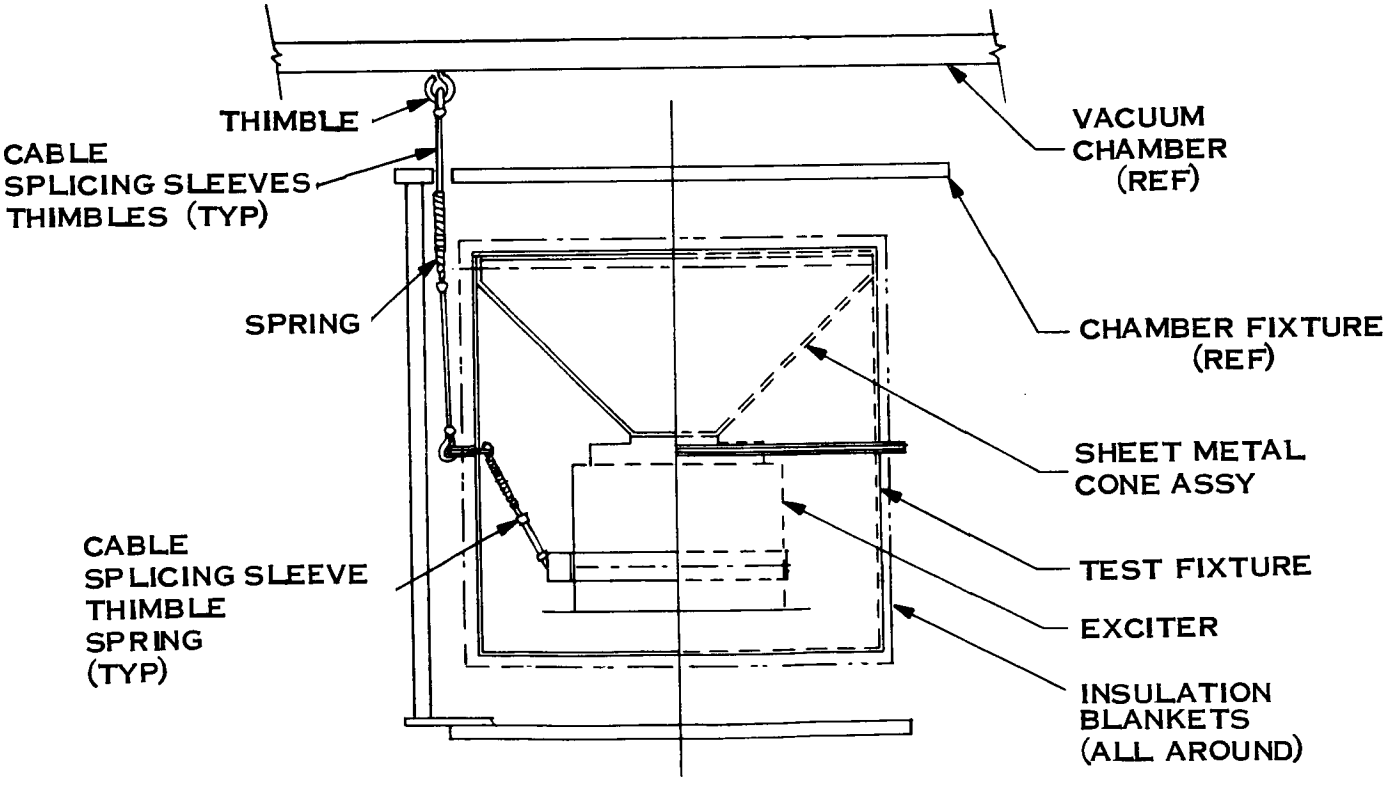

Figure 2-48. Long Term Thermal Vacuum Test Fixture

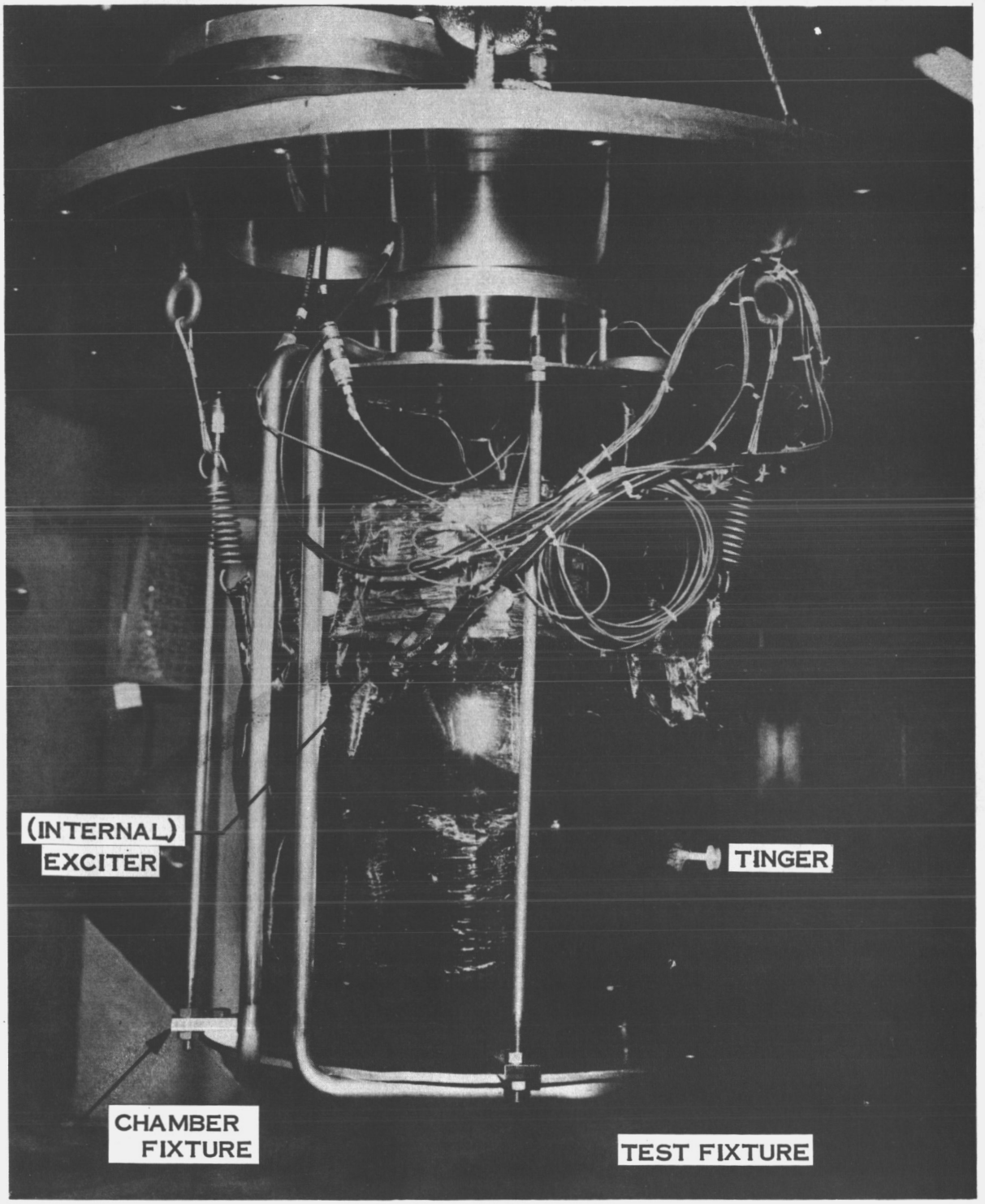

Figure 2-49. Assembled Insulated Test Fixture

TEST SAMPLES

The multilayer thermal insulation blankets specimens, for the long term vacuum test, consisted of 19 layers of gold coated 1/2 mil Kapton with a 1 layer cover sheet of 2 mil Kapton and 19 layers of gold coated 1/4 mil Mylar with a 1 layer cover sheet of 2 Mil Kapton.

The 1/4-mil gold coated Mylar and 1/2-mil gold coated Kapton were crinkled by pulling the sheet material through a Teflon die. The sheets were perforated prior to crinkling with nine 1/8-inch diameter holes per square foot. The uncoated 2-mil Kapton cover sheets were drilled with the same hole pattern. Tingers, as described in Figure 2-50, were used to mount the blankets on the test fixture. Holes, to accommodate the tinger fasteners, were 0.30 inches in diameter. The blankets were restrained on the posts by nylon split-washers snapped into the machined shoulder on top of the tinger.

The blankets were taped at the step joints with one inch wide, one mil Kapton tape coated with pressure sensitive cement. Figures 2-51 and 2-52 depict the insulation technique employed for the test fixture flange and corners. Full details of the insulation design are presented in Reference 7.

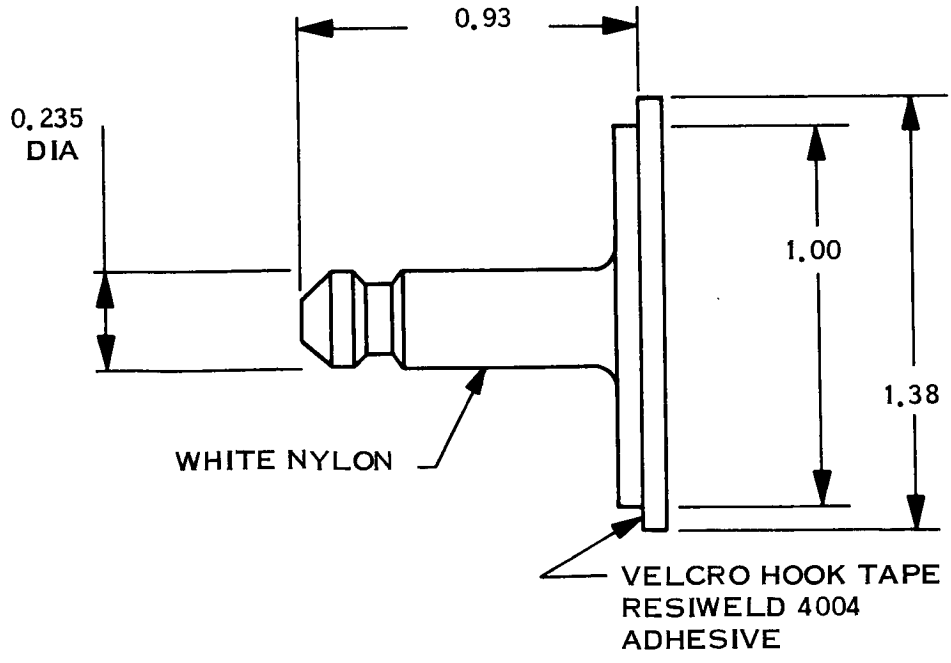

Figure 2-50. Tinger Fastener

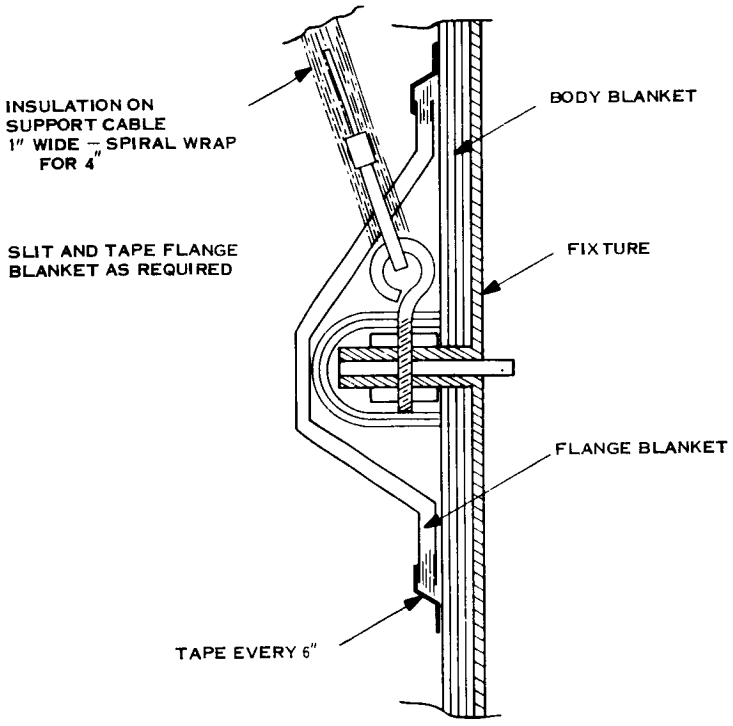

Figure 2-51. Flange Insulation Detail

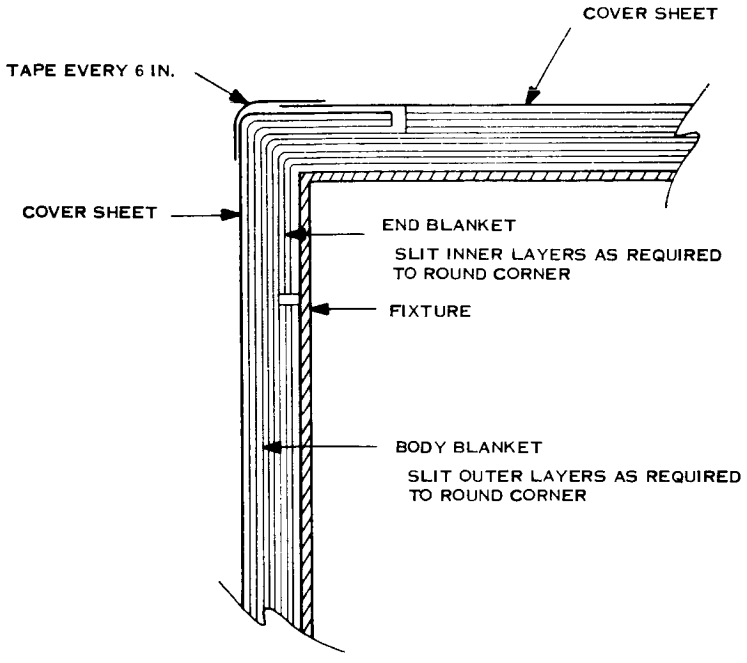

Figure 2-52. Corner Insulation Detail

TEST RESULTS

Visual Observations

The pre-test excitation of the test specimens, simulating a LEMDE thrust chamber assembly firing, produced no visible insulation system damage.

Exposure of the test specimens to 60 days of space vacuum and thermal environments, followed by excitation to the LEMDE levels, produced no visible damage to the insulation materials. The Velcro hook and pile, Tingers and Kapton tape, as well as the step joints, exhibited no noticeable damage or change in physical appearance or function after exposure to vacuum and excitation.

Thermal Performance

The long term vacuum test provided an opportunity to obtain data on the thermal effectiveness of the multilayer insulation design. The performance of the insulation on the 14-inch long cylinder should be appreciably worse than that applied to a full scale flight capsule because of the increased length of joint seams and increased number of support posts per unit area on the smaller model. In addition, the support cables and electrical lead wires will cause a greater proportionate thermal leakage in the small model.

During test with liquid nitrogen-cooled chamber walls, 3.7 watts power was required to maintain the model at about $40^{\circ}F$. At this condition, thermocouples mounted on the cylinder ends adjacent to the heaters read about $45^{\circ}F$, and thermocouples near the central parting flange were about $35^{\circ}F$. The 3.7 watts power value is an average over one day's time, with a deviation of up to $\pm$ 0.2 watt due to plant line voltage fluctuation.

The lead wire bundle included six 24-gage copper-constantan thermocouple lead wire pairs, six 20-gage copper heater power wires, two accelerometer coaxial cables, and the shaker power cable. This bundle was wrapped with insulation to about 5 inches from the model, and included a thermocouple 2.5 inches from the model. The couple read about $-65^{\circ}F$ during test. Calculations show that at least 0.5 watt could leak through this bundle at these conditions.

The model was supported by three 1/16-inch diameter steel cables. Thimbles were used at each eyebolt in the model flange. The cables and thimbles penetrated the "belly band" of insulation used to cover the flange area of the model. There is no readily available data on the thermal loss through this type of insulation penetration, but is estimated that the leak is probably as much as 0.7 watt total for the three cables. Thus, the heat loss directly through the insulation is estimated to be 2.5 watts (3.7 - 0.5 - 0.7).

Including both sides of the one-inch wide central flange, the model has 7.08 square feet of surface area. This gives a heat loss of about 0.35 watt per square foot. If the heat loss were that much from a 472 square foot full scale capsule, it would result in 165 watts loss.

Data was taken after completion of the vibration cycle and no measurable change in thermal performance was noted.

SECTION 2.0

TECHNICAL DISCUSSION

2.4 INSULATION SYSTEM–THERMAL ANALYSIS

Section 2.4 Insulation System - Thermal Analysis

Subsection 2.4.1 Thermal Control Requirements

SCOPE AND CONCLUSIONS

Up to this point, this report has dealt with the evaluation of candidate insulation materials from the standpoint of their capability to withstand the environments to which they will be exposed. At this time discussion turns to the consideration of the thermal control requirements of typical interplanetary space vehicles.

The planetary vehicle system, to be considered in this analysis, consists of a 15,000 pound spacecraft and a 5000 pound capsule. The launch vehicle is taken to be the Saturn V, and the design mission consists of Mars orbital and lander operations. The capsule is considered to be contained within a sterilization conister (biobarrier), until just prior to its landing operation, to conform with NASA planetary quarantine requirements. Figure 2-53 depicts the planetary vehicle configuration studied. The data in Table 2-29 was furnished by JPL as a guide for the insulation system analysis and design. In addition, desired operating time capability after launch was defined as follows:

a. Parking orbit: 1/2 to 1 orbit
b. Initial transfer injection: off sun for up to 6 to 7 hours
c. Cruise: 6 to 9 months
d. Mars orbit, spacecraft: minimum of 6 months continuous operation
e. Biobarrier off before capsule release: 3 to 4 hours or up to 24 hours for abort mode
f. Capsule separation: 2 to 3 hours to enter

Design Philosophy for Preliminary Analysis

The planetary vehicle configuration involves surface areas that are considerably greater than those in existing spacecraft designs and, from an area consideration alone, heat loss should be correspondingly increased. Therefore, preliminary requirements specify that internal spacecraft heat loss be minimized by the utilization of highly efficient superinsulation on the lateral surface. Performance evaluation tests, described in Section 2.2, with 1/2-inch-thick samples of an aluminized Mylar sheet layup have yielded an effective heat leak of 0.18 watt/ft^2 maximum for a temperature difference across the insulation from +72^{o}F to -320^{o}F. This value includes the heat loss effects of required attachment penetrations and step joint seams in the insulation. For design purposes, the conductance of the lateral surface insulation is considered to be 1.56×10^{-3} Btu/hr-ft^2 - ^{o}F maximum, which corresponds to a heat leak of 0.18 watt/ft^2.

Analysis and Conclusions

The analysis of the planetary vehicle thermal control requirements was performed to permit the design of a full scale thermal insulation system for a mockup test vehicle. The thermal analysis was conducted, and is presented, under the following major categories:

FOLDOUT FRAME 1

a. Spacecraft
   - Propulsion Module
   - Equipment Module
   - Orbit Insertion Engine

b. Capsule
   - Capsule prior to deorbit
   - Capsule during deorbit
   - Capsule Hardware
   - Aeroshell
   - Deorbit Motor

Based on the spacecraft thermal analysis, it was recommended that the insulation barrier between propulsion and electronic equipment modules, see Figure 2-53, be eliminated, along with the insulation attached to the rear faces of the electronic equipment bays. It was further suggested that the insulation barrier at the spacecraft/capsule interface be considered a permanent part of the spacecraft. This change will permit the propulsion compartment temperature to be controlled by the equipment bay louvers and at the same time permit sufficient insulation thickness on the sun-facing end of the propulsion compartment to reduce the solar heating effect at near-earth solar distance.

The thermal analysis for the capsule indicated that a low-emittance coating (emittance approximately = 0.05) is required on the heat shield to permit desired operational times with the forward biobarrier removed. Neither the Mars orbit nor the deorbit maneuver appears to have any significant effect on the thermal control of the capsule. The details of the analysis, and the assumptions employed, are thoroughly discussed in Reference 1.

FOLDOUT FRAME 2

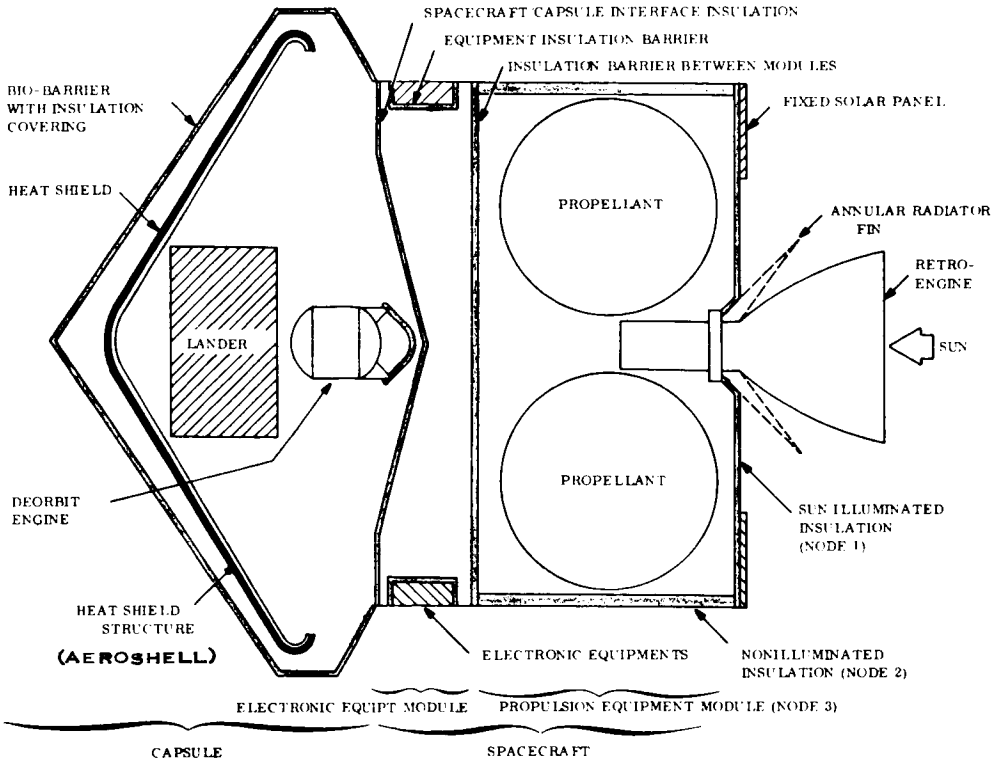

Figure 2-53. Vehicle Configuration

Table 2-29. Planetary Vehicle Design Data

	Spacecraft	Capsule
Weight	Spacecraft = 2,300 lb. Propulsion = 12,700 lb.	5,000 lb.
Internal Power	500 watts	150 to 200 watts
Temperature Limits	0°C to 40°C	0°C to 40°C
Environment	1.0 a.u. to 1.67 a.u.	Mars Atmosphere
Time for Midcourse	3 hr	3 hr
Launch Vibration	Saturn V	Saturn V
Allowable Insulation Weight	50 lb.	80 lb.
Heat Shield	-	$k = 10^{-5}$ Btu/ft-sec-°F thickness = 1/4 inch
Ster. Cannister	-	Aluminum, thickness - 1/10 inch
Aero Shell	-	Fiberglass, honeycomb
Prelaunch Air conditioning	100 lb/min, 40°F filtered air	-

Section 2.4 Insulation System - Thermal Analysis

Subsection 2.4.1 Thermal Control Requirements

A. Spacecraft Analysis

PROPULSION MODULE

In order to establish steady-state thermal control requirements, sizing of the propulsion module insulation system was performed for the "Mars Orbit" mission mode of operation. The thermal conductance of the insulation barrier at the sun-illuminated end of the spacecraft was calculated to be 2.33×10^{-2} Btu/hr-ft^2-$^\circ$F minimum. Considering the maximum conductance for lateral (nonilluminated) surfaces, the insulation details result in a minimum desired steady-state operating temperature of +40°F within the propulsion module. A maximum module temperature of +60°F is obtained when the conductance of the sun-illuminated insulation is increased by 20 percent and the conductance of the lateral surface is decreased by 20 percent.

Under the insulation conditions considered in the previous paragraph, the steady-state temperature of the propulsion module is increased to a value greater than +190°F during the cruise mode of operation at a near-earth location. In truth, this operational mode represents a transient condition, since the incident solar flux decreases as the spacecraft proceeds in its journey toward Mars. In addition, the large thermal mass of the propulsion components must be incorporated into the calculation to assess the true temperature rise of this compartment. Accordingly, a transient analysis of the propulsion module during the near-earth cruise mode results in a temperature rise of 66.5°F in 30 days (about 0.093°F/hr), starting out from an initial temperature of +60°F. If the initial temperature of the propulsion equipment is +100°F, the temperature rise is approximately 51°F after 30 days; the cruise transient is shown in Figure 2-54. In performing these calculations, the incident solar flux was taken to be 442 Btu/hr-ft^2 constant, and the insulation effective emittance assumed constant. In practice, the incident solar flux is expected to change only slightly (less than 17 percent) during the first 2 months of spacecraft flight. Hence, the consideration of a constant solar flux is conservative for demonstrating the magnitude of the problem. It would appear, then, that the spacecraft design should be provided with a suitable thermally actuated louver system designed to reject approximately 334 watts maximum and 192 watts minimum excessive heat power from the propulsion module during the near-earth portion of the Mars mission. A louver area of 8.2 square feet is required to maintain a nominal propulsion module temperature of +72°F.

Incorporated in the preceding calculations is an estimate of the net heat leak or heat gain which occurs in the spacecraft (Ref. 1) by means of thermal shorts and different modes of solar heat intake. An estimate of the heat leak (gain) effect is obtained by comparing steady-state propulsion module temperatures as determined by calculations with and without the thermal short term. Results of these calculations, corresponding to steady-state performance during Mars orbit and near-earth cruise, are presented in Table 2-30. The data indicates that an accurate evaluation of heat leaks in and from the bus is essential for a detailed evaluation of spacecraft temperatures.

Because of its high thermal mass and an absence of generated heat, the propulsion module is relatively unaffected during all other mission modes of operation. A calculation was performed to determine the temperature drop in the propulsion equipment (empty tanks and engine) during a 2-hour period of sun occultation during the Mars Orbit without capsule; the temperature drop was found to be less than $1^{O}F$. Heat leaks from the spacecraft structure and from the rocket engine were included in this calculation.

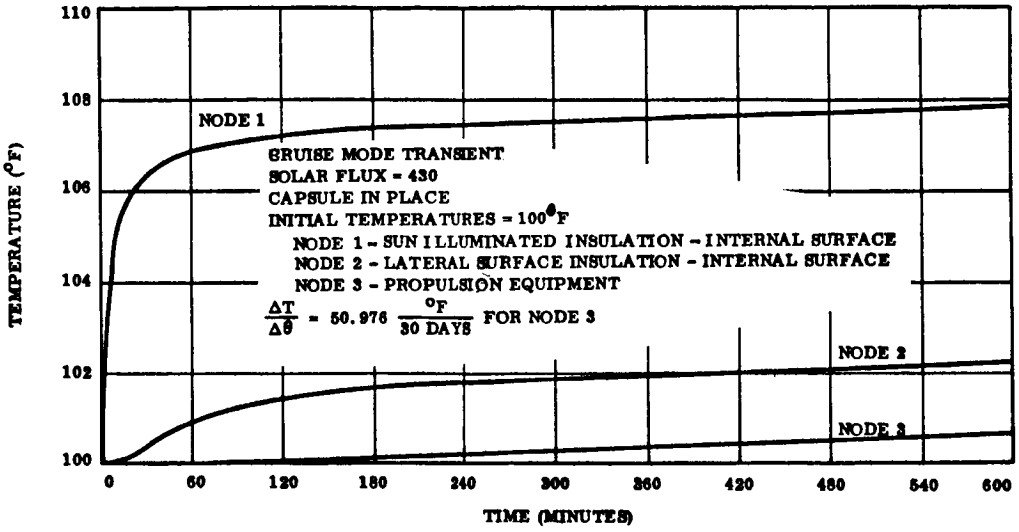

Figure 2-54. Propulsion Module Cruise Mode Transient with $100^{O}F$ Initial Temperature

Table 2-30. Propulsion Module Performance Data

Comments	Solar Flux BTU/hr-ft^2	Heat Leak BTU/hr		Inside Surface Sun-Illuminated Insulation		Temp. (°F) Outside	Propulsion Equipment Module	
		Engine Nozzle	Thermal Shorts	Conductance BTU/hr-°F	Temp. (°F) Inside		Conductance BTU/hr-°F	Temperature (°F)
Capsule Ejected Mars Orbit	195.0	+33.4	-75.1	2.47	42.7	119.2	0.401	39.7
Capsule Ejected Mars Orbit	195.0	+33.4	-75.1	2.97	62.3	119.3	0.321	59.9
Capsule Ejected Mars Orbit	195.0	+33.4	0.0	2.47	68.9	119.7	0.401	67.2
Capsule Ejected Mars Orbit	195.0	+33.4	0.0	2.97	86.0	119.9	0.321	84.7
Capsule In Place near Earth Cruise	430.0	+92.1	-33.4	2.47*	>190.6	247.1	0.401	>189.6
	*Conductance not adjusted to reflect change in outside temperature							

Section 2.4 Insulation System - Thermal Analysis

Subsection 2.4.1 Thermal Control Requirements

A. Spacecraft Analysis

EQUIPMENT MODULE

The spacecraft electronic equipment module differs from the propulsion module in that it depends primarily for its thermal control on the thermal louver system. The louvers respond to conditions of heat variation to maintain control of the equipment temperature. Several transient operational modes exist, however, where the equipments depend on their thermal mass in order to maintain desired temperature limits. Since the normal mode of operation precludes the incidence of sunlight, the transient cases of interest are those which provide excessive external heating. Such mission modes of interest include the lift-off mode and the in-flight maneuvers. Temperature control during the ground hold period is accomplished by air conditioning. Injection into the transfer trajectory is considered as a worst-case maneuver, since it involves absence of sun pointing for periods of up to 6 hours duration.

The requirement for an insulation barrier located to the rear of the equipment packages is established for the purpose of protecting the equipment after the capsule has left the spacecraft. This barrier may be situated directly behind the equipment packages or at any other equivalent location. The insulation requirement may be sized by considering a steady-state thermal balance for Mars Orbit mode of operation with capsule ejected. If the minimum power generated is reduced to a 50 percent level and the electronics are operating at a minimum temperature of $+40^{\circ}F$, the required insulation conductance is calculated to be 2.2×10^{-2} Btu-hr-ft^2-$^{\circ}F$ maximum. This calculation includes a heat leak of 0.14 watt/ft^2 from the nonlouvered areas of the electronic equipment module, as well as the heat leak from the capsule support truss. The heat loss involved with the truss members which support the capsule is estimated to be approximately 25 watts. This should not be restrictive for the maintenance of desired temperature in the equipment bays.

The significance of the insulation barrier to the rear of the electronic equipments is best evaluated by considering the two heat-up transients, lift-off and maneuvers, while at the same time allowing the insulation to vary in effectiveness from a perfect insulator to a condition where the insulation is removed. The temperature difference for the two cases during lift-off is insignificant. The effects of the insulation comparison are much more exaggerated during the maneuver transient, Figure 2-55. In this calculation the equipment radiator is illuminated by one solar constant (effective absorptance + 0.44) over a period of 6 hours. Accordingly, the existence of an internal heat sink helps to alleviate the rapid rise of temperature in the equipment bays. These data do not include a conduction link among the bays. In the two-module concept (electronic equipment and propulsion modules) an internal heat sink is nonexistent for the electronic equipment, and the degree of insulation effectiveness to the rear of the equipments has no special significance except for the steady-state operation during Mars Orbit without capsule. Consequently, it was

recommended that the insulation between the propulsion and electronic modules, as well as that to the rear of the equipment bays, be eliminated. The insulation barrier at the spacecraft/capsule interface should be considered a permanent part of the spacecraft, satisfying the Mars Orbit requirements.

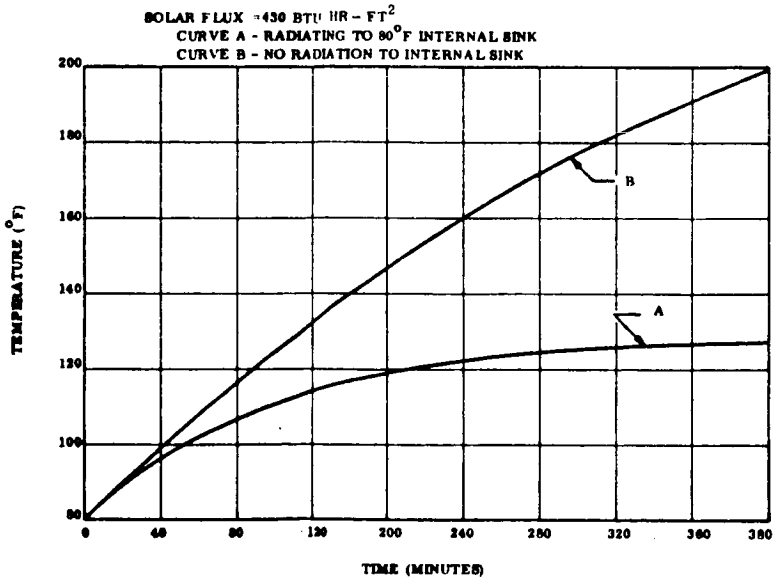

Figure 2-55. Injection into Transfer Orbit - Electronics Equipment Temperature

Section 2.4 Insulation System - Thermal Analysis

Subsection 2.4.1 Thermal Control Requirements

B. Capsule Analysis

CAPSULE PRIOR TO DEORBIT

Biobarrier In Place

During the period of vehicle transit between earth and Mars the entire exposed surface of the capsule is shaded from the sun. Thermal control of the capsule is accomplished by a blanket of thermal insulation at the exterior of the biobarrier in conjunction with a thermostatically controlled heat source within the capsule. It was assumed that the interface surface between the capsule and spacecraft is adiabatic due to the insulation included in the spacecraft at this interface and to the negligible temperature difference. The amount of capsule heat dissipation is limited by a specified power allocation of 200 watts maximum from the spacecraft. The required effectiveness of the insulation blanket over the biobarrier is a function of the desired operating temperature within the capsule and the quantity of available internal dissipated heat. A plot of the required capsule heat power and insulation weight versus insulation effectiveness, at a capsule temperature of $72^{o}F$, is given in Figure 2-56.

A capsule temperature of $+72^{o}F$ was selected for these calculations, since it represents a desirable high-side temperature for the storage batteries. A high-side temperature is desirable for the capsule in order to extend the operating time duration once the forward section of the biobarrier is ejected. For purposes of this discussion, the forward end of the capsule is defined as that side (the heat shield) which faces space, while the back end is that side which interfaces with the spacecraft.

The variation of heat loss with capsule temperature is given in Figure 2-57. These preliminary data correspond to a typical superinsulation blanket consisting of 35 layers of crinkled aluminized Mylar sheet assembled into a composite thickness of 0.5 inch. For relatively short periods of time, the spacecraft orientation may be such as to allow sun exposure of the insulation surface. However, sufficient insulation to restrict capsule heat loss to allowable levels during the shade period will also prevent appreciable warm-up during the sun-facing time.

Capsule Aeroshell

During normal cruise, with the capsule insulation in place, the following tabulated temperature profile through the aeroshell and insulation has been calculated. This analysis assumed that the effective emittance of the heat shield is 0.05 and that of the insulation outside the biobarrier is 0.00765. The latter value is attained with 24 layers of wrinkled Mylar metallized on one side with aluminum or gold as actually used. Following is the temperature profile:

Temperature at inside of aeroshell structure	$72^{o}F$
Temperature at outside of heat shield	$64^{o}F$
Temperature of biobarrier	$41^{o}F$
Temperature at outside of insulation	$-296^{o}F$

FOLDOUT FRAME /

Biobarrier Removed

Thermal control of the capsule during Mars orbit presents itself as a principal challenge to the capsule design. With the removal of the forward end of the biobarrier, the heat loss through the entry heat shield (aeroshell) is considerably increased. Considering a maximum of 200 watts of available internal heat power, calculations indicate that heat shield temperatu may decrease to values less than -200°F in 24 hours. These data correspond to a worst-cas heat shield emittance of 0.85. If a low-emittance coating is used on the heat shield, the temperature naturally does not decrease as much.

A detailed transient calculation was performed to more accurately evaluate the temperature profile of the heat shield subsequent to removal of the forward portion of the biobarrier. The capsule design should provide for distribution of the 200 watts internal heat over the heat shield. The emittance of the outside surface of the heat shield was taken to be 0.3, consider a minimum value as far as painted coatings are concerned. The capsule is attached to the spacecraft by means of several truss members; accordingly, heat is conducted to the capsule through this heat path from the spacecraft. This represents a +70°F heat source for the capsule. Figure 2-58 presents capsule temperatures as a function of time subsequent to ejection of the forward biobarrier. Notice that a heat shield temperature of -100°F minimum can be maintained for time durations up to 8 hours. Since the heat shield structure exchange heat with the capsule, the heat stored by the capsule assists in maintaining the heat shield temperature. Equipment modules on the capsule were considered insulated at their exterior surface by a 2-inch layer of Min-K insulation. Further protection of the heat shield may be accomplished by decreasing the emittance below the 0.3 figure or by placing an insulation barrier at the outside surface of the heat shield.

The effect of increasing the internal power within the capsule on prolonging heat shield cool-down was also studied. The results indicate that the power penalty involved with increasing the temperature of the heat shield is excessive. A linear extrapolation shows that with the present physical model, approximately 1000 watts of heater power would be required to maintain the heat shield above -100°F during a 24-hour duration.

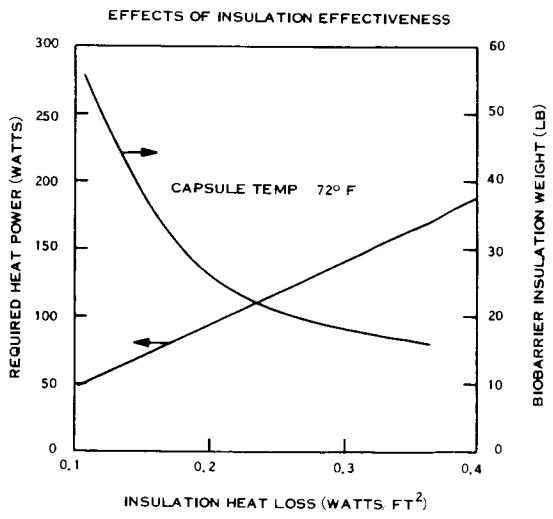

Figure 2-56. Effects of Insulation Effectiveness

FOLDOUT FRAME 2

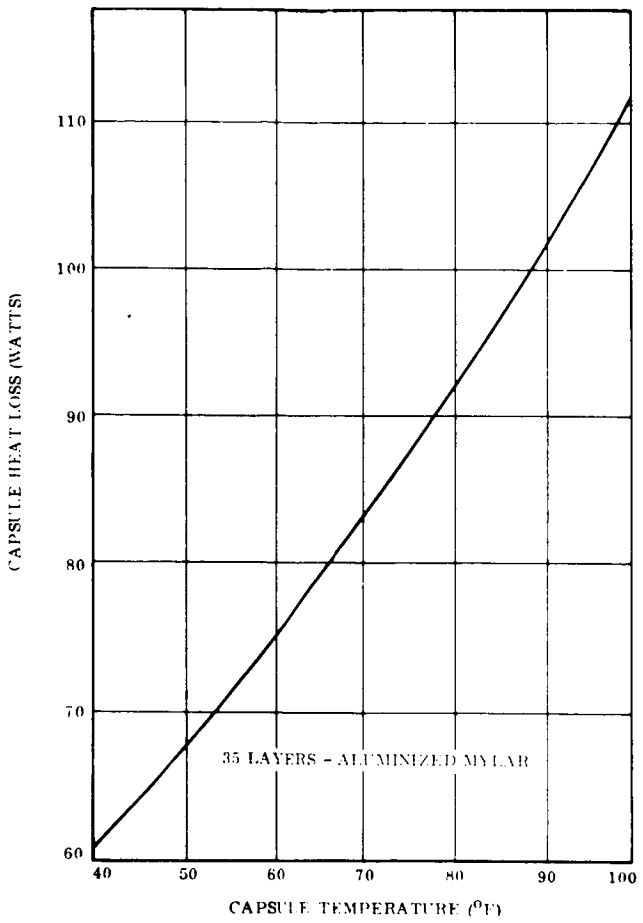

Figure 2-57. Relationship Between Capsule Temperature and Heat Loss

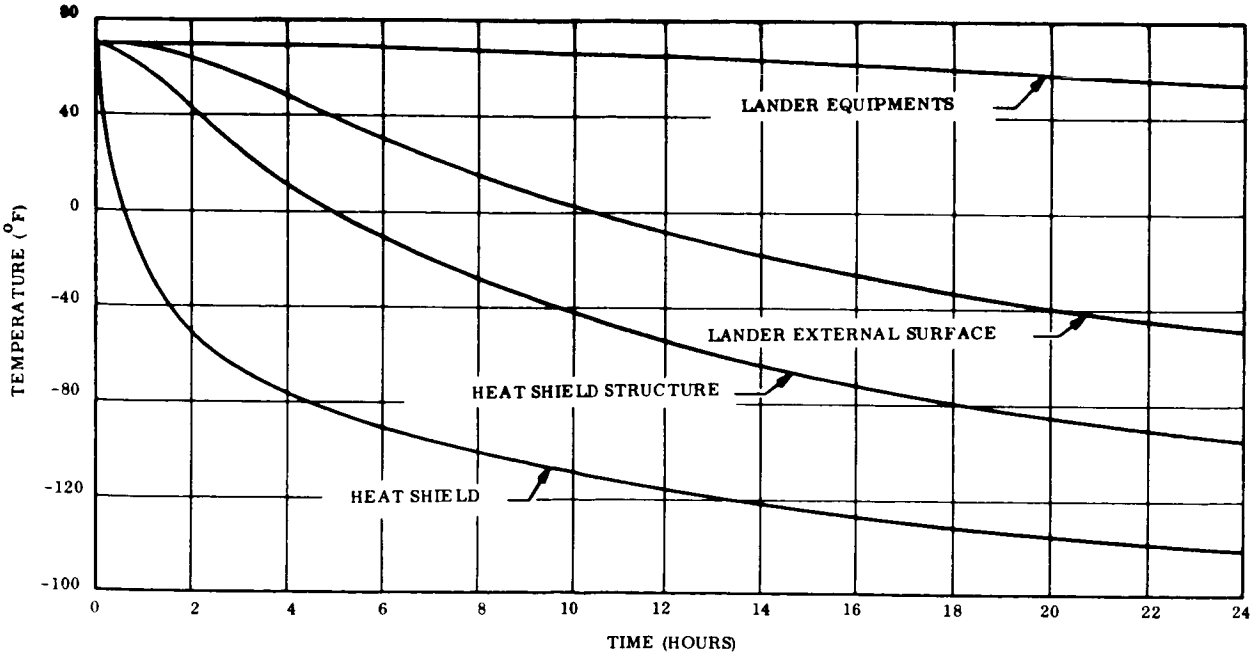

Figure 2-58. Capsule Temperature Profiles Subsequent to Ejection of the Forward Section of the Biobarrier (Heat Dissipation = 200 Watts)

Section 2.4 Insulation System - Thermal Analysis

Subsection 2.4.1 Thermal Control Requirements

B. Capsule Analysis

CAPSULE DURING DEORBIT

Subsequent to the period of capsule orbit around Mars with biobarrier removed, the capsule is detached from the spacecraft and undergoes the deorbit phase of the mission. This maneuver is estimated to last between 2 and 8 hours prior to actual entry of the capsule into the Mars atmosphere. At this time no internal power is available for heating the inside of the capsule. A control capability is provided to the capsule, however, whereby the back end is continually pointing to the sun, during descent, within a cone angle of 60 degrees. The incident sun flux assists in keeping part of the heat shield warm, but at the same time some portions will be shielded from the sun by the internal component of the capsule and may cool down to low temperatures. Data from transient heat-up and cool-down calculations are shown in Figures 2-59 and 2-60. An initial temperature of -100°F was taken for the heat shield on the assumption that the amount of temperature change from this point gives an indication of the initial temperature required to meet desired heat shield temperatures. Thus, the data indicates that the required initial temperature of the heat shield at the beginning of the deorbit maneuver should be approximately -50°F in order to meet the -100°F minimum.

The vehicle configuration for this calculation incorporates a plastic honeycomb structure behind the heat shield. Lateral heat conduction through this structure (0.007-inch faces) is relatively insignificant. The use of a metallic structure might add some improvement to the lateral conductance. A maximum difference of approximately 170°F between insolated and shaded areas of the heat shield is estimated.

A heat shield of elastometric material has been successfully tested. The shield was covered by adhesive, gold-coated, thermal control tape and has an emittance of 0.05. Figure 2-61 shows that, with 200 watts heating within the capsule, heat shield cool-down, with this low emittance, is retarded sufficiently to prevent heat shield cool-down to -100°F. With the capsule ejected 24 hours after the biobarrier is removed, an additional 20 hours of free flight without capsule power can be tolerated before -100°F is reached.

In addition to the preceding analysis that considers the gold-coated tape, heat shield material development has resulted in an elastometric heat shield material that will withstand temperatures to -200°F and below. It has a low-temperature expansion coefficient that matches that of the aeroshell structure. Thus, the technical requirement to prevent the heat shield from falling below -100°F actually may not be an overriding consideration.

Deorbit Motor

During the mission period when the forward biobarrier and it external insulation are in plac the deorbit solid motor temperature is maintained at a nominal 70°F by the thermostatically controlled electric heaters in the capsule. However, after the biobarrier is ejected, and especially after the capsule separates from the spacecraft, this motor will begin to cool dow Figure 2-62, however, shows that a small amount of insulation will retard the cool-down rat of the shaded areas of the motor surface. Solar heating of the insulated surfaces of the moto does not cause any problems because of the reduced solar intensity at Mars. Because of shading uncertainties due to sun orientation angle, it was recommended that the motor be covered with a 10-layer blanket of superinsulation to maintain the desired solid propellant temperature prior to firing.

Another question of concern involves the heating effect associated with firing the solid propel capsule deorbit engine. Heat convection from the plume is essentially nonexistent, since the exhaust materials do not make contact with any part of the capsule. The plume, however, does transfer some heat by radiation to the rear of the capsule. A basic protection for the lander equipment is provided by the 2-inch layer of Min-K insulation at the exterior surface. If the solid propellant motor, employed for capsule retropropulsion, does not possess a meta constituent, the resultant plume is composed almost completely of gaseous products of combustion. The effective emittance and temperature of this plume are similar to that for a liquid propellant ($\epsilon < 0.05$) and should not result in excessive radiant heating of the capsule.

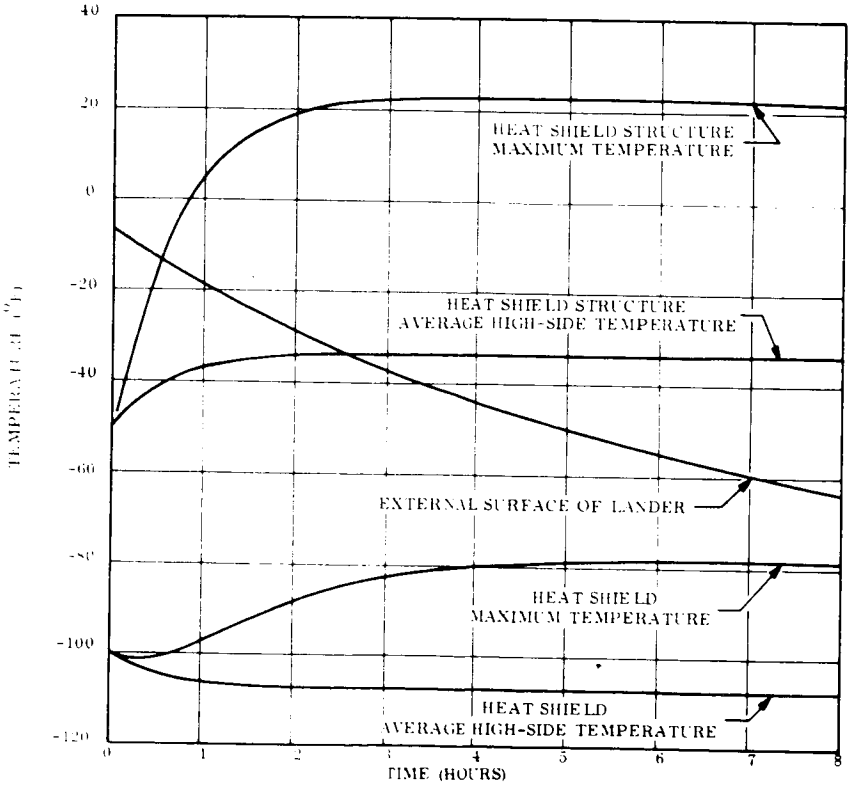

Figure 2-59. Maximum Temperature Profiles for the Capsule During Deorbit

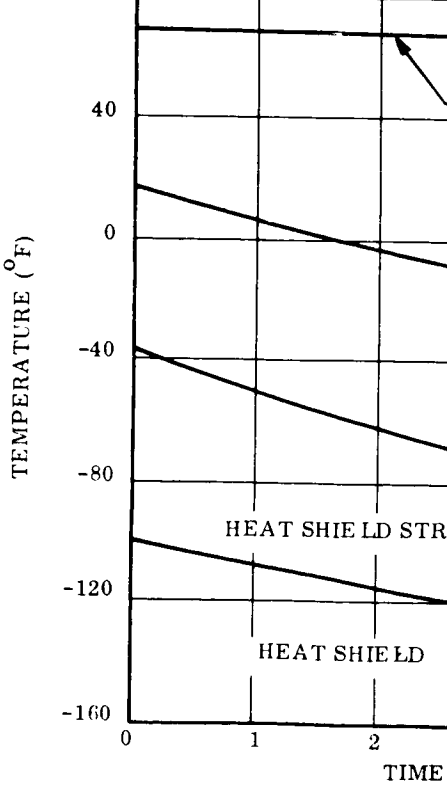

Figure 2-60. Minimum Temp

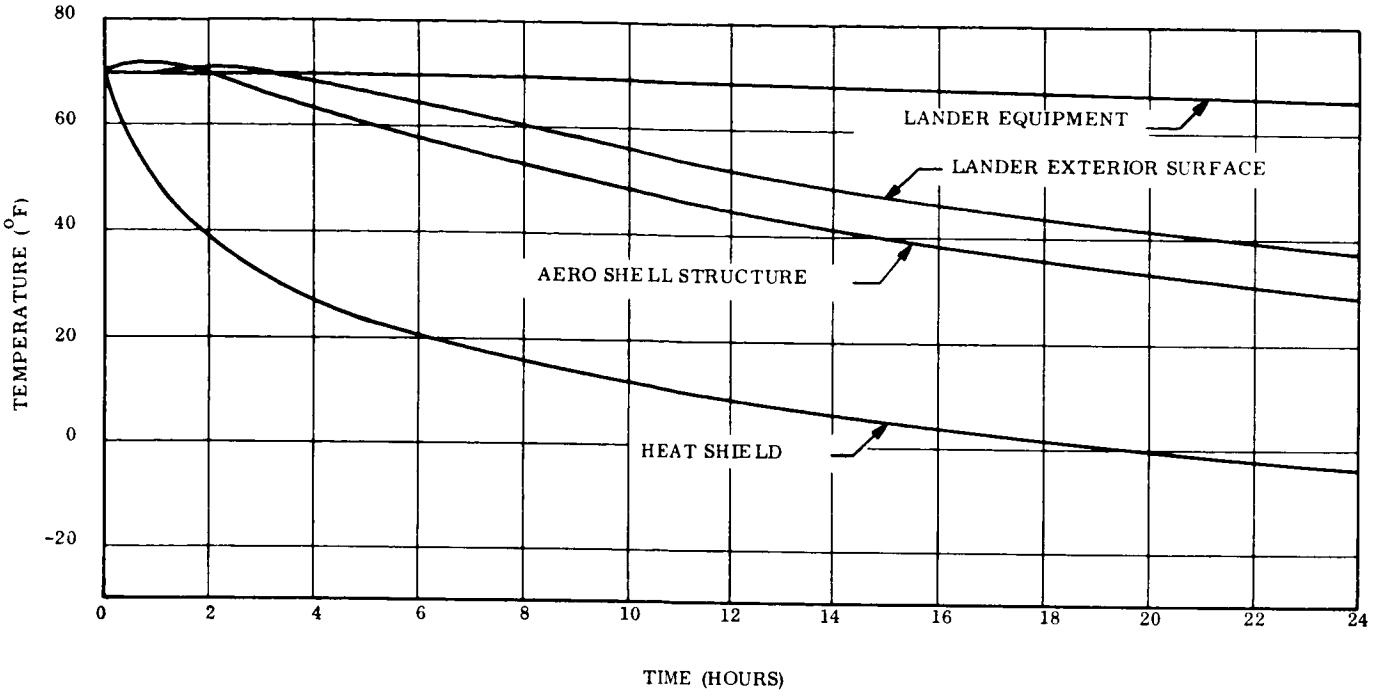

Figure 2-61. Capsule Temperature Profiles Subsequent to Ejection of the Forward Section of the Biobarrier (Heat Dissipation = 200 Watts; Emissivity = 0.05)

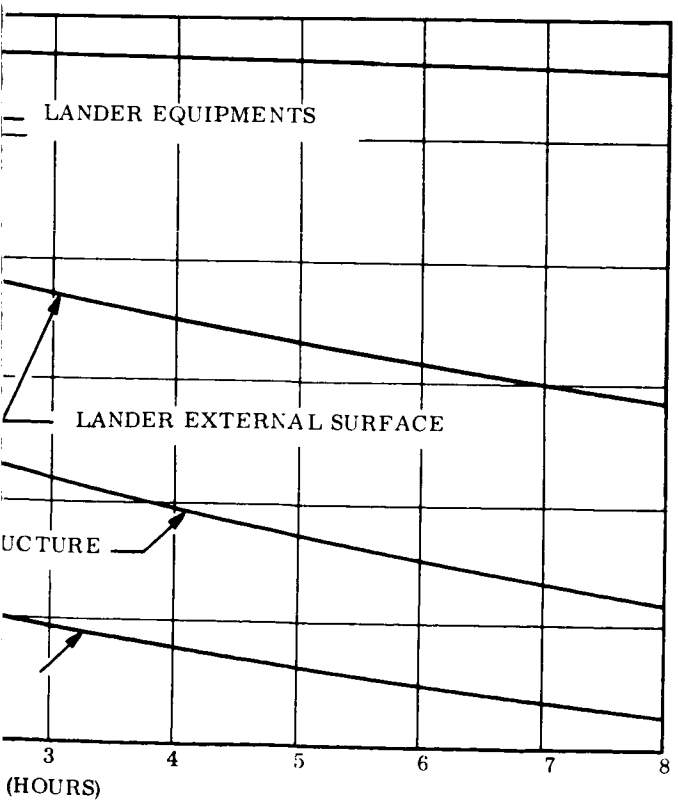

erature Profiles for the Capsule During Deorbit

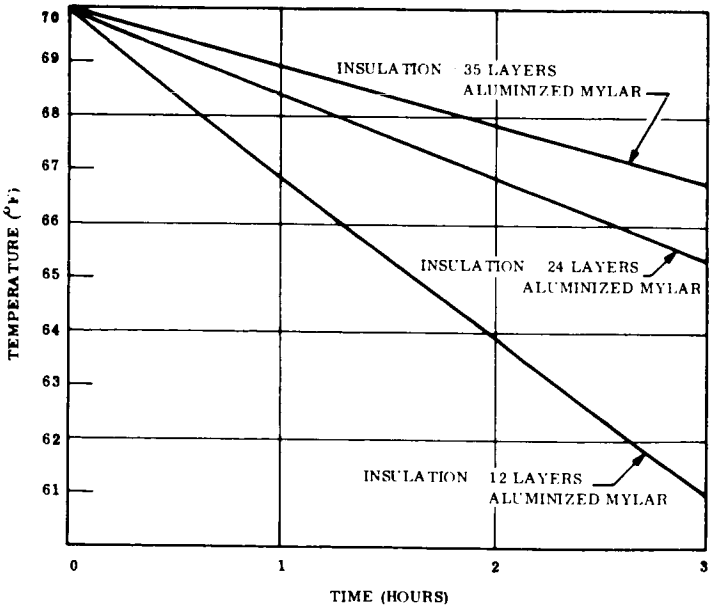

Figure 2-62. Minimum Solid Propellant Temperatures During Deorbit

Section 2.4 Insulation System - Thermal Analysis

Subsection 2.4.2 Orbit Insertion Engine Heating Study

ENGINE ANALYSIS

An orbit insertion engine is one of the requirements for the planetary vehicle considered in this study. The engine will provide retro-thrust to reduce the interplanetary cruise velocity to permit planet capture. Either a solid motor or liquid engine may be selected for this function, and a study of the heating effects which these systems may have on the spacecraft was conducted as a part of the overall insulation system thermal analysis.

Kapton, a prime candidate for multilayer insulation material at the engine end of the spacecraft, has an allowable temperature capability of 400°C or 752°F. Analyses indicate that a heat flux of 1.13 Btu/sec-ft^2 is required to cause this temperature. Consequently, engine heating in this temperature regime should be avoided, if possible, and considered in the selection of insulation materials.

Liquid Engines

The temperature profile for the radiation-cooled nozzle extension of the LEM descent engine is shown in Figure 2-63. The heat flux from this source would impose an excessively high temperature requirement on the adjacent insulation, being sufficient to damage the solar cells on the engine end of the spacecraft. Consequently, an ablation-cooled nozzle extension, despite its increased weight, is recommended for further consideration.

The low nozzle surface emittance of an ablatively cooled LEMDE nozzle limits the peak radiation flux at the insulation location to 0.085 Btu/sec-ft^2. The maximum insulation temperature caused by this flux will be less than 200°F. Consequently, the LEMDE ablative nozzle will not be a limiting consideration in insulation system design.

Solid Motors

The temperature of a solid propellant motor (Minuteman second stage) reaches 800°F and holds approximately that temperature for about 1 minute, about 2 minutes after motor cutoff, at which time plume heating has ceased. A unit area of insulation at the base of the nozzle adjacent to the cone will have a view factor to the cone of about 0.6, and with a typical emittance of 0.8 for the cone surface, the heat flux incident on the insulation from the cone emission is 0.6 Btu/sec-ft^2. This flux will cause a rate of temperature rise in a 3-mil Kapton insulation cover sheet of 66°F/sec, sufficient to ensure that the insulation will essentially reach a steady-state balance of heat absorbed and heat emitted during the time period that the nozzle cone is at or above 800°F. This steady-state insulation temperature is calculated as 590°F for the conditions listed. The transient temperature response of a ten-layer insulation panel adjacent to the nozzle is shown on Figure 2-64. The temperatures assumed for time zero are not in thermal equilibrium.

FOLDOUT FRAME 1

If a solid-fueled motor is used, thermal radiation from the solid particles in the exhaust pl may cause a heating problem to any surface exposed to this flux. Reference 8 explores this problem and correlates test data with an analytical theory. If the thermal flux, as given in that paper, is applied directly to the vehicle configuration under consideration here, severe overheating of the solar cells will result during an engine firing time of 90 seconds. Analys performed by the Aerojet-General Corporation, gave plume particle temperatures of a modified Minuteman second-stage engine with a 70:1 area ratio nozzle, as shown in Figure 2-65. The approximate size of the 23.5:1 area ratio nozzle, considered in Reference 8, is shown on the plot for comparison. This plot shows that gas convection and particle radiatic within the confines of the longer nozzle have lowered the nozzle exit particle temperature sc $750^{\circ}R$ below the exit flow temperature to be expected from the lower expansion ratio nozzle. In addition, the longer nozzle wall blocks some of the radiant flux to the engine end of the spacecraft from the free plume. The net result is that a thermal flux of about 0.25 Btu/sec from the plume is expected on the solar cells and insulation of the spacecraft. This flux would cause a peak outer insulation layer temperature of $390^{\circ}F$.

Based on the preceding analysis, an experimental program was conducted to evaluate the capability of candidate insulation materials to withstand the thermal environment created by heating from a solid motor nozzle. Subsequent pages describe this test program.

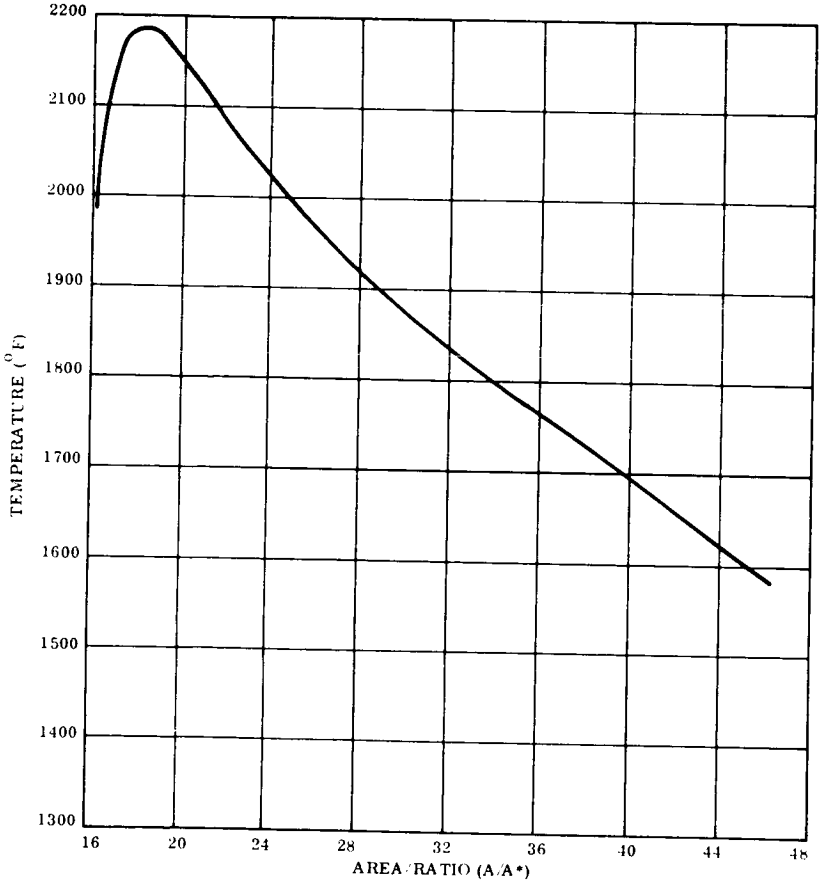

Figure 2-63. Radiation-Cooled Nozzle Extension Temperatures (LEMDE)

FOLDOUT FRAME 2

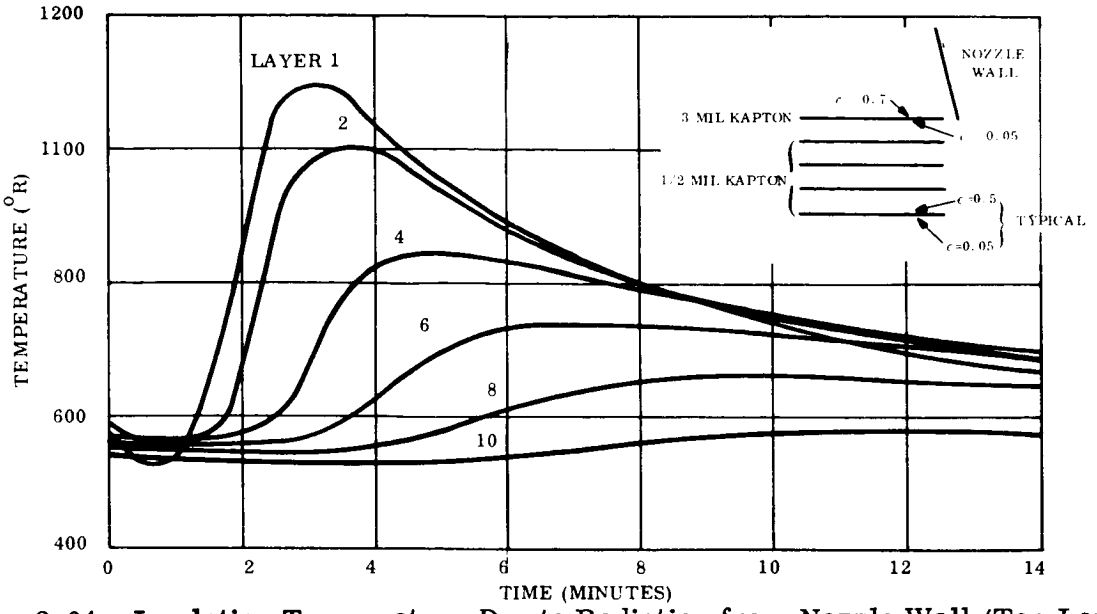

Figure 2-64. Insulation Temperature Due to Radiation from Nozzle Wall (Ten Layers)

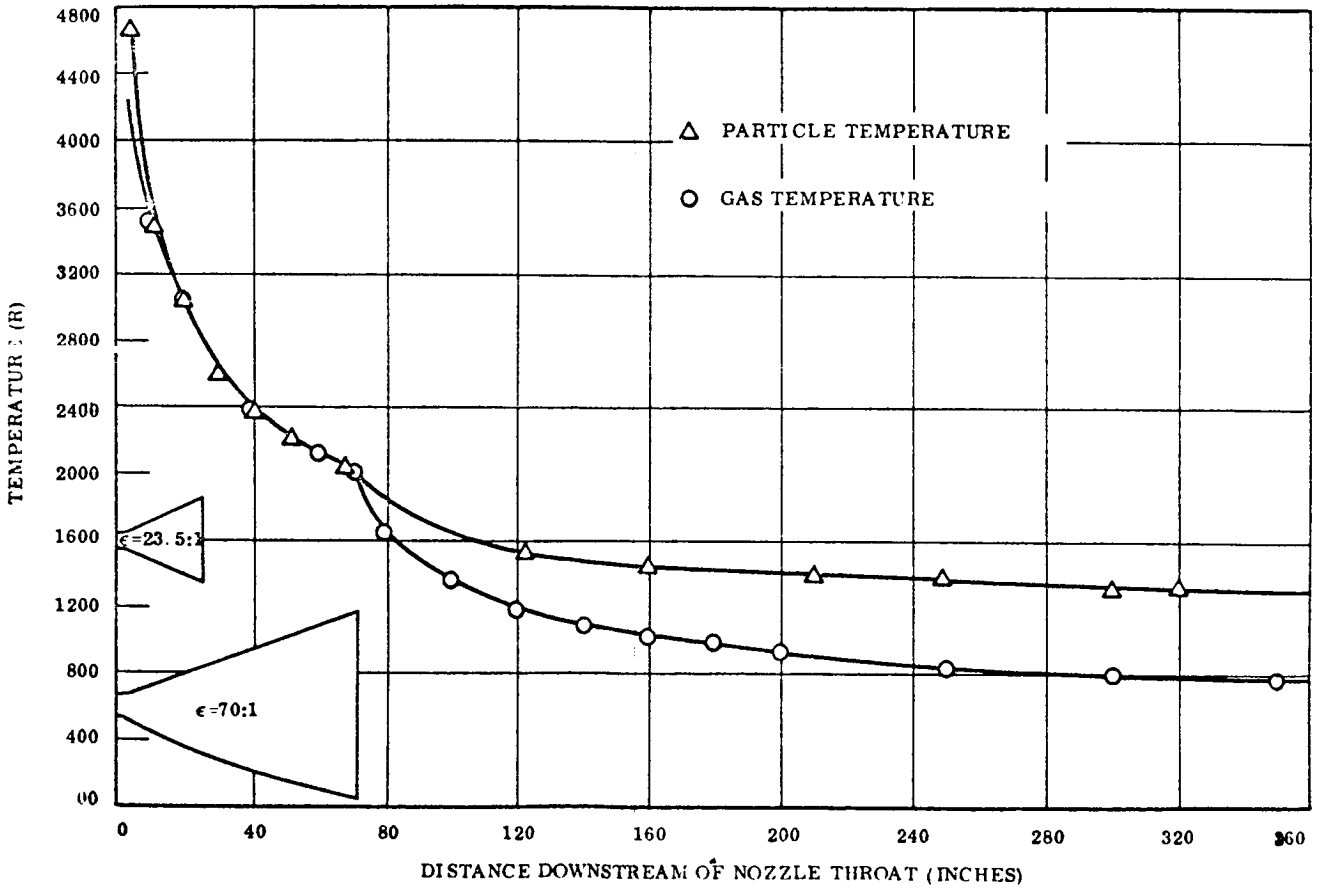

Figure 2-65. Modified Minuteman Plume Temperature Data

Section 2.4 Insulation System-Thermal Analysis

Subsection 2.4.2 Orbit Insertion Engine Heating Study

TEST PROCEDURE/APPARATUS

Nine specimens of candidate multilayer insulation blankets were exposed to a thermal heat flux that simulated heating from a solid motor nozzle. Figure 2-66 shows the heat flux incident on the insulation surface adjacent to the nozzle wall calculated from the nozzle temperature profile of a solid motor.

The test apparatus is shown in Figure 2-67. In the apparatus the irradiated face of the insulation assembly is mounted 4.75 inches from the lower bank of tungsten filament quartz lamps. Lamp bank flux at the test plane was determined by calibration as a function of lamp voltage and position in the plane. Three positions were calibrated by a 1-by-1-by-0.062-inch black calorimeter, as shown in Figure 2-68.

Heat flux calibration runs were performed by measuring the time required to raise the calorimeter temperature above its initial ambient value. Temperature runs of $25^{\circ}F$ and $50^{\circ}F$ Δt's were made, with exposure to the flux produced by lamp excitation ranging from 40 to 100 volts. The results of the calibration were corrected for radiation and convection cooling of the calorimeter; correction for convection was necessary because the calibration runs were made at ambient pressure. Actual tests of insulation temperature response were performed in vacuum.

The amount of correction required for the calibration was determined iteratively from the uncorrected heat flux, the steady-state calorimeter temperature data at 40 volts lamp excitation, and a chart of combined radiation and free convection heat transfer coefficients. The correction amounted to 0.02 Btu/sec-ft^2 for the $25^{\circ}F$ calorimeter temperature rise runs, and 0.04 Btu/sec-ft^2 for the $50^{\circ}F$ rise data. There was a small difference in heat flux with test position, but this difference is considered negligible in respect to the possibe uncertainty in heat flux to which an actual panel may have been exposed. To assure that possible error would be conservative, lamp voltage versus time was selected to duplicate the calculated heat flux due to the solid motor nozzle. Figure 2-69 depicts the lamp voltage-time transients employed in the tests.

Insulation blanket cover sheets used for this program were exposed to simulated solar radiation, as described in Section 2.1.3, prior to exposure to engine heat flux. Post-test, the optical properties of the cover sheets were measured.

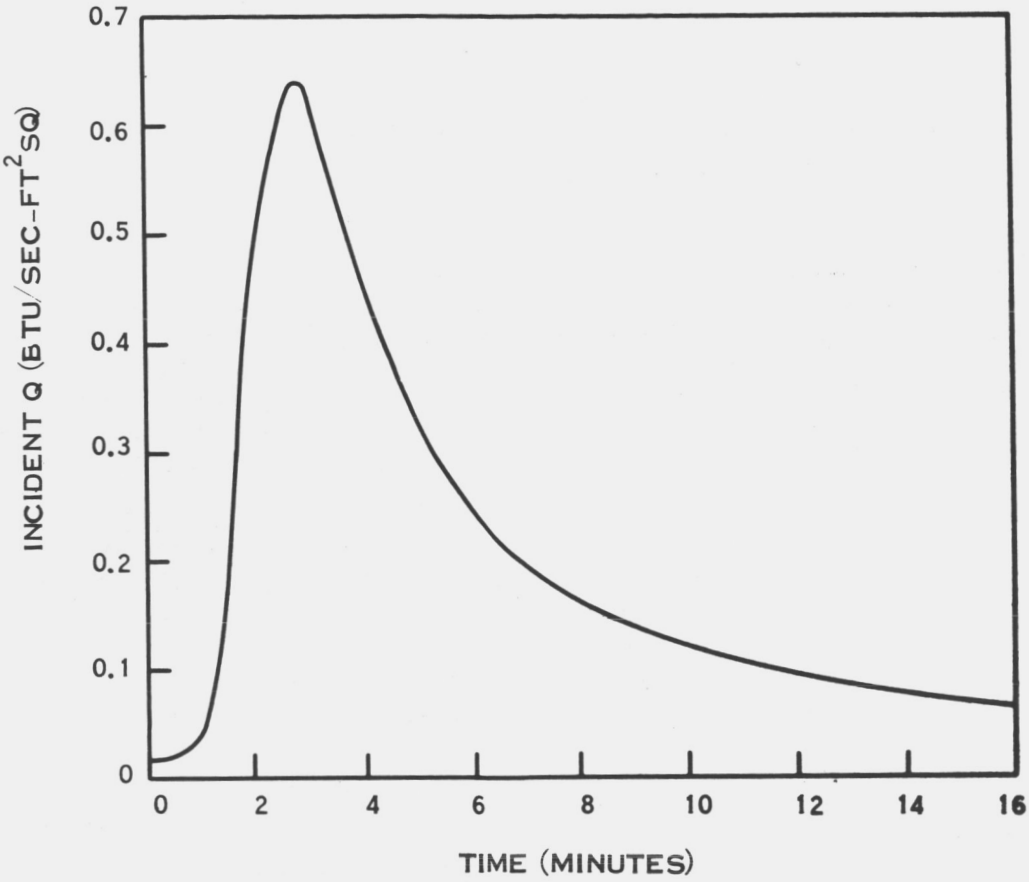

Figure 2-66. Heat Flux on Insulation Surface from Solid Orbit Insertion Motor

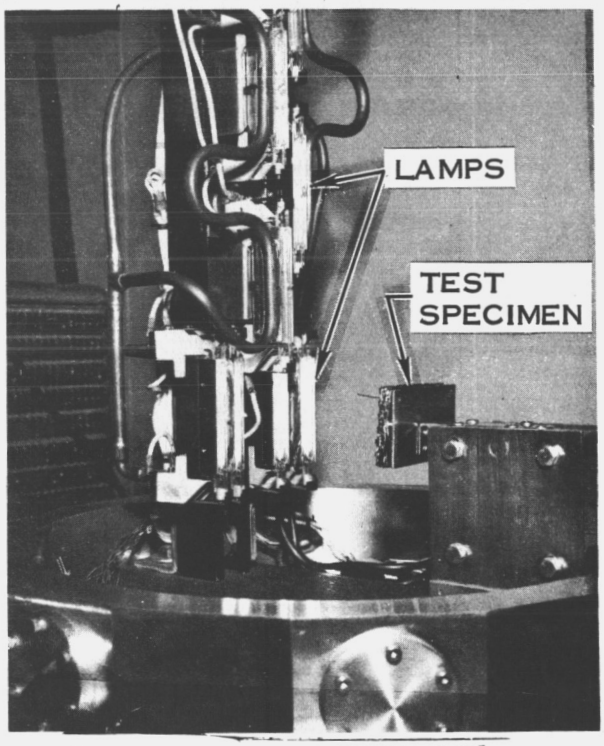

Figure 2-67. Nozzle Heat Flux Simulation Apparatus

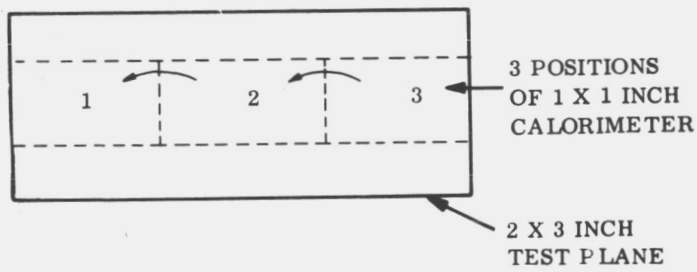

Figure 2-68. Test Calibration

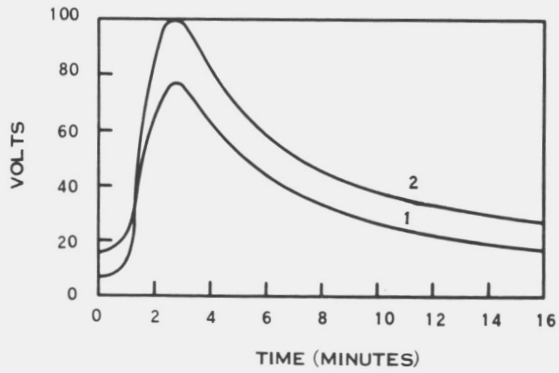

Figure 2-69. Lamp Voltage Versus Time

Section 2.4 Insulation System - Thermal Analysis

Subsection 2.4.2 Orbit Insertion Engine Heating Study

TEST SAMPLES

Nine insulation blanket configurations were tested to determine the effects of rocket engine heating. Each test specimen was 2 x 3 inches and consisted of two parts: a backing panel and a face panel. The material and configuration of the face panel changed with each test while the backing panel was the same for all specimens. The backing panel consisted of 20 layers of 1/2 mil crinkled, aluminized Kapton. Table 2-31 describes the nine face panels exposed to the test conditions. The multilayers in each of the face panels were independently assembled and held together with fiberglass thread loops, being held on the sample holder by impaling them on two small-diameter stainless steel wire pins.

The outer cover sheet of each configuration was metalized on only one side of the plastic film. It is intended that the uncoated side will be exposed to space. As the properties of this film may be degraded by solar exposure, these cover sheets were first exposed to the effects of simulated solar radiation in a combined effects chamber, described in Section 2.1.3, prior to exposure to engine heat flux. When assembled, the plastic film side of the cover sheets faced out ward, as in the insulation design being simulated.

Forty-gage Chromel-Alumel thermocouples were cemented to the inward side of the first, third, and fifth (if any) layers of the face panel material and also to the fifth layer of the backing panel. The lead wires were tacked to the insulation material with a small amount of RTV-106 adhesive.

Table 2-31. Test Samples

Sample Number	Face Panel Description*
1	Aluminized Kapton Cover sheet - 2 mil; one layer pair, 1-mil aluminized Kapton Dimplar; two layers, 1/2-mil crinkled aluminized Kapton
2	Aluminized Kapton cover sheet - 2 mil; one layer pair, 1-mil aluminized Kapton Dimplar; one layer pair, 1/2-mil aluminized Mylar Dimplar
3	Sample No. 1 with Nylatch support post and Teflon washer in center of panel
4	Aluminized Kapton cover sheet - 2 mil; three layers, 1/2-mil crinkled aluminized Kapton
5	Aluminized Teflon cover sheet - 5 mil; aluminized Mylar Dimplar separator- 1 mil; aluminized Mylar Dimplar reflector - 1/2-mil; two layers, 1/4-mil Mylar - aluminized 2 sides.
6	Aluminized Teflon cover sheet - 5 mil; one layer, 1/2-mil crinkled aluminized Kapton; one layer pair, 1-mil aluminized Kapton Dimplar; three layers, 1/4-mil Mylar - aluminized 2 sides
7	One Textolite support post with Teflon washer in center of panel; aluminized Teflon cover sheet - 5 mil; one layer pair, 1-mil aluminized Kapton Dimplar; three layers, 1/2-mil crinkled aluminized Kapton
8	Aluminized Kapton cover sheet - 2 mil; two layer pairs, 1-mil aluminized Kapton Dimplar
9	Gold-coated Kapton cover sheet - 3 mil; 3 layers, 1/2-mil crinkled aluminized Kapton; 3 layers, 1/4-mil Mylar- aluminized 2 sides

* Backing panel for all samples was 20 layers of 1/2-mil crinkled - aluminized Kapton.

TEST RESULTS

Use of the planned lamp voltage-time transient, curve 1 of Figure 2-69, resulted in an outer cover sheet temperature of about 400°F. The lamp voltage was then increased to curve 2 of Figure 2-69, which provided a black body maximum heat flux of 1.0 Btu/sec-ft^2. The outer cover sheet temperature for a Kapton cover was above 500°F. The difference between the initially planned lamp flux, with a black body peak of about 0.6 Btu/sec-ft^2, and the flux of 1.0 Btu/sec-ft^2 required to obtain desired temperature, has subsequently been found to be due to the fact that the cover sheets have a lower than unity value for the ratio of absorptance of lamp flux to thermal emittance at sheet surface temperature. With the lamp bank flux peaking at about 1.0 Btu/sec-ft^2, the following results were observed:

a. Kapton Material. None of the Kapton material was appreciably affected by the heat flux. The sheets that had been metalized on only one side showed some tendency to curl, but this should be easily restrained be insulation attachments.

b. Five-Mil Thick Aluminized Teflon Cover Sheets. These were severly affected. The material wrinkled deeply during the exposure and several samples showed severe shrinkage.

c. Aluminized Mylar. This material, either in 1/2-mil Dimplar or 1/4-mil double-sided forms, was completely unsatisfactory for at least the first five layers from the outside, having wrinkled, curled and shrunk. In sample No. 9, the Mylar was seriously distorted at the edges as far as the seventh layer.

d. Fiberglass Thread Used for Stitching, the Nylatch Post, and Teflon Washers on the Post. These did not appear to be affected.

e. Textolite Post. This appeared bleached at its outer end but did not seem to suffer any other noticeable change.

Figure 2-70 is a plot of the temperatures measured during the test for sample No. 1. This plot is typical for the nine configurations, with peak temperatures varying from 565° for sample No. 5 to 480° for sample No. 3.

The curled edges of the inner layers and temperature distribution within the sample suggests that there was a considerable flux of energy coming into the sides of the test samples. This side flux, possible because the lamps had a greater spacing between them than the 3-inch width of the samples, probably resulted in Mylar damage to a greater depth than would have been the case had the flux been only one-dimensional.

Optical measurements were taken for the cover sheet materials prior to solar irradiation, after irradiation, and after exposure to the engine heat flux. Table 2-32 presents this data. Teflon showed a considerable increase in solar absorptance post-test. Aluminized Kapton and vapor-deposited gold on Kapton did not change within the resolution of the instruments.

The results of these tests indicated that Kapton is an acceptable material for cover sheets. Teflon is not suitable for this purpose. Further, Mylar should not be used until at least the tenth layer to eliminate the possibility of material damage.

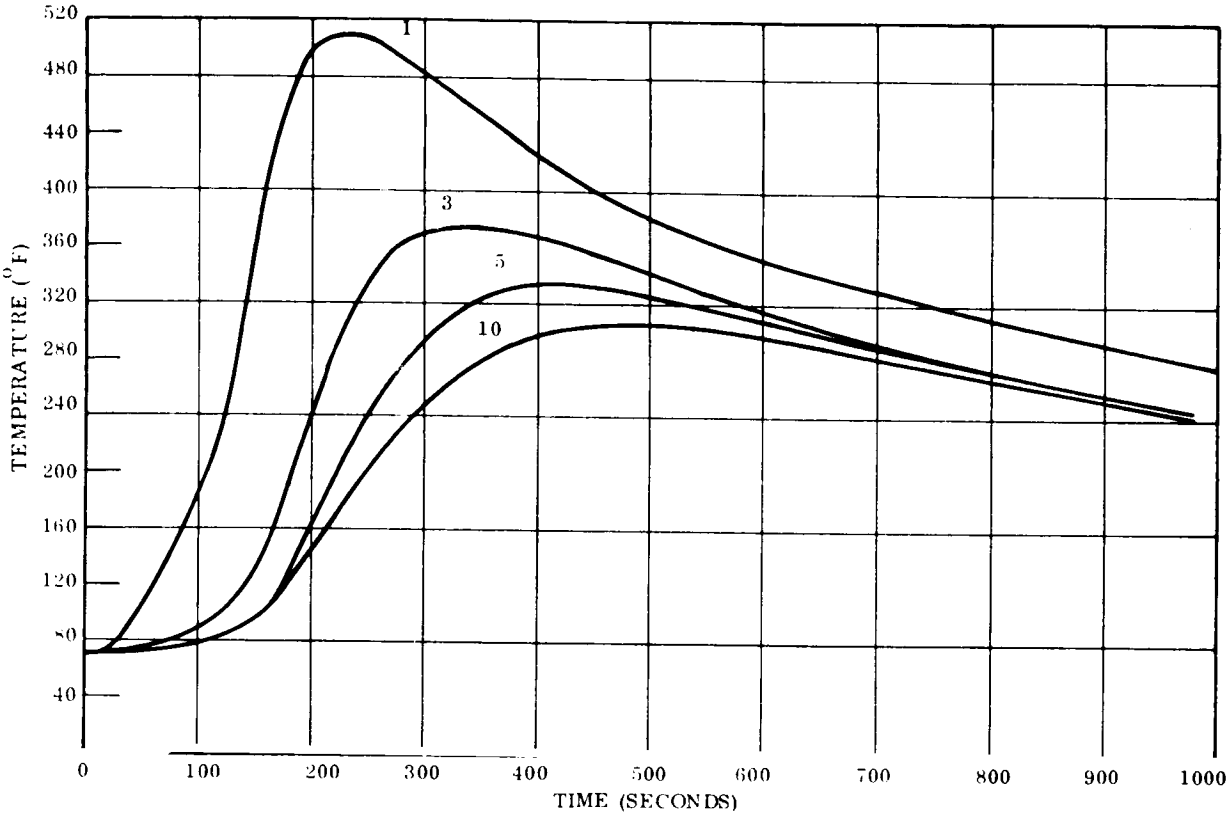

Figure 2-70. Layer Temperatures for Sample No. 1

Table 2-31. Optical Properties Measurements

Cover Sheet Material	α_s Prior to Irradiation	α_s After Irradiation*	After Engine Heating	
			α_s	ϵ_N
Alum. Kapton (2 mils)	0.460	0.447	0.443	0.768
Alum. Kapton (2 mils)	0.443	0.449	0.433	0.768
Alum. Kapton (2 mils)	0.480	0.438	0.435	0.766
Gold Kapton (3 mils)	0.430	0.409	0.422	0.797
Alum. Teflon (5 mils)	0.240	0.315	0.450	0.795

* Irradiation = 10^{16} protons/cm^2 plus 1000 UVESH.

$\epsilon_N = \pm 0.02$

$\alpha_s = \pm 0.06$

Section 2.4 Insulation System - Thermal Analysis

Subsection 2.4.3 Thermal Scale Modeling

GENERAL THEORY/CONCLUSIONS

Vickers, in Reference 9, describes the general theory of thermal scale modeling and Gabron, in Reference 10, considers the application of this theory to the thermal scaling of spacecraft, including some consideration of scaling spacecraft which are thermally isolated from the external environment with multiradiation-barrier insulation.

Gabron concludes that a thermal insulation system can best be modeled by the temperature preservation technique in which temperatures of the model match temperatures of the prototype at homologous points. This technique seems preferable as compared to the technique where all materials are kept the same between model and prototype and temperatures at homologous locations are scaled. Gabron further states that the thermal insulation system should be applied to the model in the same thickness and number of layers as it is applied to the prototype. This results from the requirement that the heat flux through the model surface duplicate that through the prototype surface. Therefore, if the same number of layers of the same materials in the same thickness of ideal, unperturbated insulation is applied to both model and prototype, the same thermal performance should be expected from each one.

Real insulation systems have joints, supports, and other penetrations which may disturb the thermal similarity between the prototype and its model. These penetrations introduce thermal disturbances which Gabron discusses as follows:

> "Unfortunately, little information exists on the nature of the heat flow around seams and penetrations. The three-dimensional heat flow patterns in these regions are complicated by the anisotropic behavior of multilayer insulation and by the nonlinearities due to radiation between and along the foils. In fact, it is practically impossible to make accurate estimates of the heat flow in such regions for penetrations of simple geometry. Until such information is developed, methods for scaling heat flows in penetrations will be subject to error."
>
> "If penetrations appear to be important in controlling the heat flow in a multilayer insulation blanket of a prototype, one method for determining a suitable procedure for scaling the heat fluxes in a model would be to make a thermal test of a single full-scale penetration, and then design and test various scale models until one arrives at a model design with the appropriate scaled heat flux. This is a rather unattractive procedure because of the iterative process involved, and the inherent difficulty in making measurements of small heat fluxes."

CONCLUSIONS

The following conclusions were arrived at for insulation scale modeling:

a. Thermal scale modeling of an insulation system using a geometrically similar model will probably lead to excessive error.

b. An adequate assessment of prototype heat flow, the objective of a thermal scale model, can probably be accomplished by using a geometrically distorted mode.in which the insulation is made of the same materials and thicknesses as the prototype; the number of insulation attachments that represent appreciable heat leak should be reduced in the model, and the length of insulation joints in the model should be reduced by a greater amount than just the scale ratio.

c. The insulation system contribution to structural penetration heat flow should be investigated as a separate problem in which the measured prototype characteristic is scaled in the model with an empirically determined design.

d. Thermal scale modeling would not significantly benefit this thermal insulation experimental evaluation program.

MODELING ANALYSIS

A spacecraft insulation system has the requirement of being readily assembled and removed from the vehicle. The attachment points necessary to accomplish this, and the insulation discontinuities resulting from division of the insulation into pieces that can be handled readily, cause perturbations that modify the ideal insulation characteristics. As thermal modeling theory requires equal heat flow per unit surface area from both the model and prototype, it is necessary to investigate the differences that the above perturbations may cause.

Considering a unit square of multilayer insulation, retained by four Nylatch posts at the corners, as the prototype. If the thermal model is kept geometrically similar to the prototype, then the number of insulation attachment posts will remain the same. As the surface area of the scaled model decreases with the square of the scale ratio.

$$\frac{A_m}{A_p} = \left(\frac{L_m}{L_p}\right)^2 \qquad \text{where} \quad \begin{aligned} A_m &= \text{model surface area} \\ A_p &= \text{prototype surface area} \\ L_m &= \text{model length} \\ L_p &= \text{prototype length} \end{aligned} \qquad (2\text{-}1)$$

The number of posts per unit surface area of the model increases with respect to the prototype according to,

$$\frac{\left(\frac{N_p}{A}\right)_m}{\left(\frac{N_p}{A}\right)_p} = \frac{A_p}{A_m} = \left(\frac{L_p}{L_m}\right)^2 \qquad (2\text{-}2)$$

where N_p = Number of posts (same for model and prototype). For equal surface heat flux:

$$\frac{(q_p)_m}{(q_p)_p} = \left(\frac{L_m}{L_p}\right)^2 \qquad (2\text{-}3)$$

where q_p = heat flow per post.

Thus, for true scaling, a quarter-sized model, for instance, would require 1/16 as much heat flow perturbation per attachment post as results in the prototype. Developing special model attachments with this reduced influence, as suggested in the quote from Gabron, would seem to be a significant problem. The joints or discontinuities between insulation panels

introduce an additional problem. Again for similar geometries, the length of model joint compares to the prototype according to,

$$\frac{(L_j)_m}{(L_j)_p} = \frac{L_m}{L_p} \tag{2-4}$$

Therefore the joint length per unit surface area changes according to:

$$\frac{(L_j/A)_m}{(L_j/A)_p} = \frac{L_m/L_p}{(L_m/L_p)^2} = \frac{L_p}{L_m} \tag{2-5}$$

The total joint heat flow penetrations per unit surface area of model and prototype is defined by,

$$\left(\frac{L_j q_j}{A}\right)_m = \left(\frac{L_j q_j}{A}\right)_p \tag{2-6}$$

where q_j = heat flow perturbation per unit length of joint.

$$\frac{(L_j/A)_m}{(L_j/A)_p} = \frac{(q_j)_p}{(q_j)_m} = L_p/L_m \tag{2-7}$$

or

$$\frac{(q_j)_m}{(q_j)_p} = \frac{L_m}{L_p} \tag{2-8}$$

Thus, for a true quarter-scale model of similar geometry to the prototype, the heat flow perturbation of the model joints needs to be one fourth that of the prototype on a unit length bas Developing low heat leak joints for the model would probably be more difficult than establishing a model post design with the necessary heat flow reduction. An example of the error that would result in scale modeling insulation heat flow if the joint leak per unit length cannot be reduced and prototype design similarity is maintained, calculates as follows:

From thermal conductivity measurements of insulation panels, it has been determined that typical 1/2-inch-thick insulation panel components have approximately the following heat leak effects between room temperature and - 320°F.

Ideal insulation	0.304 Btu/hr-ft^2
One support post	0.049 Btu/hr
One foot of joint	0.089 Btu/hr

If the prototype has one support post and 1 linear foot of joint per square foot of area, for instance, it would have a heat leak of 0.442 Btu/hr-ft^2. A geometrically similar model, in quarter scale, with the same number of the same support posts and the same joint heat leak per unit length, would have an insulation heat flow of

0.304 Btu/hr-ft^2	(ideal)	
0.784 Btu/hr	(post)	from Equation 2-2
0.356 Btu/hr	(joint)	from Equation 2-5
1.444 Btu/hr-ft^2		

and the $\frac{(q/A)_m}{(q/A)_p} = \frac{1.444}{0.442} =$ 3.27 which would be poor fidelity modeling compared to the desired ratio of 1.0.

is.

ALTERNATE MODELING APPROACHES

Thermal modeling of the insulation system may appear more attractive if similarity of design between model and prototype is discarded. This has already been "stretched" in insulation modeling recommendations where the insulation thickness on the model is made the same as the prototype, instead of reducing the thickness according to the scale ratio. If now the number of support posts per unit surface area is kept the same between model and prototype, and the model posts are made the same as the prototype, the overall heat flow perturbation that these posts cause will be the same in the model as in the prototype. This results in the number of posts in the model being reduced by the factor, $(N_p)_m/(N_p)_p = [(L_m)/(L_p)]^2$.

A prototype design, for instance, may have 4-foot by 4-foot insulation panels with support posts on 1-foot centers around its periphery. This results in one post per square foot of surface area. The corresponding panel for a quarter-scale model would be 1 foot square and contain only one post. Obviously this one post would not be able to attach the model blanket evenly and additional supports, perhaps with low-perturbation threads, would be needed for model construction. This procedure, however, should result in good thermal fidelity between model and prototype as far as the attachment posts are concerned.

It may be possible to eliminate the modeling problem caused by the insulation joints if the relative size of the model panels can be increased and the number of panels correspondingly reduced. If, for example, the total length of model insulation joint could be reduced to $(L_j)_m = (L_j)p\ (L_m/L_p)^2$, then good modeling fidelity would result, providing the heat flow perturbation effect of a unit length of model joint is the same as that of the same length of prototype joint.

For a spacecraft with regular sides, it may be relatively easy to keep the length of joint per unit area constant between model and prototype. For instance, suppose the spacecraft is a cube 12 feet on a side, and each panel face is covered by 16 insulation panels, each 3 foot square. A quarter-scale model would have 3-foot square sides, and if each side were covered by a single insulation panel, the ratio of joint length to surface area in the model will be the same as that of the prototype. The only question in scaling fidelity would be if the all-corner joints of the model would have the same heat perturbation effect as the part corner, part flat joints of the prototype.

If the insulation panels of the prototype of the previous example had been 6 feet square instead of 3 feet, there would be more of a modeling problem at quarter scale than in the previous example. The prototype of this example has a joint-length-to-surface-area ratio of 0.333 which the model should duplicate with 18.0 feet of joint. A one-piece insulation panel for a quarter-scale model, patterned after Figure 2-71, would have a joint-length-to-area ratio of 0.37 instead of 0.33. The difference would probably not be noticeable in terms of overall results.

A half-scale model, on the other hand, should have $(L_j)_m = 288\ (1/2)^2 = 72$ feet of joint. If each face of the model (6 by 6 feet) is covered with a single insulation panel, 72 feet of joint will be required and modeling fidelity should result. This again assumes that the joint between perpendicular panels has the same thermal disturbance to insulation performance as a joint between two panels in the same plane.

Other Insulation Penetrations

A real spacecraft system will have insulation penetrations for structural supports of antennas, scan packages, solar cell panels, and propulsion equipment, as well as penetrations for electronic equipment bay cooling. Because the heat disturbance to the spacecraft through these penetrations may be appreciable, it is probable that they should be modeled in true scale. The ratio of the net effect of the penetration in the model to that of the prototype should follow

$$\frac{q_m}{q_p} = \left(\frac{L_m}{L_p}\right)^2$$

This can be accomplished as far as the direct structural conduction is concerned, but the perturbation to the heat flow through the insulation may not work out as readily. The quoted suggestion, from Gabron (Ref. 10), that the model penetration be investigated empirically and the design tailored to give the desired results seems to be the only practical way to control the uncertainty in heat flow effect that scaled insulation penetrations could cause.

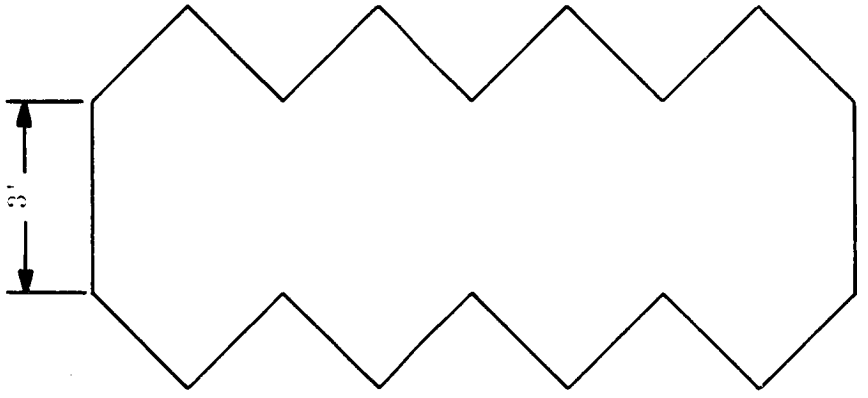

Figure 2-71. Insulation Panel

SECTION 2.0

TECHNICAL DISCUSSION

2.5 FULL SCALE THERMAL VACUUM TESTS

Section 2.5 Full Scale Thermal Vacuum Tests

SCOPE

The objective of the entire thermal insulation study program was to develop and experimentally qualify an insulation system for large interplanetary space vehicles. Figure 2-72 depicts the vehicle configuration considered in this study; the vehicle envelope is approximately 20 feet in diameter and 16 feet high.

Prior sections of this report have described the several experimental programs which were conducted to determine the capabilities and compatibilities of candidate thermal insulation materials. Furthermore, a detailed thermal analysis of the planetary vehicle has been presented, assessing the thermal control requirements associated with typical missions to Mars. Subsequent to the material evaluations and thermal analyses, a full-size test vehicle was constructed, insulated in accordance with the results of this earlier work, and evaluated under simulated interplanetary thermal vacuum environmental conditions. The full scale thermal vacuum test program is described in this section.

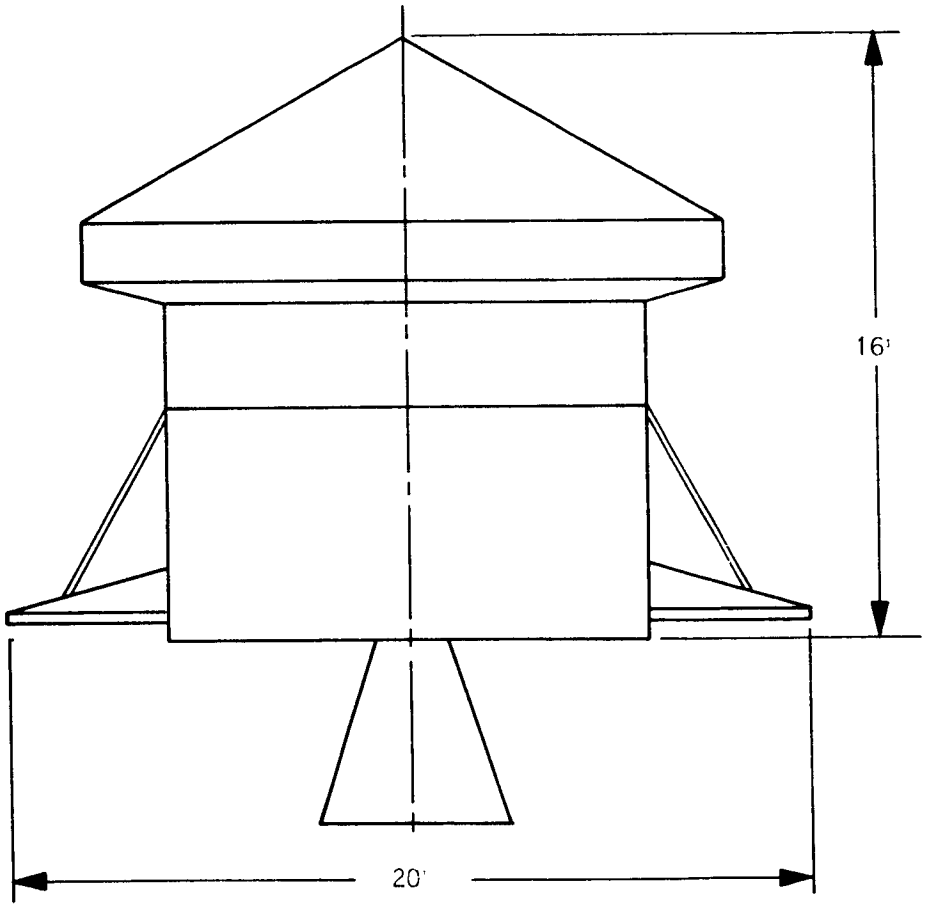

Figure 2-72. Vehicle Configuration

Section 2.5 Full Scale Thermal Vacuum Tests

SUMMARY OF RESULTS

The full scale thermal vacuum tests demonstrated that thermal control systems for large interplanetary vehicles are practical and can perform within the weight and electrical power restrictions generally applied.

Insulation Design

The following were significant developments from this portion of the program:

a. Gold coated Mylar and gold coated Kapton are effective insulation materials.
b. Required insulation weight, for the configuration studied, is less than 75 pounds.
c. Tinger fasteners, and Velcro hook and pile adhesive were shown to be effective installation and assembly retainers, allowing for rapid assembly and lessening the dimensional tolerance requirements.
d. Step (rabbet) joints and clear Kapton tape permit ease of installation and perform well.
e. Large insulation blankets are feasible, employing 1/8 inch diameter vent holes.

Thermal Performance

a. Deeply crinkled 1/4 mil gold on Mylar has high thermal performance per pound.
b. Insulation heat loss was significantly less than the design goals.
c. The insulation system is qualified for use on large interplanetary vehicles.

Section 2.5 Full Scale Thermal Vacuum Tests

Subsection 2.5.1 Insulation System Design/Analysis

CAPSULE INSULATION MATERIAL SELECTION

The insulation material for the planetary vehicle capsule must be capable of withstanding the decontamination and sterilization treatments and the interplanetary space environments. Furthermore, the material must provide effective thermal performance within the mission requirements.

Based upon the ETO compatibility tests (see Subsection 2.1.1), it was evident that gold is superior to aluminum in resisting degradation. Consequently, gold coated plastic films were employed for the capsule insulation blankets.

The purpose of the capsule insulation is to minimize capsule heating requirements and to reduce the temperature differences that would otherwise exist among the capsule components. The thermal conductance tests (Section 2.2) indicated that multilayered Mylar, metallized on one side and assembled without separators, had the lowest density-conductivity product. Crinkling of the Mylar is necessary to achieve optimum performance. Therefore, thermal performance and ETO compatibility led to the selection of crinkled gold coated Mylar for the primary capsule insulation. In addition, a cover sheet layer of 2 mil clear Kapton was specified over the Mylar, to minimize potential damage during installation.

The expected thermal performance was computed as follows:

From thermal conductivity tests of 35 layers of goldized Mylar in 1/2 inch thickness (including stitches, one attachment post, and 1 lineal foot of joint per square foot of area), effective emittance equals 0.0035 at an insulation warm-side temperature of 72°F. With 24 layers in 0.35 inch thickness, this effective emittance would be expected to increase to $\epsilon = 0.0035 \times (35/24) = 0.00510$.

Handling during installation is expected to degrade the insulation performance somewhat from the value determined by the conductivity measurements, but good manufacturing practices should keep this degradation, or increase of heat flux over measured value, from exceeding 50 percent. Using 50 percent degradation, the effective emittance increases to 0.00765.

The heat loss through the insulation then becomes $q = 0.00765 \times 474\ \sigma\ T^4$ where T is the structure temperature. At $T = 72^{\circ}F = 532^{\circ}R$:

$$q = 0.00765 \times 474 \times \frac{137.3}{3.41} = 145 \text{ watts for 24 layers (96.7 watts with 35 layers)}$$

In addition to the insulation heat loss from the capsule, there will be loss from one or more biovents. If each vent is 2 inches in diameter, as indicated by JPL, then the black-body cavity heat loss would be 0.88 watt per vent. Without any extra precautions, this loss is relatively small, but if deemed important, a hat fixture for the vent could be devised which would restrict its heat loss below the black body value.

In the calculation of capsule heat loss, the interface between the capsule and spacecraft is assumed to be adiabatic, since the design point temperatures for each component are equal. The calculated capsule power requirement of about 150 watts is in line with the allowable power of 150 to 200 watts. Increasing the number of layers and thickness of the insulation will reduce the power demand, but this is not required from a systems standpoint, since excess power is available up to the time that the capsule is separated from the spacecraft. On the other hand, reducing the insulation below the chosen 24 layers will not reduce installed insulation weight by a large amount, but will decrease the favorable operating margin that the chosen insulation provides.

Consequently, 24 layers of 1/4 mil gold on Mylar, with a 2 mil clear Kapton cover sheet, was selected for use over the capsule external surface.

Section 2.5 Full Scale Thermal Vacuum Tests

Subsection 2.5.1 Insulation System Design/Analysis

SPACECRAFT INSULATION MATERIAL SELECTION

The insulation for the spacecraft, like that for the capsule, must be capable of withstanding ETO and the space environments, and must afford effective thermal performance. The insulation is to completely cover the spacecraft except for the area of the solar cells and at the thermal control louvers. The exposed area, for the test configuration, was 296 square feet. The basic recommendation for the thermal insulation material, as discussed for the capsule, was the use of goldized Mylar.

The selected insulation materials consisted of:

a. 20 layers of gold-Mylar (1/4 mil) on the spacecraft external surfaces, e.g., sides and struts (see Figure 2-72) covered by a 2 mil layer of clear Kapton.
b. 20 layers of 1/4 mil gold-Mylar between the spacecraft and capsule. No cover sheet.
c. 10 layers of 1/2 mil gold-Kapton between the solar array and the spacecraft body.
d. 19 layers of 1/2 mil gold-Kapton between the orbit injection motor nozzle and solar cell annulus, with a 1/2 mil clear Kapton cover sheet.

The use of Kapton was specifically chosen for these latter two areas due to the high temperatures involved.

The expected thermal performance was computed as follows:

The effective emittance of the 20 layers of insulation on the cylindrical body and at the capsule end after the capsule has been ejected, is calculated from

$$\epsilon = 0.0034 \times 35/20 = 0.0060$$

Again increasing by 50 percent, the design emittance becomes

$$\epsilon = 0.0060 \times 1.5 = 0.0090$$

and the heat loss with capsule off is

$$q = 0.0090\,(296 + 122)\,\frac{\sigma T^4}{3.41} = 152 \text{ watts at } 72^{\circ} \text{ (87 watts with 35 layers)}$$

At the condition calculated above, which would occur during Mars orbit, the insulation at the engine end would operate at about 50°F. Assuming constant emittance, the heat leak for this area then becomes

$$q = 37 \times \frac{0.0090}{3.41}\,(\sigma T_{72}^4 - \sigma T_{50}^4) = 2 \text{ watts}$$

In addition, there is heat from the adjacent solar cells operating at 119°F.

$$q = 69 \times \frac{0.018}{3.41} (\sigma T_{119}^4 - \sigma T_{72}^4) = 21 \text{ watts}$$

and a net heat leak from all the thermal shorts of 83 watts.

The above heat losses sum as follows:

Heat loss at Mars at 72°F

From shaded surfaces exposed to space	152 watts
From insolated insulation	2 watts
From spacecraft mounted solar cells	-21 watts
From all thermal shorts	83 watts
Total nonlouvered heat loss at Mars	216 watts (151 watts with 35 layers)

For the flight period near earth, the insolated spacecraft surface will be considerably warmer. The Kapton insulation layer temperature will increase to 160°F, and the solar cells to 247°F. This will increase the net heat addition from these areas to about 106 watts, allowing for a slight decrease in effective emittance which will occur at the evaluated temperature. This condition, with capsule in place, will result in the following spacecraft heat loss through other than louvered surfaces:

Heat loss at earth at 72°F

From cylindrical spacecraft body	98 watts
From insolated surfaces	-106 watts
From thermal shorts	-17 watts
Total nonlouvered heat loss at earth	-25 watts

The tabulations of the nonlouvered heat losses of the spacecraft show a small gain at near-earth condition, indicating that the louvered equipment bays must have the capability of rejecting essentially all of the internally generated heat. At Mars, however, the nonlouvered heat loss has increased to more than 40 percent of the maximum expected heat dissipation.

Considering that one high-powered equipment bay may not have louvers, and assuming 0.2 minimum effective emittance for the louver operation of the other bays, a spacecraft average temperature of about 55°F in Mars orbit will result with the 20-layer insulation blanket at the minimum expected illuminated Mars orbit power demand. At the minimum Mars eclipse power demand, the average temperature would approach 45°F with the louvers nearly closed, except that the spacecraft heat capacity will prevent significant cool-down during the eclipse period, which is short relative to the spacecraft time constant.

As can be seen from the preceding paragraph, there is considerable margin in the spacecraft thermal design to maintain satisfactory temperatures in Mars orbit following capsule ejection. An additional reduction of 51 watts must occur in spacecraft internal heat release below minimum Mars occulted power before the average temperature would reach 40°F. If 35 layers of insulating material were used instead of 20, the total nonequipment bay heat loss at 40°F would reduce from 151 watts with 20 layers to 100 watts. Thus, the spacecraft would maintain minimum desired temperatures with 51 watts less internal power. The same result could be achieved by separating from the spacecraft the part of the biobarrier that would normably remain after capsule ejection. This shell, considered uninsulated on its exposed face, causes a 50-watt heat leak if it remains attached to the spacecraft. Essentially all of this loss would be eliminated if the remaining part of the biobarrier were ejected.

Section 2.5 Full Scale Thermal Vacuum Tests

Subsection 2.5.1 Insulation System Design/Analysis

CAPSULE BLANKET DESIGN

Figure 2-73 shows the basic outline of the capsule tested in this program. The capsule consisted of a forward conical section, a cylindrical section, and a lower conical section. The insulation blanket design for the capsule comprised:

a. A 31.5 inch diameter blanket over the nose of the forward conical section.
b. 20 triangular pieces, 36 inches at the base by 110 inches long, for the forward cone.
c. Six 109 by 21 inch rectangular sections for the cylinder.
d. Seven curved sections, 66 inches long by 30 inches wide with an outer radius of 103 inches, for the lower cone.

Blankets for all capsule sections were 24 layers of 1/4 mil gold-Mylar with a 2 mil clear Kapton cover sheet.

In general, a 2 inch overlap step joint was used due to its thermal efficiency and ease of manufacture and handling demonstrated during the structural properties evaluations (Section 2.3). Several joint types were considered, as shown in Figure 2-74. A weighting analysis was performed, and is depicted in Table 2-33, from which the step joint was selected. All joints were intermittently taped with Tech Floro clear Kapton, pressure-sensitive tape at approximately 6 inch intervals.

A significant aspect of the blanket design was that fasteners were employed which did not require disassembly of the fastener to remove the blanket. The "Tinger" fastener, developed during this program, is shown in Figure 2-75. Velcro "pile," attached to the vehicle,fastens to the Velcro "hook" on the Tinger; disassembly requires a 5 pound force peeling action. Four Tingers were used for the nose blanket, 16 for each of the upper cone triangular segments (leaving no more than 2 feet between fasteners as shown to be desirable in the depressurization tests, Subsection 2.3.1), 19 for each cylindrical section, and 10 for each of the lower conical sections. Based on the shock tests, holes for the Tingers were 0.296 inch in diameter.

As a result of depressurization test results, vent holes were provided in all blankets, there being four 1/8 inch diameter holes per square foot.

The total capsule insulated area was 474 square feet; the insulation weighed 35.3 pounds.

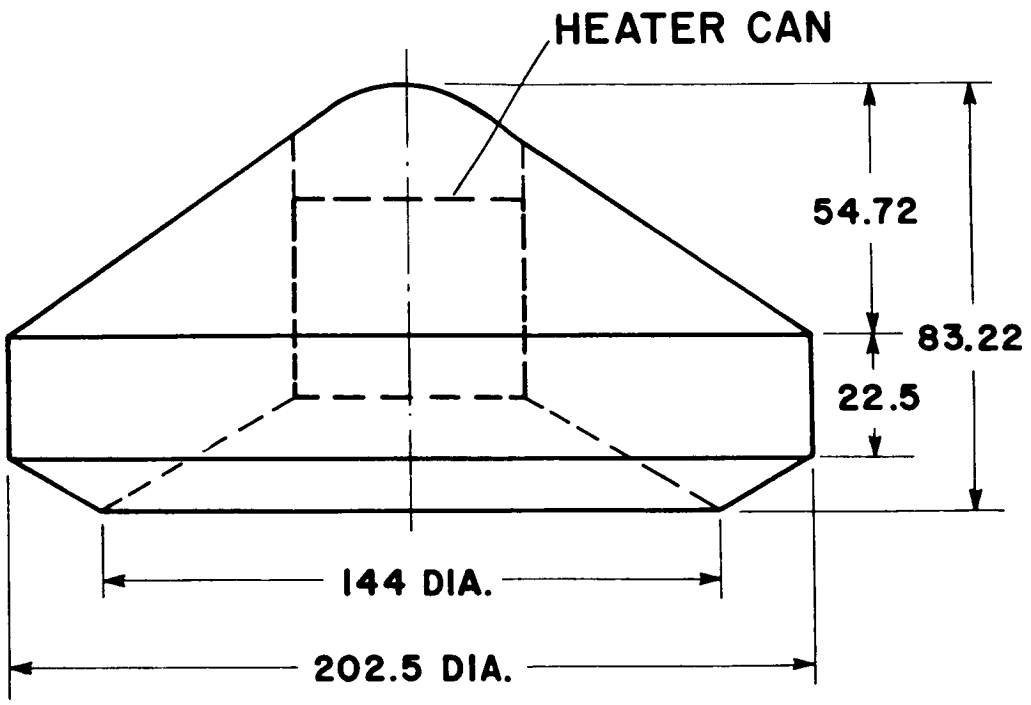

Figure 2-73. Capsule Configuration

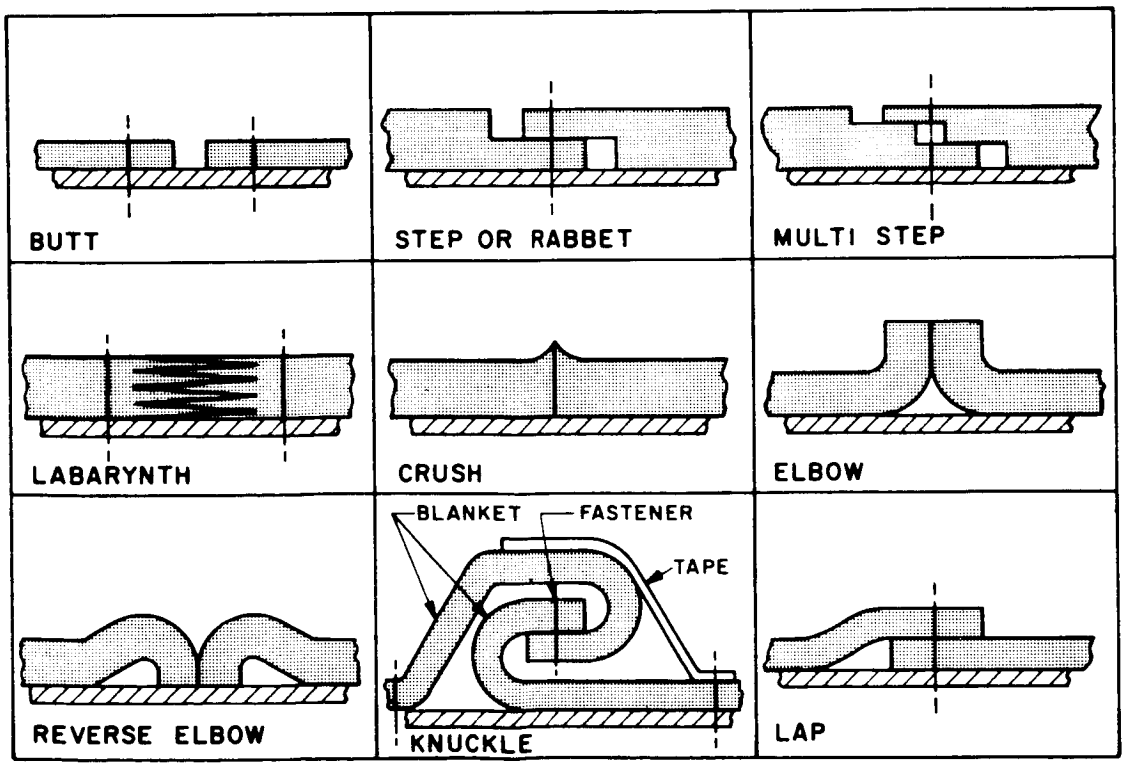

Figure 2-74. Joint Designs Considered

FOLDOUT FRAME 2

Table 2-33. Joint Selection Table

CRITERIA \ JOINT	STEP	MULTI STEP	LABARYNTH	CRUSH	ELBOW	REVERSE ELBOW	KNUCKLE	LAP	BUTT	WEIGHT
HEAT LOSS	+	+	+	+	–	O	+	O	–	25
VENTING	O	O	–	O	+	–	–	+	+	25
EASY TO INSTALL	O	O	O	+	O	O	–	O	+	5
EASY TO REMOVE	O	O	O	+	O	O	–	O	+	5
INEXPENSIVE TO MFG.	+	–	O	+	O	O	–	+	+	10
RELIABLE	+	+	+	O	O	O	–	+	O	25
CONFORMANCE TO GEOM.	+	+	+	+	–	–	–	+	+	10
HOLDS UP UNDER ENV.	+	+	O	+	–	–	–	–	+	
	87.5	77.5	70.0	80.0	47.5	35.0	25	67.5	67.5	

+ FULL VALUE O 1/2 VALUE – NO VALUE

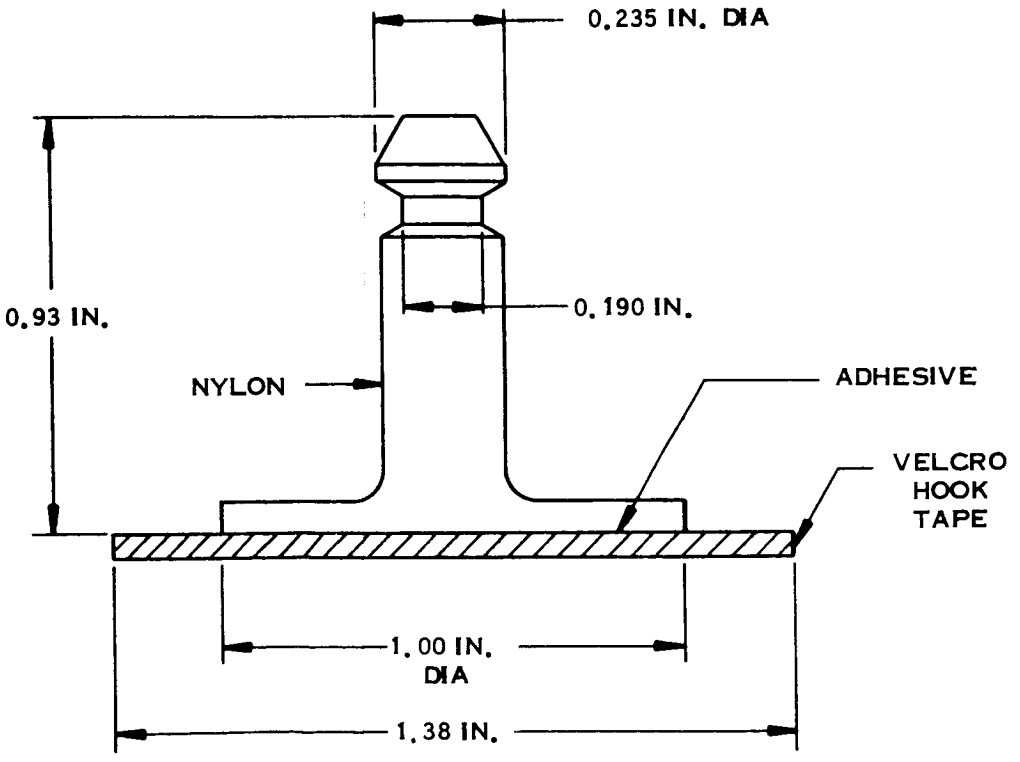

Figure 2-75. Tinger Configuration

Section 2.5 Full Scale Thermal Vacuum Tests

Subsection 2.5.1 Insulation System Design/Analysis

SPACECRAFT BLANKET DESIGN

Figure 2-76 depicts the basic outline of the spacecraft test configuration. The insulation requirements, as discussed under "Spacecraft Insulation Material Selection" (Subsection 2.5.1), are shown in Table 2-34.

Spacecraft side insulation consisted of 16 individual blankets, 102.5 by 30 inches wide, with 15 fasteners per section. Eight of the blankets had cutouts for simulated thermal louvers. At the base of the structure, the Kapton insulation between the engine and the solar array consisted of nine triangular segments, 34-inch arc length by 41.88 inches long, employing five Tinger fasteners per section. The insulation between the solar array and the spacecraft body was composed of 8 sections, 26 inches wide, with 6 fasteners per section. As with the capsule insulation, all joints were step joints, covered by clear Kapton tape.

All penetrations, i.e., struts, electrical harnesses and simulated scan platform, were insulated with specially configured blankets, described in Reference 6.

The total spacecraft insulation weight was 38.8 pounds, insulating a total area of 599 square feet. Coupled with the capsule insulation, the total vehicle insulation weighed 74.1 pounds and covered 1073 square feet.

Table 2-34. Spacecraft Insulation Requirements

Location	Number of Layers	Area (sq ft)	Weight (lb)
Side of spacecraft	20 layers gold on 1/4 mil Mylar 1 layer clear 2 mil Kapton	370	25.0
Interface-Capsule to spacecraft	20 layers gold on 1/4 mil Mylar	119	5.8
Spacecraft Between thrust chamber nozzle and solar panel	19 layers gold on 1/2 mil Kapton 1 layer clear 2 mil Kapton	45	4.7
Between base mounted solar array and spacecraft	10 layers gold on 1/2 mil Kapton	65	3.3
		599	38.8

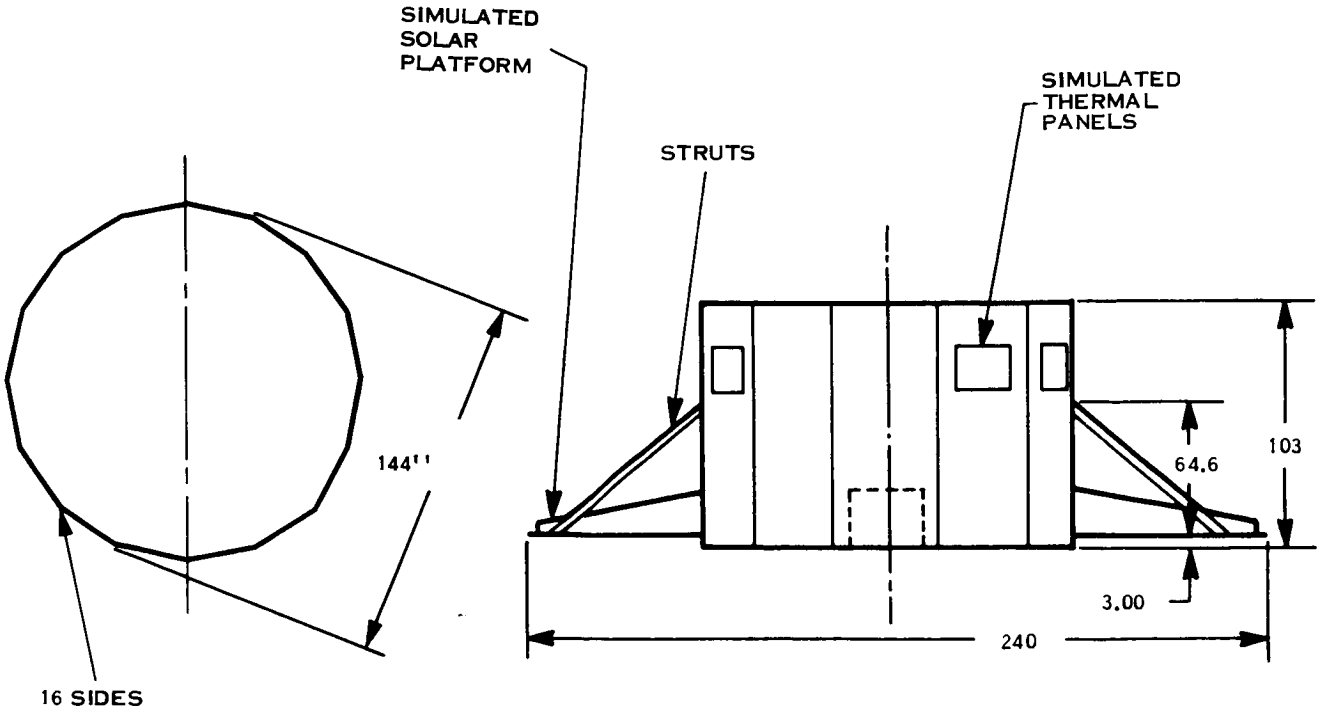

Figure 2-76. Spacecraft Configuration

Section 2.5 Full Scale Thermal Vacuum Tests

Subsection 2.5.1 Insulation System Design/Analysis

CAPSULE INSULATION THERMAL ANALYSIS

At the completion of the insulation system design, just discussed, a thermal analysis was conducted to refine the earlier analysis and to determine the temperature patterns expected during the thermal vacuum test, and to predict the power required to maintain the desired operating temperatures. The steady state analyses were performed for near-earth cruise and Mars orbit environments.

The capsule analysis was performed for two configurations: one with the nodal division as shown on Figure 2-77, and the other with the heat shield and aeroshell structure removed (nodes 8 to 17). Thus, the first configuration is generally representative of an actual capsule configuration, with the surface laboratory represented by the cylindrical heater of node 1, while the second configuration, which does not incorporate the heat shield and aeroshell structure within the sterilization canister, is similar to the capsule test fixture designed for the thermal vacuum tests.

All of the capsule nodes are symmetrical about the centerline. Planar nodes 2 and 3 are used to represent the actually conical insulated interface between the capsule and spacecraft. Nodes 2, 3, and 4 are considered adiabatic, since the spacecraft and capsule may be at the same temperature, except for one low temperature capsule case where the spacecraft is assumed warmer. Nodes 5, 6, 7 and 18 through 22 are assigned to that part of the sterilization canister that is exposed to space. It is assumed that no external radiation is incident on this external surface, since it is shaded from the sun by the spacecraft, and that radiation to space through the surrounding insulation is controlled by an effective emittance term applied to these nodes. Each of the nodes exchanges internal radiation with all other nodes in view, except that radiation between the heat shield and the adjacent canister is restricted to nodes that are immediately opposite; e.g., node 13 to node 18, node 14 to node 19, etc. Details of the internodal connections are presented in Reference 6.

Figure 2-78 plots temperatures of some typical nodes of the capsule-with-aeroshell for a range of heater power. Reference 6 presents data for all the nodes. Heat is assumed to be generated uniformly over the entire heater surface that is represented by node 1. Thus, the figure should be entered at values of heater power and the resulting temperature pattern determined. Figure 2-79 shows similar values for the configuration that does not include the shield and aeroshell, demonstrating that the test configuration temperatures within the capsule will be more uniform than would be expected for an actual capsule and aeroshell situation.

The low power point on Figure 2-79, designated by the symbol ◊, represents the test situation where the capsule is colder than the spacecraft. Therefore, capsule nodes 2, 3, and 4, receive heat by radiation through the spacecraft-capsule interface insulation, and node 4 receives conductive heat through the spacecraft-capsule structural connection, with the spacecraft assumed to be at the upper test temperature of 115°F.

FOLDOUT FRAME /

The net results for the two capsule configurations considered show that the low effective emittance of the capsule external insulation results in relatively small capsule temperature differences. As expected, the test configuration without the shield is more nearly isothermal, but the difference is not sufficient to warrant increasing the complexity of the test fixture to include this component.

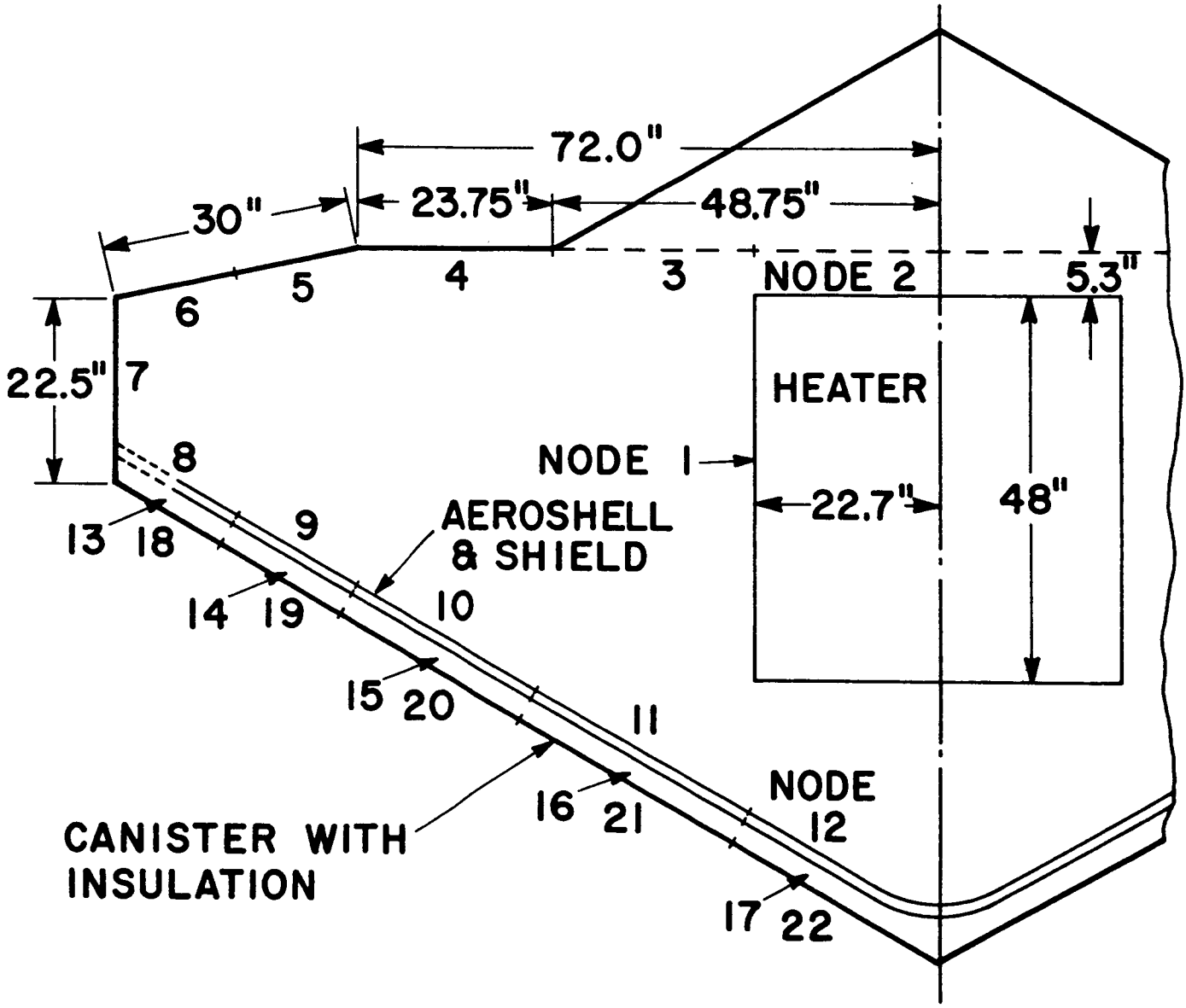

Figure 2-77. Capsule Nodal Configuration

FOLDOUT FRAME 2

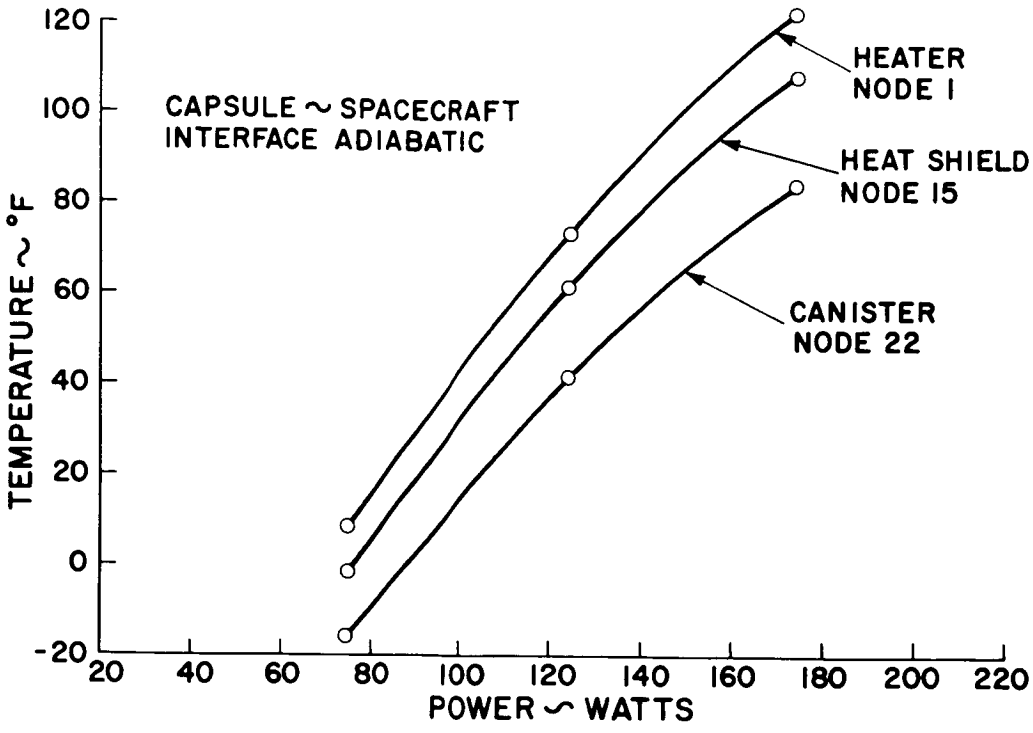

Figure 2-78. Capsule with Shield

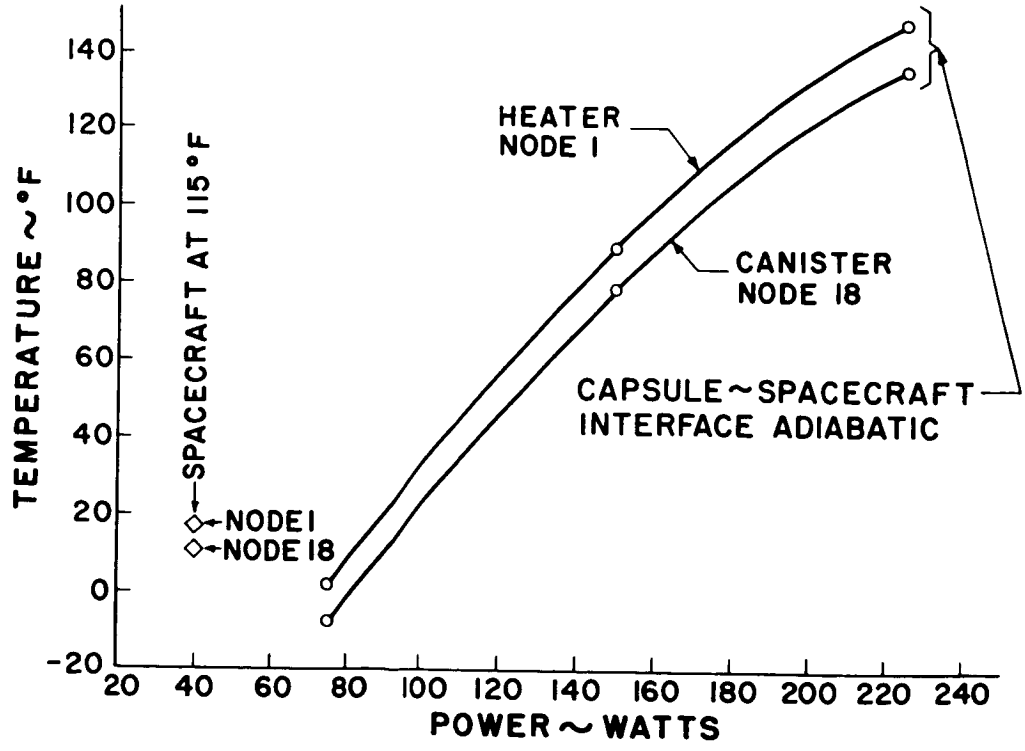

Figure 2-79. Capsule without Shield

Section 2.5 Full Scale Thermal Vacuum Tests

Subsection 2.5.1 Insulation System Design/Analysis

SPACECRAFT INSULATION THERMAL ANALYSIS

The spacecraft analysis configuration included a liquid fueled midcourse correction and orbit insertion engine. Although internal spacecraft analysis details such as engine piping to tankage connections, and external engine nozzle shading were not included, the spacecraft thermal analysis was more complex than that of the capsule.

The spacecraft analyzed here, and shown in Figure 2-80, was a prism comprised of 16 sides. Heat flow, from electronic equipment mounted to eight of these sides, was simulated by electrical heaters mounted on the equipment bay panels. Four main engine fuel tanks are located within the body. In an attempt to reduce the number of nodes required to analyze this situation, the spacecraft was divided into eight equal parts. Each part includes an equipment bay panel, an adjacent plain panel, and one half of a fuel tank. The nodal network made up one of these one-eighth circumferential sections.

In the symmetrical spacecraft, each of the equipment bays will have a radiation connection to each of the fuel tanks. Consequently, radiation from the equipment bay to the tank in the one-eighth section was set up to include the view factor summation of a bay to all the tanks. In like manner, the internal radiation interchange between all nodes of the one-eighth section mathematical model includes the total view factor that would occur between similar type nodes in the full sized case. In this fashion, the spacecraft analysis was performed with 32 nodes whereas several hundred nodes would be required to give this much detail for a whole spacecraft. Reference 6 presents the spacecraft nodal connection details. Five conditions or cases were considered. In each case the solar flux was assumed incident on nodes 28, 29, 31 and 32. Specific details of each case are given in Table 2-35. In this table, the node 1 (equipment bay panel) heater power is stated as eight times the value actually used in the one-eighth section mathematical model, and is thereby applicable to the entire spacecraft. The principle nodal temperatures that result for each case are given in Tables 2-36 and 2-37.

Cases 3, 4, and 5 of the spacecraft analysis included a radiation and conduction term of the capsule instead of the normally assumed adiabatic interface. In case 5, the capsule was assumed to be at 10^{o}F, and spacecraft power was adjusted to give approximately 115^{o}F spacecraft temperature. Thus, this computed point shows the influence of the capsule on the spacecraft in the inverse sense that the effect of the spacecraft on the capsule had been previously shown.

Cases 3 and 4 represent Mars orbit conditions where the capsule has been separated from the spacecraft but the uninsulated aft biobarrier remained attached. Previous calculations had indicated that 50 watts would be conducted from the spacecraft, at 40^{o}F, to the aft biobarrier, and this heat leak was incorporated in the analysis. This previous analysis indicated that the biobarrier would become very cold, and so the radiation connection from node 10 was assumed to be the same as directly to space. These cases show that appreciable temperature differences can exist within the spacecraft structure, primarily in the region directly affected by the heat leak connections.

Cases 1, 3, and 5 were computed with the assumption that the external equipment bay radiating panels have a constant emittance of 0.05. In an actual design, the emittance of these panels will be automatically adjusted by louvers to accommodate power changes without the large temperature changes shown. For such a louvered thermal control system, the 0.05 emittance assumed is below the normally expected closed louver emittance. This value was chosen for the analysis, however, to represent the test configuration which does not include the extra detail of louvers.

To demonstrate the effect of equipment bay panel emittance, cases 2 and 4 were performed for an emittance of 0.3. The results show that the chief effect of equipment bay panel emittance is to shift the power scale by the increment representative of the change in emittance, although a slightly low choice of power for case 4 tends to confuse this comparison. For the test conditions, however, there was some uncertainty in the amount of external radiant heat flow that would occur from the equipment bay panels, due to uncertainties in surface emittance and degree of thermal interaction with the back of the spacecraft solar array and the capsule outer surface that is within "view" of the panels. Low panel emittance reduced this heat flow, and so reduced the absolute amount of heat flow uncertainty that could occur from this effect.

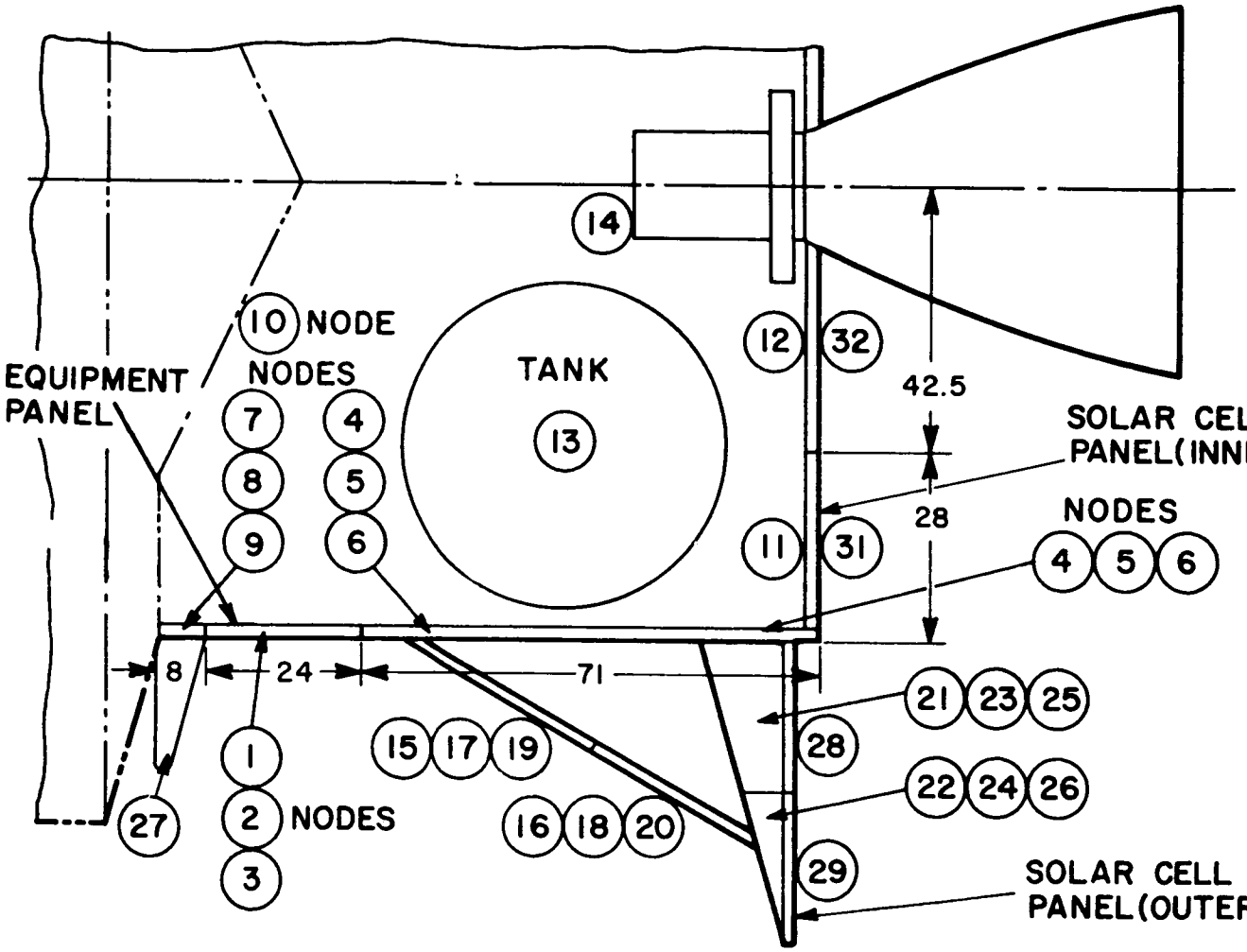

Figure 2-80. Spacecraft Nodal Configuration

FOLDOUT FRAME 2

Table 2-35. Case Descriptions

Case	Mode	ϵ Node 1	q Node 1 (watts)	Solar Flux (Btu/hr-ft^2)	Condition
1	Near earth	0.05	99.2	442	Spacecraft-capsule interface adiabatic
2	Near earth	0.30	456.8	442	Spacecraft-capsule interface adiabatic
3	Near Mars	0.05	181.6	200	Heat leak through spacecraft-capsule interface to space included
4	Near Mars	0.30	356.8	200	Heat leak through spacecraft-capsule interface to space included
5	Near earth	0.05	150.4	442	Heat leak through spacecraft-capsule interface to 10^{o}F capsule included

Table 2-36. Spacecraft Near-Earth Temperature

Capsule Interface	Adiabatic		10^{o}F
Equipment Panel Emittance Equipment Power (watts)	(Case 1) 0.05 99	(Case 2) 0.30 457	(Case 5) 0.50 150
Node 1 (equip panel) (^{o}F)	113	117	121
Node 4 (middle side) (^{o}F)	108	109	109
Node 9 (top side) (^{o}F)	102	104	99
Node 13 (tank) (^{o}F)	110	111	110
Node 14 (engine) (^{o}F)	125	126	125
Node 29 (outer array) (^{o}F)	145	145	145
Node 31 (base array) (^{o}F)	230	230	230

Table 2-37. Spacecraft Near Mars Temperatures (After Capsule Ejection)

Equipment Panel Emittance	0.05 (Case 3)	0.30 (Case 4)
Equipment Power (watts)	182	357
Node 1 (equip panel) (^{o}F)	62	49
Node 4 (middle side) (^{o}F)	36	28
Node 9 (top side) (^{o}F)	13	4
Node 13 (tank) (^{o}F)	38	30
Node 14 (engine) (^{o}F)	46	38
Node 29 (outer array) (^{o}F)	53	53
Node 31 (base array) (^{o}F)	106	106

Section 2.5 Full Scale Thermal Vacuum Tests

Subsection 2.5.2 Test Apparatus

TEST FIXTURE DESIGN/FABRICATION

The full scale thermal vacuum test fixture consisted of a spacecraft and a capsule structure. The capsule and spacecraft fixtures were fabricated separately and joined for testing. The insulation barrier between capsule and spacecraft was supported by a sheet metal platform. The uninsulated test fixture weighed about 2800 pounds.

The capsule fixture under construction is shown in Figure 2-81. Basically, the capsule consisted of an upper long conical section, a cylindrical section, and a lower short conical section. Detail drawings of the capsule fixture are presented in Reference 6. The structural material was all 6061-T6 aluminum. Four handling lugs were provided at the 144 inch diameter of the upper cone. A cylindrical heater was located in the center of the capsule structure, being attached to the skin of the forward cone by suspension bars and to the cylindrical section by cables and structures.

The spacecraft structural configuration is shown in Figure 2-82. The structure, a 100 inch high 16-sided figure, was fabricated in four identical 90 degree segments from 6061-T6 aluminum. A central platform, supported by struts and braces, provides the mounting for a simulated rocket motor.

Figure 2-83 depicts the completely assembled thermal vacuum test fixture. Special handling equipment, e.g., dolly and lift sling, may be seen. The spacecraft is shown with the simulated louver panels in place and with the "solar array" and struts mounted.

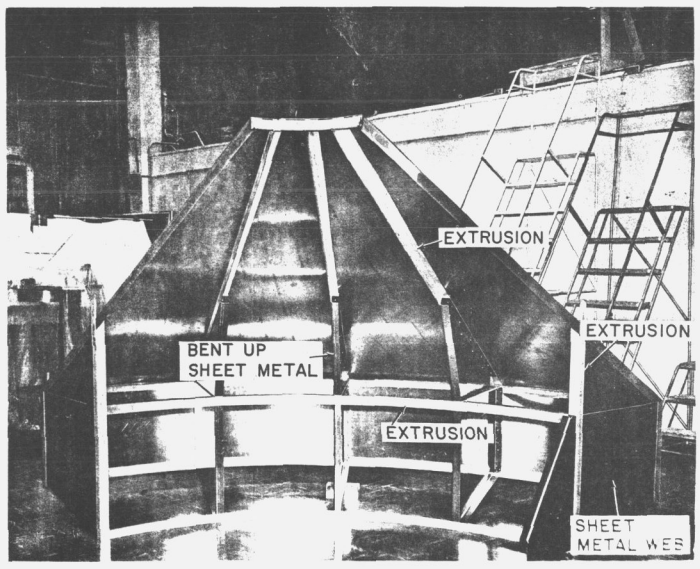

Figure 2-81. Capsule Test Fixture - Construction

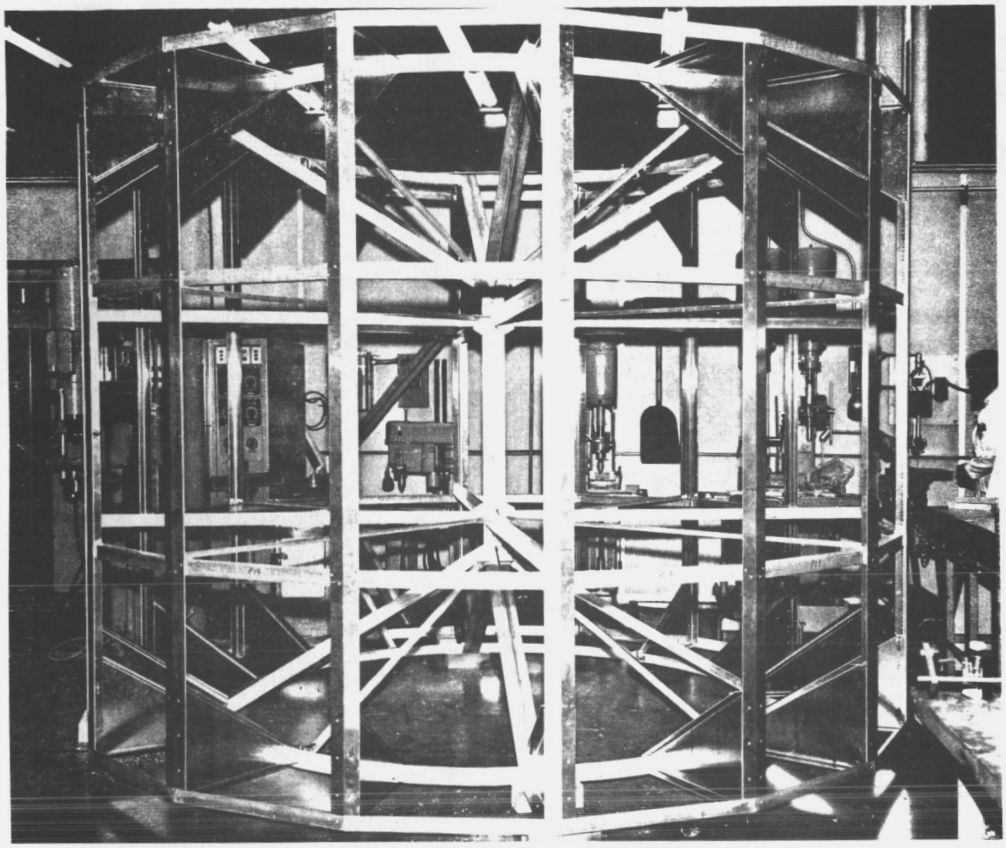

Figure 2-82. Spacecraft Test Fixture - Structural Configuration

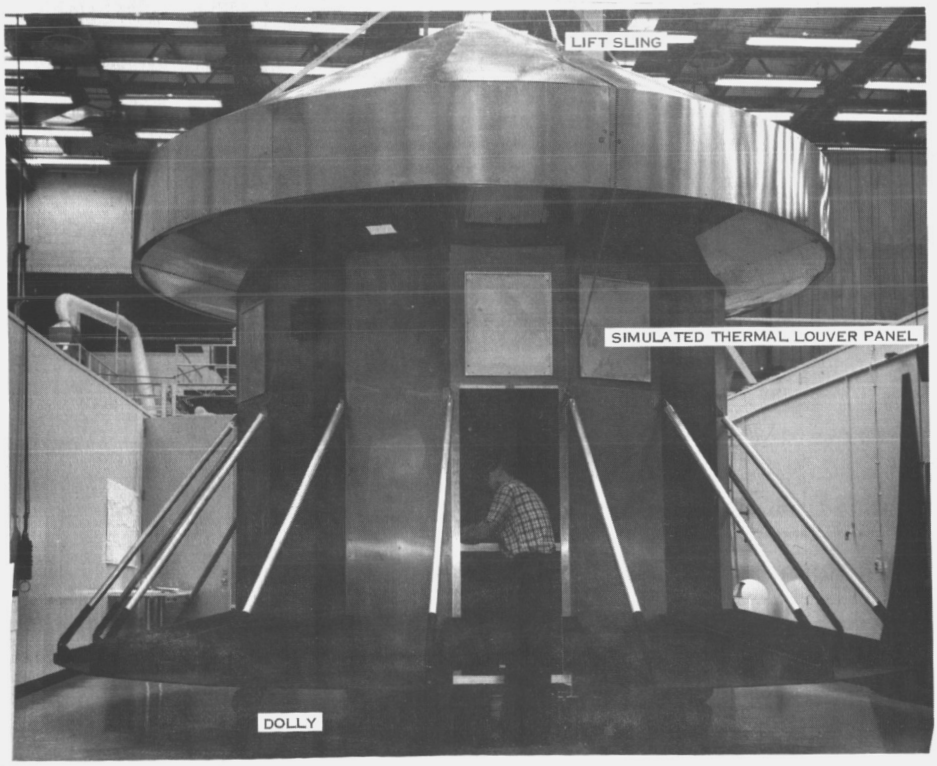

Figure 2-83. Complete Test Fixture

Section 2.5 Full Scale Thermal Vacuum Tests

Subsection 2.5.2 Test Apparatus

THERMAL BLANKET FABRICATION/ASSEMBLY

Fabrication and installation of the insulation blankets, due to their large size and sensitivity to handling, required the development of special procedures and techniques. Figure 2-84 schematically presents the blanket fabrication steps.

To enhance the thermal properties of the gold coated Mylar, the as-received material was drawn through a teflon die which imparted random permanent creases to the material. Figure 2-85 shows the crinkling process. After the crinkled metalized film came out of the die, it was re-rolled onto a large drum. The number of turns put on the drum was determined by the quantity of layers required by the insulation blanket. When the correct amount of turns was registered on a counter, the material was cut off and laid flat on a table to be further processed.

Metal templates were made of the desired blanket profile and penetrations. The mounting holes, into which the Tinger mounting posts were placed, were also located by the templates. A cover sheet of 2 mil Kapton was placed on top of the lay-up of insulation material on the table. The metal template was placed on top and clamped to the table. An X-acto knife was used to cut the blanket to shape, using the metal sides of the template to guide the blade (Figure 2-86 depicts this operation). The use of Tinger fasteners, employing 2 by 2 inch Velcro "pile" cemented to the spacecraft, eliminate the requirement for precise location of mounting holes. The spacecraft skin is not penetrated for mounting. Tingers provide several other advantages: namely, the need for blanket stitching is eliminated, blanket removal is facilitated without need for disturbing other blankets, ease of alignment permits better fit-up, and blanket installation on the vehicle is simplified.

The blankets were designed so that they were fabricated 1/2 percent larger than the surface area to be covered, permitting the spacecraft and blankets to have generous tolerances. Handling frames, used to pick up and install the blankets, had the mounting holes located so that they were in a nominal position, giving assurance that the installed blanket would always have some degree of slack.

The method employed to install large blankets is to lay the blanket out in a flat position, placing the handling frame on the blanket so that the support posts (Tingers) are in the locating holes of the frame. Spring loaded collets lock the Tinger to the frame, making the frame and blanket a unit. The assembly is then placed in the proper location on the spacecraft.

The pattern of the Velcro pile pads match the pattern of the Tinger posts as they are both positioned with the same handling frame as formerly noted. The collets are unfastened and the frame is carefully removed, leaving the insulation in place.

FOLDOUT FRAME |

The final fitting of the insulation blanket on the vehicle was accomplished by moving the support post so that the joints were all closed and, at the same time, the blanket was not tau between supports. The cover sheets of the blankets were interwoven and taped together acr the seams using 1 inch wide pressure sensitive Kapton tape (Tech Floro).

Care was exercised by all personnel that handled the blankets. White nylon gloves were wo prevent fingerprints on the insulation. The blankets were stored on flat trays, in a rack tha was kept covered with a plastic cover to keep the blankets as clean as possible. The trays, which could be removed from the rack, made the blankets accessible to install the handling frames, minimizing the danger of damage to the insulation blankets. The rack was mounted wheels so that the distance the blanket had to be carried to the spacecraft was minimal.

The installation of the complete insulation took eight man days, including the installation of blankets. There was no need to rework any blankets and every joint closed fully.

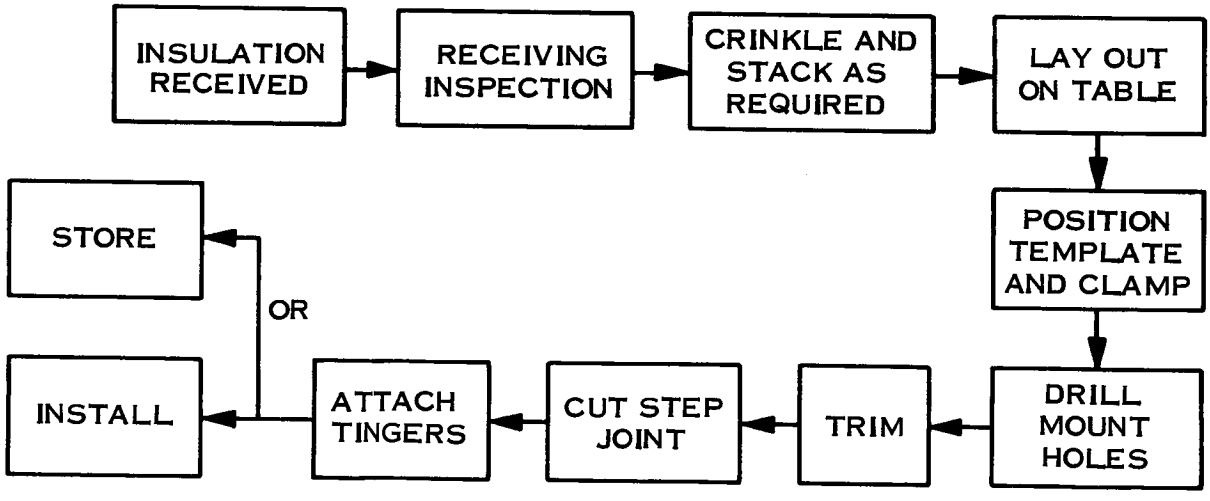

Figure 2-84. Blanket Fabrication

FOLDOUT FRAME 2

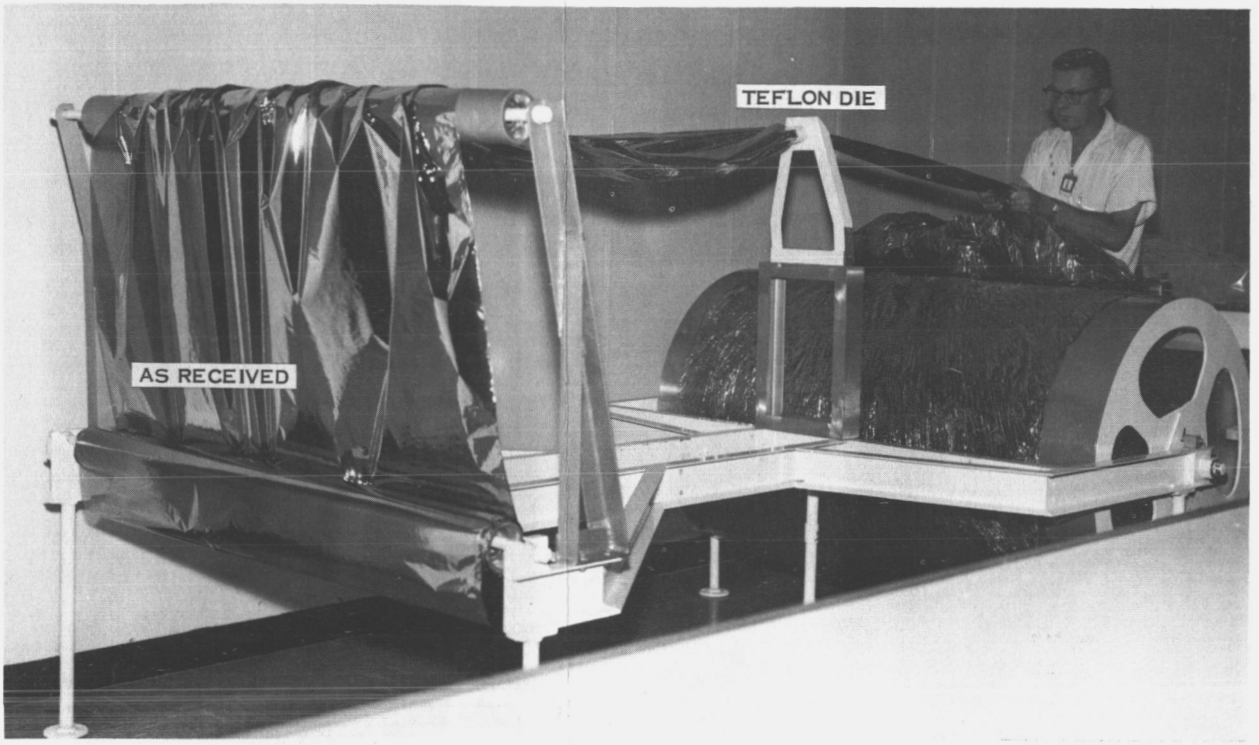

Figure 2-85. Crinkling Operation

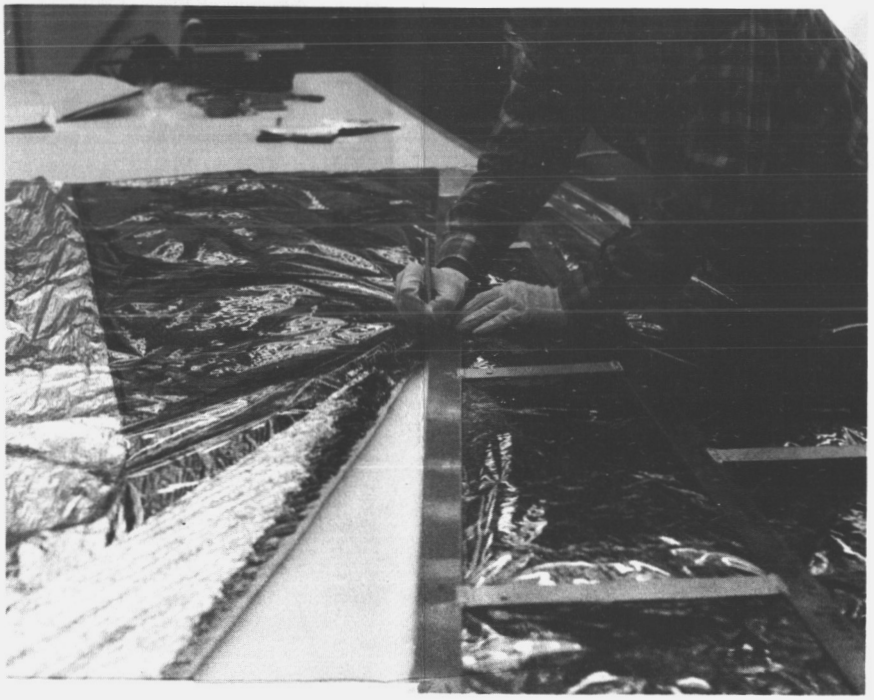

Figure 2-86. Fabrication

Section 2.5 Full Scale Thermal Vacuum Tests

Subsection 2.5.2 Test Apparatus

FACILITY DESCRIPTION

The full scale thermal vacuum test was conducted in a 39 foot diameter thermal vacuum chamber at the General Electric Valley Forge facility. Figure 2-87 depicts the test fixture being prepared for test. The fixture is suspended by the lift sling and supported by the utility dolly, permitting ease of rotation. The overhead crane is capable of lifting the test fixture along with the thermal vacuum chamber lid, as shown.

Figure 2-88 shows the test fixture in the vacuum chamber in the test position. Note that the fixture is suspended from the chamber lid by cables, the lift sling having been removed. An IR heater, attached to the bottom of the fixture, provides simulated solar heating to the insolated end of the spacecraft.

Figure 2-89 is a photograph of the completely assembled and insulated test fixture prior to testing.

The temperature control equipment, used on these tests, consisted of Research, Inc. LABAC controllable dc power supplies and Thermac temperature controllers. The equipment had the capability of controlling temperature within $\pm 2^{o}F$ of the set point. Heat-up to the set point was accomplished automatically, manual control being employed for final power adjustments. The rate of temperature change was restricted to less than $0.20^{o}F$/hour.

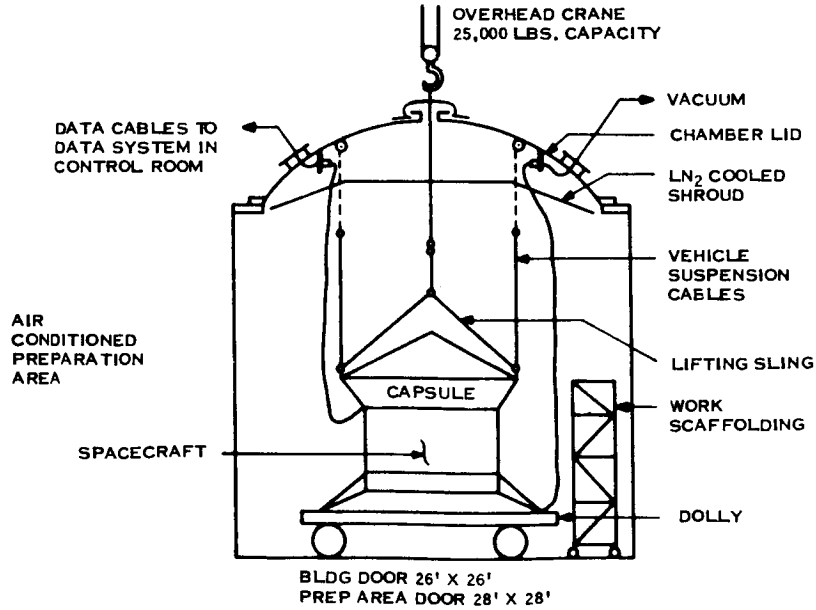

Figure 2-87. Test Preparation

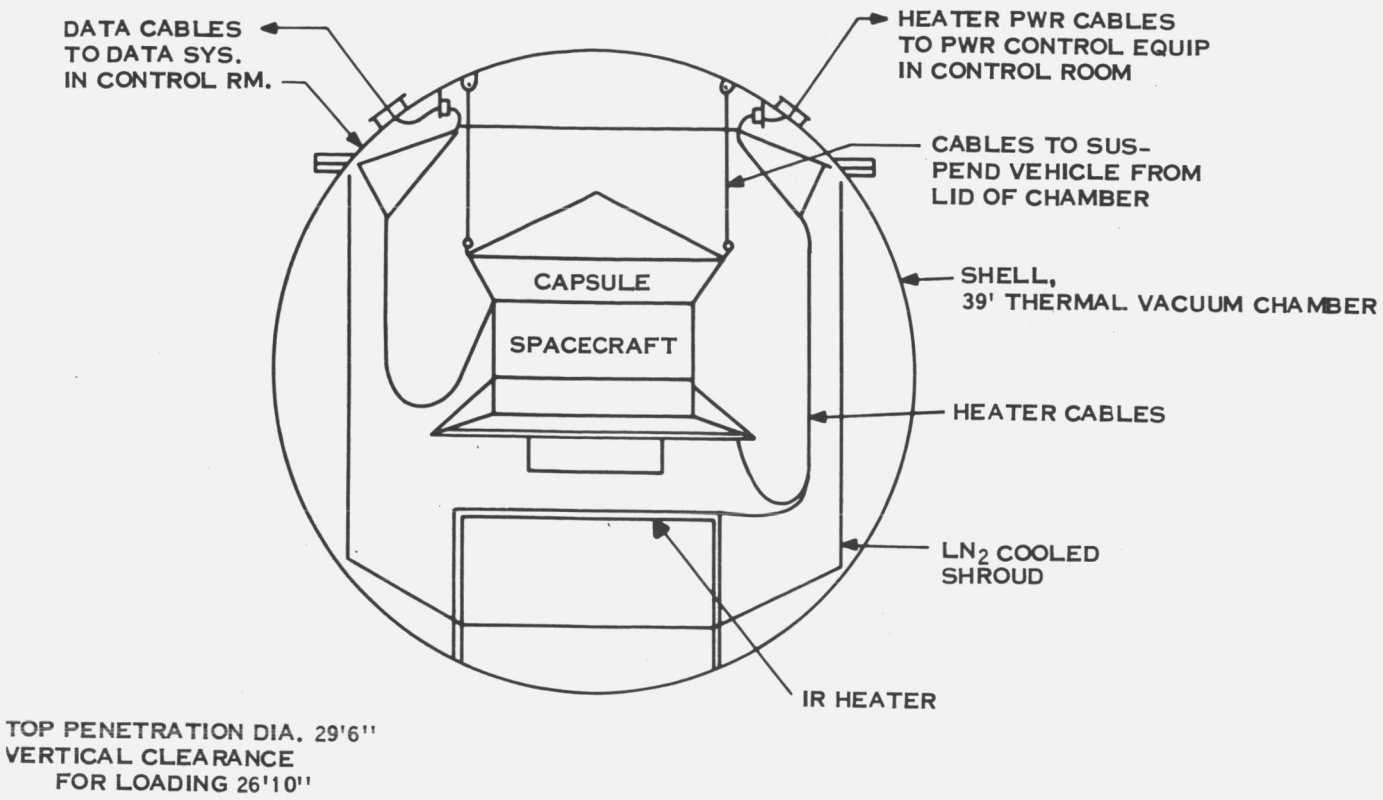

Figure 2-88. Chamber/Fixture Integration

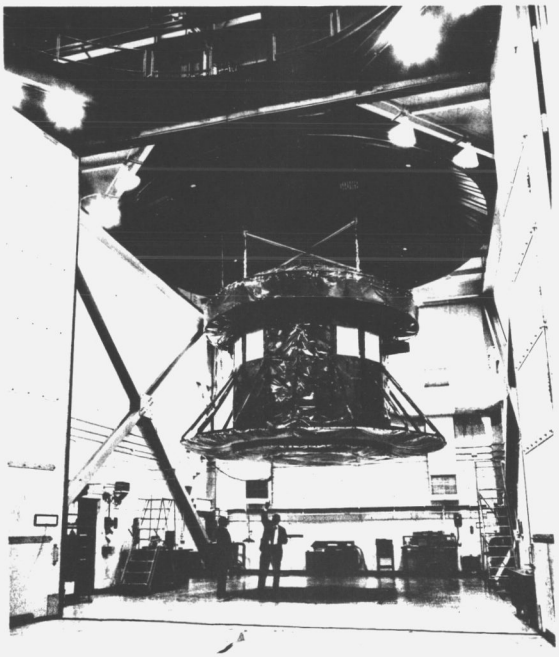

Figure 2-89. Complete Test Article

Section 2.5 Full Scale Thermal Vacuum Tests

Subsection 2.5.2 Test Apparatus

THERMOCOUPLE INSTRUMENTATION

Temperatures of the thermal vacuum test vehicle and test chamber were closely monitored throughout the program by approximately 200 thermocouples. The thermocouples were fabricated of premium grade 24 gage copper-constantan wire. Table 2-38 describes the thermocouple locations for the spacecraft, capsule, and test chamber walls.

The thermocouples were terminated in a bulkhead-type connector on the test fixture. Extension cables then carried the thermocouple signals into the control room. The reference junction was a $32^{\circ}F$ ice chest. Use of the General Electric computer facilities made it possible for reduced temperature data to be available at the test site within 20 minutes or less of a data scan.

Proper evaluation of the preponderance of thermocouple data required the establishment of temperature zones, each zone consisting of several thermocouple measurements. Table 2-39 presents the make-up of each of the 44 temperature zones, depicting the thermocouple channels involved and describing the location monitored by each zone. The zone temperature, described under Thermal Vacuum Test Results, Subsection 2.5.4, is arrived at via an arithmetic average of the thermocouple channels within the zone.

FOLDOUT FRAME /

Table 2-38. Thermocouple Locations

Thermocouple Channel No.	Location
1 thru 40	Equipment Bay Panels - 5 T/C Each
41 thru 48	S/C Structure at Capsule Attachment
49 thru 64	S/C Side Panels 37.5 Inch Above Bottom
65 thru 68	S/C Structure at Array Strut Attachment
69 thru 72	S/C Structure at Array Beam Attachment
73 thru 78	S/C-Capsule Insulation Support at 54 Inch Ra
79 thru 84	S/C Bottom at 51 Inch Radius
85 thru 86	Top of Engine
87 thru 88	Engine Throat Heater Plate
89 thru 90	S/C Structure at Scan Platform Bracket
91 thru 92	Scan Platform Bracket 4 Inch From S/C
93 thru 94	Array Strut 6 Inch From Attachment to S/C
95 thru 96	Array Beam 6 Inch From S/C
97 thru 98	Spares
99 thru 100	S/C-Capsule Harness at Midpoint
101 thru 102	S/C-Capsule Harness at S/C Penetration
103 thru 104	S/C at Chamber Cable Connector
105 thru 106	Chamber Harness 18 Inch From S/C
107 thru 120	External Solar Panels at 99 Inch Radius
121 thru 123	External Solar Panels at Periphery
124 thru 126	External Solar Panels at S/C Side Panels
127 thru 130	Spares
131 thru 134	Body Array Solar Panels at 58 Inch Radius
135 thru 136	Body Array Solar Panels at Outer Periphery
137 thru 138	Body Array Solar Panels at Inner Periphery
139 thru 142	Bottom I.R. Heater Can at 30 Inch Radius
143 thru 150	Spares
151	Capsule Top Skin at Center
152 thru 154	Capsule Top Skin at 24 Inch Radius
155 thru 157	Capsule Top Skin at 48 Inch Radius
158 thru 160	Capsule Top Skin at 72 Inch Radius
161 thru 163	Capsule Top Skin at 96 Inch Radius
164 thru 166	Capsule Skin at Midpoint of Outer Cylinder
167 thru 169	Capsule Bottom Skin at About 86 Inch Radius
170 thru 171	Capsule at Harness Connector
172 thru 179	Capsule Structure at S/C Attachment
180	Spare
181 thru 186	Capsule Heater 24 Inches From End of Cylinder
187 thru 190	Capsule Structure at Lifting Points
191 thru 192	Capsule Lift Cables 18 Inch From Capsule Skir
193 thru 199	Spares or Open Circuit
200	Equipment Bay Heater Current Shunt
201	Equipment Bay Heater Voltage Divider
202	Capsule Heater Current Shunt
203	Capsule Heater Voltage Divider
204 thru 236	Test Chamber Inner Wall

FOLDOUT FRAME 2

Table 2-39. Temperature Zones

Zone No.	Location	T/C Channels
1.	Equipment Bay Panel #1	1-5
2.	Equipment Bay Panel #2	6-10
3.	Equipment Bay Panel #3	11-15
4.	Equipment Bay Panel #4	16-20
5.	Equipment Bay Panel #5	21-25
6.	Equipment Bay Panel #6	26-30
7.	Equipment Bay Panel #7	31-35
8.	Equipment Bay Panel #8	36-40
9.	All Equipment Bay T/C	1-40
10.	S/C Structure at Capsule Attachment	41-48
11.	S/C Skin Between Eq. Bay and Base	49-64
12.	S/C Structure at Array Strut	65-68
13.	S/C Structure at Array Beam	69-72
14.	S/C Capsule Insulation Support (51" Radius)	73-78
15.	S/C Base Structure at 51" Radius	79-84
16.	Base Solar Panel at 58" Radius	131-134
17.	Base Solar Panel at O.D.	135-136
18.	Base Solar Panel at I.D.	137-138
19.	Base Solar Panel O.D. and I.D.	135-138
20.	All Base Solar Panel T/C	131-134
21.	External Solar Panel at 99" Radius	107-120
22.	External Solar Panel at O.D.	121-123
23.	External Solar Panel at I.D.	124-126
24.	External Solar Panel O.D. and I.D.	121-126
25.	All External Solar Panel T/C	107-126
26.	S/C Structure at Planet Scan Platform	89-90
27.	Head of Simulated Engine	85-86
28.	Engine Throat Solar Simulator	87-88
29.	I.R. Heater Can at 30" Radius	139-142
30.	Solar Array Support Strut	93-94
31.	Solar Array Support Beam	95-96
32.	Planet Scan Platform Support	91-92
33.	S/C Capsule Harness at S/C	101-102
34.	S/C Structure at Chamber Harness Connectors	103-104
35.	Chamber Harness 6 in. from S/C	105-106
36.	Capsule Structure at S/C Attachment	172-179
37.	Capsule Skin	151-169
38.	Capsule Heat Source	181-186
39.	Capsule Lift Cable	191-192
40.	Capsule Structure at Support Cable	187-190
41.	Capsule Skin and Heater T/C	151-169 & 181-186
42.	Capsule Structure at Harness Connectors	
43.	Midpoint of S/C Capsule Harness	170-171
44.	Test Chamber Shroud	99-100 204-236

Section 2.5 Full Scale Thermal Vacuum Tests

Subsection 2.5.3 Test Procedures

PROCEDURES AND PREPARATION

A full scale thermal model of a large interplanetary spacecraft was tested in a thermal vacuum chamber to evaluate the performance level of an insulation system under simulated environmental conditions. The insulation materials used, and the detailed design of the insulation system and test fixture (thermal model of the spacecraft), are described in Subsections 2.5.1 and 2.5.2. This section outlines the specific tests and procedures used.

Test Conditions and Accuracies

The test objective was to subject the full scale planetary vehicle fixture and insulation system to the following conditions:

Vacuum level	1×10^{-5} torr or lower
Temperature/emittance	$-280^{\circ}F$ ambient or lower, with wall emissivity $\geqq 0.90$
Solar array temperature	To $235^{\circ}F \pm 2^{\circ}F$
IR can	To $160^{\circ}F \pm 2^{\circ}F$ with emissivity = 0.90
Capsule and spacecraft temperature	$10^{\circ}F$, $60^{\circ}F$, and $115^{\circ}F \pm 3^{\circ}F$ at each set point level
Heater power measurements	$\pm 1\%$

Test Preparations

Figure 2-90 is a block flow diagram of the test vehicle movement prior to and following the thermal vacuum tests. Basically, the capsule and spacecraft were moved from the aseembly area to the preparation area adjacent to the test chamber. Figure 2-86, of Subsection 2.5.2, shows the fixture during preparation. Heaters, thermocouples, insulation and instrumentation were installed and checked out. After installation in the test chamber, the system was pumped down, the tests performed and the chamber warmed up and vented. Post-test, the insulated test fixture was removed from the chamber and returned to the preparation area for visual observation.

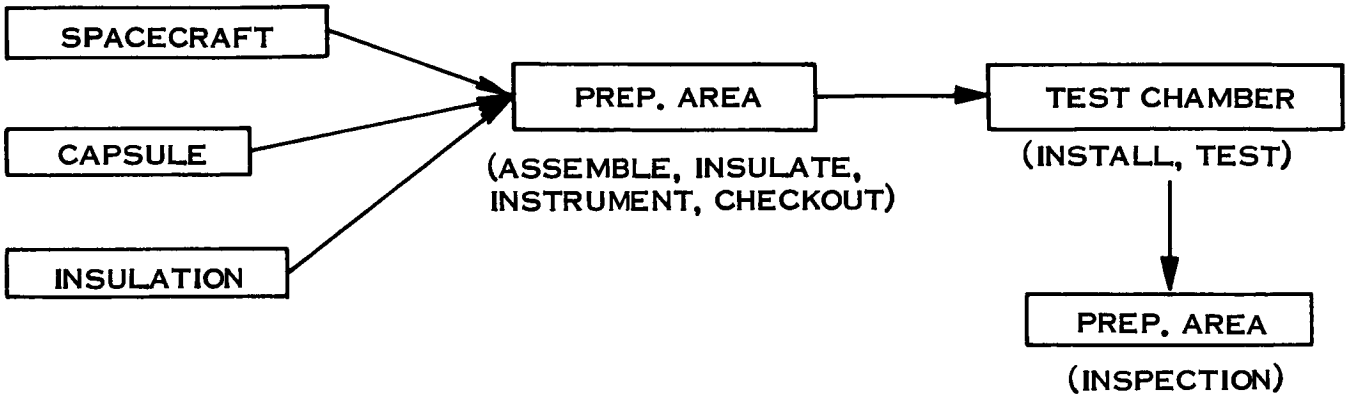

Figure 2-90. Test Fixture Flow

Section 2.5 Full-Scale Thermal Vacuum Tests

Subsection 2.5.3 Test Procedures

TEST SEQUENCE

The thermal vacuum test program consisted of pumping down the test chamber to approximately 10^{-6} torr, stabilizing the temperatures at the desired levels, conducting four tests, warm-up and venting. Figure 2-91 depicts the pressure-temperature history of the test chamber during the program. The figure shows the key events in the test cycle, as described below.

Heater controls were turned on prior to LN_2 shroud cool-down, to maintain close temperature control and to minimize the time required to reach steady-state conditions. Liquid nitrogen was admitted to the test chamber traps at approximately 40 mm Hg pressure to prevent back-streaming of diffusion pump oil. The test period started as soon as the chamber pressure was below 10^{-5} torr, the chamber walls cooled below $-280^{o}F$, and the test model had reached the first stable temperature point. This occurred approximately 7 hours after start of pump-down. Data scans were taken periodically from start of pump-down through the vent period.

During post-test warm-up, pressure was held at about 0.5 mm Hg to assure that there would be no condensation on the test vehicle.

Test Points

During the stable part of the test program, as shown in Figure 2-91, four test points were monitored. Each test point represented the attainment of specified spacecraft and capsule temperatures for approximately 10 hours. Table 2-40 presents the specified temperature and voltage controller setting for each of the four test points, the tests being monitored in numerical order. Test Point No. 1 and 2 were readily achievable. However, Test Point No. 3 could not be attained; the spacecraft temperature increased at a relatively rapid rate at $10^{o}F$, though no power was supplied to the heaters. The temperature was re-set at $25^{o}F$. Test Point No. 4 had similar difficulties with the capsule, particularly with the spacecraft at $115^{o}F$.

Table 2-40. Test Points

Temp. Controller	Test Point No.			
	1	2	3	4
Engine Throat Heater	66 volts	52 volts	52 volts	65 volts
IR Heater Can	$160^{o}F$	$50^{o}F$	$50^{o}F$	$160^{o}F$
Solar Array Simulator	$150^{o}F$	$60^{o}F$	$60^{o}F$	$150^{o}F$
Spacecraft	$115^{o}F$	$60^{o}F$	$10^{o}F(25^{o}F)$	$115^{o}F$
Capsule (Central Heater)	$115^{o}F$	$60^{o}F$	$10^{o}F$	$10^{o}F(25^{o}F)$
Body Mounted Array	$235^{o}F$	$106^{o}F$	$106^{o}F$	$235^{o}F$

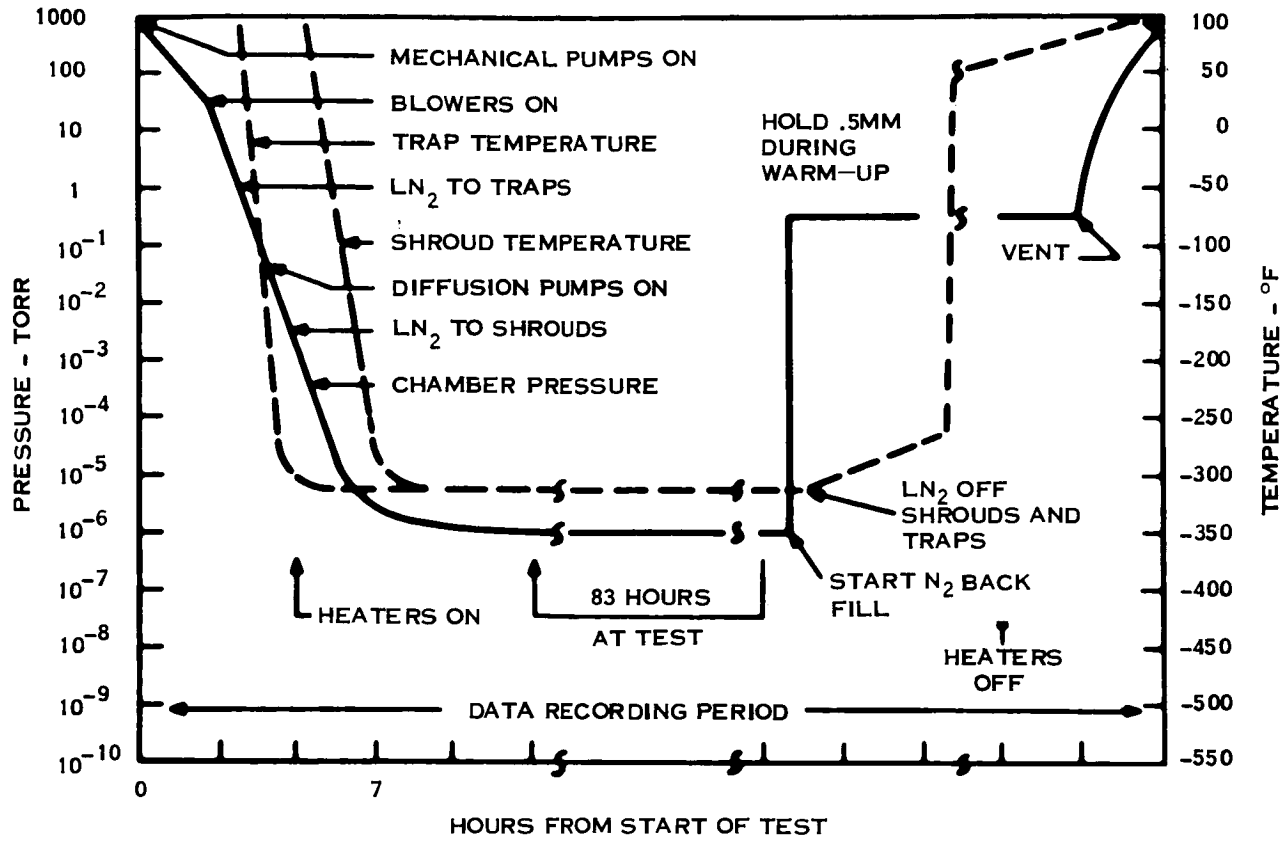

Figure 2-91. Test Profile

Section 2.5 Full Scale Thermal Vacuum Tests

Subsection 2.5.4 Thermal Vacuum Test Results

SYSTEM PERFORMANCE

Full scale test of the capsule and spacecraft demonstrated excellent thermal performance. The test was planned around four temperature conditions as shown in Table 2-41 and described in Subsection 2.5.3. Because temperature differences exist in the spacecraft and capsule, the tabulated temperatures are representative of the equipment bay heater panels of the spacecraft and the central heater of the capsule.

The first and second test point temperatures were met within the $\pm 3^{\circ}F$ objective, but for the third point, the spacecraft increased in temperature at a relatively rapid rate at $10^{\circ}F$ even though no power was supplied to the equipment bay heaters. This point was then adjusted to provide a spacecraft temperature at $25^{\circ}F$ without any electrical power to the bay heaters. The fourth point had similar difficulty, but this time with the capsule. It would not remain at $10^{\circ}F$ with the spacecraft maintained at $115^{\circ}F$, and so was raised to $25^{\circ}F$.

Figures 2-92 and 2-93 show representative capsule and spacecraft temperatures, respectively. The temperatures are averaged from the test data, averaging being accomplished as discussed in Subsection 2.5.2 (THERMOCOUPLE INSTRUMENTATION). In each case, the vertical columns in the figures represent temperatures from Test Point No. 1 through Test Point No. 4, reading from the top down. Detailed temperature data and zone averages for the four test points are presented in Appendix A.

Table 2-42 shows the gross power required to maintain the test temperatures. Gross power is defined as electrical power input, adjusted for the heat capacity contribution of the spacecraft or capsule structure due to its test slope of temperature change, vs time. The heat capacity calculated from the measured weight of the structures and the specific heat of the aluminum material is 63.5 watt-hr/$^{\circ}F$ for the spacecraft, discounting the outer solar array, and 69 watt-hr/$^{\circ}F$ for the capsule.

At each of the four test points, spacecraft and capsule temperatures and heater powers were adjusted, when possible, to give desired test conditions. The temperatures are given in Table 2-41; the test procedure calls for maintaining these temperatures within $\pm 3^{\circ}F$. In addition, it was desired that the rate of temperature change of the spacecraft and capsule structures, at essentially constant power, be restricted to less than $0.20^{\circ}F/hr$ as determined from a data plot maintained for 10 hours. The average rate of temperature change over this 10-hour span was used to calculate the structural heat flow term that modifies the heater electrical power for the gross power determination. Heater power was determined from a time integrated average of the power readings during each 10-hour data run.

FOLDOUT FRAME /

Table 2-41. Test Sequence

Test Point No.	Spacecraft (^{O}F)	Capsule (^{O}F)
1	115	115
2	60	60
3	10 (25^{O}F)	10
4	115	10 (25^{O}F)

Table 2-42. Gross Power

Test Point No.	Spacecraft (watts)	Capsule (watts)
1	225	107
2	127	66
3	-11*	32
4	305	-28*

* No electrical power.

FOLDOUT FRAME 2

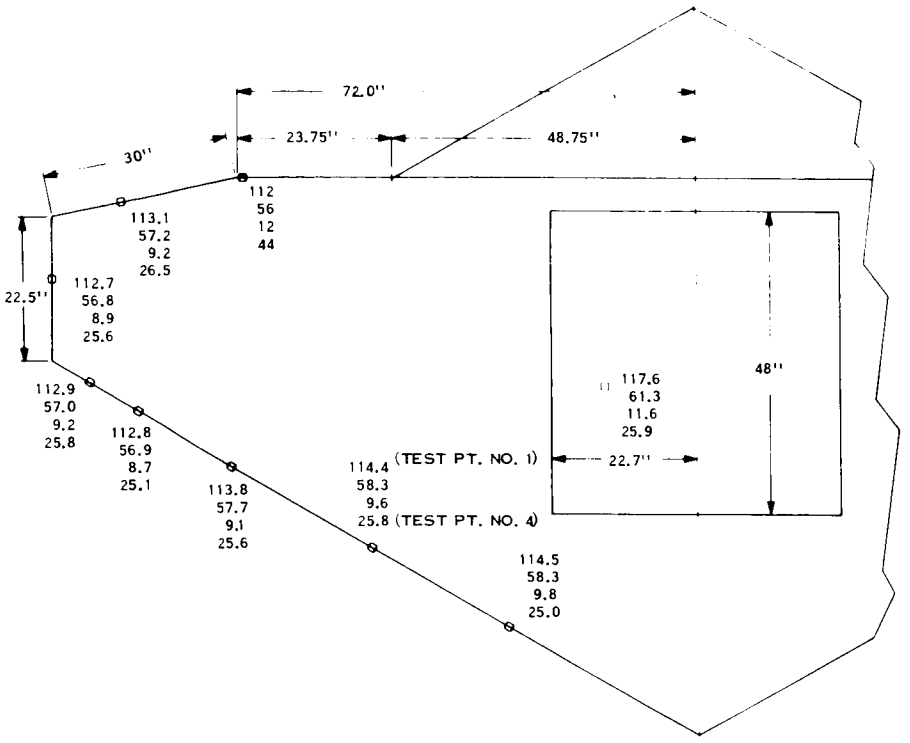

Figure 2-92. Capsule Temperatures

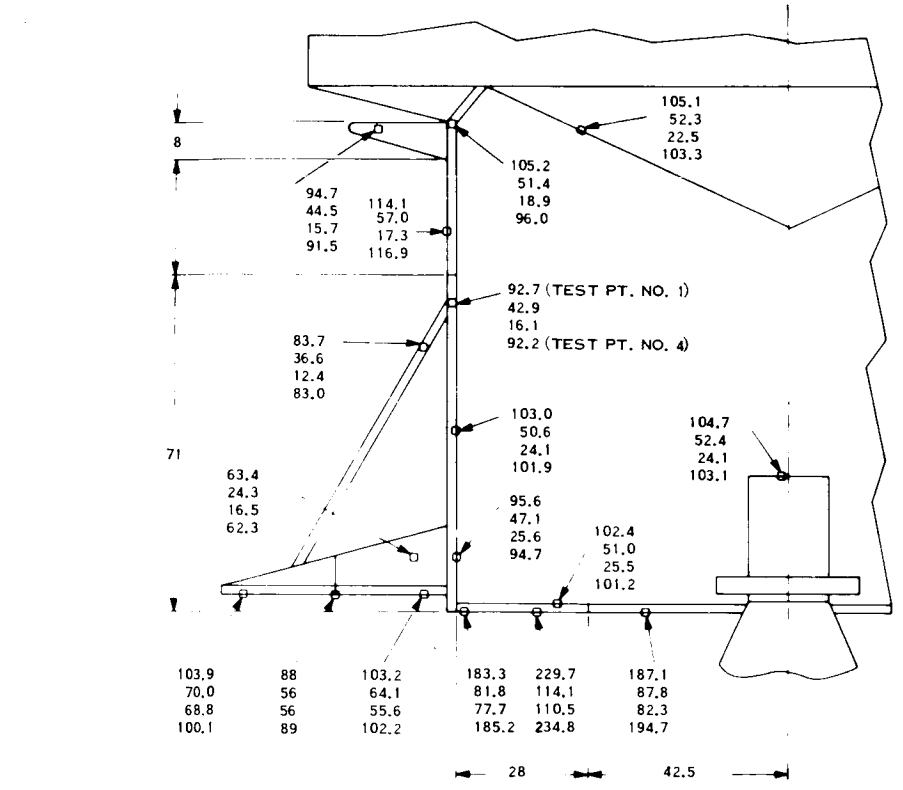

Figure 2-93. Spacecraft Temperatures

Section 2.5 Full Scale Thermal Vacuum Tests

Subsection 2.5.4 Thermal Vacuum Test Results

CAPSULE INSULATION PERFORMANCE

The capsule was a completely insulated body, having only three concentrated heat leaks or thermal shorts. The major capsule thermal short occurs at the capsule-spacecraft bolted attachment. The thermal conductance of this attachment was designed to give about 50 watts heat leak from the spacecraft for the condition of a very cold capsule structure. Temperatures on both the spacecraft and capsule side of the eight bolt locations were measured so that the actual thermal interconnection could be evaluated. Spacecraft power conditions from Test Point No. 1 and 4 were compared to provide heat flow data at a particular set of temperature conditions. By holding the spacecraft temperatures of Test Point No. 4 as closely as possible to Test Point No. 1, the measured spacecraft power difference was basically due to the spacecraft-capsule thermal interchange. Table 2-43 presents this calculation, resulting in an actual-to-estimated ratio of 2.97 for this interchange heat flow.

The other capsule thermal shorts are due to the four lifting lugs from which the capsule and spacecraft were suspended in the test chamber, and to the capsule-to-spacecraft electrical harness. These points were also instrumented to give data from which heat leaks could be calculated.

The lower conical area of the capsule is exposed to both the external solar array and side panels of the spacecraft. Both of these surfaces block the view of this part of the outer capsule surface to the test chamber cold walls, and thereby partially block the insulation heat flow by raising the outer surface temperature. Since the outer insulation temperature was not measured, an analysis was performed to estimate the conical surface temperature before the overall insulation effective emittance could be determined. The analysis indicated that the outer surface temperature of the lower cone was about $-100^{\circ}F$. The net effect of this condition, which applies to 115 square feet of the 474 square feet total capsule area, is to increase the average effective emittance by 4 percent from the value determined, with the assumption that all the insulated surfaces view only the chamber cold walls.

As has been noted, the spacecraft-capsule thermal interconnection is nearly three times (2.97) greater than calculated from the pretest estimate of thermal conductance. This interconnection includes both the direct conduction through the attachment bolts and spacers and the radiation through the insulation thermal barrier between the spacecraft and capsule. If this combined conductive and radiative thermal interchange is applied to the design prototype of the capsule and spacecraft for the condition where the forward part of the biobarrier and the lander assembly have been ejected, it is calculated that the total spacecraft heat loss to the remaining biobarrier structure will be 167 watts at a spacecraft temperature of $70^{\circ}F$. This assumes that the inner surface of the aft biobarrier has a net effective emittance of 0.1 and a projected open area of 285 square feet. The biobarrier structure temperature would be $-131^{\circ}F$.

Table 2-44 presents the detailed data reduction for Test Point No. 1. Complete capsule data reduction for the four test points is presented in Appendix B. Figure 2-94 plots the capsule external insulation heat flow as a function of temperature as determined from the four test points. In addition, the figure shows initial predictions based on calorimeter tests of hand-wrinkled gold coated 1/4 mil Mylar, and revised predictions based on additional calorimeter tests of more deeply die-crinkled material. Both of the predicted curves, as discussed in Subsection 2.5.1, include a 25 percent heat flow increase over base material for support posts and joints and an additional 50 percent heat flow increase for nonidealized conditions caused by actual manufacturing and installation procedures. The actual test result curve shows about a 39 percent increase in heat flow over calorimeter measurements for the basic unpenetrated crinkled insulation material. Capsule thermal balance calculations are presented in Appendix C.

Capsule insulation effective emittance, calculated from the four test points, is shown in Table 2-45. The effective emittance values show agreement within a tolerance of $\pm$ 3 percent. Achieving this degree of uniformity is considered to be a major achievement for a test of this type. Comparing the results shown on this table suggests that the spacecraft-capsule thermal interchange is slightly higher than computed, since a higher net conductance would decrease the spread between points to an even smaller value.

Table 2-43. Evaluation of Spacecraft-Capsule Thermal Interchange

Test Point No. 1 - 102°F Side Structure Temperature	
Electrical Power	218.6 Watts
Cooling at 0.1073°F/hr	6.8
Gross Power	225.4 Watts
Heat Flow From Capsule (reiterated)	11.5
Gross Power Plus Capsule Contribution	236.9
Test Point No. 4 - 102°F Side Structure Temperature	
Electrical Power	301.6 Watts
Cooling at 0.06°F/hr	3.8
Gross Power	305.4 Watts
Net Gain (No. 4 vs. No. 1) (See Appendix D)	3.9
Adjusted Gross Power	309.3 Watts
Less Adjusted Gross Power (Test Point No. 1)	236.9
Net to Capsule (Test Point No. 4)	72.4 Watts
$\frac{\text{Net to Capsule}}{\text{Calculated to Capsule}} = \frac{72.4}{24.4} =$	2.97

Table 2-44. Capsule Detailed Data Reduction

TEST POINT NO. 1		
Structural Temperature Change		+0.156°F/hour
Structural Capacity Contribution		- 11 watts
Electrical Power		118 watts
Gross Power		107 watts
Capsule Heat Leaks		
External Supports		4 watts
Wiring Harness		1 watt
Spacecraft Interchange (Predicted)		
Support Bolts	1.3	
Radiation	2.6	
	3.9 watts	
Interchange Factor from 4th Point	2.97	
Corrected Interchange (3.9 x 2.97)		11 watts
Total Leaks less Insulation		16 watts
Insulation Heat Flow (Gross Power minus leaks)		91 watts
Effective Emittance at 114°F Average Temperature		0.00366

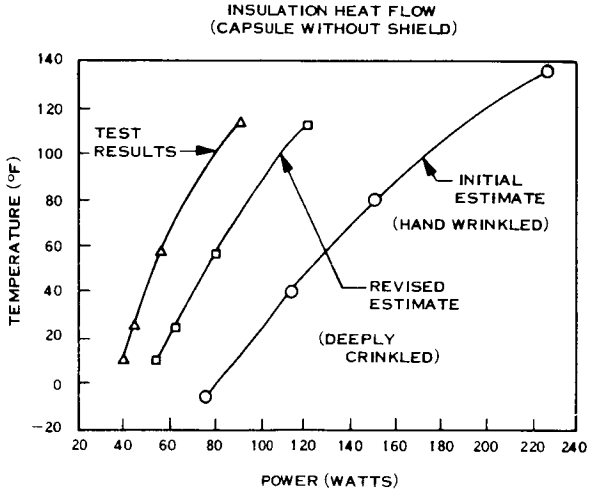

Figure 2-94. Insulation Heat Flow

Table 2-45. Capsule Insulation Performance

Test Point No.	Emissivity	Temperature (°F)
1	$\epsilon_1 = 0.00366$	114
2	$\epsilon_2 = 0.00344$	57
3	$\epsilon_3 = 0.00354$	10
4	$\epsilon_4 = 0.00347$	25

Section 2.5 Full Scale Thermal Vacuum Tests

Subsection 2.5.4 Thermal Vacuum Test Results

SPACECRAFT INSULATION PERFORMANCE

The capsule insulation performance has been relatively simple to determine. However, this is not the case for the spacecraft. The external insulation heat flow of the spacecraft is small relative to the heat flows from the exposed equipment bay panels, the external solar array support, struts and beams, and the heat flow from the base solar array and bottom heater can that simulates solar heating of the base surfaces. There are no calibrated conductances in these several heat flow paths. Therefore, anything approaching precise knowledge of these heat flow values is not available. Attempts to find adjusted conductance constants for the heat flow balance for all of the test points has not been successful. Such a balance is required if the true insulation heat flow is to be established. An evaluation of these heat flows and the spacecraft heat balance calculations are presented in Appendix C.

The overall spacecraft thermal performance was very good. At Mars solar intensity, only a small amount of electrical equipment heat rejection will maintain the spacecraft at a desirable temperature level. Due to test equipment limitations, it was not possible to raise the external solar panel to the near-earth calculated temperature, and so the full thermal effect of the external array was not duplicated during Test Point No. 1 and 4. However, it is evident that the heat rejection range of louvered equipment bay panels would be sufficient to provide satisfactory spacecraft temperatures over the full range of spacecraft equipment power that could reasonably be expected. Analysis performed pretest (Subsection 2.5.1) predicted a net spacecraft non-louvered heat loss of 146 watts at 40°F for the Mars orbit condition with forward biobarrier and capsule ejected. Table 2-46 depicts the gross power calculations for Test Point No. 2 and 3. In Table 2-47, the predicted value is compared to the test data. This comparison shows that even with the factor of three increase in spacecraft-to-capsule interconnection, the measured performance brackets the estimated value.

Table 2-46. Spacecraft Gross Power

Test Point No. 2 - 51° F Side Structure Temperature	
Electrical Power	122.8 Watts
Cooling at 0.07° F/hr.	4.4
Gross Power	127.2 Watts
Test Point No. 3 - 24° F Side Structure Temperature	
Electrical Power	0 Watts
Heating at 0.18° F/hr.	-11.4
Gross Power	-11.4 Watts

Table 2-47. Spacecraft Mars Orbit Heat Loss
(Not Including Louvers)

PRETEST ESTIMATE		TEST NO. 2	TEST NO. 3
$40^{o}F$		51^{o} F	24^{o} F
	Gross Power (Watts)	127	-11
	From Capsule (Watts)	6	-9
	Less Bay Panels (Watts)	57	41
	Plus Canister (Watts)	152	132
146	Total Non-Louvered Loss (Watts)	228	71

SECTION 3.0

PROGRAM CONCLUSIONS

SECTION 4.0

PROGRAM RECOMMENDATIONS

PROGRAM 5.0

NEW TECHNOLOGY

SECTION 6.0

REFERENCES

Section 3.0 Program Conclusions

The results of the Planetary Vehicle Thermal Insulation program have led to the following definitive conclusions:

a. The gold on Mylar and gold on Kapton insulation system tested provides adequate thermal protection throughout all mission phases.

b. Incorporation of vent holes in the insulation blankets prevents excessive ballooning during launch depressurization.

c. Gold on Mylar and gold on Kapton materials are compatible with currently recommended decontamination and sterilization environments.

d. Aluminized plastic films are unreliable in ethylene oxide environments.

e. Tinger fasteners are compatible with typical acoustic, vibration and shock loads, and afford an effective means for blanket assembly and disassembly.

f. Pressure sensitive Velcro hook and pile is compatible with the environments and conditions imposed, and works well in conjunction with Tinger fasteners.

g. Pressure sensitive clear Kapton (Tech Floro) tape appears to be satisfactory for completing insulation joints.

h. The step (or rabbet) joint appears to be superior to all other candidates.

i. Post holes, for fasteners, should be larger than the fastener diameter to avoid tears.

j. Minimal handling of the insulation is desirable.

k. Kapton-based insulations are most suitable for outer layers.

Section 4.0 Program Recommendations

On the basis of the worked performed during the program and the conclusions drawn in Section 3.0, the following recommendations are presented:

a. Gold on Mylar and gold on Kapton insulation materials should be employed for interplanetary vehicles. Kapton-based materials should comprise the outer layer.

b. Vent holes should be provided in the insulation blankets at the rate of four-1/8 inch holes per square foot of surface.

c. Fasteners should be spaced no more than 12 inches apart along joints,and a maximum unsupported distance should not exceed two feet to minimize tearing and ballooning.

d. Tinger fasteners, in conjunction with Velcro hook and pile, are recommended. Tinger post diameters of 0.25 inches should have 0.296 inch diameter holes in the insulation.

The following new technology item is reported from the subject program.

5.1 Title: Insulation Attachment Device

5.2 Inventor: Donald Ting
Member, Technical Staff
Jet Propulsion Laboratory
Pasadena, California

5.3 Progress Report for Information

Information on this item was included in "Voyager Thermal Insulation System Phase II Summary Report", DIN 67SD4405, 11 September 1967, pages 2-17 and 2-19.

5.4 Date Reported to NASA

The information was reported to NASA on 26 May 1967, Invention Report 30-1135, Jet Propulsion Laboratory.

Section 6.0 References

1. Planetary Vehicle Thermal Insulation Systems, Phase I Summary Report, GE Document No. 67SD4289, dated 3 March 1967.

2. Karp, G. S. and Lankton, C. S., A Guarded Hot Plate Thermal Conductivity Apparatus for Multilayer Cryogenic Insulation, ASTM publication STP411, April 1967.

3. NRC-2 Insulation, Brochure of National Research Corporation.

4. Getty, R. C., Clay, J. P. and Kremzier, E. J., Experimental Investigation of Some Selected Lightweight Superinsulation for Space Vehicles, Paper B-3, Advances in Cryogenic Engineering, Volume II, 1965.

5. Basic Investigations of Multi-Layer Insulation Systems, NASA CR-54191, ADL 65958-00-04, Arthur D. Little, Inc.

6. Voyager Thermal Insulation Systems, Phase II Summary Report, GE Document No. 67SD4405, dated 11 September 1967.

7. Long Term Thermal Vacuum Storage Test and Vibration Effects Evaluation on Multi-Layer Super Insulation Blankets, GE Document No. 67SD4405-5, dated 1 November 1967.

8. Morizumi, S. J. and Carpenter, H. J., Thermal Radiation from the Exhaust Plume of an Aluminized Composite Rocket Propellant, September-October, 1964.

9. Vickers, J.M.F., A Study of Thermal Scale Modeling Techniques, JPL Technical Memorandum No. 33-153.

10. Gabron, F., Thermal Scale Modeling Techniques for Voyager-type Spacecraft, Arthur D. Little, Inc., Contract No. 951417, June 15, 1966.

APPENDIXES

APPENDIX A

TEMPERATURE DATA

A1. TEST TEMPERATURES

Tables A-1 through A-4 present typical temperature values for Test Point No. 1 through 4, respectively. These data are taken at the midpoint of the 10 hour run with near constant conditions.

A2. TEMPERATURE ZONE AVERAGES

The average values for the temperature zones* for Test Point No. 1 through 4 are shown in Tables A-5 through A-8, respectively. Also tabulated under the "Net" heading are the number of channels used in the average, and tabulated under "Total" are the number of channels available for the average. Channels which deviate beyond certain limits are automatically excluded from the calculated averages. The maximum plus and minus deviations of values used in the average are also shown. The large deviations in Test Chamber Shroud temperatures (Zone 44) are believed due to the epoxy attached thermocouples popping off the LN_2 cooled walls.

*Temperature zones are defined in Subsection 2.5.2, under THERMOCOUPLE INSTRUMENTATION

Table A-1. Test Point No. 1 - Temperatures (^{O}F)

SEQ	TEMPERATURE READINGS TIMES 10									
	0	1	2	3	4	5	6	7	8	9
0	-9999	1180	1125	1138	1124	1118	1170	1147	1147	1115
10	1132	1179	1130	1127	1133	1113	1168	1127	1131	1105
20	1106	1174	1122	1129	1115	1107	1166	1129	1130	1103
30	1122	1170	1125	1121	1101	1118	1157	1122	1117	1116
40	1115	1053	1050	1046	1049	1049	1041	1047	1049	1027
50	1020	1028	1022	1027	1026	1026	1012	1024	1024	1026
60	1024	1019	1021	1020	1021	943	932	931	873	962
70	941	950	950	1054	1035	1042	1052	1050	1041	1015
80	1017	-9999	1016	1016	1020	998	1081	1821	1864	1008
90	1009	936	940	832	826	640	621	754	754	1039
100	1015	1025	1009	978	976	121	119	970	851	888
110	851	932	840	866	857	854	819	932	834	859
120	916	999	1106	1011	1009	1071	1015	760	760	760
130	756	2485	2273	2473	2409	1857	1813	2326	2269	1880
140	1878	1909	1835	760	760	759	760	760	758	762
150	756	1136	1155	1155	1155	1153	1154	1151	1139	1142
160	1143	1130	1134	1139	1134	1137	1138	1136	1143	1141
170	1107	1108	1113	1110	1120	1116	1127	1123	1127	1127
180	763	1186	1181	1176	1178	1179	1178	1134	1132	1132
190	1139	127	-19	761	761	760	756	760	760	759
200	9999	9999	9999	9999	-2453	-2038	-2710	-2481	-1498	-2161
210	-1069	-1723	-2244	-2398	-2773	-2877	-2907	-2740	-2467	-3008
220	-3131	-2792	-2901	-2864	-9999	-9999	-3019	-3041	-3009	-3510
230	-3031	-3019	-3015	-9999	-9999	-2987	-2946	2397	322	-2724

NOTE: Thermocouple numbers by tens are shown in the left hand column with digit numbers shown across the top. Temperature readings shown include the first decimal point. For example: T/C 112 reads 84.0^{O}F.

Table A-2. Test Point No. 2 - Temperatures (^{o}F)

SEQ	TEMPERATURE READINGS TIMES 10									
	0	1	2	3	4	5	6	7	8	9
0	-9999	605	564	573	562	561	595	579	579	556
10	541	603	570	569	575	547	597	569	569	548
20	550	598	564	569	559	552	595	569	568	549
30	565	595	566	556	549	558	581	564	560	559
40	9999	520	516	514	515	513	503	514	515	506
50	497	506	499	509	510	507	489	506	502	508
60	508	507	508	509	508	444	435	441	392	483
70	462	470	469	529	512	522	524	523	522	506
80	512	-9999	507	508	514	493	554	1104	1103	497
90	492	443	445	364	366	240	248	753	751	497
100	477	498	484	458	456	-303	-300	591	492	574
110	562	583	511	534	532	541	515	615	557	550
120	618	693	776	716	580	678	674	755	756	756
130	751	1227	1114	1223	1190	815	796	1130	1126	881
140	889	905	841	756	757	757	759	758	756	762
150	758	579	587	586	585	581	581	582	571	576
160	577	567	573	575	572	572	571	568	576	572
170	545	547	554	558	563	564	569	568	566	562
180	762	624	611	607	609	612	611	572	570	567
190	573	-328	-444	761	760	760	755	759	758	757
200	9999	9999	9999	9999	-2430	-2020	-2711	-2463	-1408	-9999
210	-1028	-1320	-2202	-2305	-2779	-2878	-2925	-9999	-2334	-9999
220	-9999	-2847	-9999	-2880	-9999	-9999	-3042	-3055	-3033	-9999
230	-3054	-3033	-9999	-9999	-9999	-9999	-2955	2396	322	-2722

Table A-3. Test Point No. 3 - Temperatures (^{o}F)

SEQ	TEMPERATURE READINGS TIMES 10									
	0	1	2	3	4	5	6	7	8	9
0	-9999	179	166	167	168	169	166	168	165	168
10	146	173	171	174	169	166	178	174	169	169
20	169	178	178	178	179	178	172	170	167	172
30	172	175	175	170	179	173	175	174	174	180
40	9999	181	179	184	188	195	194	191	198	241
50	237	242	241	242	242	243	236	238	239	239
60	238	239	239	241	239	168	162	174	137	267
70	253	257	244	220	224	225	224	225	225	253
80	253	-9999	256	248	257	190	288	922	928	203
90	204	156	157	119	126	147	175	712	712	114
100	95	172	166	155	154	-525	-520	585	491	556
110	538	586	511	587	594	605	590	556	498	525
120	586	683	-9999	646	465	595	578	719	720	719
130	715	1221	1092	1217	1172	770	766	1103	1084	823
140	828	847	783	719	719	719	719	718	719	720
150	714	92	101	97	95	94	95	97	94	96
160	94	90	90	89	90	91	91	95	94	91
170	84	86	128	134	124	127	110	104	109	98
180	722	127	116	114	114	115	113	89	88	86
190	90	-687	-761	722	721	720	718	720	720	719
200	9999	9999	9999	9999	-2453	-2031	-2725	-2475	-1143	-1370
210	-1043	-1341	-2226	-2125	-2775	-2924	-2938	-2935	-2734	-9999
220	-9999	-2860	-9999	-2899	-9999	-9999	-3053	-3067	-9999	-3067
230	-3070	-3053	-9999	-9999	-9999	-9999	-2971	2394	318	-2729

Table A-4. Test Point No. 4 - Temperatures (^{o}F)

SEQ	TEMPERATURE READINGS TIMES 10									
	0	1	2	3	4	5	6	7	8	9
0	-9999	1230	1150	1171	1163	1156	1221	1171	1172	1153
10	1171	1227	1151	1153	1174	1156	1212	1147	1144	1142
20	1145	1226	1142	1161	1152	1147	1217	1165	1163	1147
30	1164	1223	1149	1162	1132	1155	1208	1157	1145	1155
40	9999	938	911	946	946	970	978	976	1002	1020
50	1020	1021	1020	1021	1021	1021	1018	1019	1020	1020
60	1018	1017	1016	1015	1015	938	931	934	878	958
70	940	949	949	1036	1012	1025	1047	1041	1031	1010
80	1011	9999	1012	1011	1016	989	1073	1802	1785	992
90	997	914	918	829	828	635	633	722	722	594
100	563	866	904	934	932	89	87	980	849	908
110	867	944	847	888	876	876	838	947	851	877
120	932	1025	9999	1031	1021	1074	1018	728	729	729
130	723	2544	2363	2479	2486	1894	1819	2383	2317	1953
140	1953	1977	1905	727	726	726	726	726	728	730
150	726	231	247	242	239	252	256	250	253	254
160	249	254	252	250	259	257	248	262	262	253
170	302	307	502	537	503	481	387	355	395	331
180	731	261	255	254	255	255	248		250	245
190	245	-628	-709	728	729	729	728	729	728	748
200	9999	9999	9999	9999	-2439	-2018	-2714	-2468	-1092	-9999
210	-1030	-1328	-2209	-2094	-2727	-2858	-2899	-2709	-2409	9999
220	9999	-2789	9999	-2863	-9999	-9999	-3025	-3047	-9999	-3042
230	-3040	-3029	-9999	-9999	-9999	-9999	-2955	2392	317	-2732

Table A-5. Zone Temperature Averages (°F) - Test Point No. 1

ZONE NO	TEMP X10	T/C NET*	T/C TOT**	DEV(X10) +	DEV(X10) -
1	1137	5	5	43	-19
2	1142	5	5	28	-27
3	1136	5	5	43	-23
4	1127	5	5	41	-22
5	1129	5	5	45	-22
6	1130	5	5	36	-27
7	1127	5	5	43	-26
8	1125	5	5	32	-10
9	1132	40	40	48	-31
10	1048	8	8	5	-7
11	1023	16	16	5	-11
12	920	4	4	23	-47
13	951	4	4	11	-10
14	1046	6	6	8	-11
15	1017	5	6	3	-2
16	2410	4	4	75	-137
17	1835	2	2	22	-22
18	2298	2	2	28	-29
19	2066	4	4	260	-253
20	2238	8	8	247	-425
21	876	14	14	94	-57
22	1039	3	3	67	-40
23	1032	3	3	39	-23
24	1035	6	6	71	-36
25	924	20	20	182	-105
26	1009	2	2	0	-1
27	1040	2	2	41	-42
28	1843	2	2	21	-22
29	1876	4	4	33	-41
30	829	2	2	3	-3
31	631	2	2	9	-10
32	938	2	2	2	-2
33	1017	2	2	8	-8
34	977	2	2	1	-1
35	120	2	2	1	-1
36	1120	8	8	7	-10
37	1143	19	19	12	-13
38	1180	6	6	6	-4
39	54	2	2	73	-73
40	1134	4	4	5	-2
41	1152	25	25	34	-22
42	1108	2	2	0	-1
43	1027	2	2	12	-12
44	-2462	20	33	1393	-669

NOTE:

* No. of channels used for average.

** No. of channels available for average (see Table 2-38, Subsection 2.5.2).

Table A-6. Zone Temperature Averages (^{O}F) - Test Point No. 2

ZONE NO	TEMP X10	T/C NET	T/C TOT	DEV(X10) +	DEV(X10) -
1	573	5	5	32	-12
2	570	5	5	25	-29
3	573	5	5	30	-26
4	567	5	5	30	-19
5	568	5	5	30	-16
6	569	5	5	26	-20
7	565	5	5	30	-16
8	566	4	5	15	-7
9	569	39	40	36	-28
10	514	8	8	6	-11
11	505	16	16	5	-16
12	428	4	4	16	-36
13	471	4	4	12	-9
14	522	6	6	7	-10
15	509	5	6	5	-3
16	1189	4	4	38	-75
17	806	2	2	9	-10
18	1128	2	2	2	-2
19	967	4	4	163	-171
20	1078	8	8	149	-282
21	555	14	14	63	-63
22	728	3	3	48	-35
23	644	3	3	34	-64
24	686	6	6	90	-106
25	595	20	20	181	-103
26	495	2	2	2	-3
27	524	2	2	30	-31
28	1104	2	2	0	-1
29	879	4	4	26	-38
30	365	2	2	1	-1
31	244	2	2	4	-4
32	444	2	2	1	-1
33	491	2	2	7	-7
34	457	2	2	1	-1
35	-302	2	2	2	-1
36	563	8	8	6	-9
37	576	19	19	11	-9
38	612	6	6	12	-5
39	-386	2	2	58	-58
40	571	4	4	2	-4
41	585	25	25	39	-18
42	546	2	2	1	-1
43	487	2	2	10	-10
44	-2302	15	33	1274	-623

Table A-7. Zone Temperature Averages (^{O}F) - Test Point No. 3

ZONE NO	TEMP X10	T/C NET	T/C TOT	DEV(X10) +	DEV(X10) -
1	170	5	5	9	-4
2	163	5	5	5	-17
3	171	5	5	3	-5
4	172	5	5	6	-3
5	178	5	5	1	0
6	171	5	5	1	-4
7	174	5	5	5	-4
8	176	4	5	4	-2
9	172	39	40	8	-26
10	189	8	8	9	-10
11	240	16	16	3	-4
12	160	4	4	14	-23
13	255	4	4	12	-11
14	224	6	6	1	-4
15	253	5	6	4	-5
16	1176	4	4	45	-84
17	768	2	2	2	-2
18	1094	2	2	9	-10
19	931	4	4	172	-165
20	1053	8	8	168	-287
21	558	14	14	47	-67
22	665	2	3	18	-19
23	546	3	3	49	-81
24	593	5	6	90	-128
25	567	19	20	116	-102
26	204	2	2	0	-1
27	239	2	2	49	-49
28	925	2	2	3	-3
29	820	4	4	27	-37
30	123	2	2	3	-4
31	161	2	2	14	-14
32	157	2	2	0	-1
33	169	2	2	3	-3
34	155	2	2	0	-1
35	-523	2	2	3	-2
36	117	8	8	17	-19
37	93	19	19	8	-4
38	117	6	6	10	-4
39	-724	2	2	37	-37
40	88	4	4	2	-2
41	99	25	25	28	-10
42	85	2	2	1	-1
43	105	2	2	9	-10
44	-2294	17	33	1251	-644

Table A-8. Zone Temperature Averages (^{O}F) - Test Point No. 4

ZONE NO	TEMP X10	T/C NET	T/C TOT	DEV(X10) +	DEV(X10) -
1	1174	5	5	56	-24
2	1178	5	5	43	-25
3	1172	5	5	55	-21
4	1158	5	5	54	-16
5	1166	5	5	60	-24
6	1171	5	5	46	-24
7	1164	5	5	59	-32
8	1166	4	5	42	-21
9	1169	39	40	61	-37
10	958	8	8	44	-47
11	1019	16	16	2	-4
12	920	4	4	18	-42
13	949	4	4	9	-9
14	1032	6	6	15	-20
15	1012	5	6	4	-2
16	2468	4	4	76	-105
17	1857	2	2	37	-38
18	2350	2	2	33	-33
19	2103	4	4	280	-284
20	2286	8	8	258	-467
21	891	14	14	89	-53
22	1028	2	3	3	-3
23	1038	3	3	36	-20
24	1034	5	6	40	-16
25	929	19	20	145	-91
26	995	2	2	2	-3
27	1031	2	2	42	-42
28	1794	2	2	8	-9
29	1947	4	4	30	-42
30	829	2	2	0	-1
31	634	2	2	1	-1
32	916	2	2	2	-2
33	885	2	2	19	-19
34	933	2	2	1	-1
35	88	2	2	1	-1
36	436	8	8	101	-105
37	251	19	19	11	-20
38	255	6	6	6	-7
39	-669	2	2	41	-40
40	716	4	4	1408	-471
41	252	25	25	10	-21
42	305	2	2	2	-3
43	579	2	2	15	-16
44	-2290	16	33	1260	-609

APPENDIX B

CAPSULE INSULATION PERFORMANCE

The capsule insulation performance is given below for each of the four data points.

B1. TEST POINT NO. 1 - 114°F CAPSULE STRUCTURE TEMPERATURE

Calculated Capsule Thermal Shorts

Support Cables		4.1 watts
Electrical Harness		0.6
S/C Conduction 1.3 S/C Radiation 2.6	3.9 x 2.97	11.5
Total Shorts		16.2 watts
Electrical Power		118.1 watts
Heating at 0.156°F/hr.		-10.8
Gross Power		107.3 watts
Less Thermal Shorts		16.2
Net Out Capsule Insulation		91.1 watts

Average Heat Flow Per Unit Area = 0.192 watts/sq. ft.
Insulation Effective Emittance =

$$0.192 \text{ watts/ft}^2 \frac{(3.41 \text{ BTU/hr-watt})}{(186.1 \text{ BTU/hr-ft}^2)} (1.04) = 0.00366$$

B2. TEST POINT NO. 2 - 57° STRUCTURE TEMPERATURE

Calculated Thermal Shorts

Support Cables			2.7 watts
Harness			0.4
S/C Conduction	0.9	2.1 x 2.97	6.2
S/C Radiation	1.2		
Total Shorts			9.3 watts
Electrical Power			71.2
Heating at 0.08°F/hr			-5.5
Gross Power			65.7 watts
Less Thermal Shorts			-9.3
Net Out Capsule Insulation			56.4 watts

Heat Flow Per Unit Area = 0.119 watts/sq. ft.
Insulation Effective Emittance = 0.00344

B3. TEST POINT NO. 3 - 9.5° STRUCTURE TEMPERATURE

Calculated Thermal Shorts

Support Cables			1.8 watts
Harness			-0.2
S/C Conduction	-1.3	-3.1 x 2.97	-9.2
S/C Radiation	-1.8		
Total Shorts			-7.6 watts
Electrical Power			29.8 watts
Cooling at 0.03°F/hr			2.1
Gross Power			31.9 watts
Less Thermal Shorts		-(-)	7.6
Net Out Capsule Insulation			39.5 watts

Heat Flow Per Unit Area = 0.0833 watts/sq. ft.
Insulation Effective Emittance = 0.00354

B4. TEST POINT NO. 4 - 25°F STRUCTURAL TEMPERATURE

Calculated Thermal Shorts

Support Cables			2.1 watts
Harness			-2.0
S/C Conduction 9.3 S/C Radiation 15.1	24.4 x 2.97		-72.4
Total Shorts			-72.3 watts
Electrical Power			0 watts
Heating at 0.41°F/hr			-28.3
Gross Power			-28.3 watts
Less Thermal Shorts		-(-)	72.3
Net Out Capsule Insulation			44.0 watts

Heat Flow Per Unit Area = 0.093 watts/sq. ft.

Insulation Effective Emittance = 0.00347

APPENDIX C

HEAT FLOW ANALYSIS - HEAT BALANCE

Heat flow equations were established to evaluate the thermal performance of the spacecraft and capsule as the tests were in progress. The heat balance equations are presented in Table C-1. The equation constants for the spacecraft were established according to the following discussion:

a. Solar Array Beams - The solar array beams support the external solar panels from the spacecraft side structure near the base. In the test fixture these beams, 16 in all, were attached to the structure with sheet metal screws. The beam heat flow was assumed proportional to the temperature difference between a point on the beam web and the spacecraft structure at the attachment location. The composite thermal conductance between the point on the beam web six inches from the spacecraft attachment and the attachment structure was estimated to be 7.85 watts/^{o}F, including an allowance for contact resistance at the beam attachment joint.

b. Array Support Struts - The 16 array support struts connect the spacecraft side structure to the outer end of the array support beams. The strut heat flow was assumed to be proportional to the temperature difference between the spacecraft structure side mounting lug and a point on the strut tube six inches from the lug. The total strut conductance of 4.27 watts/^{o}F includes an allowance for the bolted joint between the lug and strut.

c. Equipment Bay Panels - The eight panels simulating the exposed side of the equipment bays had uncoated aluminum faces "looking" out. A hemispherical emittance of 0.055 was estimated, from a normal emittance measurement of 0.045 made on a coupon cut from similar material, resulting in a total radiative conductance of 0.491 watt-hr-ft^{2}/Btu from the panels. The view to the bottom capsule insulation was neglected for return radiation on the assumptions that the outer capsule insulation temperature was much lower than that of the equipment bay panels and that return reflection is negligible. The radiative conductance from the external solar array, of 0.021 watt-hr-ft^{2}/Btu, includes the view factor of 0.05 between the panels and the array. The inside of each bay panel had two strip heaters, and was painted black, as was the entire interior of the spacecraft.

d. Scan Platform Mounting Bracket - The scan platform mounting bracket was attached to the spacecraft structure with sheet metal screws and the interface was coated with silicone grease at assembly for increased conductance. The insulation over the bracket structure had openings at the outer end to simulate an uninsulated swing joint with the scan platform support arm. The arm was not included. The heat flow from the spacecraft structure to the platform bracket was assumed proportional to the temperature difference between the spacecraft structure and a point 4 inches out from the spacecraft. The resulting conductance was 1.64 watts/^{o}F.

Table C-1. Heat Balance Equations

Equation No.	Spacecraft
1.	Equipment bay heat rejection $q_{eb} = C_1 \sigma T_9^4 - C_2 \sigma T_{25}^4$ watts Where C_1 & C_2 are constants that include area, view factor, emittance, conductivity, contact conductance, and absorptance, if applicable, and the temperature subscript number refers to the previously listed temperature averages.
2.	Spacecraft-Capsule conductance $q_{cb} = C_3 (T_{10} - T_{36})$
3.	Engine solar heating $q_e = C_4 (\sigma T_{28}^4 - \sigma T_{27}^4)$
4.	Body solar array $q_{bsa} = C_5 (\sigma T_{20}^4 - \sigma T_{15}^4)$
5.	Base insulation $q_{bi} = C_6 (\sigma T_{29}^4 - \sigma T_{15}^4)$
6.	Array support strut $q_{as} = C_7 (T_{12} - T_{30})$
7.	Array support beam $q_{ab} = C_8 (T_{13} - T_{31})$
8.	Scan platform structure $q_{sp} = C_9 (T_{26} - T_{32})$
9.	S/C capsule harness $q_{bh} = C_{10} (T_{33} - T_{43})$
10.	Chamber harness $q_{mh} = C_{11} (T_{34} - T_{35})$
11.	S/C capsule radiation $q_{ii} = C_{12} (\sigma T_{14}^4 - \sigma T_{41}^4)$
12.	S/C side insulation $q_{si} = C_{13} (\sigma T_{11}^4)$
13.	S/C heat loss $q_{s/c}$ = Eqs. 1+2-3-4-5+6+7+8+9+11+12
14.	S/C Power $q_{bp} = C_{14}$ (ch 200) (ch 201)
15.	S/C heat loss deviation $D_{s/c} = \frac{14 - 13}{14}$
	Capsule
16.	Capsule support $q_{cs} = C_{20} (\sigma T_{40}^4)$
17.	Capsule harness $q_{ch} = C_{21} (T_{42} - T_{43})$
18.	Capsule insulation $q_{ci} = C_{23} (\sigma T_{37}^4)$
20.	S/C Capsule interchange $q_{bci} = 2 + 11 - 17$
21.	Capsule heat loss $q_c = 17 + 16 - 2 - 11 + 18 + 19$
22.	Capsule power $q_{cp} = C_{24}$ (ch 202) (ch 203)
23.	Capsule heat loss deviation $D_c = \frac{22 - 21}{22}$

Where

$C_1 = 0.491$
$C_2 = 0.021$
$C_3 = 0.178$
$C_4 = 0.0924$
$C_5 = 0.360$
$C_6 = 0.130$
$C_7 = 4.270$
$C_8 = 7.85$
$C_9 = 1.64$
$C_{10} = 0.075$
$C_{11} = 0.031$
$C_{12} = 0.196$
$C_{13} = 0.506$
$C_{14} = 2.675$
$C_{20} = 0.022$
$C_{21} = 0.075$
$C_{23} = 0.652$
$C_{24} = 2.94$

ch 200 = S/C heater current shunt (millivolts)
ch 201 = S/C heater voltage divider (millivolts)
ch 202 = Capsule heater current shunt (millivolts)
ch 203 = Capsule heater voltage divider (millivolts)

e. Spacecraft-Chamber Harness - The heat flow from the spacecraft to the chamber wiring harness was based on the temperature difference between the connector panel and a point in the insulated bundle 18 inches from the spacecraft. The conductance rate was 0.03 watts/^{o}F.

f. Spacecraft-Capsule Harness - The spacecraft-capsule wiring harness conductance of 0.075 watts/^{o}F was calculated, for the spacecraft, from the point in the insulated wire bundle at the spacecraft electrical panel penetration to the harness midpoint between the spacecraft and capsule. Thermocouples at each point provided the temperature difference.

g. Side Insulation - The radiative conductance of 0.506 watt-hr-ft^{2}/Btu assumed that the inner insulated area was exposed to the chamber cold wall through an emittance of 0.00562. If this insulation actually performed as well as the capsule insulation, adjusted for the relative number of layers, the emittance used in the heat flow calculations should have been 0.00408. Actually, radiant heat to the outer insulation surface from the solar panels probably increases the outer surface temperature considerably over the temperature that would result from cold wall exposure only and causes a further reduction in the insulation heat flow. This effect may reduce the actual insulation heat flow to little more than half the amount shown in the calculations.

h. Spacecraft-Capsule Interconnection - The spacecraft and capsule were conductively interconnected through the attachment bolts and spacer bushings and radiatively connected through the spacecraft top insulation blanket. The conductive coupling of 0.178 watts/^{o}F was calculated on the basis of no thermal interaction between the eight bolts and the surrounding spacer bushings. The radiative conductance of 0.196 watt-hr-ft^{2}/Btu assumed an insulation effective emittance of 0.00562.

Test data show that the thermal interchange between the spacecraft and capsule was about three times the calculated sum of the conductive and radiative terms. It is impossible to tell from the data whether one or the other or both of the heat transfer paths was responsible for this increase. Conjecture indicates that perhaps the aluminum bushing contacted the bolt and caused a thermal short circuit as illustrated in Figure C-1. Inspection after disassembly does show evidence of this contact in several of the bolt-spacer assemblies.

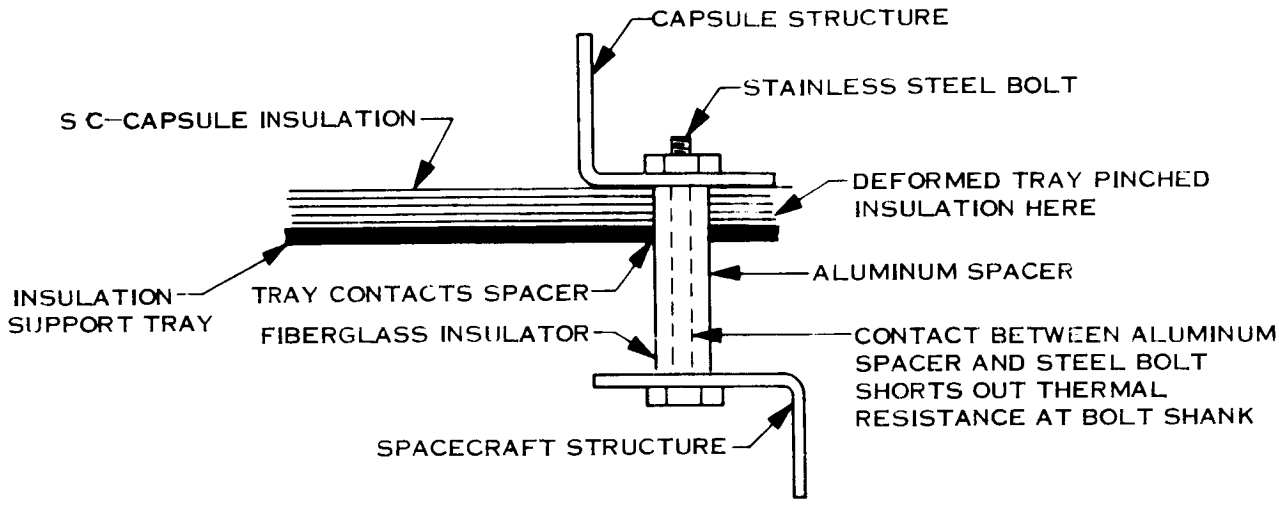

Figure C-1. Bolt-spacer Assemblies

On the other hand, it was also noticed at assembly that the insulation support tray at the top of the spacecraft did not lay tight to the spacecraft structure at the outer periphery, but instead was sprung toward the capsule. Although not thought to be of any consequence at the time, this tray may have been distorted sufficiently to press the separating insulation against the lower capsule structure, thus increasing the heat flow. Post disassembly did show that the insulation was firmly squeezed by the support tray against the capsule structure in four locations. In addition, the insulation tray touched the aluminum spacer bushing at several clearance hole locations. As both the radiative and conductive coupling terms may be contributing to the heat flow increase, their sum was used in evaluating the increased heat flow rate as compared to the test predictions.

i. Engine Solar Heating - In the spacecraft prototype design, the sun would be directly incident on the orbit insertion engine nozzle, shining through the nozzle throat area into the engine combustion chamber. In test this solar heat flux was simulated by a heater plate located in the simulated engine throat. It was intended that this plate would be suspended in the throat with a high conductive resistance so that heat transfer from the plate would be primarily by radiation. Due to manufacturing tolerances, however, the plate fit very tightly into the throat so that it is likely that a considerable amount of contact conduction exists. This agreed with the test operation where it was noted that heater plate temperature was much lower than plate power would require. Consequently, plate power calculated from the electrical voltage panel meter reading and the room temperature heater resistance was used

to set the test points. It is likely that the actual heat flow to the simulated engine was somewhat less than indicated because of line losses in the chamber electrical system and because of increased heater resistance with temperature.

j. Body Array Solar Heating - Heat flow from the base mounted solar array was calculated from the radiative conductance of 0.360 watt-hr-ft^2/Btu. This conductance was based on insulation effective emittance of 0.0185 and included a 2 percent factor to include heat flow through the plastic standoff posts that attach the simulated array panel to the bottom of the spacecraft.

k. Base Insulation Solar Heating - The base insulation radiative conductance of 0.130 watt-hr-ft^2/Btu was calculated from an insulation effective emittance of 0.0099.

Table C-2 shows typical calculated heat flow values for each of the four test points. As can be seen from Equation 15, the ratio of calculated heat loss to electrical power input has considerable deviation from unity. For some cases, such as Test Point 3, this is primarily due to the fact that the heat input term does not include the test fixture structural heat capacity contribution. In addition, the local heat flow factors are more complex, in most cases, than the simple equations can consider. Electrical input is believed to be a better evaluation of engine solar heating than the radiation only calculation of Equation 3. The capsule-spacecraft interconnections of Equations 2 and 11 have not been corrected to agree with test results.

The insulation heat loss calculation for the capsule (QC) corresponds to the revised prediction curve of Figure 2-94 in Subsection 2.5.4. It is probable that the spacecraft insulation loss is also over valued.

Table C-3 lists the Spacecraft Heat Flow values revised from test data analysis. Only the first three test points are listed, as Test Point No. 4 was essentially like Test Point No. 1, subject to the minor changes listed in Table C-4.

Table C-2. Heat Flow (watts)

Equation* No.	Test Point Number			
	1	2	3	4
1 QEB =	87.2532	57.2791	40.9372	89.6046
2 QCB =	-1.2816	-0.8722	1.2816	9.2916
3 QE =	11.2447	5.8346	6.0597	10.5272
4 QBSA =	73.3419	22.0465	28.7215	77.3812
5 QBI =	16.9764	4.8878	6.8534	18.7990
6 QAS =	38.8570	26.9010	15.7990	38.8570
7 QAB =	251.2000	178.1950	73.7900	247.2750
8 QSP =	11.6440	8.3640	7.7080	12.9560
9 QBH =	-0.0750	0.0300	0.4800	2.2950
10 QMH =	2.6567	2.3529	2.1018	2.6195
11 QII =	-2.6312	-1.1561	1.8090	15.1467
12 QSI =	86.4565	58.7195	47.4358	86.2105
13 QS/C =	372.5166	297.0444	149.7077	397.5486
14 QBP =	218.7590	122.9928	0.0055	259.5560
15 DS/C =	-0.7029	-1.4151	27219.5801	-0.5316
16 QCS =	4.0649	2.6877	1.8151	3.0024
17 QCH =	0.6075	0.4425	-0.1500	-2.0550
18 QV =	0.	0.	0.	0.
19 QCI =	121.2281	79.9636	54.0231	61.6809
20 QBCI =	-4.5203	-2.4708	3.2406	26.4933
21 QC =	129.8133	85.1221	52.5975	38.1899
22 QCP =	117.6684	70.8755	29.5904	-0.0035
23 DC =	-0.1032	-0.2010	-0.7775	10825.8068

*Equation No. corresponds to numbers in Table C-1.

Table C-3. Spacecraft Heat Flow - Calculated (Watts)

COMPONENT	TEST POINT 1	TEST POINT 2	TEST POINT 3	TEMPERATURES USED IN CALCULATIONS (°F) TEST POINT 1	TEST POINT 2	TEST POINT 3	
External Solar Array (Inner-Avg.)				103.2 - 87.6	64.1 - 55.5	55.6 - 55.8	
Solar Array Beam Loss	251.2	178.2	73.8	95.6 - 63.4	47.1 - 24.3	25.6 - 16.5	
Array Strut Loss	38.9	26.9	15.8	92.7 - 83.7	42.9 - 36.6	16.1 - 12.4	
Equipment Bay Rejection	87.3	57.3	40.9	114.1*	57.0*	17.3*	
Scan Platform Loss	11.6	8.4	7.7	100.9 - 93.8	49.5 - 44.4	20.4 - 15.7	
S/C Chamber Harness Loss	2.6	2.4	2.1	97.7 - 12.0	45.7 - (-30.2)	15.5 - (-52.3)	
S/C Capsule Harness Loss	-0.1	0	0.5	101.7 - 102.7	49.1 - 48.7	16.9 - 10.5	
Side Insulation Loss	86.4	58.7	47.7	102.3*	50.6*	24.1*	
Capsule Interconnection Loss	-11.5	-9.3	9.2	104.8 - 112.0 104.6* - 115.2*	51.4 - 56.3 52.2* - 58.5*	18.9 - 11.7 22.4* - 9.9*	Conduction Radiation
Total S/C Loss	466.4	322.6	197.7				
Engine Solar Heating	35.2	22.5	22.5	184.3* - 104.0*	110.4* - 52.4*	92.5* - 23.9*	Probably more conductive than radiative
Body Solar Array Heating	73.3	22.0	28.7	229.7* - 102.4*	114.1* - 51.0*	110.5* - 25.5*	
Base Insulation Solar Heating	17.0	4.9	6.9	187.1* - 102.4*	87.8* - 51.0*	82.3* - 25.5*	
Gross Power	225.4	127.2	-11.4				
Total Heating	350.9	176.6	46.7				
Excess Loss	115.5	146.0	151.0				

* Denotes Radiation

Table C-4. Spacecraft Heat Flow (Watts) (Calculated)

Component	Test Point 1		Test Point 4		Difference Test Point 4 - Test Point 1		Net Gain Test Point No. 4 vs No. 1
	Gain	Loss	Gain	Loss	Gain	Loss	
Solar Array Beam		251.2		247.3	3.9		
Engine Solar Heating	35.2		35.2		0		
Equipment Bay Rejection		87.3		89.6		2.3	
Body Array Solar Heating	73.3		77.4		4.1		
Base Insolation Solar Htg.	17.0		18.8		1.8		
Array Strut Loss		38.9		38.9		0	
Scan Platform Loss		11.6		13.0		1.4	
Spacecraft/Capsule Harness	0.1			2.3		2.4	
Spacecraft/Chamber Harness		2.6		2.6		0	
Side Insolation		86.4		86.2	0.2		
Total	125.6	478.0	131.4	479.9	10.0	6.1	3.9
S/C Capsule Conduction	1.3			9.3			
S/C Radiation	2.6			15.1			